Die Rolle des Adhäsions-GPCR VLGR1/ADGRV1 in Mitochondrien-assoziierten ER-Membranen

Dissertation

Zur Erlangung des Grades

„Doktor der Naturwissenschaften"

Am Fachbereich Biologie

der Johannes Gutenberg-Universität

in Mainz

von Jacek Krzysko

Mainz, Dezember 2022

1. Berichterstatter: Univ.-Prof. Dr. Uwe Wolfrum,

Institut für molekulare Physiologie

Tag der mündlichen Prüfung: 13.03.2022

Anmerkungen:

Die hier vorliegende Arbeit ist kumulativ gestaltet und besteht aus vier veröffentlichten Publikationen (I, II, III & IV).

I. Knapp B, Roedig J, Boldt K, Krzysko J, Horn N, Ueffing M and Wolfrum U (2019). Affinity proteomics identifies novel functional modules related to adhesion GPCRs. Ann N Y Acad Sci 1456(1): 144-167.

II. Knapp B, Roeding J, Roeding H, Krzysko J, Horn N, Güler E.G, Kusuluri D.K, Yildirim A, Boldt K, Ueffing M, Liebscher I and Wolfrum U (2022). Affinity Proteomics Identifies Interaction Partners and Defines Novel Insights into the Function of the Adhesion GPCR VLGR1/ADGRV1. Molecules 2022, 27(10), 3108.

III. Güler B, Krzysko J and Wolfrum U, Isolation and Culturing of Primary Astrocytes of Mouse Models for the Analysis of Focal Adhesion Dynamics. STAR Protocols, Volume 2, Issue 4, 2021, 100954,

IV. Krzysko J, Maciag F, Mertens A, Güler B, Linnert J, Knapp B, Boldt K, Ueffing M, Nagel-Wolfrum K, Heine M, and Wolfrum U (2022). The Adhesion GPCR VLGR1/ADGRV1 Regulates the Ca^{2+} Homeostasis at Mitochondria-Associated ER Membranes. Cells 2022, 11, 2790.

Publikation I ist in der Zeitschrift "Annals of the New York Academy of Sciences" veröffentlicht (2019). Publikation II wurde in "Molecules" 2022 publiziert. Publikation III wurde 2021 im "STAR Protocols Journals" veröffentlicht. Publikation IV ist in der Zeitschrift "Cells MDPI" 2022 publiziert.

Kongressbeiträge:

Auszüge dieser Dissertation wurden auf Kongressen präsentiert:

Krzysko J., Kusuluri D., Knapp B., Wolfrum U. (2017) „VLGR1 signaling at focal adhesions and ICD release as a non-canonical signaling pathway of aGPCRs." DFG Research Unit FOR 2149. Elucidation of Adhesion-GPCR signaling. Leipzig, Germany.

Krzysko J., Mertens A., Wolfrum U. (2019) „The adhesion GPCR VLGR1 controls Ca^{2+} homeostasis at ER-mitochondria membrane contacts." Retreat Research Unit FOR 2149. Eisenach, Germany.

Krzysko J., Güler E.B., Linnert J., Kusuluri D.K., Knapp B., Wolfrum U. (2022) „Novell insights into cellular functions of the adhesion GPCR VLGR1/ADGRV1 in cell migration, autophagy and Ca^{2+} homeostasis." Adhesion GPCR Workshop 2020/22. Copenhagen. Denmark.

Abkürzungsverzeichnis

ADGR	Adhäsions GPCR
CTF	C-terminales Fragment
DAPI	4,6-Diamidino-2-Phenylindol
DNA	Deoxyribonucleic acid
ER	Endoplasmatisches Retikulum
GFP	Green fluorescent protein
GAIN	GPCR Autoproteolysis inducing
GPCR	G-Protein gekoppelter Rezeptor
GPS	GPCR proteolysis site
HEK	Human embryonic kidney
HeLa	Henrietta Lacks
MAM	Mitochondrien-assoziierte Membran
NTF	N-terminales Fragment
PBM	PDZ- Bindemotif
RFP	Red fluorescent protein
RNA	Ribonucleic acid
RP	Retinitis Pigmentosa
TAP	Tandem Affinity Purification (Tandem-Affinitäts-Aufreinigung)
TM	Transmembran-Domäne
USH	Usher-syndrome
VLGR1	Very Large G Protein-coupled Receptor 1
WT	Wildtyp

Inhalt

1. Einleitung

Die vorliegende Arbeit beschäftigt sich im Kern mit dem Very large G protein-coupled receptor (VLGR1), einem der Unterfamilie der G-Protein gekoppelten Rezeptoren (GPCRs) zugeordneten Adhäsions-GPCR. VLGR1, auch bekannt als USH2C-Protein, ist assoziiert mit dem humanen Usher Syndrom (USH), der häufigsten erblich bedingten Form von Taub-Blindheit. Zudem führen Mutationen im *VLGR1* Gen zu einer Suszeptibilität für audiogen induzierte epileptische Anfälle bei Mäusen. Ebenfalls gibt es zunehmend Hinweise auf einen Zusammenhang von VLGR1 und Epilepsie beim Menschen. Die Validierung und Charakterisierung von VLGR1 an speziellen subzellulären Kompartimenten, den Mitochondrien-assoziierten ER-Membranen (MAMs), vertieft und erweitert das Verständnis bisher unbekannter molekularer Funktionen dieses Rezeptors und trägt zur Aufklärung dessen Pathomechanismen bei. Interaktionen von MAM-Proteinen mit VLGR1, die Lokalisation in diesem exklusiven Bereich, sowie der Einfluss von VLGR1 auf die Beschaffenheit und Funktionalität der MAMs, sind von zentraler Bedeutung für das Verständnis molekularer Mechanismen von VLGR1 zwischen Mitochondrien und ER.

1.1 Adhäsions G-Protein gekoppelter Rezeptoren

GPCRs sind in einer Protein-Superfamilie klassifiziert, die in fünf Hauptfamilie: Klasse A (Rhodopsin-Rezeptoren), Klasse B (Sekretin-Rezeptoren), Klasse C (Glutamat-Rezeptoren) Klasse E (Adhäsions-Rezeptoren) und Klasse F (Frizzled/Smoothened) aufgegliedert ist (Favara et al. 2014) (Abb. 1). Klasse D zu der die Fungal mating pheromone receptors gehören, kommen in Säugetieren nicht vor. Zu den Kernfunktionen der GPCRs zählt die Übertragung extrazellulärer Signale in die Zellen, ein für die Zellkommunikation wesentlicher Mechanismus. Ein strukturbildendes und für die Signalübertragung bedeutendes Element aller GPCRs ist eine Transmembrandomäne bestehend aus sieben α-helikalen Segmenten, die durch alternierende intra-bzw. extrazelluläre Loops verbunden sind (7TM). Intrazellulär setzt sich die Signalübertragungskaskade über heterotrimere G-Proteine fort (Rosenbaum et al. 2009), bestehen aus Gα- und Gβγ-Untereinheiten, mit einer GDP / GTP-Bindungsstelle an ihrer Alpha-Untereinheit. Nach der Aktivierung durch einen Liganden (Neurotransmitter, Hormone, Duft-/Geschmacksstoffe, Licht oder mechanische Stimulation), kommt es zu einer Konformationsänderung, welche den Austausch von GDP zu GTP (Guanosintriphosphat) beim assoziierten G-Protein zu Folge hat (Gether and Kobilka 1998, Ji et al. 1998). Dadurch dissoziieren die Gα- und Gβγ-Untereinheiten und aktivieren verschiedenen Effektoren (Hamm 1998). Der GPCRs Signalweg ist selbstterminierend, Gα hydrolysiert GTP zu GDP, was zu

einer Reassoziation der Gα- und Gβγ-Untereinheiten führt und somit der inaktive Zustand hergestellt wird.

GPCR Superfamilie

Klasse A	Klasse B	Klasse C	Klasse E	Klasse F
Rhodopsin (701)	Sekretin (15)	Glutamat (22)	Adhäsion (33)	Frizzled (11)

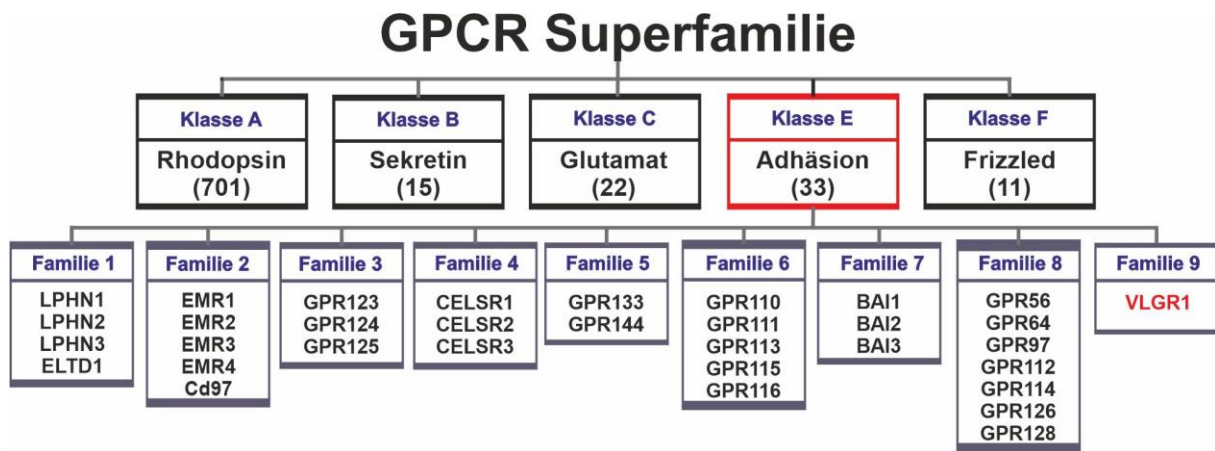| Familie 1	Familie 2	Familie 3	Familie 4	Familie 5	Familie 6	Familie 7	Familie 8	Familie 9
LPHN1 LPHN2 LPHN3 ELTD1	EMR1 EMR2 EMR3 EMR4 Cd97	GPR123 GPR124 GPR125	CELSR1 CELSR2 CELSR3	GPR133 GPR144	GPR110 GPR111 GPR113 GPR115 GPR116	BAI1 BAI2 BAI3	GPR56 GPR64 GPR97 GPR112 GPR114 GPR126 GPR128	VLGR1

Abb. 1: GPCR Klassifikation mit Fokus auf die Adhäsions-GPCRs. GPCRs lassen sich anhand der Sequenzhomologie ihrer 7 transmembran Domänen in 5 Klassen unterteilen (A, B, C, E und F). Die Klasse der Adhäsions-GPCRs umfasst 33 Rezeptoren, die sich wiederum phylogenetisch in 9 Subfamilien einteilen lassen. Rezeptoren jeder Unterfamilie sind namentlich gelistet.

Die Adhäsions-GPCRs (ADGRs) stellen innerhalb der Superfamilie der GPCRs (Klasse A 701, Klasse B 15, Klasse C 22 und Klasse F 11) mit 33 Vertretern die zweitgrößte Gruppe dar (Favara et al. 2014), die sich wiederum in 9 Subfamilien klassifizieren lässt (Abb. 1). Ältere systematische Klassifizierungen zählten ADGRs und Klasse B (Sekretin-Rezeptoren) zu einer Gruppe (Baud et al. 1995). Fundiert auf genetischen Analysen, lassen sich ADGRs jedoch zu einer eigenständigen Subfamilie zusammenfassen (Hamann et al. 2015). Ein wesentlicher Unterschied der ADGRs zu den Sekretin-Rezeptoren ist die meisten sehr große extrazelluläre N-terminale Domäne, die Zell-Zell- oder Zell-Matrix-Adhäsion generiert. Ebenfalls können ADGRs durch Kopplung von Adhäsions- und Signaleigenschaften, die Funktion von Mechanosensoren einnehmen (Luo et al. 2011, Langenhan 2020, Scholz et al. 2015). Des Weiteren besitzen ADGRs eine besondere GAIN Proteindomäne N-Terminal der Transmembranhelix. In der GAIN Domäne befindet sich die GPCR proteolytic site (GPS), an der durch autokatalytische Spaltung im Endoplasmatischen Retikulum (Lin et al. 2010) zwei funktionale Untereinheiten des Proteins resultieren. Das N-terminale Fragment (NTF) bleibt extrazellulär und das C-terminale Fragment membrangebunden (Arac et al. 2012). Beide Fragmente bleiben meistens als Dimer assoziiert, können aber auch voneinander unabhängige Signalfunktionen ausüben und sogar Heterodimere mit Fragmenten von anderen ADGRs bilden (Hu et al. 2014, Hamann et al. 2015, Knapp et al. 2019, Promel et al. 2012, Patra et al. 2013). Bemerkenswert hierbei ist die Tatsache, dass die C-terminalen Fragmente vieler ADGRs eine

höhere Rezeptoraktivität als die vollständigen Proteine aufweisen (Okajima et al. 2010, Paavola et al. 2011, Ward et al. 2011). Dabei spielen die ersten ~10 Aminosäuren des CTFs, das sogenannte *Stachel-Peptid* eine entscheidende Rolle. Nach Dissoziation oder einer Konformationsänderung des NTF, ist das *Stachel-Peptid* nicht mehr an das NTF gebunden und kann durch Bindung an die Transmembrandomäne den Rezeptor aktivieren (Abb. 2) (Liebscher et al. 2014, Demberg et al. 2015, Stoveken et al. 2015, Wilde et al. 2016). Somit unterdrückt das NTF die Rezeptoraktivität (Paavola et al. 2011), indem es die *Stachel*-Sequenz vor der Abspaltung maskiert. Somit wird der *Stachel* auch als „angebundener" Agonist (tethered agonist) definiert. Eine weitere Hypothese zur Aktivierung von ADGRs, bezieht sich auf mögliche mechanosensorischen Funktionen der Rezeptoren, nach dem diese als Mechanorezeptoren wirken könnten (Luo et al. 2011, Karpus et al. 2013, Scholz et al. 2016).
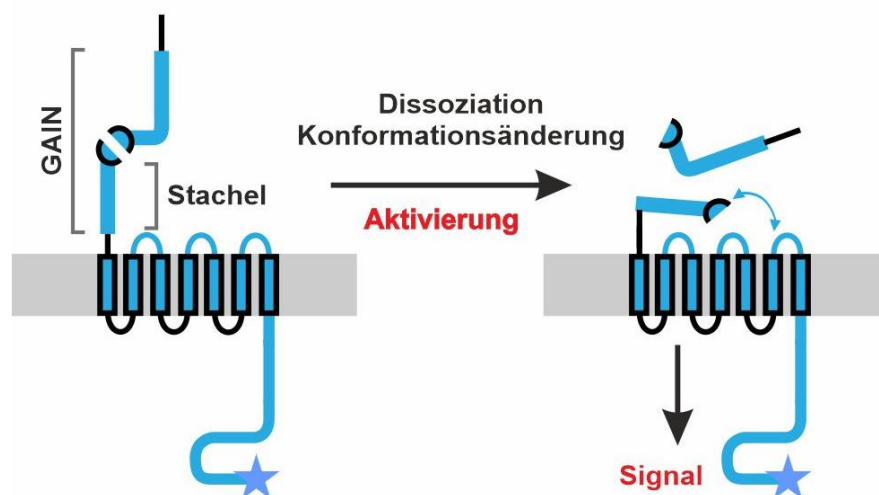

Abb. 2: Aktivierungsmechanismus von Adhäsions-GPCRs mittels Stachel-Peptid. Dissoziation oder Konformationsänderung des NTFs, führt zu einer Abspaltung an der GAIN-Domäne. Dadurch kann das Stachel-Peptid an die Transmembranhelix binden und den Rezeptors aktivieren.

ADGRs stehen mit zahlreichen Krankheiten in Verbindung, jedoch stellen dieses bislang keine Zielmoleküle für therapeutische Ansätze dar (Bassilana et al. 2019). Dies liegt am fehlenden Wissen und Verständnis über/für die Funktionen, die Signalwege, die Interaktionspartner und die übergeordneten Proteinnetzwerke (Knapp and Wolfrum 2016). So entwickelt und steigert sich über die letzten Jahre das Interesse an der Erforschung von ADGRs enorm. Bisherige Daten zeigen, dass einige ADGRs an der Aktivierung der Rho-GTPasen Rho, CDC42 oder

Rac1 beteiligt sind und zudem in Wnt/PCP-Signalwegen eine Rolle spielen (Hamann et al. 2015, Knapp and Wolfrum 2016, Knapp et al. 2019). Auch konnten Interaktionen mit Gerüstproteinen gezeigt werden, die auf Modellierung von Rezeptoraktivität hindeuten (Stephenson et al. 2013, Hu et al. 2014). Jedoch bleibt im Feld der ADGRs noch Vieles zu erforschen. Um den Kenntnisstand zu erweitern und ein genaueres Bild zu erhalten, sind besonders die Identifizierung, Charakterisierung und Validierung von Liganden und Interaktionspartnern von ADGRs von Bedeutung.

1. 2 Der Very Large G protein-coupled Receptor 1 (VLGR1)

Der very large G protein coupled receptor 1 (VLGR1), auch GPR98, ADGRV1 oder MASS1 bezeichnet, ist das Produkt des *GPR98* (*USH2C*) Gens und gehört zur Proteinunterfamilie der Adhäsions-G-Protein gekoppelten Rezeptoren (ADGRs) (McMillan and White 2010, Hamann et al. 2015). Wobei die die Abkürzung ADGRV1 die aktuelle gültige nach der aGPCR Nomenklatur darstellt (Hamann et al. 2015). In den meisten Publikationen wird jedoch, die dem eigentlichen Namen des Rezeptors nahliegende Form, VLGR1 verwendet. Diese wird auch in dieser Arbeit und den dazugehörenden Publikationen benutzt. Das Gen umfasst über 600 kb und codiert 90 Exons, die längste Isoform VLGR1b besteht aus 6306 Aminosäuren mit einem Molekulargewicht von ~ 730 kDa. VLGR1 ist der größte bekannte GPCR und bildet innerhalb der Unterfamilie der ADGRs eine eigene Gruppe (Hamann and Petrenko 2016, McMillan et al. 2002). Strukturelle Besonderheiten des Proteins, sind die sehr lange extrazelluläre Domäne mit 35 Calx-beta (Calxβ) Domänen, sowie Epilepsie-assoziierte Regionen bestehend aus sieben Epitempin Wiederholungssequenzen (EPTP/EAR) und einer Laminin G (LamG)/Pentraxin (PTX) Domäne. N-terminal der sieben Transmembrandomäne (7TM) befindet sich die GPCR autoproteolysis-inducing (GAIN) Domäne, in welcher eine GPCR proteolytic site (GPS) lokalisiert ist. Am intrazellulären C-Terminus befindet sich eine PDZ binding motif (PBM) (McMillan and White 2010). Neben VLGR1b der „full-lenght" Form des Proteins, sind 8 weitere Isoformen beschrieben (Skradski et al. 2001, Nikkila et al. 2000, McMillan and White 2004, Yagi et al. 2009) welche Spleiß-Varianten der b Isoform Form sind (Abb. 3). VLGR1a ist die einzige bekannte Isoform, die neben VLGR1b eine 7TM und eine intrazelluläre Domäne aufweist und somit auch als GPCR fungieren kann. Die Isoformen VLGR1c-e bestehen aus unterschiedlichen großen Teilen des nativen N-Terminus von VLGR1b und besitzen somit ein Signalpeptid zur Sekretion aus den Zellen. Drei weitere Isoformen MASS1.1, MASS1.2 and MASS1.3 sind ebenfalls Fragmente der N-terminalen Domäne, jedoch ohne hydrophobes Signalpeptid, weshalb diese wahrscheinlich intrazellulär lokalisiert sind. Die Expressionslevel

einiger Isoformen sind sehr gering, so wird MASS1.1 nur zu unter 1% von VLGR1b exprimiert, was die Relevanz verschiedener Isoformen in Frage stellt (Yagi et al. 2005). Neben den beschriebenen Isoformen, stehen weitere Varianten in Diskussion. VLGR1f-1h, VLGR1j und VLGR1o wurden mittels der RACE (rapid amplification of cDNA-ends) Methode identifiziert, jedoch noch nicht validiert, weshalb diese nur als mögliche Isoformen klassifiziert werden.
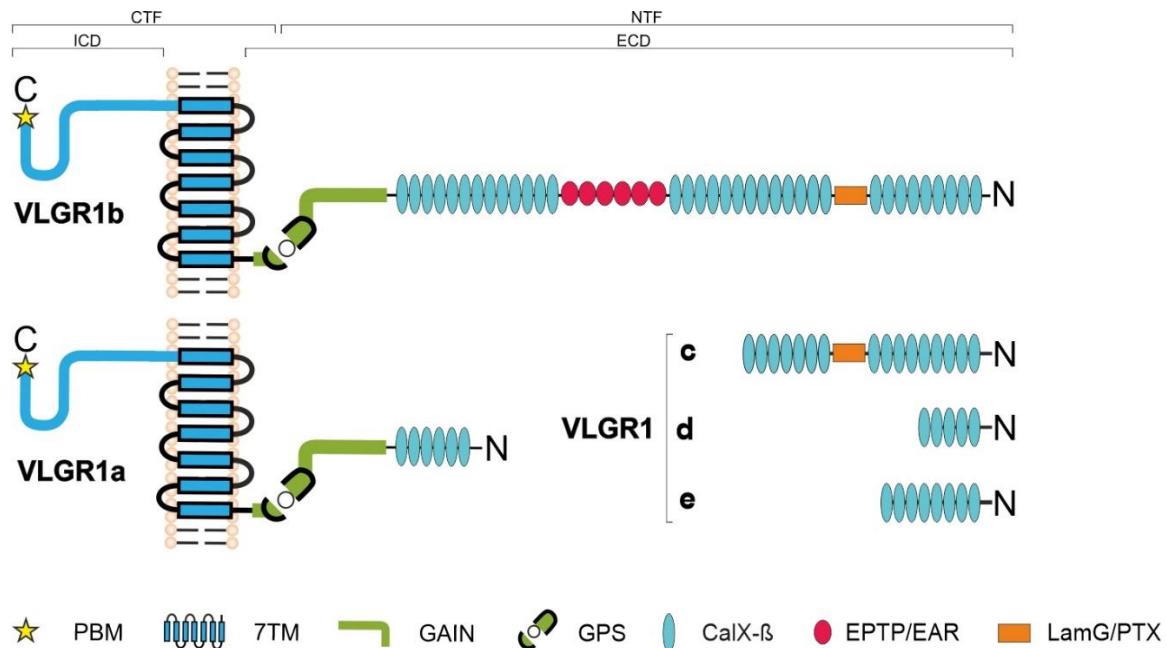

Abb. 3: Proteinstruktur der VLGR1-Isoformen a-e. VLGR1b ist die "full-length" Isoform mit PDZ-binding motif (PBM), 7 transmembrane domain (7TM), GPCR autoproteolysis inducing domain (GAIN), GPCR proteolytic site (GPS), 7 epilepsy associated repeats (EAR), calcium-binding motifs (Calx-β) und Laminin G(LamG)/Pentraxin(PTX) domain. Durch Autoprotolyse am GPS entsteht ein C-terminales Fragment (CTF) und N-terminales Fragment (NTF). ICD = intracellular domain. ECD = extracellular domain. Domänen Größenverhältnis: CTF-NTF 1:15.

1.3 VLGR1 im humane Usher-Syndrom und anderen Krankheiten

Mutationen im *VLGR1* Gen, führen zur Entwicklung schwerer Krankheiten bei Menschen und ausgeprägter Phänotypen bei Mausmodellen. Zurzeit sind über 40 pathogene humane Mutation in *VLGR1* identifiziert, die sich über die gesamte Spanne der Gensequenz erstrecken (https://databases.lovd.nl/shared/ genes/GPR98). Zusammenhänge von Epilepsie und Mutationen im *VLGR1* Gen wurden ebenso beschrieben (Nakayama et al. 2002, Wang et al. 2015a, Zhou et al. 2016, Myers et al. 2018, Han et al. 2020, Dahawi et al. 2021 Liu et al. 2022) , wie Hinweise auf die Struktur von Knochengewebe und Osteoporose (Urano et al. 2012). VLGR1 wird ubiquitäre exprimiert, jedoch unterliegt die Expression temporären und lokalen Regulationen. In zahlreichen adulten Gewebe ist VLGR1 zu finden, auch wenn in geringen

Konzentrationen (Nikkila et al. 2000, Skradski et al. 2001, McMillan et al. 2002, McGee et al. 2006, Michalski et al. 2007). Hohe Expressionslevel lassen sich im Gehirn, Retina und Cochlea detektieren (Reiners et al. 2005, van Wijk et al. 2006, Maerker et al. 2008, Shin et al. 2013).

Obwohl ein direkter funktioneller Kontext mit Epilepsien noch nicht gezeigt wurde, konnte nachgewiesen werden, dass VLGR1 sowohl in Oligodendrozyten stark exprimiert wird, als auch bei der Erhaltung der Myelin-Scheiden von Bedeutung ist, indem VLGR1 stabilisierenden Einfluss auf das Myelin-assoziierte Glykoprotein (MAG) nimmt (Shin et al. 2013). Zusätzlich legen Expressionsanalysen eine Beteiligung von VLGR1 in der Entwicklung des zentralen Nervensystems nahe (McMillan and White 2010). Interessanterweise neigen Mausmodelle mit einer *Vlgr1*-Mutation (u.a. del7TM Mäuse) zu audiogen induzierbaren epileptischen Anfällen (Skradski et al. 2001, McMillan and White 2004, Yagi et al. 2005). Dieser ausgeprägte Phänotyp macht die Mausmodelle zu geeigneten Objekten, die molekularen Grundlagen der Rolle von VLGR1 auf die Entwicklung neuronaler Defekte zu untersuchen.

Die bislang prominenteste Rolle von VLGR1, ist die in der Genese des humanen Usher Syndroms (USH). Es ist eines von 10 identifizierten Genen, deren Fehlfunktionen diese heterogenen autosomal-rezessiv vererbte Krankheit verursachen. USH ist mit einer Prävalenz von 1:10.000 (Hope et al. 1997) bis 1:6.000 (Kimberling et al. 2010), die häufigste Form von erblich bedingter Taub-Blindheit (Bonnet et al. 2016), welche auch Störungen des vestibulären Systems beinhalten kann. Diese progrediente Krankheit ist charakterisiert durch eine progressive Degeneration der Retina (*Retinitis Pigmentosa*), kombiniert mit einer gestörten Entwicklung von Haarsinneszellen im Innenohr. Es werden drei klinische Subtypen des USH klassifiziert: USH1, USH2 und USH3 (Tabelle 1.). Zur Einstufung werden Kriterien wie Alter bei Krankheitsbeginn, der zeitliche Verlauf, sowie die Schwere der Symptome herangezogen. USH1 ist die schwerwiegendste Form und zeichnet sich durch ausgeprägte Hörschäden aus, die entweder kongenital oder frühkindlich auftreten (Kimberling and Moller 1995). RP und vestibuläre Störungen treten schon präpubertär auf und sind fortschreitend (Petit 2001). Die häufigste Form ist USH2, welche 56-67% der Fälle darstellt und sich im Wesentlichen von USH1 durch einen späteren Beginn der RP (während oder postpubertär), mildere Beeinträchtigungen des Hörvermögens (besonders bei hohen Frequenzen) und einen intakten Gleichgewichtssinn differenzieren lässt (Ebermann et al. 2009). Mutationen von *VLGR1 (USH2C)* bedingen dabei 3-8% der USH2 Erkrankungen (Millan et al. 2011, Bonnet et al. 2016). Die seltenste und mildeste Form ist USH3. Etwa 50% der USH3 Fälle wurden aus Finnland berichtet. Hörbeeinträchtigungen treten bei dieser Form frühstens im fortgeschrittenen

Kindesalter auf und auch RP und Gleichgewichtsstörungen entwickeln sich im Erwachsenenalter (Pakarinen et al. 1995).

Neben den klinischen Unterschieden ist auch die genetische Heterogenität von USH bemerkenswert. Obwohl bisher 10 Gene identifiziert wurden, deren Mutationen USH hervorrufen (Tabelle 1.), sind die zugrundeliegenden molekularen Mechanismen der Krankheit unzureichend bekannt.

Tabelle 1: USH-Formen und identifizierte USH Gene. Das im Fokus dieser Arbeit steht der USH2C Subtyp, der von Defkten im *ADGRV1* Gen das VLGR1/ADGRV1 Protein kodiert (umrahmt). PDZ = PDZ-Domäne. GPCR = G protein coupled receptor.

Typ	Locus	Gen	Protein	Funktion	Referenz
USH1B	11q13.5	*MYO7A*	Myosin VIIa	Motorprotein	Weil *et al.*, 1995
USH1C	11p14-15.1	*USH1C*	Harmonin	PDZ-Gerüstprotein	Smith *et al.*, 1992
USH1D	10q22.1	*CDH23*	Cadherin 23	Zell-Zell Adhäsion, Transmembran-protein	Bolz *et al.*, 2001
USH1E	21q21	-	-	-	-
USH1F	10q21.1	*PCDH15*	Protocadherin 15	Zell-Zell Adhäsion, Transmembran-protein	Alagramam *et al.*, 2001
USH1G	17q25.1	*USH1G*	SANS	Gerüstprotein	Weil *et al.*, 2003
USH1H	15q22-q23	-	-	-	-
USH1J	15q25.1	*CIB2*	CIB2	Calcium Homeostasis	Riazuddin *et al.*, 2012
USH1K	10p11.21-q21.1	-	-	-	-
USH2A	1q41	*USH2A*	USH2a/Usherin	Transmembran-protein	Eudy *et al.*, 1998
USH2C	5q13	*ADGRV1*	VLGR1/ADGRV1	Adhesion-GPCR, Transmembrane-protein	Johnson *et al.*, 2005
USH2D	9q32	*DFNB31*	Whirlin	PDZ-Gerüstprotein	Ebermann *et al.*, 2007
USH3A	3q25	*CLRN1*	Clarin 1	4-Transmembran-protein, Zell Adhäsion	Adato *et al.*, 2002

Die aus den USH Genen resultierende Proteine gehören unterschiedlichen Proteinfamilien an und variieren in ihren Funktionen, jedoch bilden sie das sogenannte USH-Protein-Netzwerk (Usher-Interaktom) (Adato et al. 2005, Reiners et al. 2005, Wolfrum 2011). Das Resultat von

identischen Phänotypen, hervorgerufen von Fehlfunktionen strukturell unterschiedlicher Proteine, lässt sich mit der Integration dieser Proteine in ein funktionelles Netzwerk erklären, dessen korrekte Ausbildung und Funktion von den Interaktionen der einzelnen Proteine untereinander abhängt. USH-Proteine und insbesondere VLGR1 stehen neben USH in Verbindung mit zahlreichen anderen Proteinen und Zellkompartimenten und repräsentieren somit ein vielversprechendes und interessantes Arbeitsfeld für die Erforschung pathogener Mechanismen neben dem USH (Knapp et al. 2019).

1.4 Mitochondrien-assoziierten ER-Membranen (MAMs)

Um die Entstehung und Entwicklung, der von VLGR1-Fehlfunktionen bedingten Krankheiten besser zu verstehen, ist die Lokalisation der Prozesse innerhalb der Zelle entscheidend. Im Zuge dieser Arbeit, ergaben sich Hinweise auf eine Assoziation von VLGR1 an den Mitochondrien-assoziierten ER-Membranen (MAMs). Die MAMs stellen spezielle subzelluläre Kompartimente dar, welche sich aus Membranen des Endoplasmatischen Retikulums (ER) und den äußeren Mitochondrienmembranen dynamisch und reversibel bilden. Definiert wird dieses Kompartiment als Kontaktstelle zwischen ER und Mitochondrien mit einem Abstand von 10-80 nm. Diese Schnittstelle zwischen den beiden Organellen, wird durch bestimmte Ankerproteine „tethers" und Protein-Protein-Interaktion, für diesen Bereich charakteristischer Proteinen definiert. Generell können MAMs als eine besonders wichtige Plattform für zahlreiche biochemische Prozesse in eukaryotischen Zellen beschrieben werden (Giacomello and Pellegrini 2016).

Fehlfunktionen an MAMs beziehungsweise von an MAMs beteiligten Proteinen stehen oft in Verbindung mit neurodegenerativen Krankheiten wie Alzheimer und Stoffwechselstörungen wie Diabetes (Lee et al. 2018, Paupe and Prudent 2018). So existieren zahlreiche Hypothesen, welche den MAMs eine Rolle an den molekularen Prozessen die Alzheimer zugrunde liegen, zusprechen. Die β-Amyloid Theorie, ist ein Ansatz zur Erklärung der Bildung und Akkumulation von extrazellulären Plaques in Gehirn von Alzheimer Patienten. Dabei spielt die Spaltung des Amyloid-precursor Proteins (APP) durch die γ-Sekretase eine zentrale Rolle (Pimplikar 2009). Es konnte gezeigt werden, dass beide katalytischen Untereinheiten der γ-Sekretase, Präsinilin 1 & 2 (PSEN1, PSEN2) an den MAMs angereichert sind (Area-Gomez et al. 2009, Knapp et al. 2019). Eine veränderte Ca^{2+}-Homöostase, erhöhte Cholesterol Spiegel sowie Phospholipid-Synthese, sind weitere Eigenschaften, die bei der Alzheimer-Krankheit auftreten und deren molekularer Hintergrund eng mit MAMs assoziiert ist. Diese Indikatoren stützen die sogenannte „MAM-Hypothese" in Bezug auf die Alzheimer-Krankheit, im

Speziellen, dass beeinträchtigte MAM-Funktionen zu einer gestörten Kommunikation von ER und Mitochondrien führen und dies, die Ursache für die Entwicklung der Krankheit darstellt (Schon and Area-Gomez 2013, Area-Gomez et al. 2009).

MAMs besitzen zum Teil die Charakteristik von *lipid rafts* (Lipidflöße). Dies sind spezielle Membrandomänen, die sich durch einen relativ hohen Gehalt an Sphingomyelinen, Glycosphingolipiden und Cholesterin auszeichnen und sich als flüssigkristalline Phasenstruktur in der Zellmembran einordnen (Hayashi and Fujimoto 2010, Area-Gomez et al. 2012, Annunziata et al. 2018). Lipid Rafts dienen als Plattformen in der Zellmembran für die Integration und Sortierung bestimmter Proteine und sind so wesentlich an der Kompartimentierung beteiligt (Lingwood and Simons 2010). Aufgrund ihrer relativen Stabilität gegenüber Detergenzien wie Tensiden, werden *lipid rafts* auch als *detergent-resistant membranes* (DRMs) bezeichnet und lassen sich mithilfe dieser isolieren (Simons and Vaz 2004, Area-Gomez et al. 2012).

Untersuchungen deuten darauf hin, dass das spezielle Zellkompartiment der MAMs, eine Schlüsselfunktione in verschiedenen zellulären Mechanismen einnimmt. Darunter sind die Ca^{2+}-Homöostase, Lipidsynthese- und Umbau, Regulation der mitochondrialen Morphologie und die Autophagozytose (Hamasaki et al. 2013, Ilacqua et al. 2017). Lipid- und Phospholipidsynthese sind die ersten Mechanismen, die den MAMs zugeordnet wurden (Vance 2014). Weiter Untersuchungen konnten die Umwandlungskaskaden aufschlüsseln und zeigten, dass diese Prozesse stark an die Kontaktstellen zwischen ER und Mitochondrien gekoppelt sind und legen ein Zusammenspiel von Proteinkomplexen nahe, welches den Lipidtransfer an den MAMs bewerkstelligt (Vance 2014, De Mario et al. 2017).

Von zentraler Bedeutung für die Signalübermittlung und Bioenergetik in Zellen ist Ca^{2+} (Hayashi and Su 2007). Es wird durch einen Brückenkomplex aus dem Inositol triphosphate receptor (IP3R, am ER) und dem Voltage dependent anion channels (VDAC, Mitochondrienmembran) vom ER in die Mitochondrien transferiert. Vermutlich sind auch weiteren Proteinen wie GPR75 und der Sigma-1-Rezeptor an diesem Vorgang beteiligt (Hedskog et al. 2013, Ilacqua et al. 2017).

Im Grunde bieten MAMs ebenso eine Ebene für (unter anderen) Proteine und Mechanismen der Lipid- und Ca^{2+}-Homöostase oder Autophagie und werden aber auch durch diese definiert. Eine Veranschaulichung dieser Struktur ist in Abbildung 4 illustriert, welche mitunter putative und validierte Interaktionspartner von VLGR1 beinhaltet.
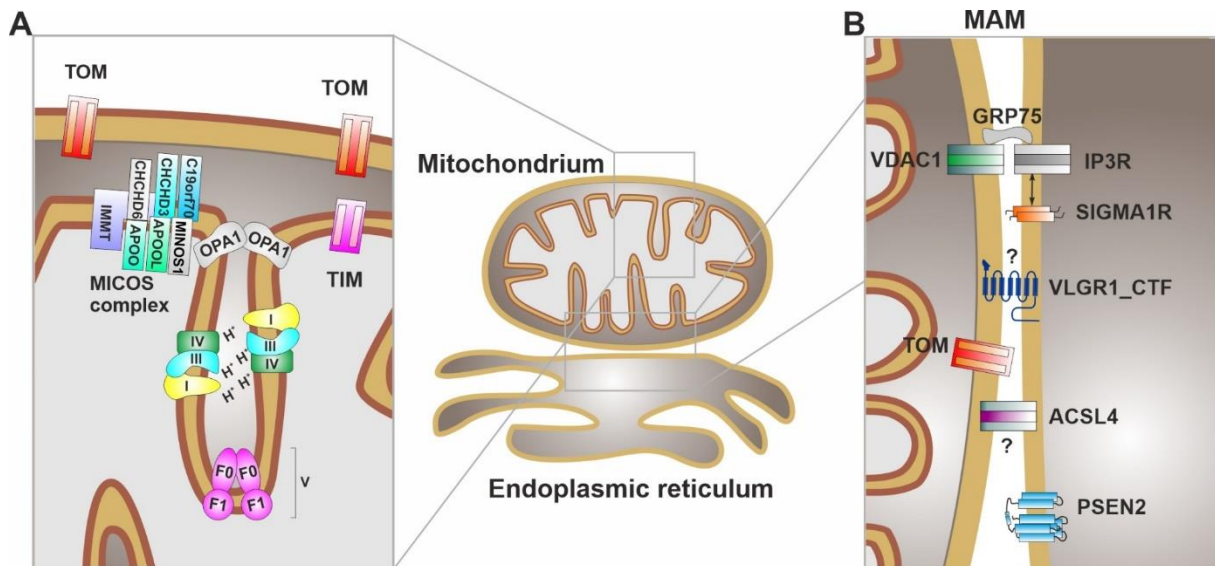
Abb. 4: Schematische Übersicht der MAMs mit in VLGR1_CTF TAPs identifizierten Proteinen. (A) VLGR1_CTF ist assoziiert mit dem mitochondrialen Protein-Komplex der Atmungskette (complex I, III, IV, V), MICOS komplex und Translokasen der inneren und äußeren Mitochondrienmembran (TIM, TOM). (B) VLGR1_CTF ist assoziiert mit verschiedenen Proteinen der Mitochondrien-assoziierten ER Membranen (MAMs): VDAC1, SIGMA1R, ACSL4 und Komponenten des γ-Sekretase-Komplex (PSEN1, PSEN2). Proteine, die in TAPs identifiziert wurden sind farbig gestaltet, andere sind in grau gehalten. Abbildung wurde modifiziert nach Knapp et al., 2019.

1.5 Zielsetzung der Arbeit

VLGR1 ist der größte bekannte Adhäsions-GPCR und eines von 10 Genen (USH2C), deren Mutationen das Humane Usher Syndrom (USH), die häufigste Form erblicher Taub-Blindheit hervorrufen. Erkenntnisse über die molekulare Funktion und die Signalwege dieses Rezeptors, sind essentiell für das Verständnis der Pathogenese von USH und andere Krankheiten, in denen VLGR1 beteiligt ist. VLGR1 ist ein sehr komplexes Protein mit unterschiedlichen Domänenstrukturen, die auf verschiedene Funktionen dieses Moleküls hinweisen und somit interessante Felder zu Erforschung dieses aGPCRs bieten. Um Aufschluss über die Beteiligung von VLGR1 in bestimmten zellulären Prozessen zu erhalten, ist es nötig, seine Interaktionspartner und Lokalisation zu ermitteln. Um die Relevanz von VLGR1 auf diese Prozesse zu definieren, sind gut etablierte VLGR1-Modelle unabdingbar. Diese schaffen die Grundlagen für funktionelle Studien und tragen bei der Erforschung des Potentials dieses besonderen Rezeptors eine tragende Rolle.

Somit ergaben sich für die folgenden Ziele, die in den jeweiligen Forschungsarbeiten zu VLGR1 formuliert wurden:

(1) **Identifizierung von Interaktionspartner von VLGR1, die Hinweise auf die Beteiligung von VLGR1 in Zellmodulen liefern**

(2) **Etablierung primäre Astrozyten als zelluläres Model für Vlgr1-Defekte**

(3) **Validierung und Charakterisierung der Rolle von VLGR1 an Mitochondrien-assoziierten ER-Membranen**

Zu (1) Identifizierung von Interaktionspartner von VLGR1 und deren Beteiligung an zellulären Prozessen

Als Grundlage für die Erforschung noch nicht bekannter Funktionen von VLGR1 auf molekularer und zellulärer Ebene, dienten Protein-Interaktions-Analysen wie die Tandem-Affinitäts-Aufreinigungen (TAPs). Mittels der TAPs, die mit verschiedenen Fragmenten von VLGR1 durchgeführt wurden, sollten putative Interaktionspartner identifizierte werden. In Kombination mit Massenspektrometrie (Gloeckner et al. 2007, Boldt et al. 2016) und anschließender bioinformatischen Auswertungen wurden Modele von VLGR1-Proteinnetzwerken erstellt werden. Diese Proteomdaten zeigten neue Ansätze für die Beteiligung von VLGR1 in verschiedenen biologischen Prozessen auf (**Publikation I und II**).

Zu (2) Etablierung von VLGR1-defizienten Zelllinien basierend auf Maus Modellen

Um die Relevanz, also den Einfluss und Beteiligung, von Proteinen auf molekulare Prozesse zu definieren und zu beurteilen, sind robuste *in vitro* Modele von großer Bedeutung. Primäre Astrozyten gewinnen immer mehr Aufmerksamkeit als wichtige und nützliche Modelle zu Erforschung biologischer und biochemischer Prozesse. Ausgehend von zwei VLGR-defizienten Mausmodellen: *Vlgr1*/del7TM und *Drum B* (Potter et al. 2016), sollte eine effektive Isolationsmethode etabliert werden, welche die Kultivierung von primären murinen Astrozyten, zur Analysezwecken gewährleistet (**Publikation III**).

Zu (3) Validierung und Charakterisierung von VLGR1 an Mitochondrien-assoziierten ER Membranen

Die Analyse der VLGR1-Proteinnetzwerke, in Hinblick auf ihre Beteiligung in biologische und molekulare Prozesse, sowie der zellulären Komponenten, zeigt u.a., dass VLGR1 mit vielen Proteinen interagiert, die im ER bzw. Mitochondrien lokalisiert sind. Signifikant für VLGR1 wurden viele Proteine identifiziert, die hauptsächlich mit Mitochondrien-assoziierten ER-

Membranen (MAMs) assoziiert sind, was neue, bisher nicht bekannte Funktionen von VLGR1 impliziert. Eine Beteiligung von VLGR1 in den MAMs, sollte durch die Validierung direkter Interaktionen zu MAM-Schlüsselproteinen, die Lokalisation in diesem subzellulären Kompartiment sowie durch Präsenz von VLGR1 in isolierten MAM-Fraktionen bestätigt werden. Weiter sollte die Rolle von VLGR1 in den MAMs näher beschrieben werden, indem die Komposition der MAMs in den relevanten Organen von VLGR1-defizienten Mausmodellen analysiert wurde. Für eine funktionelle Analyse von VLGR1 an den MAMs sollte der Ca^{2+}-Fluss von ER und Mitochondrien untersucht werden. (**Publikation IV**).

2. Publikationen

Publikation I

Knapp B, Roedig J, Boldt K, Krzysko J, Horn N, Ueffing M and Wolfrum U (2019). **Affinity proteomics identifies novel functional modules related to adhesion GPCRs.** Ann N Y Acad Sci 1456(1): 144-167.

Publikation II

Knapp B, Roeding J, Roeding H, Krzysko J, Horn N, Güler E.G, Kusuluri D.K, Yildirim A, Boldt K, Ueffing M, Liebscher I and Wolfrum U (2022). **Affinity Proteomics Identifies Interaction Partners and Defines Novel Insights into the Function of the Adhesion GPCR VLGR1/ADGRV1.** Molecules 2022, 27(10), 3108.

Publikation III

Güler B, Krzysko J and Wolfrum U. (2021). **Isolation and Culturing of Primary Astrocytes of Mouse Models for the Analysis of Focal Adhesion Dynamics**

Publikation IV

Krzysko J, Maciag F, Mertens A, Güler B, Linnert J, Knapp B, Boldt K, Ueffing M, Nagel-Wolfrum K, Heine M, Wolfrum U (2022). **The Adhesion GPCR VLGR1/ADGRV1 Regulates the Ca^{2+} Homeostasis at Mitochondria-Associated ER Membranes**. Cells 2022, 11, 2790. https://doi.org/10.3390/11182790

Publikation I

ANNALS OF THE NEW YORK ACADEMY OF SCIENCES
ORIGINAL ARTICLE

Affinity proteomics identifies novel functional modules related to adhesion GPCRs

Barbara Knapp,[1] Jens Roedig,[1] Karsten Boldt,[2] Jacek Krzysko,[1] Nicola Horn,[2] Marius Ueffing,[2] and Uwe Wolfrum[1]

[1]Institute of Molecular Physiology, Molecular Cell Biology, Johannes Gutenberg University of Mainz, Mainz, Germany.
[2]Institute for Ophthalmic Research and Medical Bioanalytics, Centre for Ophthalmology, Eberhard-Karls University Tübingen, Tübingen, Germany

Address for correspondence: Prof. Dr. Uwe Wolfrum, Institute of Molecular Physiology, Molecular Cell Biology, Johannes Gutenberg University of Mainz, J.J. Becherweg 7, 55099 Mainz, Germany. wolfrum@uni-mainz.de

Adhesion G protein–coupled receptors (ADGRs) have recently become a target of intense research. Their unique protein structure, which consists of a G protein–coupled receptor combined with long adhesive extracellular domains, suggests a dual role in cell signaling and adhesion. Despite considerable progress in the understanding of ADGR signaling over the past years, the knowledge about ADGR protein networks is still limited. For most receptors, only a few interaction partners are known thus far. We aimed to identify novel ADGR-interacting partners to shed light on cellular protein networks that rely on ADGR function. For this, we applied affinity proteomics, utilizing tandem affinity purifications combined with mass spectrometry. Analysis of the acquired proteomics data provides evidence that ADGRs not only have functional roles at synapses but also at intracellular membranes, namely at the endoplasmic reticulum, the Golgi apparatus, mitochondria, and mitochondria-associated membranes (MAMs). Specifically, we found an association of ADGRs with several scaffold proteins of the membrane-associated guanylate kinases family, elementary units of the γ-secretase complex, the outer/inner mitochondrial membrane, MAMs, and regulators of the Wnt signaling pathways. Furthermore, the nuclear localization of ADGR domains together with their physical interaction with nuclear proteins and several transcription factors suggests a role of ADGRs in gene regulation.

Keywords: G protein–coupled receptors; aGPCR; ADGR; synaptic scaffold proteins; mitochondria-associated membranes; gamma-secretase; Wnt signaling

Introduction

Over the last two decades, the adhesion G protein–coupled receptor (aGPCR or ADGR) protein family and their functional roles in cell adhesion and signaling have received increasing attention.[1] The ADGR protein family comprises 33 members, characterized by a unique protein structure composed of a large extracellular domain with adhesive function and a seven transmembrane (7TM) moiety that resembles G protein–coupled receptors (GPCRs) of the secretin family. According to the molecular signature of their 7TM domains, the 33 human AGPRs are categorized into nine distinct subfamilies (I–IX).[2]

A characteristic feature of ADGRs is their ability to undergo autocleavage at the G protein–coupled receptor proteolytic site (GPS), which is located near the first transmembrane domain and embedded in the GPCR autoproteolysis-inducing (GAIN) domain (Fig. 1A).[3] ADGR autocleavage results in an N-terminal fragment (NTF) and a C-terminal fragment (CTF) that usually stay associated as a dimer.[4] However, there is increasing evidence that the NTF and CTF can act independently.[5,6] Many CTFs show increased activation compared with the full-length receptor when overexpressed in cellular systems[7–10] and it has been presumed that the signaling function of ADGRs is regulated by their NTFs.[3,11,12] More
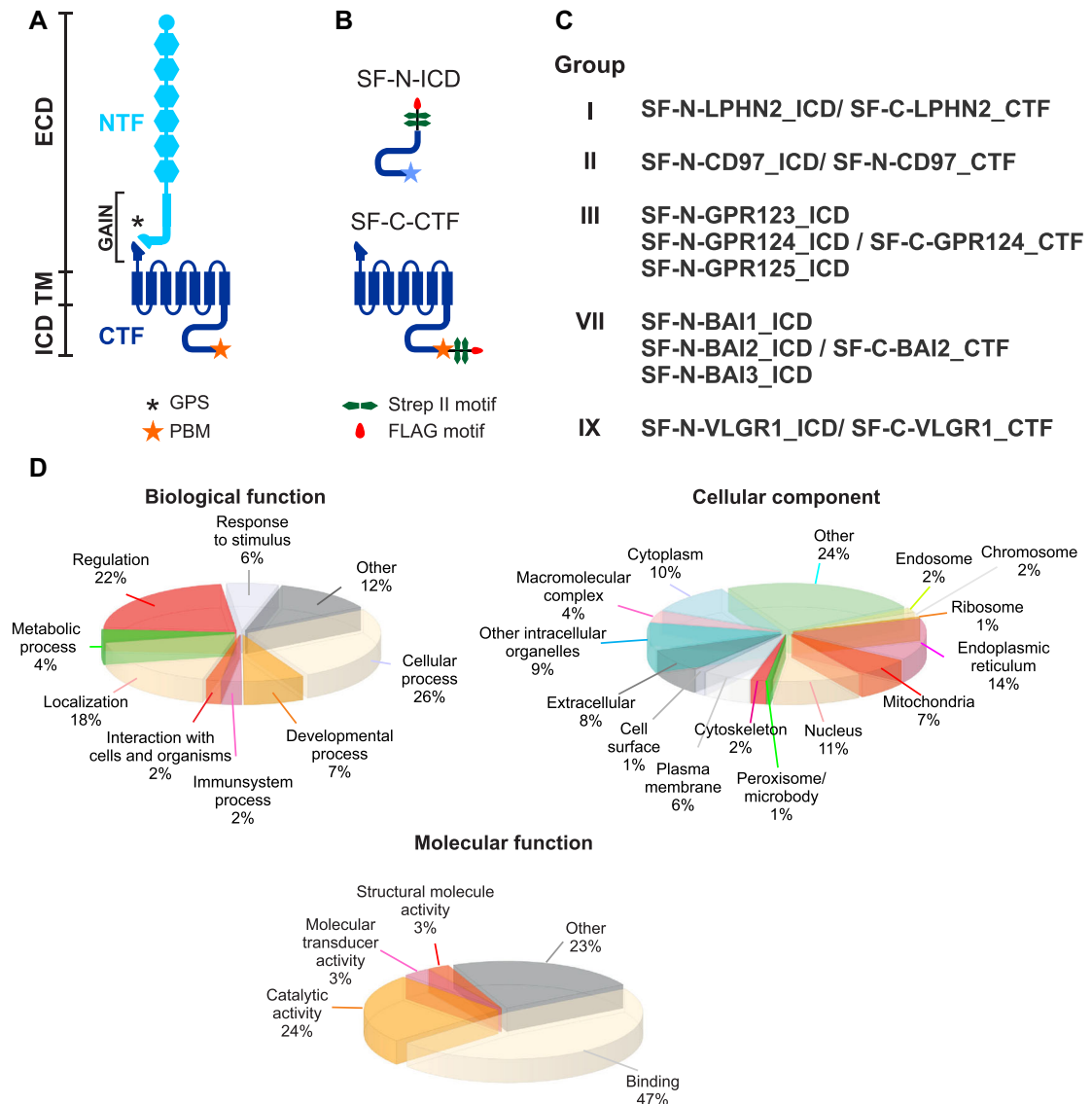
Figure 1. ADGR protein domain structure and TAP constructs and GO term analysis of TAP data. (A) General protein structure of ADGRs. (B) Schematic representation of ADGR protein fragments that were fused to a STREP II-FLAG tag. (C) ADGR fragments that were used in the TAPs. ICD, intracellular domain; TM, transmembrane domain; ECD, extracellular domain; GAIN, G protein–coupled receptor autoproteolysis-inducing domain; CTF, C-terminal fragment; NTF, N-terminal fragment; GPS, GPCR proteolytic site; PBM, PDZ-binding motif. (D) GO term analysis for ADGR TAP preys. TAP preys that are included in all ADGR_CTF datasets were grouped according to assigned GO terms using STRAP.[25] ADGR preys are mainly involved in cellular processes and regulation. They predominantly localize to the endoplasmic reticulum, nucleus, and mitochondria. The prevalent molecular functions are binding and catalytic activity.

recently, it has been demonstrated that the first ∼5–10 amino acids of the CTF, called *Stachel*, mediate the activation of ADGRs upon NTF removal or conformational change.[13,14] However, there is also evidence for *Stachel*-independent signaling that requires alternative, more complex activation.[15,16]

Despite considerable progress in ADGR research, many functions of these unique receptors and their underlying molecular mechanisms remain largely elusive. The elucidation of ADGR function is hampered by the lack of known ligands and intracellular interaction partners.[17]

Identification of such interacting partners should provide a more comprehensive view of ADGR functions in defined cellular modules. In the present study, we used a powerful affinity proteomics approach to identify physically interacting partners and protein complexes of nine ADGRs from five different ADGR groups, namely LPHN2 (ADGRL2, group I), CD97 (ADGRE5, group II), GPR123 (ADGRA1, group III), GPR124 (ADGRA2, group III), GPR125 (ADGRA3, group III), BAI1 (ADGRB1, group VI), BAI2 (ADGRB2, group VI), BAI3 (ADGRB3, group VI), and VLGR1 (ADGRV1, group IX). To identify proteins and protein complexes interacting with the cellular parts of the ADGR, we tagged the intracellular domain (ICD) or CTF of the ADGRs with the Strep II/FLAG tandem affinity purification (SF-TAP) tag and expressed the SF-tagged proteins in HEK 293T cells. We subsequently performed tandem affinity purification (TAP) to isolate ADGR-associated complexes close to their native functional state from cell lysates.[18] Subsequently, the content of purified protein complexes was analyzed by liquid chromatography coupled with tandem mass spectrometry (LC–MS/MS). Analysis of the identified complex components revealed novel intracellular ADGR interaction partners, including synaptic scaffold proteins, nuclear proteins, and regulatory phosphatases. In addition, we determined for the first time the association of ADGRs with intracellular membrane networks associated with the endoplasmic reticulum (ER), the Golgi apparatus, and mitochondria. Specifically, we identified the subunits of the γ-secretase complex as a common interaction partner for VLGR1, CD97, LPHN2, and GPR124. A large overlap in the interactomes of VLGR1, CD97, and LPHN2 indicates a common joint protein interactome. Moreover, their nuclear localization paired with their physical interaction with nuclear proteins and several transcription factors suggest an unexpected role of ADGRs in gene regulation.

Materials and methods

Plasmids

Plasmids used for TAP were coding for the Strep II-FLAG (SF)-tagged versions of the following proteins: hsVLGR1 (Uniprot ID Q8WXG9-1) a.a. 6155–6306 (ICD) and a.a. 5891–6306 (CTF); hsCD97 (P48960-1) a.a. 789–835 (ICD) and a.a. 531–835 (CTF); mGPR123 (Q52KJ6-1) a.a. 202–469 (ICD); mGPR124 (Q91ZV8-1) a.a. 1066–1336 (ICD) and a.a. 745–1336 (CTF); mGPR125 a.a. 1046–1321 (ICD); mBAI1 (Q30HD1-1) a.a. 1188–1582; mBAI2 (Q8CGM1-1) a.a. 1169–1561; mBAI3 (Q80ZF8-1) a.a. 1147–1522; and mLPHN2 (Q8JZZ7-1) a.a. 1112–1487 (ICD) and a.a. 829–1487 (CTF). The cDNAs for GPR123, GPR124, GPR125, BAI1, BAI2, and BAI3 were kindly provided by Dr. Ines Liebscher (University of Leipzig); the cDNA for LPHN2 was kindly provided by Dr. Simone Prömel (University of Leipzig); and the cDNA for CD97 was kindly provided by Dr. Gabriela Aust (University of Leipzig).

Cell culture

We used HEK 293T cells, which are commonly used as human cell models for the TAP analyses,[19] including studies on GPCRs.[20] With the exception of BAI3 and GPR123, all analyzed ADGRs are expressed in HEK 293T cells[21] (VLGR1, own unpublished data). For the present experiments, HEK 293T cells and HeLa cells were cultured in Dulbecco's modified Eagle's medium containing 10% heat-inactivated fetal calf serum. Cells were transfected with GeneJuice® (Merck Millipore, Darmstadt, Germany) according to manufacturer's instructions.

Tandem affinity purification

TAP was performed as described previously,[22] allowing the isolation of protein complexes under mild conditions. For this, we tagged the N- or C-terminus of the ICDs and CTFs of ADGRs with the SF-TAP (Fig. 1A–C). SF-tagged proteins were expressed in HEK 293T cells for 48 hours. Since we observed apoptosis in the cells expressing CD97_CTF, BAI2_CTF, and LPHN2_CTF, we shortened the time of expression to 18 hours. Mock-treated HEK 293T cells were used as controls. The cells were lysed and the lysate was cleared by centrifugation. The supernatant was then subjected to a two-step purification on Strep-Tactin® Superflow® beads (IBA, Göttingen, Germany) and anti-FLAG M2 agarose beads (Sigma-Aldrich, Hamburg, Germany). Competitive elution was achieved using desbiothin (IBA) in the first step and FLAG® peptide (Sigma-Aldrich) in the second step. The eluate was precipitated by methanol-chloroform and then subjected to mass spectrometry analysis. Eluted affinity

purified complexes were subsequently analyzed by LC–MS/MS.

Mass spectrometry

LC–MS/MS was performed as previously described.[19] In brief, SF-TAP–purified protein complexes were solubilized before subjected to trypsin cleavage. The resulting peptides were desalted and purified using stage tips before separation on a Dionex™ RSLC system. Eluted peptides were directly ionized by nanospray ionization and detected by an LTQ Orbitrap™ Velos mass spectrometer (Thermo Fisher Scientific). We search the raw spectra against the human SwissProt database using Mascot and verified the results by Scaffold (version Scaffold 4.02.01, Proteome Software Inc.) to validate MS/MS–based peptide and protein identifications.

Data processing

Mass spectrometry data of all TAPs were compared with the corresponding data for mock-transfected cells. Proteins that occurred in the mock dataset were not considered for subsequent analysis. We also compared our datasets with a total of 140 TAPs of the protein RAF1, commonly used as an unrelated control TAP analysis.[18,19] Furthermore, we compared hits with the data listed in the Contaminant Repository for Affinity Purifications (CRAPome) database.[23] The CRAPome is a collection of common contaminants in affinity proteomic MS data and contains data for control experiments from an increasing number of affinity purifications. We further analyzed only those with an occurrence below 5%. The gene names of ADGR preys were used as input for the Cytoscape plugins STRING and ClueGO and the STRAP software. The parameter *confidence (score) cutout* was set to 0.4 and the parameter *maximum number of interactors* was set to 0 for STRING analysis. ClueGO v2.3.3 was used for Gene Ontology (GO) term enrichment analysis. Network specificity was set to default (medium).

Antibodies

Mouse anti-FLAG M2 (Sigma-Aldrich) and mouse anti-SIGMAR1 (sc-166392, Santa Cruz Biotechnology) were used as the primary antibodies for immunocytochemistry. Secondary antibody conjugated to Alexa568 was purchased from Molecular Probes™ (Life Technologies, Darmstadt, Germany). Nuclear DNA was stained with DAPI (1 mg/mL) (Sigma-Aldrich).

Immmunocytochemistry

Cells were fixed and permeabilized in ice-cold methanol for 10 min and washed with phosphate-buffered saline. After washing, the cells were covered with blocking solution and incubated overnight with the primary antibody at 4 °C. Cells were washed and then incubated with the secondary antibody in blocking solution containing DAPI for 1.5 h at room temperature. After washing, sections were mounted in Mowiol® (Roth). Specimens were analyzed on a Leica DM6000B microscope and images were processed with Leica imaging software and Adobe Photoshop CS (intensity adjustment). For the analysis of the colocalization of VLGR1 and SIGMAR1, the Leica DMi8 system in combination with the Thunder software was used.

Colocalization analysis

The Pearson correlation coefficient (R) was used to determinate the degree of colocalization between VLGR1_CTF_HA and SIGMAR1 in HeLa cells. Calculation of the Pearson correlation coefficient is a mathematical method to measure the strength of a linear association between two variables.[24] The correlation value has a range from $+1$ to -1. A value of 0 indicates no association, greater than 0 indicates a positive association, and less than 0 indicates a negative association between the two variables. The stronger the positive association of the two variables, the closer R is to $+1$. The Pearson coefficient was calculated using the Coloc 2 plugin of ImageJ (https://imagej.nih.gov/ij/).

γ-Secretase inhibitor assays

Both potent γ-secretase inhibitors LY411575 and DAPT (*N*-[*N*-(3,5-difluorophenacetyl)-ʟ-alanyl]-*S*-phenylglycine *t*-butyl ester) were purchased from Sigma Aldrich and were added to culture media at a final concentration of 100 nM in DMSO after transfection of HEK 293T cells. As control, the same volume DMSO was added to the cells after transfection.

Results

We aimed to identify interacting partners in protein complexes associated with ADGRs by affinity proteomics in HEK 293T cells, applying TAPs in combination with mass spectrometric determination

of the protein content of eluates.[18,19] We analyzed the proteomic datasets by STRAP[25] and grouped proteins according to their assigned GO terms (Fig. 1D). We used ClueGO,[26] a Cytoscape (http://www.cytoscape.org/) plugin, for GO term enrichment analysis (e.g., Figs. S1 and S2, online only) and evaluated the specificity of the identified prey proteins by comparing our data with the CRAPome dataset. We excluded from further analyses the molecules identified in our TAPs that were in the controls and the ones that are present in the CRAPome in 5% of the datasets in order to secure a high probability of specific interaction with ADGRs.

ADGRs physically interact with scaffold proteins and synaptic proteins

Our TAP datasets reveal that ADGR subgroups I, III, VII, and IX interact with PDZ (PSD-95, discs large, zona occludens 1) domain–containing scaffold proteins (Fig. 2A). The dataset for VLGR1_ICD contained the two scaffold proteins whirlin (WHRN; previously DFNB31 or USH2D) and harmonin (USH1C). TAPs of other ADGRs revealed that the ICDs of ADGR groups III (GPR123, GPR124, and GPR125) and VII (BAI1 and BAI3) bind scaffold proteins of the membrane-associated guanylate kinases (MAGUK) family. For the BAI group, we identified CASK, LIN7C, and DLG1 (Fig. 2A). For ADGR group III, we identified the scaffold proteins CASK, DLG1, LIN7A, LIN7C, MPP2, MPP6, MPP7, and MAGI3.

In TAPs for BAI3, we also found the scaffold protein SNTB2, and for GPR124 and GPR125, we found the scaffold protein SCRIB, which was also present in TAPs of LPHN2. Both SNTB2 and SCRIB do not belong to the MAGUK family but do contain PDZ domains. In TAPs with CD97 constructs, we did not find any scaffold proteins.

Notably, we also did not identify any of the above-mentioned scaffold proteins in TAPs with the CTFs of VLGR1, BAI2, GPR124, and LPHN2, potentially due to the C-terminal SF-tag, which may block binding to the ADGR PDZ-binding motif (PBM). However, the TAP data that we acquired with ADGR_CTFs indicated synaptic localization and functions of the receptors: they contain various proteins involved in vesicle fusion and numerous interactors that are associated with synapse-related GO terms, such as *synaptic signaling* and *synaptic vesicle cycle* (Fig. 2B).

TAP data indicate binding of phosphatases and kinases to ADGRs

In TAPs of all ADGRs except GPR123, we identified diverse phosphatases and kinases (Table 1). For most ADGRs, we identified catalytic and regulatory subunits of protein phosphatases 2 (PP2) and 6 (PP6). BAI proteins also interacted with subunits of protein phosphatases 1 and 4. Interestingly, the ICDs (except in the case of VLGR1) were sufficient to interact with these phosphatases (Table 1), indicating that phosphatases preferentially bind to the ICD of ADGRs. In TAPs with CTFs of GPR124, BAI2, CD97, and VLGR1, the protein phosphatase Mg^{2+}/Mn^{2+}-dependent 1B was also found. Furthermore, our TAPs revealed casein kinase 2 (CK2), calcium/calmodulin-dependent protein kinase II (CAMK2), cyclin-dependent kinase 4 (CDK4), and mitogen-activated protein kinase 1 or 3 (MAPK1/MAPK3) as possible candidates that phosphorylate ADGRs. *In silico* analysis of ADGR amino acid sequences using the kinasephos 2.0 tool (http://kinasephos2.mbc.nctu.edu.tw/predict.php) predicts phosphorylation sites in all ADGRs studied, defining them as potential targets for phosphorylation. All ADGRs contain potential CK2 and CDK phosphorylation motifs in their ICD. A potential MAPK phosphorylation site was predicted for all ADGRs except CD97. Potential CAMK target sites were predicted for LPHN2, BAI2, and BAI3.

ADGR presence in protein complexes of the ER, the Golgi apparatus, and mitochondria

Comparing the TAP datasets of ADGR_CTFs, we identified 116 molecules present in all TAPs of all five ADGRs (Table S1, online only). We grouped these proteins according to their assigned GO terms with STRAP (Fig. 1D) and analyzed them for enriched GO terms with ClueGO (Fig. S1, Table S1, online only). Our analysis demonstrated that the most significantly enriched GO terms in the category *Cellular Component* were related to the ER, the Golgi apparatus, mitochondria, and the nucleus (Fig. S1A, online only). In the GO term category *Biological Process,* we found an enrichment in the terms *mitochondrial ATP synthesis coupled proton transport, membrane lipid biosynthetic process, protein import into nucleus*, and *response to ER stress* (Fig. S1B, online only). Notably, many of the ADGR-associated proteins were amino acid and
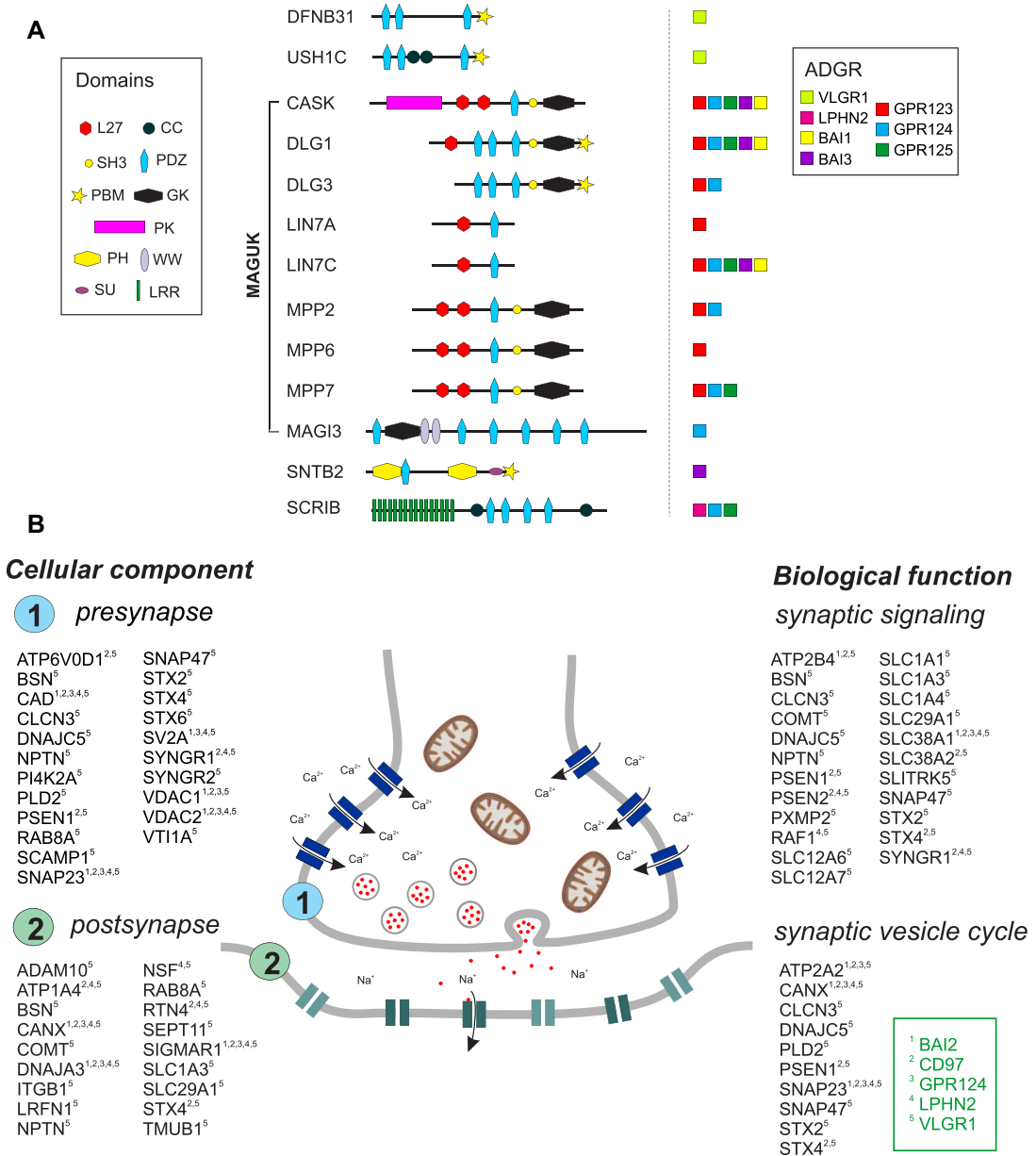
Figure 2. ADGRs interact with scaffold proteins and other proteins associated with synaptic functions. (A) ADGR_ICDs are associated with scaffold proteins. ADGR_ICDs bind to scaffold proteins containing PDZ domains. L27, Lin2/Lin7 domain; CC, coiled-coil domain; SH3, Src homology 3 domain; PK, protein kinase; PH, pleckstrin homology; PDZ (PSD-95, DLG, ZO-1) domain; PBM, PDZ-binding motif; GK, guanylate kinase domain; WW, WW domain; SU, SU domain; LRR, leucine-rich repeat. (B) ADGR_CTFs bind to synaptic proteins. GO term enrichment analysis with ClueGO[26] reveals that TAP preys of ADGR_CTFs localize to the *pre-* and *postsynapse* and are involved in *synaptic signaling* and the *synaptic vesicle cycle.*

zinc transporters of the solute carrier (SLC) family and ATPases that are coupled to H^+ and Ca^{2+} transmembrane transport (Table S1, online only). Several of our TAP preys were enriched in mitochondria-associated membranes (MAMs) (Table 2). MAMs are contact sites of the ER to the outer mitochondrial membrane.[27] The association with MAM proteins was most prevalent for VLGR1 and the

Table 1. Protein phosphatases and kinases identified in ADGR-TAPs

Phosphatase/ kinase	BAI1	BAI2	BAI3	CD97	GPR124	GPR125	LPHN2	VLGR1
Protein phosphatase 1		PPP1CA PPP1CC PPP1R9B						
Protein phosphatase 2	PPP2CB PPP2R1A PPP2R2A PPP2R2D	PPP2CA PPP2R2A PPP2R3A PPP2R1A* PPP2R2A*	PPP2CB PPP2R1A PPP2R2A	PPP2CA PPP2R1A PPP2R2A PPP2R1B*	PPP2CA PPP2R2A PPP2R1A*	PPP2CA PPP2CB PPP2R1A PPP2R2A PPP2R2D	PPP2CA PPP2R1A PPP2R2A PPP2R5E PPP2R1A* PPP2R1B* PPP2R2A*	PPP2R1A* PPP2R1B*
Protein phosphatase 4	PPP4C PPP4R2 PPP4R3A PPP4R3B							
Protein phosphatase 6		PPP6C PPP6R3 PPP6C* PPP6R1* PPP6R3*		PPP6C*	PPP6C PPP6R3 PPP6C* PPP6R1* PPP6R3*		PPP6C PPP6R3 PPP6C* PPP6R1* PPP6R3*	PPP6C*
Protein phosphatase, $Mg2^+$/$Mn2^+$ dependent, 1B		PPM1B*		PPM1G*	PPM1B*			PPM1B*
Casein kinase 2					CSNK2A1 CSNK2A2 CSNK2B CSNK2A1* CSNK2B*		CSNK2B*	
Calcium/calmodulin-dependent protein kinase II		CAMK2D CAMK2G	CAMK2D CAMK2G CAMK2D*		CAMK2D*			
Cyclin-dependent kinase 4				CDK4			CDK4	
Mitogen-activated protein kinase 1				MAPK1				MAPK1
Mitogen-activated protein kinase 3								MAPK3

NOTE: Listed are the phosphatase subunits and kinases that were found by TAP for each ADGR. Most subunits were identified with the ICD; those marked with * were identified with the CTF. Only those that show a low occurrence in the CRAPome (less than 5%) are listed.

least prevalent for BAI2. Immunocytochemical double labeling of VLGR1 and the MAM core protein sigma1R (SIGMAR1) in human HeLa cells transfected with VLGR1_CTF_HA revealed partial colocalization of SIGMAR1 and VLGR1 (Fig. 3C).

We also identified proteins that are located at the outer and inner mitochondrial membrane as putative interactors for all ADGR_CTFs (Table 3). These include proteins that are mainly involved in transmembrane transport and membrane folding. We found that all ADGR_CTFs associate with components of the respiratory chain, namely subunits for NADH-ubiquinone oxidoreductase (complex I), the cytochrome bc1 complex (complex III), cytochrome c oxidase (complex IV), and the F_1F_0 ATP synthase (complex V) (Fig. 3 and Table 3). In addition to components of the respiratory chain complex, we identified proteins that are involved in the assembly of mitochondrial complexes. These include COA3, OXA1L, and TIMM21, which are necessary for complex IV assembly,[28–30] as well as NDUFAF-1, -3, and -4, and TMEM126B, which participate in complex I assembly.[31–33] For VLGR1,

Table 2. Molecules related to mitochondria-associated membranes (MAMs) identified in ADGR-CTF-TAPs

Gene	Protein function	Reference	BAI2	CD97	GPR124	LPHN2	VLGR1
ACSL4	Lipid biosynthesis and fatty acid degradation	105	−	−	−	−	+
AIFM1	Apoptosis, mitochondria morphology	106	−	+	−	+	+
AMFR	Ubiquitination	107	+	+	+	+	+
BCAP31	Apoptosis	108	−	−	+	−	+
BSG	Regulatory component of γ-secretase	109	−	+	−	+	+
CANX	Calcium pumping	110	−	+	+	+	+
CISD2	Calcium homeostasis	111	−	+	−	−	+
ERLIN2	Targets IP3Rs for degradation	112	−	−	−	−	+
ERP44	ER protein retention	113	−	−	−	−	+
FUS	RNA splicing	114	+	−	+	−	−
G6PC3	Gluconeogenesis	115	−	−	−	−	+
HMOX1	Catalyzes the degradation of heme	116	−	+	−	−	−
HSPA5	ER stress, chaperone	117	−	+	+	+	+
HSPA9	Binds VDAC	76	−	+	−	+	+
LCLAT1	Cardiolipin acyl chain remodeling	118	−	−	−	−	+
LMAN1	Mannose-specific lectin	119	−	−	−	−	+
MAVS	Activation of NF-κB/IRF3	120	−	−	−	−	+
P4HB	ER protein retention	121	−	+	+	+	+
PIGN	GPI syn:transferase	118	−	−	−	−	+
PSEN1	Component of γ-secretase	122	−	+	−	−	+
PSEN2	Component of γ-secretase	122	−	+	−	+	+
PTDSS1	Phospholipid metabolism	123	+	−	+	−	+
PTDSS2	Phospholipid metabolism	123	−	+	−	−	+
RHOT1	Mitochondrial trafficking	124	−	−	−	−	+
RTN2	Generation of tubular ER	125	−	−	−	−	+
RTN4	ER–mitochondria tethering	126	−	+	−	+	+
SCD	Fatty acid transport	127	+	+	+	+	+
SIGMAR1	Lipid transport and calcium signaling	117	+	+	+	+	+
SLC27A4	Fatty acid transport	128	+	+	+	+	+
SOAT1	Cholesterol metabolism	119	−	−	−	−	+
VAPB	ER–mitochondria tethering	114	−	−	−	−	+
VDAC1	Ion exchange	76	+	+	+	−	+

Note: Only identified molecules that show a low occurrence in the CRAPome (less than 5%) are listed.

we further identified BCS1L, which is necessary for complex III assembly.[34]

All ADGR_CTFs were associated with translocases of the inner mitochondrial membrane (TIMs) and to a lesser extent with translocases of the outer mitochondrial membrane (TOMs) (Table 3). Moreover, all ADGR_CTFs bound to components of the MICOS complex that is crucial for the formation and maintenance of the mitochondrial cristae structure.[35] In addition, we found YME1L1 in TAPs for GPR124, BAI2, and LPHN2, as well as PARL for VLGR1. Both YME1L1 and PARL also maintain cristae morphology and have an antiapoptotic effect.[36,37]

CTFs of ADGR physically interact with components of the γ-secretase complex

Strikingly, we found LPHN2 as a prey for CD97_CTF and VLGR1_CTF, and CD97 as a prey for VLGR1_CTF. This indicates that these three ADGRs may be part of the same protein complexes. This prompted us to check for preys shared by CD97, LPHN2, and VLGR1 TAPs, and we found that 196 proteins were common for all three of these ADGRs (Fig. S2A, online only). After filtering out proteins that occur in more than 5% of the negative controls in the CRAPome, we performed a GO term enrichment analysis with the remaining 89 interacting proteins. Our analyses

Table 3. Molecules that localize to mitochondria identified in ADGR-CTF-TAPs

Protein	BAI2	CD97	GPR124	LPHN2	VLGR1	
Complex I NADH–ubiquinone oxidoreductase	NDUFA4 NDUFA5 NDUFA13 NDUFS1 NDUFS3	NDUFA13 NDUFA4 NDUFB10 NDUFS1 NDUFS2 NDUFS3 NDUFV1	NDUFA4 NDUFA5 NDUFS1 NDUFS2 NDUFS3	NDUFA4 NDUFA5 NDUFA9 NDUFA13 NDUFS2 NDUFS3	NDUFA4 NDUFA5 NDUFA8 NDUFA9 NDUFA11 NDUFA13 NDUFAB1 NDUFB4 NDUFB5	NDUFB10 NDUFB11 NDUFS1 NDUFS2 NDUFS3 NDUFS8 NDUFV1 NDUFV2
Complex I assembly	NDUFAF4	NDUFAF1	NDUFAF3 NDUFAF4	NDUFAF4	NDUFAF1 NDUFAF3 NDUFAF4	
Complex III Cytochrome bc1	UQCRC1 UQCRQ	UQCR10 UQCRC1 UQCRH UQCRQ	UQCRC2 UQCRQ	UQCRC2	UQCR10 UQCRB UQCRC2 UQCRFS1 UQCRQ	
Complex IV Cytochrome c oxidase	COX6C COX7B	COX4I1	COX6C COX7B	COX15 COX4I1 COX5A COX6C COX7B	COX15 COX4I1 COX5A COX6C COX7B	
Complex V F_1F_0 ATP synthase	ATP5B ATP5C1 ATP5F1 ATP5H ATP5O	ATP5A1 ATP5B ATP5C1 ATP5D ATP5F1 ATP5H ATP5O	ATP5B ATP5C1 ATP5F1 ATP5H ATP5O	ATP5C1 ATP5EP2 ATP5F1 ATP5H ATP5J2 ATP5O	ATP5A1 ATP5B ATP5C1 ATP5D ATP5EP2 ATP5F1	ATP5H ATP5I ATP5J ATP5J2 ATP5L ATP5O
MICOS complex	C19orf70	IMMT	C19orf70 IMMT	APOOL C19orf70 IMMT	APOO C19orf70 CHCHD3 IMMT	
Translocase of the inner membrane	TIMM17A TIMM21 TIMM23B TIMM50	TIMM17B TIMM23 TIMM50	TIMM17A TIMM21 TIMM23B TIMM50 TIMMDC1	TIMM17A TIMM21 TIMM23B TIMM50 TIMMDC1	TIMM17B TIMM23 TIMM50 TIMMDC1	
Translocase of the outer membrane	TOMM22	TOMM22 TOMM70A	TOMM22	–	TOMM22 TOMM40	
Mitochondrial SLC transporters	SLC16A1 SLC25A1 SLC25A10 SLC25A11 SLC25A22 SLC25A6	SLC16A1 SLC25A13 SLC25A22 SLC25A3 SLC25A5 SLC25A6	SLC16A1 SLC25A1 SLC25A10 SLC25A11 SLC25A22 SLC25A3 SLC25A5 SLC25A6	SLC16A1 SLC25A10 SLC25A11 SLC25A12 SLC25A13 SLC25A19 SLC25A22 SLC25A3 SLC25A5 SLC25A6	SLC16A1 SLC1A3 SLC25A1 SLC25A10 SLC25A11 SLC25A12 SLC25A13 SLC25A19 SLC25A21 SLC25A22	SLC25A24 SLC25A3 SLC25A33 SLC25A4 SLC25A40 SLC25A46 SLC25A5 SLC25A6 SLC27A3

NOTE: Only identified molecules that show a low occurrence in the CRAPome (less than 5%) are listed.
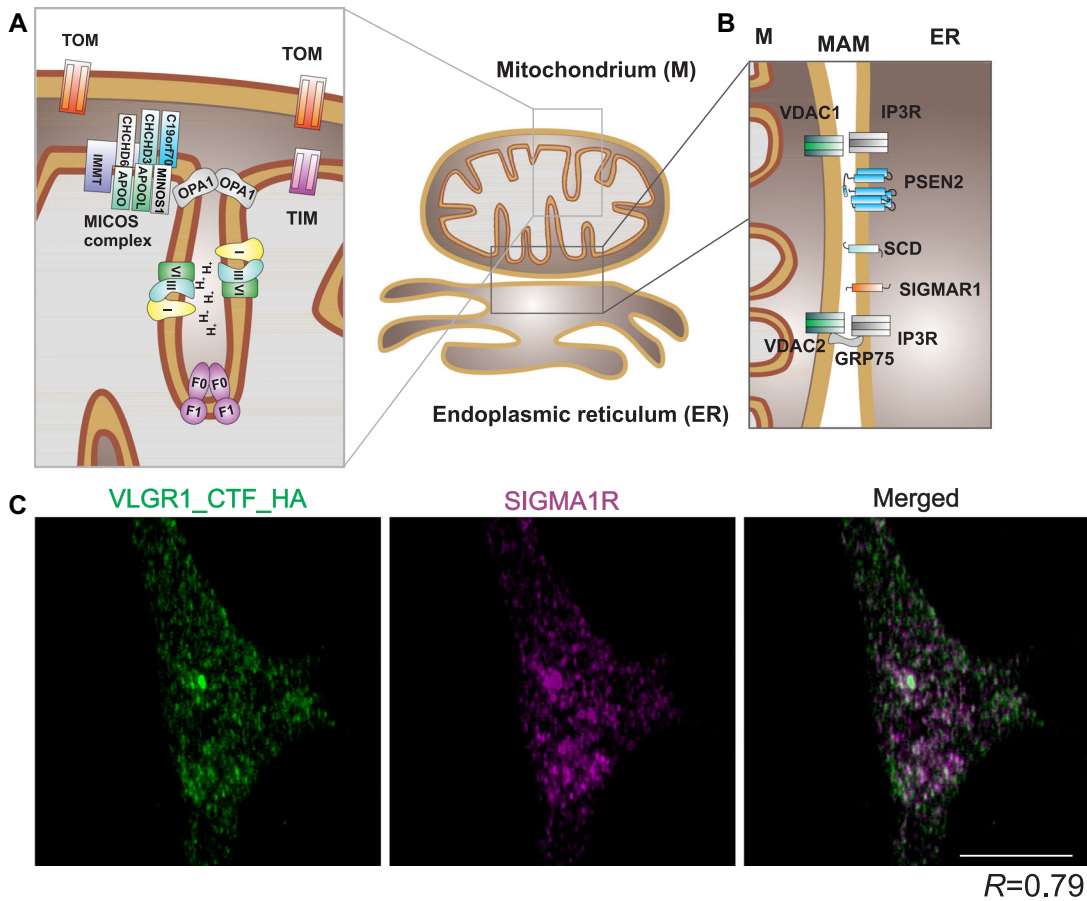
Figure 3. Mitochondrial proteins identified in ADGR TAPs. (A) Schema of mitochondria. Colored: mitochondrial proteins from the respiratory chain (complexes I, III, and IV), F_0F_1 ATP synthase, components of the MICOS complex, and translocases in the inner and outer membrane (TIMs/TOMs) (see also Table 2). Colored: proteins were identified in TAPs. Gray: other key components of mitochondrial cristae and MAMs. (B) Diverse proteins that are enriched in mitochondria-associated membranes (MAMs) were precipitated with ADGR_CTFs (see also Table 3). (C) Immunocytochemical staining of the MAM core protein SIGMAR1 and VLGR1_CTF_HA in HeLa cells reveals partial colocalization of SIGMAR1 and VLGR1. The Pearson coefficient $R = 0.79$ indicates positive association of both proteins in the cell. Exemplary analysis from three independent experiments.

revealed that the GO terms were mostly related to ER and mitochondria localization and function (Fig. S2 and Table S3, online only). We observed that all three TAPs contained subunits of the γ-secretase complex (Fig. 4A and B). Interestingly, the γ-secretase complex has recently been reported to be present in MAMs.[38–40] In TAPs of VLGR1 and CD97, we identified nicastrin (NCSTN), presenilins 1 and 2 (PSEN1 and PSEN2), as well as aph-1 homolog A (APH1A), but not presenilin enhancer 2 (PEN2), which is important for endoproteolysis of presenilins, activating the enzyme. In TAPs of LPHN2, the proteins NCSTN, PSEN2, and APH1A were present (Fig. 4B). Notably, we also found that

GPR124_CTF interacts with NCSTN. In contrast, we did not identify any γ-secretase subunits in the BAI2_CTF TAP dataset.

Besides the γ-secretase complex itself, we also found several γ-secretase modulators in the ADGR TAPs. In all ADGR_CTF TAPs, the regulatory subunit basigin (BSG) was present.[41] Furthermore, we identified the presenilin cleavage proteins histocompatibility minor 13 (HM13) and the transmembrane p24 trafficking protein 10 (TMED10) in all ADGR_CTF TAPs, with the exception of BAI2 TAP.[42,43]

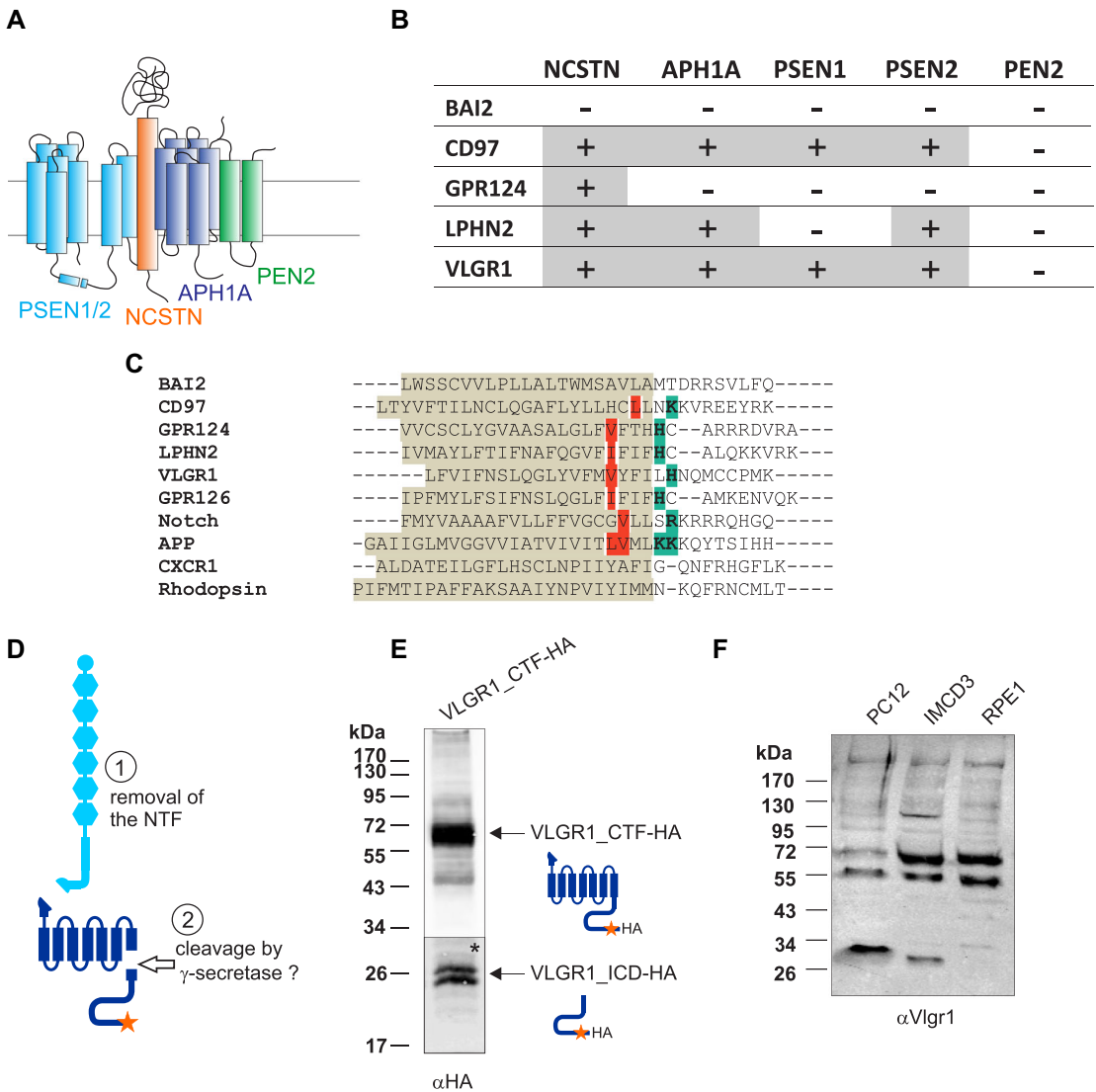We further aimed to determine whether ADGRs may be substrates for the γ-secretase complex

A

B

	NCSTN	APH1A	PSEN1	PSEN2	PEN2
BAI2	−	−	−	−	−
CD97	+	+	+	+	−
GPR124	+	−	−	−	−
LPHN2	+	+	−	+	−
VLGR1	+	+	+	+	−

PEN2
APH1A
PSEN1/2   NCSTN

C

```
BAI2       ----LWSSCVVLPLLALTWMSAVLAMTDRRSVLFQ-----
CD97       --LTYVFTILNCLQGAFLYLLHCLLNKKVREEYRK-----
GPR124     ----VVCSCLYGVAASALGLFVFTHHC--ARRRDVRA---
LPHN2      ----IVMAYLFTIFNAFQGVFIFIFHC--ALQKKVRK---
VLGR1      ------LFVIFNSLQGLYVFMVYFILHNQMCCPMK-----
GPR126     ----IPFMYLFSIFNSLQGLFIFIFHC--AMKENVQK---
Notch      ----FMYVAAAAFVLLFFVGCGVLLSRKRRRQHGQ-----
APP        -GAIIGLMVGGVVIATVIVITLVMLKKKQYTSIHH-----
CXCR1      --ALDATEILGFLHSCLNPIIYAFIG-QNFRHGFLK----
Rhodopsin  PIFMTIPAFFAKSAAIYNPVIYIMMN-KQFRNCMLT----
```

D

① removal of the NTF

② cleavage by γ-secretase ?

E

VLGR1_CTF-HA

kDa
170 —
130 —
95 —
72 —   ← VLGR1_CTF-HA
55 —
43 —
34 —
26 —   ← VLGR1_ICD-HA
*
17 —

αHA

F

PC12 IMCD3 RPE1

kDa
170 —
130 —
95 —
72 —
55 —
43 —
34 —
26 —

αVlgr1

Figure 4. ADGR_CTFs bind to the γ-secretase complex. (A) Components of the γ-secretase complex: nicastrin (NCSTN), aph-1 homolog A (APH1A), presenilin 1/2 (PSEN1/2), and presenilin-enhancer 2 (PEN2). (B) Table of γ-secretase subunits that bound to ADGR_CTFs in TAP. (C) Amino acid sequence alignments of positively charged residues (colored) at the junction of the trans-membrane helix 7 only of ADGRs and other receptors. Positively charged residues in Notch and APP (three to four residues after the ε cleavage sites) are the primary determinants for substrate binding.[44] (D) Schematic representation of ADGR cleavage by γ-secretase. (E) VLGR1_CTF-HA is cleaved, releasing a smaller band of ∼26 kDa. *The intensity of the lower part was increased relative to the upper part of the blot. (F) VLGR1-CTF and smaller VLGR1 fragments at ∼26 kDa are detected in PC12, IMCD3, and RPE1 cell lysates. Panels E and F each show an exemplary western blot from three independent experiments.

(Fig. 4C–F). Amino acid sequence alignments revealed conserved, positively charged residues at the junction of transmembrane helix 7 only in the ADGRs for which we found interactions with γ-secretase components (Fig. 4C). Charged residues located three to four residues after the ε cleavage sites were recently described

for NOTCH and the amyloid precursor protein (APP) as the primary determinants for substrate binding.[44]

Since most γ-secretase subunits were found with VLGR1 and yet overexpression of VLGR1_CTF did not induce apoptotic effects, we chose VLGR1 for further investigation. Upon recombinant

expression of C-terminally tagged VLGR1_CTF-HA in HEK 293T cells, we observed that, in addition to the full-length CTF with a molecular weight of ∼50 kDa, two smaller bands at ∼26 kDa occurred (Fig. 4E). This size corresponds to the molecular size of the ICD of VLGR1. In addition, corresponding protein fragments were detected in cell lysates of PC12, IMCD3, and RPE1 cells (Fig. 4F).

In conclusion, these data suggested that like other γ-secretase substrates, VLGR1 is proteolytically cleaved in the transmembrane helix 7 by the γ-secretase. However, in several preliminary experiments applying well-established γ-secretase inhibitors, namely LY-411575 and DAPT, we demonstrated the inhibition of APP cleavage but did not observe any effect on ICD release from ADGRs (data not shown).

ADGRs interact with nuclear proteins and localize to the nucleus

We observed that all ADGRs studied here associated with resident nuclear proteins, which are involved in nuclear-specific functions, such as gene regulation, RNA splicing, and transcription. This was the case for both the ADGR_CTF and ADGR_ICD baits and was most prominent for GPR124, BAI1, and BAI2.

In TAPs of the GPR124_ICD and GPCR124_CTF, we found an enrichment of proteins that were assigned to the GO term *nuclear speckles*, the chromatin-free nuclear compartment of RNA splicing. For GPR124_CTF and BAI2_CTF, we observed an enrichment in proteins assigned with the GO term *nucleolus,* the site of ribosomal RNA transcription. Furthermore, the ICDs of BAI1 and GPR124 interacted with the PAF1 complex, which is involved in RNA polymerase II transcription elongation and transcription-coupled histone modifications.[45] GO terms related to histone modification, splicing, and DNA unwinding were enriched for all ADGRs; however, the numbers greatly varied.

BAI1_ICD, GPR124_CTF, GPR124_ICD, BAI2_CTF, LPHN2_ICD, CD97_ICD, and CD97_CTF were additionally associated with karyopherins (importins), which mediate nuclear import. Strikingly, we observed that the ICDs of GPR123, GPR124, GPR125, and BAI2 clearly show nuclear localization when they are recombinantly expressed in HEK 293T cells (Fig. 5A). GPR123_ICD, GPR124_ICD, and GPR125_ICD show a punctate-like enrichment in the nucleus, resembling nuclear speckles, whereas BAI2_ICD showed much larger nuclear accumulations.

The association with nuclear import proteins and the nuclear localization of some of the ADGR_ICDs led us to check whether ADGR_ICDs contain nuclear localization sequences (NLSs). For this, we applied the NLS prediction tool cNLS Mapper.[46] We found high scores for BAI1 and BAI2 and medium scores for BAI3 and GPR123. GPR124, GPR125, and LPHN2 gave only low scores, whereas no NLSs were predicted for VLGR1 and CD97 ICDs (Fig. 5B).

The results from our TAPs, together with our immunocytochemical localization analysis and the presence of NLS in some ADGRs, indicate that the ICDs of ADGRs may be cleaved and potentially act as transcription factors in the nucleus. We therefore checked our TAP data for proteins that act as transcriptional regulators. Indeed, we found numerous proteins that are related to transcriptional regulation. The molecules involved in transcriptional regulation identified in our ADGR TAPs are included in Table 4.

Identification of modulators of the Wnt signaling pathway in ADGR TAPs

The GO term analyses of our TAP data also revealed an enrichment for the GO term *Wnt signaling* in the BAI2_CTF, GPR124_CTF, and VLGR1_CTF datasets. Furthermore, single proteins involved in Wnt pathways were also found in TAPs of CD97_CTF and LPHN2_CTF (Table 5). Most of these molecules modulate Wnt signaling by targeting β-catenin. Some prey proteins have functions in the nucleus. SLC30A9 is part of the β-catenin transcription complex and participates in the regulation of Wnt downstream genes.[47]

Discussion

In the present study, we identified previously described binding partners and numerous novel putative interactors of ADGRs by TAPs in combination with subsequent mass spectrometry. Nevertheless, our affinity capture approach bears limitations, which have to be considered for the interpretation of our datasets. In our study, we used HEK 293T cells as established human cellular models for the ADGR TAPs.[19,20] Therefore, we were not able to capture tissue- or cell-specific interacting partners that are

Table 4. Molecules involved in transcriptional regulation identified in ADGR TAPs

Gene	Protein function	References	BAI2 ICD	CD97 ICD	GPR124 ICD	LPHN2 ICD	VLGR1 ICD
BTAF1	Regulates transcription in association with TATA binding protein (TBP)	129	–	–	+	–	–
BZW1	Enhances histone H4 gene transcription	130	+	+	+	+	+
BZW2	Controls translation by inhibition of eIF2	131	–	+	–	+	+
HOXA5	Transcription factor, essential for embryonic development and the nervous system	132	+	–	+	–	–
MAGEA1	Acts as an transcriptional repressor	133	–	–	+	–	–
MLF1	Posttranscriptional inhibitor and activator of gene expression	134	+	–	+	+	–
PREB	Transcription factor, probable role in cell fate	135	+	+	+	+	+
TCF25	Transcription factor important for embryonic development	136	+	–	+	+	–
UBR2	E3 ubiquitin-protein ligase plays a critical role in chromatin inactivation	137	+	–	–	+	–
UBR5	Involved in maturation and/or transcriptional regulation of mRNA	138	+	–	–	–	+

Gene	Protein function	References	BAI2 ICD	CD97 ICD	GPR123 ICD	GPR124 ICD	LPHN2 ICD	VLGR1 ICD
CTR9	Component of the PAF1 complex required for Hox gene transcription	139	+	–	–	+	–	–
ELOB	Activates elongation by RNA polymerase II	140	–	+	–	–	+	–
FHL2	Inhibits the transcriptional activity of FOXO1	141	–	–	–	–	+	+
HMGN5	Nucleosomal binding and transcriptional activation	142	+	–	–	–	–	–
MAPK1	Transcriptional repressor	143	–	–	–	–	+	+
MAPK3	Regulation of transcription factors	144	–	–	–	–	–	+
SETD7	Transcriptional activation of genes (e.g., collagenase and insulin)	145	–	–	–	+	–	–
SIRT1	Regulates epigenetic gene silencing	146	+	–	–	+	+	–
TCEAL1	Modulates various viral and cellular promoters	147	–	–	+	–	+	–

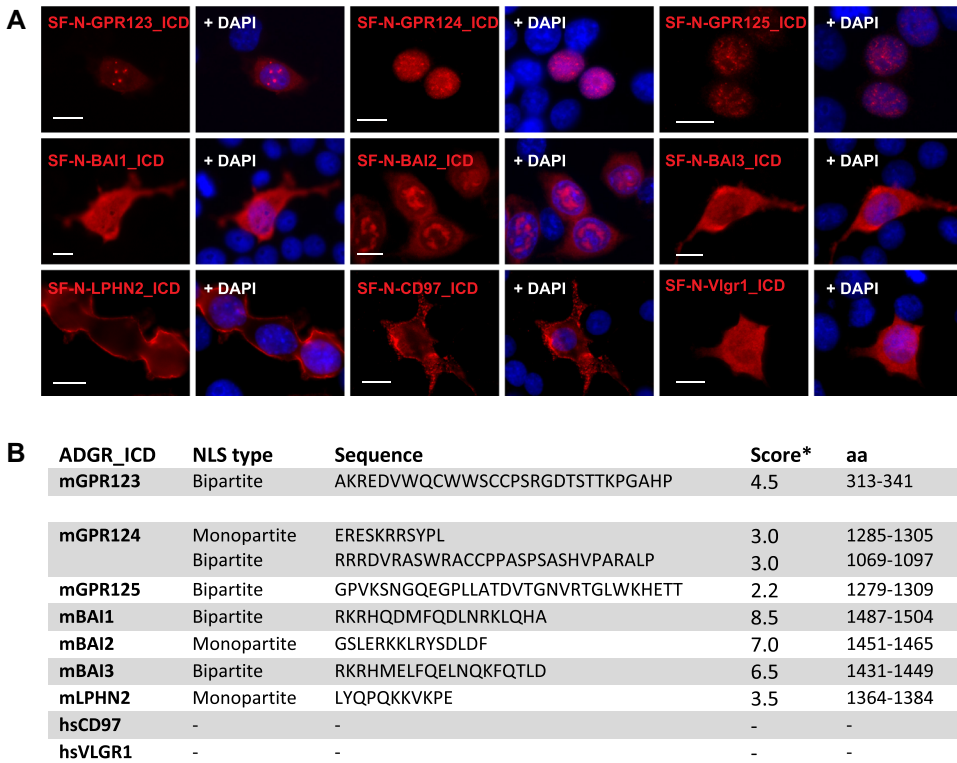NOTE: Only identified molecules that show a low occurrence in the CRAPome (less than 5%) are listed.

ADGR_ICD	NLS type	Sequence	Score*	aa
mGPR123	Bipartite	AKREDVWQCWWSCCPSRGDTSTTKPGAHP	4.5	313-341
mGPR124	Monopartite	ERESKRRSYPL	3.0	1285-1305
	Bipartite	RRRDVRASWRACCPPASPSASHVPARALP	3.0	1069-1097
mGPR125	Bipartite	GPVKSNGQEGPLLATDVTGNVRTGLWKHETT	2.2	1279-1309
mBAI1	Bipartite	RKRHQDMFQDLNRKLQHA	8.5	1487-1504
mBAI2	Monopartite	GSLERKKLRYSDLDF	7.0	1451-1465
mBAI3	Bipartite	RKRHMELFQELNQKFQTLD	6.5	1431-1449
mLPHN2	Monopartite	LYQPQKKVKPE	3.5	1364-1384
hsCD97	-	-	-	-
hsVLGR1	-	-	-	-

Figure 5. Localization of ADGR_ICDs in the nucleus. (A) Immunocytochemical staining of SF-tagged ADGR_ICDs expressed in HEK 293T cells by anti-FLAG antibodies. Exemplary analysis from three independent experiments. (B) Predictions of nuclear localization signals (NLS) in ADGR_ICDs. *Scores: 8–10, exclusively localized to the nucleus; 6–7, partially localized to the nucleus; 3–5, localized to both the nucleus and cytoplasm; 1–2, localized to the cytoplasm. Scale bars, 10 μm.

not expressed in HEK 293T cells. Since we cultured the cells under standard conditions, we also missed proteins that require specific physiological conditions for binding to ADGRs, such as mechanical or chemical ligand stimulation. Although TAP protein complexes are purified in close-to-native conditions, the membrane protein complexes lose their membrane context during the purification steps and therefore are difficult to obtain in general.[20] In addition, overexpression of ADGR domains may lead to changes in the stoichiometry of purified protein complex compositions. In any case, as in other screens, it is necessary to validate all newly identified putative binary interactions by applying independent, complementary experiments from the molecular to organismic level to sort out false positive hits. Nevertheless, the obtained datasets highlight the usefulness of our affinity capture approach even for membrane proteins. The identified ADGR-

interacting proteins support previously discussed functions of ADGRs, but more importantly define novel physiological functions related to ADGRs.

ADGR subfamilies interact with scaffold proteins

The TAP data of our study reveal numerous interactions of ADGRs and scaffold proteins. All identified scaffold proteins possess PDZ domains and all ADGRs investigated in the present study contain a PBM at their C-terminal end (Fig. 1) that is predetermined to bind to PDZ domains. Therefore, their mutual interaction most probably occurs via the binding of ADGRs' PBM to PDZ domains. This is also confirmed by previous experimental data. We have previously shown that VLGR1 (USH2D) directly binds the two other Usher syndrome proteins, harmonin (USH1C) and whirlin (USH2D), both of which serve as cytoplasmic anchors in

Table 5. Modulators of the Wnt signaling pathway identified in ADGR TAPs

Gene	Protein function	Reference	BAI2 CTF	CD97 CTF	GPR124 CTF	LPHN2 CTF	VLGR1 CTF
AMER1	Regulator of the canonical Wnt signaling pathway	148	+	−	+	−	−
ATP6AP2	Functions as an adaptor between Wnt receptors and V-ATPase	149	−	−	−	−	+
LRP1	Represses canonical Wnt signaling	150	−	−	−	−	+
PSEN1	Inhibitor for β-catenin	151	−	+	−	−	+
PTK7	Modulates Wnt signaling activity via LRP6	152	−	−	−	−	+
RRM2	Inhibits Wnt signaling	153	−	−	−	−	+
SKP1	Mediates degradation of β-catenin	154	−	−	−	−	+
SLC30A9	Participates in transcriptional activation of Wnt-responsive genes	47	−	−	+	−	+
UBR5	Ubiquitinates and upregulates β-catenin	155	+	−	+	−	+
USP34	Regulates axin stability	156	−	−	+	−	−
WLS	Regulates Wnt protein sorting and secretion	157	+	+	+	+	+

NOTE: Only identified molecules that show a low occurrence in the CRAPome (less than 5%) are listed.

membrane adhesion complexes of the inner ear hair cells and retinal photoreceptor cells.[48–50] It has also been reported previously that BAI1 and GPR124 interact with DLG1 (SAP97).[10,51] Interestingly, although the direct interaction of DLG1 with the C-terminal PBM of CD97 has been shown recently,[52] we did not find DLG1 or any other PDZ-containing protein in our TAPs of CD97. This is most probably due to the fact that the interaction of DLG1 with CD97 is induced by phosphorylation of the PBM of CD97. However, this phosphorylation is induced by mechanical stimulation, a condition not present in our TAPs. Nevertheless, our TAP data revealed the interaction of ADGRs of group I (latrophilins), group III (GPR123, GPR124, and GPR125), and group VII (BAIs) with the same set of scaffold proteins (Fig. 2B). The question of whether the ADGRs are integrated in common protein networks and signaling hubs organized by scaffold proteins in cells and tissues will be reserved for future studies.

ADGR subfamilies are part of protein networks at synapses

Although the identified scaffold proteins are ubiquitously expressed, they are essential components of the protein networks of synapses, particularly of the postsynaptic density of neurons.[53] These scaf-

fold proteins are mainly members of the MAGUK family, which are involved in the establishment and maintenance of cell polarity and the dynamic arrangement of receptors and channels at synaptic membranes.[10,54,55] In addition, we identified several proteins involved in the targeting and fusion of synaptic vesicles as putative interaction partners of ADGRs (Fig. 2B), suggesting an involvement of ADGRs in these processes too. For example, SNAP23, which interacts with all ADGR_CTFs, is known to be involved in the exocytosis of glutamate receptors to the postsynaptic membrane.[56] Our findings are also in line with the enrichment of ADGRs, namely VLGR1, latrophilins, and BAIs, at the postsynapse of dendrites[50,57–59] and the function of latrophilins and BAIs in synaptic remodeling.[55,60–62] Although the ADGRs CD97, GPR123, GPR124, and GPR125 have not been mapped to synaptic subdomains, a role in synaptic function cannot be ruled out yet.

ADGR interaction with the γ-secretase complex

Our TAP data for the ADGR_CTFs also revealed a close relationship of ADGR with the γ-secretase complex. With the exception of BAI2, we identified subunits of the γ-secretase complex in the TAPs of all other ADGR_CTFs, indicating their close

relationship with this intramembranous complex. The γ-secretase complex is well known for the generation of the β-amyloid peptide protein by the sequential proteolysis of the APP, which is a crucial step in the development of Alzheimer's disease.[63] However, in addition to APP, the γ-secretase also proteolytically cleaves a variety of integral membrane proteins that initiate downstream pathways involved in transcriptional regulation in the nucleus.[64] Indeed, we also observed the release from several ADGRs of a fragment with the size of the ICD in cultures of diverse cell lines (Fig. 4). In addition, we demonstrated the localization of ADGR fragments in the nucleus, which is further supported by the presence of NLS sequences in the ICDs of diverse ADGRs (Fig. 5). Together, our findings suggest a novel signaling mechanism of ADGRs that comprises the release of an ICD upon γ-secretase cleavage and subsequent translocation of the ICD into the nucleus for gene regulation. This scenario is similar to the described signaling pathway related to the γ-secretase substrate polycystin 1 (PKD1).[65] PKD1 shows high structural similarity to ADGRs: it is also a multispanning transmembrane protein that undergoes autocleavage at a GPS, analogous to ADGRs.[66,67] Upon γ-secretase cleavage, a small (∼30 kDa) PKD1_ICD fragment is released and directed into the nucleus.[68,69] The release of PKD1_ ICD is most probably induced by mechanical stimuli,[68] an activation mechanism that has also been discussed for ADGRs.[70–72]

Although our data favor a noncanonical signaling pathway triggered by γ-secretase cleavage, our approach of applying established γ-secretase inhibitors did not alter the release of ICDs from the ADGR. ADGRs may alternatively play a role in γ-secretase positioning in specific membrane domains (e.g., lipid rafts) or in its regulation. This is supported by the fact that, besides γ-secretase subunits, we also identified γ-secretase regulators in our TAPs, such as BSG, TMED10, and HM13. In particular, BSG was found in the TAP datasets for LPHN2, CD97, and VLGR1 CTFs and was previously described as a potential additional γ-secretase regulatory subunit.[41] TMED10 was present in all ADGR_CTF TAPs except for BAI2. It is part of presenilin complexes and regulates γ-secretase cleavage activity.[73] Finally, HM13 was identified as a TAP prey for all ADGR_CTFs. It is an activa-

tor for PSEN1 and thereby promotes γ-secretase cleavage.[43]

In any case, our TAP data revealing the interaction of ADGR with the γ-secretase complex pave the way for further investigations to identify the role of this interplay. Interestingly, the γ-secretase complex is not only present in the plasma membrane but is even more prominently associated with internal cell membranes, such as the ER or MAMs.[38–40]

Evidence for association of ADGRs with MAMs and participation at biogenesis of mitochondria

In the present TAPs, we identified many proteins known to locate mainly to specific intracellular compartments, such as the ER and mitochondria. The high number of molecules related to intracellular compartments suggests novel roles of ADGRs in the cell that have not been described so far. In particular, we found various proteins located at contact sites between the ER and mitochondria, namely the MAMs. Interestingly, the γ-secretase subunits PSEN2 and PSEN1 are enriched in this compartment. Besides γ-secretase subunits, we identified the MAM protein SIGMAR1 as an interactor for all ADGRs analyzed. The present immunocytochemistry demonstrates partial colocalization of this MAM core protein with VLGR1. SIGMAR1 regulates ITP3R-dependent calcium efflux at the ER and the biogenesis of lipids.[74] The spatial regulation of calcium homeostasis and lipid biogenesis are both major processes associated with MAMs.[27,75] In addition, our analyses of TAPs indicate that all ADGRs interact with the voltage-dependent anion channels 1 and 2 (VDAC1 or VDAC2) that localize to the outer mitochondrial membrane and allow the exchange of small hydrophilic molecules.[76,77] It is conceivable that ADGRs assist in the function of the highly dynamic MAMs.[78]

Surprisingly, we identified various ADGR interactors that localize to the mitochondrial inner membrane. The majority of the identified mitochondrial proteins have very low occurrence in the CRAPome, indicating the specificity of their interaction with ADGRs. These TAP hits are subunits of the respiratory chain complexes I, III, and IV, as well as subunits of the F_0F_1 ATP synthase, all localizing to mitochondrial cristae (Fig. 4).[79,80] In

addition, we identified components of the MICOS complex, which is essential for cristae formation,[35] and proteins that are involved in complex assembly of the respiratory chain. Furthermore, we found inner and outer membrane translocases (TIMs and TOMs), which are essential for transmembrane translocations.

ADGRs have not been found in mitoproteomes so far.[81,82] However, a previous report indicated a substantial role of GPR126, a group VII ADGR, in the biogenesis of mitochondria.[6] GPR126 deficiency results in mitochondrial defects in the developing heart of mice. These defects manifest in defective differentiation of mitochondrial cristae. The present identification of putative ADGR interactors that are localized to cristae or support the formation of cristae suggests that ADGRs may regulate the biogenesis of mitochondria in general. Patra *et al.*[6] also observed the accumulation of lipids in *Gpr126*$^{-/-}$ cardiomyocytes, indicating defective lipid metabolism. This is in line with a function of ADGRs in MAMs, which are very important for lipid biogenesis and represent sites of constant lipid exchange.

It is noteworthy that the respiratory chain subunits that we identified are all transcribed in the nucleus and have to be imported into mitochondria. There is growing evidence that MAMs play an essential role in this translocation processes. Based on our findings, we hypothesize that ADGRs are part of the dynamic MAMs and participate in the control of the delivery of mitochondrial components into mitochondria during mitochondrial biogenesis. For this, they may interact only transiently with mitochondrial proteins, which may also explain why ADGRs are not present in the existing mitoproteomes.

TAP data indicate regulation of ADGRs by phosphorylation

The identification of diverse kinases and phosphatases in the present TAPs (Table 1) indicates that both kinases and phosphatases bind to ADGRs. ADGRs may serve as scaffolds for these enzymes. Alternatively, they may regulate the ADGR function by the yin and yang of protein phosphorylation and dephosphorylation. The latter hypothesis is supported by previous data demonstrating that extracellular domain phosphorylation may facilitate ADGR signaling.[12] However, most putative phosphorylation sites have been identified in the ICD of ADGRs.[12] This is also in line with the predicted phosphorylation sites of all kinases identified by the present TAPs. The phosphorylation of residues in the PBMs of the ICD may regulate the binding to PDZ domains of diverse scaffold proteins also identified as potential interactors in the present study (see above). Such regulation has recently been described for the binding of CD97 to one of the PDZ domains of the DLG1 scaffold protein triggered by the phosphorylation of the C-terminal PBM of CD97.[52] This mechanism might be a general mechanism for the regulation of PBM and PDZ domain interaction.

It is notable that we did not identify any member of the GPCR kinase (GRK) family by TAPs. GRKs phosphorylate activated canonical GPCRs, which promotes the binding of arrestins, precluding further G protein coupling.[83] GRKs phosphorylate GPCRs usually at serine, threonine, or tyrosine residues present in the third intracellular loop of the 7TM domain and the ICD. However, GRKs for ADGR phosphorylation have not been identified so far. Therefore, the absence of GRKs in our TAPs can be due to the fact that we did not stimulate the ADGRs in our TAPs or that indeed no GRKs exist for ADGRs.

The identified kinases are part of signaling pathways, which may be related to ADGR. For example, MAPK1 and MAPK3 (also known as extracellular signal–regulated kinases (ERK1/2)) are central kinases of the ERK pathway that plays an important role in integrating external signals into signaling events promoting cell growth and proliferation in many mammalian cell types.[84] One of the targets of the MAPK/ERK kinase cascade is another identified kinase, CDK4, which controls the G_1-S phase in the cell cycle. The elucidation of the role of ADGRs and their putative interacting kinases in signaling pathways has to be reserved for future experimental investigations.

ADGRs interact with Wnt/planar cell polarity signaling proteins

Our TAP data provide several lines of evidence that ADGRs are modulators of Wnt signaling. This is in line with previous reports describing crosstalk between the Wnt and ADGR pathways, which focused on GPR124 and GPR125.[85–89] In particular for GPR124, it has been shown that this

interplay facilates angiogenesis in the central nervous system.[86,89–91] Since ADGRs and their interacting partners (e.g., synaptic scaffold proteins, see above) are localized at both the pre- and postsynapse, it is conceivable that ADGRs act together with WLS in the transsynaptic translocation of the Wnt1 ligand.[92]

Other Wnt-related interactors identified in TAPs differ between the ADGRs analyzed. However, all Wnt-related interactors indicate a modulating role in Wnt signaling. The most Wnt-related preys were identified in TAPs with VLGR1 constructs. These include molecules previously linked to Wnt signaling, such as ATP6AP2 and PTK7. As a planar cell polarity (PCP) core protein, ATP6AP2 also interacts with another ADGR, namely CELSR1.[93–95] PTK7 is a regulator of both canonical and noncanonical (PCP) Wnt signaling, and like VLGR1 it is essential for hair cell development in the cochlea.[96–98]

For GPR124_CTF and VLGR1_CTF, we also identified SLC30A9, which directly interacts with β-catenin and is part of a complex that activates Wnt-responsive gene transcription.[99,100] Importantly, the transcriptional regulator FHL2, which we found in the VLGR1_ICD dataset, is part of the same complex. Moreover, GPR124_CTF and BAI2_CTF interacted with AMER1, which negatively regulates Wnt signaling by promoting β-catenin degradation.[101,102] Two additional proteins identified in our TAP datasets, namely NONO and SFPQ, further support the relevance of this finding. The transcriptional activator NONO, which colocalizes with AMER1 at nuclear speckles,[99] was found in TAPs of BAI2_CTF. SFPQ, which forms heterodimers with NONO,[103,104] was found in both the GPR124_CTF and BAI2_CTF datasets.

In summary, our data support the prominent role of GPR124 in the regulation of the Wnt signaling pathway.[86,89–91] In addition, our findings indicate that the crosstalk of ADGRs and Wnt signaling is not only restricted to GPR124 or GPR125[85] but may also be mediated by other ADGRs, namely VLGR1 and BAI2.

Concluding remarks

In conclusion, we identified protein networks related to ADGRs by an affinity capture approach. Our data not only support previous findings but also reveal novel molecular relationships, which

suggest novel cellular functions for ADGRs. Our data demonstrate that ADGRs of groups I, II, III, VII, and IX are involved in synaptic processes and are modulators of Wnt signaling. In addition, we found evidence for an association of ADGRs with the γ-secretase complex and cleavage of their ICDs, which may act in transcriptional regulation in the nucleus. Whether ADGRs are substrates of the γ-secretase or other proteases remains to be determined. Moreover, our data indicate that ADGRs may have novel roles associated with the intracellular membranes of the ER and mitochondria, and in particular with the joint protein complexes of the MAMs. In any case, we regard the outcome of the present study as springboard for future investigations that should be carried out in order to understand the complex function of ADGRs in health and disease.

Acknowledgments

Author contributions

B.K. conducted most of the experiments, analyzed data, and prepared most of the figures for publication. J.R. performed sets of tandem affinity purifications. J.K. contributed to experiments analyzing γ-secretase and MAM complexes. K.B., N.H., and M.U. carried out mass spectrometry analysis and analyzed data. B.K. and U.W. designed the studies and wrote the manuscript. All authors read, contributed to, and approved the final manuscript.

Supporting information

Additional supporting information may be found in the online version of this article.

Table S1. Overlap all ADGRs ClueGO results.xls

Table S2. Occurrence of mitochondrial proteins in RAF1 TAPs.xls

Table S3. Overlap LPHN2 CD97 ClueGO results CRAPome cutout.xls

Figure S1. GO term enrichment analysis of ADGR_CTF TAP preys. GO term enrichment analysis in (a) the category *Cellular Component* and (b) the category *Biological Process* for prey proteins that are identical in all ADGR_CTF TAPs.

Figure S2. GO term enrichment analysis of LPHN2, CD97, and VLGR1 interactors. (a) 196 TAP preys are identical for LPHN2, CD97, and VLGR1 CTFs. (b) GO term enrichment analysis in the category *Cellular Component* and (c) the category *Biological Process* for all 196 proteins.

Competing interests

The authors declare no competing interests.

References

1. Hamann, J. & A.G. Petrenko. 2016. Introduction: history of the adhesion GPCR field. *Handb. Exp. Pharmacol.* **234:** 1–11.

2. Hamann, J., G. Aust, D. Arac, *et al.* 2015. International Union of Basic and Clinical Pharmacology. XCIV. Adhesion G protein-coupled receptors. *Pharmacol. Rev.* **67:** 338–367.

3. Arac, D., A.A. Boucard, M.F. Bolliger, *et al.* 2012. A novel evolutionarily conserved domain of cell-adhesion GPCRs mediates autoproteolysis. *EMBO J.* **31:** 1364–1378.

4. Yona, S., H.H. Lin, W.O. Siu, *et al.* 2008. Adhesion-GPCRs: emerging roles for novel receptors. *Trends Biochem. Sci.* **33:** 491–500.

5. Promel, S., M. Frickenhaus, S. Hughes, *et al.* 2012. The GPS motif is a molecular switch for bimodal activities of adhesion class G protein-coupled receptors. *Cell Rep.* **2:** 321–331.

6. Patra, C., M.J. van Amerongen, S. Ghosh, *et al.* 2013. Organ-specific function of adhesion G protein-coupled receptor GPR126 is domain-dependent. *Proc. Natl. Acad. Sci. USA* **110:** 16898–16903.

7. Okajima, D., G. Kudo & H. Yokota. 2010. Brain-specific angiogenesis inhibitor 2 (BAI2) may be activated by proteolytic processing. *J. Recept. Signal Transduct. Res.* **30:** 143–153.

8. Paavola, K.J., J.R. Stephenson, S.L. Ritter, *et al.* 2011. The N terminus of the adhesion G protein-coupled receptor GPR56 controls receptor signaling activity. *J. Biol. Chem.* **286:** 28914–28921.

9. Ward, Y., R. Lake, J.J. Yin, C.D. Heger, *et al.* 2011. LPA receptor heterodimerizes with CD97 to amplify LPA-initiated RHO-dependent signaling and invasion in prostate cancer cells. *Cancer Res.* **71:** 7301–7311.

10. Stephenson, J.R., K.J. Paavola, S.A. Schaefer, *et al.* 2013. Brain-specific angiogenesis inhibitor-1 signaling, regulation, and enrichment in the postsynaptic density. *J. Biol. Chem.* **288:** 22248–22256.

11. Paavola, K.J. & R.A. Hall. 2012. Adhesion G protein-coupled receptors: signaling, pharmacology, and mechanisms of activation. *Mol. Pharmacol.* **82:** 777–783.

12. Langenhan, T., G. Aust & J. Hamann. 2013. Sticky signaling—adhesion class G protein-coupled receptors take the stage. *Sci. Signal.* **6:** re3.

13. Liebscher, I., J. Schon, S.C. Petersen, *et al.* 2014. A tethered agonist within the ectodomain activates the adhesion G protein-coupled receptors GPR126 and GPR133. *Cell Rep.* **9:** 2018–2026.

14. Liebscher, I. & T. Schoneberg. 2016. Tethered agonism: a common activation mechanism of adhesion GPCRs. *Handb. Exp. Pharmacol.* **234:** 111–125.

15. Kishore, A. & R.A. Hall. 2016. Versatile signaling activity of adhesion GPCRs. *Handb. Exp. Pharmacol.* **234:** 127–146.

16. Purcell, R.H. & R.A. Hall. 2018. Adhesion G protein-coupled receptors as drug targets. *Annu. Rev. Pharmacol. Toxicol.* **58:** 429–449.

17. Knapp, B. & U. Wolfrum. 2016. Adhesion GPCR-related protein networks. *Handb. Exp. Pharmacol.* **234:** 147–178.

18. Gloeckner, C.J., K. Boldt & M. Ueffing. 2009. Strep/FLAG tandem affinity purification (SF-TAP) to study protein interactions. *Curr. Protoc. Protein Sci.* Chapter 19: Unit19 20. http://doi.org/10.1002/0471140864.ps1920s57.

19. Boldt, K., J. van Reeuwijk, Q. Lu, *et al.* 2016. An organelle-specific protein landscape identifies novel diseases and molecular mechanisms. *Nat. Commun.* **7:** 11491.

20. Daulat, A.M., P. Maurice, C. Froment, *et al.* 2007. Purification and identification of G protein-coupled receptor protein complexes under native conditions. *Mol. Cell. Proteomics* **6:** 835–844.

21. Atwood, B.K., J. Lopez, J. Wager-Miller, *et al.* 2011. Expression of G protein-coupled receptors and related proteins in HEK293, AtT20, BV2, and N18 cell lines as revealed by microarray analysis. *BMC Genomics* **12:** 14.

22. Gloeckner, C.J., K. Boldt, A. Schumacher, *et al.* 2007. A novel tandem affinity purification strategy for the efficient isolation and characterisation of native protein complexes. *Proteomics* **7:** 4228–4234.

23. Mellacheruvu, D., Z. Wright, A.L. Couzens, *et al.* 2013. The CRAPome: a contaminant repository for affinity purification-mass spectrometry data. *Nat. Methods* **10:** 730–736.

24. Adler, J. & I. Parmryd. 2010. Quantifying colocalization by correlation: the Pearson correlation coefficient is superior to the Mander's overlap coefficient. *Cytometry A* **77:** 733–742.

25. Bhatia, V.N., D.H. Perlman, C.E. Costello & M.E. McComb. 2009. Software tool for researching annotations of proteins: open-source protein annotation software with data visualization. *Anal. Chem.* **81:** 9819–9823.

26. Bindea, G., B. Mlecnik, H. Hackl, *et al.* 2009. ClueGO: a Cytoscape plug-in to decipher functionally grouped gene

ontology and pathway annotation networks. *Bioinformatics* **25:** 1091–1093.

27. Vance, J.E. 2014. MAM (mitochondria-associated membranes) in mammalian cells: lipids and beyond. *Biochim. Biophys. Acta* **1841:** 595–609.

28. Clemente, P., S. Peralta, A. Cruz-Bermudez, *et al.* 2013. hCOA3 stabilizes cytochrome c oxidase 1 (COX1) and promotes cytochrome c oxidase assembly in human mitochondria. *J. Biol. Chem.* **288:** 8321–8331.

29. Molina-Gomes, D., N. Bonnefoy, V.C. Nguyen, *et al.* 1995. The OXA1L gene that controls cytochrome oxidase assembly maps to the 14q11.2 region of the human genome. *Genomics* **30:** 396–398.

30. Mick, D.U., S. Dennerlein, H. Wiese, *et al.* 2012. MITRAC links mitochondrial protein translocation to respiratory-chain assembly and translational regulation. *Cell* **151:** 1528–1541.

31. Saada, A., S. Edvardson, M. Rapoport, *et al.* 2008. C6ORF66 is an assembly factor of mitochondrial complex I. *Am. J. Hum. Genet.* **82:** 32–38.

32. Saada, A., R.O. Vogel, S.J. Hoefs, *et al.* 2009. Mutations in NDUFAF3 (C3ORF60), encoding an NDUFAF4 (C6ORF66)-interacting complex I assembly protein, cause fatal neonatal mitochondrial disease. *Am. J. Hum. Genet.* **84:** 718–727.

33. Heide, H., L. Bleier, M. Steger, *et al.* 2012. Complexome profiling identifies TMEM126B as a component of the mitochondrial complex I assembly complex. *Cell Metab.* **16:** 538–549.

34. Moran, M., L. Marin-Buera, M.C. Gil-Borlado, *et al.* 2010. Cellular pathophysiological consequences of BCS1L mutations in mitochondrial complex III enzyme deficiency. *Hum. Mutat.* **31:** 930–941.

35. van der Laan, M., S.E. Horvath & N. Pfanner. 2016. Mitochondrial contact site and cristae organizing system. *Curr. Opin. Cell Biol.* **41:** 33–42.

36. Stiburek, L., J. Cesnekova, O. Kostkova, *et al.* 2012. YME1L controls the accumulation of respiratory chain subunits and is required for apoptotic resistance, cristae morphogenesis, and cell proliferation. *Mol. Biol. Cell* **23:** 1010–1023.

37. Cipolat, S., T. Rudka, D. Hartmann, *et al.* 2006. Mitochondrial rhomboid PARL regulates cytochrome c release during apoptosis via OPA1-dependent cristae remodeling. *Cell* **126:** 163–175.

38. Pinho, C.M., P.F. Teixeira & E. Glaser. 2014. Mitochondrial import and degradation of amyloid-β peptide. *Biochim. Biophys. Acta* **1837:** 1069–1074.

39. Schreiner, B., L. Hedskog, B. Wiehager & M. Ankarcrona. 2015. Amyloid-β peptides are generated in mitochondria-associated endoplasmic reticulum membranes. *J. Alzheimers Dis.* **43:** 369–374.

40. Leal, N.S., B. Schreiner, C.M. Pinho, *et al.* 2016. Mitofusin-2 knockdown increases ER–mitochondria contact and decreases amyloid β-peptide production. *J. Cell. Mol. Med.* **20:** 1686–1695.

41. Zhou, S., H. Zhou, P.J. Walian & B.K. Jap. 2005. CD147 is a regulatory subunit of the gamma-secretase complex

in Alzheimer's disease amyloid beta-peptide production. *Proc. Natl. Acad. Sci. USA* **102:** 7499–7504.

42. Weihofen, A., K. Binns, M.K. Lemberg, *et al.* 2002. Identification of signal peptide peptidase, a presenilin-type aspartic protease. *Science* **296:** 2215–2218.

43. Moliaka, Y.K., A. Grigorenko, D. Madera & E.I. Rogaev. 2004. Impas 1 possesses endoproteolytic activity against multipass membrane protein substrate cleaving the presenilin 1 holoprotein. *FEBS Lett.* **557:** 185–192.

44. Langosch, D., C. Scharnagl, H. Steiner & M.K. Lemberg. 2015. Understanding intramembrane proteolysis: from protein dynamics to reaction kinetics. *Trends Biochem. Sci.* **40:** 318–327.

45. Tomson, B.N. & K.M. Arndt. 2013. The many roles of the conserved eukaryotic Paf1 complex in regulating transcription, histone modifications, and disease states. *Biochim. Biophys. Acta* **1829:** 116–126.

46. Kosugi, S., M. Hasebe, M. Tomita & H. Yanagawa. 2009. Systematic identification of cell cycle-dependent yeast nucleocytoplasmic shuttling proteins by prediction of composite motifs. *Proc. Natl. Acad. Sci. USA* **106:** 10171–10176.

47. Chen, Y.H., C.K. Yang, M. Xia, *et al.* 2007. Role of GAC63 in transcriptional activation mediated by beta-catenin. *Nucleic Acids Res.* **35:** 2084–2092.

48. Reiners, J., E. van Wijk, T. Marker, *et al.* 2005. Scaffold protein harmonin (USH1C) provides molecular links between Usher syndrome type 1 and type 2. *Hum. Mol. Genet.* **14:** 3933–3943.

49. van Wijk, E., B. van der Zwaag, T. Peters, *et al.* 2006. The DFNB31 gene product whirlin connects to the Usher protein network in the cochlea and retina by direct association with USH2A and VLGR1. *Hum. Mol. Genet.* **15:** 751–765.

50. Reiners, J., K. Nagel-Wolfrum, K. Jurgens, *et al.* 2006. Molecular basis of human Usher syndrome: deciphering the meshes of the Usher protein network provides insights into the pathomechanisms of the Usher disease. *Exp. Eye Res.* **83:** 97–119.

51. Yamamoto, Y., K. Irie, M. Asada, *et al.* 2004. Direct binding of the human homologue of the *Drosophila* disc large tumor suppressor gene to seven-pass transmembrane proteins, tumor endothelial marker 5 (TEM5), and a novel TEM5-like protein. *Oncogene* **23:** 3889–3897.

52. Hilbig, D., D. Sittig, F. Hoffmann, *et al.* 2018. Mechano-dependent phosphorylation of the PDZ-binding motif of CD97/ADGRE5 modulates cellular detachment. *Cell Rep.* **24:** 1986–1995.

53. Langenhan, T., X. Piao & K.R. Monk. 2016. Adhesion G protein-coupled receptors in nervous system development and disease. *Nat. Rev. Neurosci.* **17:** 550–561.

54. Wu, H., C. Reissner, S. Kuhlendahl, *et al.* 2000. Intramolecular interactions regulate SAP97 binding to GKAP. *EMBO J.* **19:** 5740–5751.

55. Stephenson, J.R., R.H. Purcell & R.A. Hall. 2014. The BAI subfamily of adhesion GPCRs: synaptic regulation and beyond. *Trends Pharmacol. Sci.* **35:** 208–215.

56. Washbourne, P., X.B. Liu, E.G. Jones & A.K. McAllister. 2004. Cycling of NMDA receptors during trafficking in

neurons before synapse formation. *J. Neurosci.* **24:** 8253–8264.

57. Silva, J.P., V.G. Lelianova, Y.S. Ermolyuk, *et al.* 2011. Latrophilin 1 and its endogenous ligand Lasso/teneurin-2 form a high-affinity transsynaptic receptor pair with signaling capabilities. *Proc. Natl. Acad. Sci. USA* **108:** 12113–12118.

58. O'Sullivan, M.L., J. de Wit, J.N. Savas, *et al.* 2012. FLRT proteins are endogenous latrophilin ligands and regulate excitatory synapse development. *Neuron* **73:** 903–910.

59. Specht, D., S.B. Wu, P. Turner, *et al.* 2009. Effects of presynaptic mutations on a postsynaptic Cacna1s calcium channel colocalized with mGluR6 at mouse photoreceptor ribbon synapses. *Invest. Ophthalmol. Vis. Sci.* **50:** 505–515.

60. Sando, R., E. Bushong, Y. Zhu, *et al.* 2017. Assembly of excitatory synapses in the absence of glutamatergic neurotransmission. *Neuron* **94:** 312–321.e313.

61. Duman, J.G., C.P. Tzeng, Y.K. Tu, *et al.* 2013. The adhesion-GPCR BAI1 regulates synaptogenesis by controlling the recruitment of the Par3/Tiam1 polarity complex to synaptic sites. *J. Neurosci.* **33:** 6964–6978.

62. Kreienkamp, H.J., H. Zitzer, E.D. Gundelfinger, *et al.* 2000. The calcium-independent receptor for alpha-latrotoxin from human and rodent brains interacts with members of the ProSAP/SSTRIP/Shank family of multidomain proteins. *J. Biol. Chem.* **275:** 32387–32390.

63. O'Brien, R.J. & P.C. Wong. 2011. Amyloid precursor protein processing and Alzheimer's disease. *Annu. Rev. Neurosci.* **34:** 185–204.

64. Haapasalo, A. & D.M. Kovacs. 2011. The many substrates of presenilin/γ-secretase. *J. Alzheimers Dis.* **25:** 3–28.

65. Merrick, D., H. Chapin, J.E. Baggs, *et al.* 2012. The γ-secretase cleavage product of polycystin-1 regulates TCF and CHOP-mediated transcriptional activation through a p300-dependent mechanism. *Dev. Cell* **22:** 197–210.

66. Qian, F., A. Boletta, A.K. Bhunia, *et al.* 2002. Cleavage of polycystin-1 requires the receptor for egg jelly domain and is disrupted by human autosomal-dominant polycystic kidney disease 1-associated mutations. *Proc. Natl. Acad. Sci. USA* **99:** 16981–16986.

67. Yu, S., K. Hackmann, J. Gao, *et al.* 2007. Essential role of cleavage of polycystin-1 at G protein-coupled receptor proteolytic site for kidney tubular structure. *Proc. Natl. Acad. Sci. USA* **104:** 18688–18693.

68. Chauvet, V., X. Tian, H. Husson, *et al.* 2004. Mechanical stimuli induce cleavage and nuclear translocation of the polycystin-1 C terminus. *J. Clin. Invest.* **114:** 1433–1443.

69. Low, S.H., S. Vasanth, C.H. Larson, *et al.* 2006. Polycystin-1, STAT6, and P100 function in a pathway that transduces ciliary mechanosensation and is activated in polycystic kidney disease. *Dev. Cell* **10:** 57–69.

70. Luo, R., S.J. Jeong, Z. Jin, *et al.* 2011. G protein-coupled receptor 56 and collagen III, a receptor-ligand pair, regulates cortical development and lamination. *Proc. Natl. Acad. Sci. USA* **108:** 12925–12930.

71. Karpus, O.N., H. Veninga, R.M. Hoek, *et al.* 2013. Shear stress-dependent downregulation of the adhesion-G protein-coupled receptor CD97 on circulating leukocytes

72. upon contact with its ligand CD55. *J. Immunol.* **190:** 3740–3748.

73. Scholz, N., J. Gehring, C. Guan, *et al.* 2015. The adhesion GPCR latrophilin/CIRL shapes mechanosensation. *Cell Rep.* **11:** 866–874.

74. Chen, F., H. Hasegawa, G. Schmitt-Ulms, *et al.* 2006. TMP21 is a presenilin complex component that modulates gamma-secretase but not epsilon-secretase activity. *Nature* **440:** 1208–1212.

75. Pal, A., D. Fontanilla, A. Gopalakrishnan, *et al.* 2012. The sigma-1 receptor protects against cellular oxidative stress and activates antioxidant response elements. *Eur. J. Pharmacol.* **682:** 12–20.

76. Krols, M., G. van Isterdael, B. Asselbergh, *et al.* 2016. Mitochondria-associated membranes as hubs for neurodegeneration. *Acta Neuropathol. (Berl.)* **131:** 505–523.

77. Szabadkai, G., K. Bianchi, P. Varnai, *et al.* 2006. Chaperone-mediated coupling of endoplasmic reticulum and mitochondrial Ca^{2+} channels. *J. Cell Biol.* **175:** 901–911.

78. Rostovtseva, T.K., W. Tan & M. Colombini. 2005. On the role of VDAC in apoptosis: fact and fiction. *J. Bioenerg. Biomembr.* **37:** 129–142.

79. Tagaya, M. & K. Arasaki. 2017. Regulation of mitochondrial dynamics and autophagy by the mitochondria-associated membrane. *Adv. Exp. Med. Biol.* **997:** 33–47.

80. Scorrano, L., M. Ashiya, K. Buttle, *et al.* 2002. A distinct pathway remodels mitochondrial cristae and mobilizes cytochrome c during apoptosis. *Dev. Cell* **2:** 55–67.

81. Gilkerson, R.W., J.M. Selker & R.A. Capaldi. 2003. The cristal membrane of mitochondria is the principal site of oxidative phosphorylation. *FEBS Lett.* **546:** 355–358.

82. Cotter, D., P. Guda, E. Fahy & S. Subramaniam. 2004. MitoProteome: mitochondrial protein sequence database and annotation system. *Nucleic Acids Res.* **32:** D463–D467.

83. Calvo, S.E., K.R. Clauser & V.K. Mootha. 2016. MitoCarta2.0: an updated inventory of mammalian mitochondrial proteins. *Nucleic Acids Res.* **44:** D1251–D1257.

84. Pierce, K.L., R.T. Premont & R.J. Lefkowitz. 2002. Seven-transmembrane receptors. *Nat. Rev. Mol. Cell Biol.* **3:** 639–650.

85. Yoon, S. & R. Seger. 2006. The extracellular signal-regulated kinase: multiple substrates regulate diverse cellular functions. *Growth Factors* **24:** 21–44.

86. Li, X., I. Roszko, D.S. Sepich, *et al.* 2013. Gpr125 modulates Dishevelled distribution and planar cell polarity signaling. *Development* **140:** 3028–3039.

87. Zhou, Y. & J. Nathans. 2014. Gpr124 controls CNS angiogenesis and blood–brain barrier integrity by promoting ligand-specific canonical wnt signaling. *Dev. Cell* **31:** 248–256.

88. Li, Q., A. Kannan, A. Das, *et al.* 2013. WNT4 acts downstream of BMP2 and functions via β-catenin signaling pathway to regulate human endometrial stromal cell differentiation. *Endocrinology* **154:** 446–457.

89. Morgan, R., A.M. El-Kadi & C. Theokli. 2003. Flamingo, a cadherin-type receptor involved in the Drosophila planar polarity pathway, can block signaling via the canonical wnt pathway in *Xenopus laevis*. *Int. J. Dev. Biol.* **47:** 245–252.

89. Posokhova, E., A. Shukla, S. Seaman, *et al.* 2015. GPR124 functions as a WNT7-specific coactivator of canonical β-catenin signaling. *Cell Rep.* **10:** 123–130.

90. Vanhollebeke, B., O.A. Stone, N. Bostaille, *et al.* 2015. Tip cell-specific requirement for an atypical Gpr124- and Reck-dependent Wnt/β-catenin pathway during brain angiogenesis. *elife* **4**. http://doi.org/10.7554/eLife.06489.

91. Cho, C., P.M. Smallwood & J. Nathans. 2017. Reck and Gpr124 are essential receptor cofactors for Wnt7a/Wnt7b-specific signaling in mammalian CNS angiogenesis and blood–brain barrier regulation. *Neuron* **95:** 1056–1073.e1055.

92. Korkut, C., B. Ataman, P. Ramachandran, *et al.* 2009. Trans-synaptic transmission of vesicular Wnt signals through Evi/Wntless. *Cell* **139:** 393–404.

93. Buechling, T., K. Bartscherer, B. Ohkawara, *et al.* 2010. Wnt/Frizzled signaling requires dPRR, the *Drosophila* homolog of the prorenin receptor. *Curr. Biol.* **20:** 1263–1268.

94. Hermle, T., M.C. Guida, S. Beck, *et al.* 2013. *Drosophila* ATP6AP2/VhaPRR functions both as a novel planar cell polarity core protein and a regulator of endosomal trafficking. *EMBO J.* **32:** 245–259.

95. Schafer, S.T., J. Han, M. Pena, *et al.* 2015. The Wnt adaptor protein ATP6AP2 regulates multiple stages of adult hippocampal neurogenesis. *J. Neurosci.* **35:** 4983–4998.

96. Lee, J., A. Andreeva, C.W. Sipe, *et al.* 2012. PTK7 regulates myosin II activity to orient planar polarity in the mammalian auditory epithelium. *Curr. Biol.* **22:** 956–966.

97. McGee, J., R.J. Goodyear, D.R. McMillan, *et al.* 2006. The very large G-protein-coupled receptor VLGR1: a component of the ankle link complex required for the normal development of auditory hair bundles. *J. Neurosci.* **26:** 6543–6553.

98. Michalski, N., V. Michel, A. Bahloul, *et al.* 2007. Molecular characterization of the ankle-link complex in cochlear hair cells and its role in the hair bundle functioning. *J. Neurosci.* **27:** 6478–6488.

99. Rivera, M.N., W.J. Kim, J. Wells, *et al.* 2009. The tumor suppressor WTX shuttles to the nucleus and modulates WT1 activity. *Proc. Natl. Acad. Sci. USA* **106:** 8338–8343.

100. Wei, Y., C.A. Renard, C. Labalette, *et al.* 2003. Identification of the LIM protein FHL2 as a coactivator of beta-catenin. *J. Biol. Chem.* **278:** 5188–5194.

101. Grohmann, A., K. Tanneberger, A. Alzner, *et al.* 2007. AMER1 regulates the distribution of the tumor suppressor APC between microtubules and the plasma membrane. *J. Cell Sci.* **120:** 3738–3747.

102. Major, M.B., N.D. Camp, J.D. Berndt, *et al.* 2007. Wilms tumor suppressor WTX negatively regulates WNT/beta-catenin signaling. *Science* **316:** 1043–1046.

103. Shav-Tal, Y. & D. Zipori. 2002. PSF and p54(nrb)/NonO—multi-functional nuclear proteins. *FEBS Lett.* **531:** 109–114.

104. Knott, G.J., C.S. Bond & A.H. Fox. 2016. The DBHS proteins SFPQ, NONO and PSPC1: a multipurpose molecular scaffold. *Nucleic Acids Res.* **44:** 3989–4004.

105. Lewin, T.M., C.G. Van Horn, S.K. Krisans & R.A. Coleman. 2002. Rat liver acyl-CoA synthetase 4 is a peripheral-membrane protein located in two distinct subcellular organelles, peroxisomes, and mitochondrial-associated membrane. *Arch. Biochem. Biophys.* **404:** 263–270.

106. Chiang, S.F., C.Y. Huang, T.Y. Lin, *et al.* 2012. An alternative import pathway of AIF to the mitochondria. *Int. J. Mol. Med.* **29:** 365–372.

107. Goetz, J.G., H. Genty, P. St-Pierre, *et al.* 2007. Reversible interactions between smooth domains of the endoplasmic reticulum and mitochondria are regulated by physiological cytosolic Ca^{2+} levels. *J. Cell Sci.* **120:** 3553–3564.

108. Iwasawa, R., A.L. Mahul-Mellier, C. Datler, *et al.* 2011. Fis1 and Bap31 bridge the mitochondria–ER interface to establish a platform for apoptosis induction. *EMBO J.* **30:** 556–568.

109. Hashimoto, T., R. Hussien & G.A. Brooks. 2006. Colocalization of MCT1, CD147, and LDH in mitochondrial inner membrane of L6 muscle cells: evidence of a mitochondrial lactate oxidation complex. *Am. J. Physiol. Endocrinol. Metab.* **290:** E1237–E1244.

110. Myhill, N., E.M. Lynes, J.A. Nanji, *et al.* 2008. The subcellular distribution of calnexin is mediated by PACS-2. *Mol. Biol. Cell* **19:** 2777–2788.

111. Wang, C.H., Y.F. Chen, C.Y. Wu, *et al.* 2014. Cisd2 modulates the differentiation and functioning of adipocytes by regulating intracellular Ca2$^+$ homeostasis. *Hum. Mol. Genet.* **23:** 4770–4785.

112. Browman, D.T., M.E. Resek, L.D. Zajchowski & S.M. Robbins. 2006. Erlin-1 and erlin-2 are novel members of the prohibitin family of proteins that define lipid-raft-like domains of the ER. *J. Cell Sci.* **119:** 3149–3160.

113. Gilady, S.Y., M. Bui, E.M. Lynes, *et al.* 2010. Ero1alpha requires oxidizing and normoxic conditions to localize to the mitochondria-associated membrane (MAM). *Cell Stress Chaperones* **15:** 619–629.

114. Stoica, R., S. Paillusson, P. Gomez-Suaga, *et al.* 2016. ALS/FTD-associated FUS activates GSK-3β to disrupt the VAPB–PTPIP51 interaction and ER–mitochondria associations. *EMBO Rep.* **17:** 1326–1342.

115. Bionda, C., J. Portoukalian, D. Schmitt, *et al.* 2004. Subcellular compartmentalization of ceramide metabolism: mAM (mitochondria-associated membrane) and/or mitochondria? *Biochem. J.* **382:** 527–533.

116. Lynes, E.M., M. Bui, M.C. Yap, *et al.* 2012. Palmitoylated TMX and calnexin target to the mitochondria-associated membrane. *EMBO J.* **31:** 457–470.

117. Hayashi, T. & T.P. Su. 2007. Sigma-1 receptor chaperones at the ER–mitochondrion interface regulate Ca(2$^+$) signaling and cell survival. *Cell* **131:** 596–610.

118. Kinoshita, T. & N. Inoue. 2000. Dissecting and manipulating the pathway for glycosylphos-phatidylinositol-anchor biosynthesis. *Curr. Opin. Chem. Biol.* **4:** 632–638.

119. Rusinol, A.E., Z. Cui, M.H. Chen & J.E. Vance. 1994. A unique mitochondria-associated membrane fraction from rat liver has a high capacity for lipid synthesis and contains pre-Golgi secretory proteins including nascent lipoproteins. *J. Biol. Chem.* **269:** 27494–27502.

120. Horner, S.M., H.M. Liu, H.S. Park, *et al.* 2011. Mitochondrial-associated endoplasmic reticulum membranes (MAM) form innate immune synapses and are

targeted by hepatitis C virus. *Proc. Natl. Acad. Sci. USA* **108:** 14590–14595.

121. Hoffstrom, B.G., A. Kaplan, R. Letso, *et al.* 2010. Inhibitors of protein disulfide isomerase suppress apoptosis induced by misfolded proteins. *Nat. Chem. Biol.* **6:** 900–906.

122. Area-Gomez, E., A.J. de Groof, I. Boldogh, *et al.* 2009. Presenilins are enriched in endoplasmic reticulum membranes associated with mitochondria. *Am. J. Pathol.* **175:** 1810–1816.

123. Stone, S.J. & J.E. Vance. 2000. Phosphatidylserine synthase-1 and -2 are localized to mitochondria-associated membranes. *J. Biol. Chem.* **275:** 34534–34540.

124. Saotome, M., D. Safiulina, G. Szabadkai, *et al.* 2008. Bidirectional Ca2+-dependent control of mitochondrial dynamics by the Miro GTPase. *Proc. Natl. Acad. Sci. USA* **105:** 20728–20733.

125. Hubner, C.A. & I. Kurth. 2014. Membrane-shaping disorders: a common pathway in axon degeneration. *Brain* **137:** 3109–3121.

126. Sutendra, G., P. Dromparis, P. Wright, *et al.* 2011. The role of Nogo and the mitochondria-endoplasmic reticulum unit in pulmonary hypertension. *Sci. Transl. Med.* **3:** 88ra55.

127. Man, W.C., M. Miyazaki, K. Chu & J. Ntambi. 2006. Colocalization of SCD1 and DGAT2: implying preference for endogenous monounsaturated fatty acids in triglyceride synthesis. *J. Lipid Res.* **47:** 1928–1939.

128. Jia, Z., Z. Pei, D. Maiguel, *et al.* 2007. The fatty acid transport protein (FATP) family: very long chain acyl-CoA synthetases or solute carriers? *J. Mol. Neurosci.* **33:** 25–31.

129. Pereira, L.A., M.P. Klejman & H.T. Timmers. 2003. Roles for BTAF1 and Mot1p in dynamics of TATA-binding protein and regulation of RNA polymerase II transcription. *Gene* **315:** 1–13.

130. Mitra, P., P.S. Vaughan, J.L. Stein, *et al.* 2001. Purification and functional analysis of a novel leucine-zipper/nucleotide-fold protein, BZAP45, stimulating cell cycle regulated histone H4 gene transcription. *Biochemistry* **40:** 10693–10699.

131. Hiraishi, H., J. Oatman, S.L. Haller, *et al.* 2014. Essential role of eIF5-mimic protein in animal development is linked to control of ATF4 expression. *Nucleic Acids Res.* **42:** 10321–10330.

132. Hutlet, B., N. Theys, C. Coste, *et al.* 2016. Systematic expression analysis of Hox genes at adulthood reveals novel patterns in the central nervous system. *Brain Struct. Funct.* **221:** 1223–1243.

133. Laduron, S., R. Deplus, S. Zhou, *et al.* 2004. MAGE-A1 interacts with adaptor SKIP and the deacetylase HDAC1 to repress transcription. *Nucleic Acids Res.* **32:** 4340–4350.

134. Ruvolo, V., E. Wang, S. Boyle & S. Swaminathan. 1998. The Epstein–Barr virus nuclear protein SM is both a post-transcriptional inhibitor and activator of gene expression. *Proc. Natl. Acad. Sci. USA* **95:** 8852–8857.

135. Taylor Clelland, C.L., B. Levy, J.M. McKie, *et al.* 2000. Cloning and characterization of human PREB; a gene that maps to a genomic region associated with trisomy 2p syndrome. *Mamm. Genome* **11:** 675–681.

136. Steen, H. & D. Lindholm. 2008. Nuclear localized protein-1 (Nulp1) increases cell death of human osteosarcoma

cells and binds the X-linked inhibitor of apoptosis protein. *Biochem. Biophys. Res. Commun.* **366:** 432–437.

137. Sheng, K., X. Liang, S. Huang & W. Xu. 2014. The role of histone ubiquitination during spermatogenesis. *Biomed. Res. Int.* **2014:** 870695.

138. Cojocaru, M., A. Bouchard, P. Cloutier, *et al.* 2011. Transcription factor IIS cooperates with the E3 ligase UBR5 to ubiquitinate the CDK9 subunit of the positive transcription elongation factor B. *J. Biol. Chem.* **286:** 5012–5022.

139. Muntean, A.G., J. Tan, K. Sitwala, *et al.* 2010. The PAF complex synergizes with MLL fusion proteins at HOX loci to promote leukemogenesis. *Cancer Cell* **17:** 609–621.

140. Garrett, K.P., T. Aso, J.N. Bradsher, *et al.* 1995. Positive regulation of general transcription factor SIII by a tailed ubiquitin homolog. *Proc. Natl. Acad. Sci. USA* **92:** 7172–7176.

141. Yang, Y., H. Hou, E.M. Haller, *et al.* 2005. Suppression of FOXO1 activity by FHL2 through SIRT1-mediated deacetylation. *EMBO J.* **24:** 1021–1032.

142. Rochman, M., Y. Postnikov, S. Correll, *et al.* 2009. The interaction of NSBP1/HMGN5 with nucleosomes in euchromatin counteracts linker histone-mediated chromatin compaction and modulates transcription. *Mol. Cell* **35:** 642–656.

143. Deak, M., A.D. Clifton, L.M. Lucocq & D.R. Alessi. 1998. Mitogen- and stress-activated protein kinase-1 (MSK1) is directly activated by MAPK and SAPK2/p38, and may mediate activation of CREB. *EMBO J.* **17:** 4426–4441.

144. Ouwens, D.M., N.D. de Ruiter, G.C. van der Zon, *et al.* 2002. Growth factors can activate ATF2 via a two-step mechanism: phosphorylation of Thr71 through the Ras-MEK-ERK pathway and of Thr69 through RalGDS-Src-p38. *EMBO J.* **21:** 3782–3793.

145. Fujimaki, K., T. Ogihara, D.L. Morris, *et al.* 2015. SET7/9 enzyme regulates cytokine-induced expression of inducible nitric-oxide synthase through methylation of lysine 4 at histone 3 in the islet β cell. *J. Biol. Chem.* **290:** 16607–16618.

146. Jesko, H. & R.P. Strosznajder. 2016. Sirtuins and their interactions with transcription factors and poly(ADP-ribose) polymerases. *Folia Neuropathol.* **54:** 212–233.

147. Pillutla, R.C., A. Shimamoto, Y. Furuichi & A.J. Shatkin. 1999. Genomic structure and chromosomal localization of TCEAL1, a human gene encoding the nuclear phosphoprotein p21/SIIR. *Genomics* **56:** 217–220.

148. Pfister, A.S., K. Tanneberger, A. Schambony & J. Behrens. 2012. Amer2 protein is a novel negative regulator of Wnt/β-catenin signaling involved in neuroectodermal patterning. *J. Biol. Chem.* **287:** 1734–1741.

149. Cruciat, C.M., B. Ohkawara, S.P. Acebron, *et al.* 2010. Requirement of prorenin receptor and vacuolar H+-ATPase-mediated acidification for Wnt signaling. *Science* **327:** 459–463.

150. Zilberberg, A., A. Yaniv & A. Gazit. 2004. The low density lipoprotein receptor-1, LRP1, interacts with the human frizzled-1 (HFz1) and down-regulates the canonical Wnt signaling pathway. *J. Biol. Chem.* **279:** 17535–17542.

151. Murayama, M., S. Tanaka, J. Palacino, *et al.* 1998. Direct association of presenilin-1 with beta-catenin. *FEBS Lett.* **433:** 73–77.

152. Bin-Nun, N., H. Lichtig, A. Malyarova, *et al.* 2014. PTK7 modulates Wnt signaling activity via LRP6. *Development* **141:** 410–421.

153. Tang, L.Y., N. Deng, L.S. Wang, *et al.* 2007. Quantitative phosphoproteome profiling of Wnt3a-mediated signaling network: indicating the involvement of ribonucleoside-diphosphate reductase M2 subunit phosphorylation at residue serine 20 in canonical Wnt signal transduction. *Mol. Cell. Proteomics* **6:** 1952–1967.

154. Latres, E., D.S. Chiaur & M. Pagano. 1999. The human F box protein beta-Trcp associates with the Cul1/Skp1 complex and regulates the stability of beta-catenin. *Oncogene* **18:** 849–854.

155. Hay-Koren, A., M. Caspi, A. Zilberberg & R. Rosin-Arbesfeld. 2011. The EDD E3 ubiquitin ligase ubiquitinates and up-regulates beta-catenin. *Mol. Biol. Cell* **22:** 399–411.

156. Lui, T.T., C. Lacroix, S.M. Ahmed, *et al.* 2011. The ubiquitin-specific protease USP34 regulates axin stability and Wnt/β-catenin signaling. *Mol. Cell. Biol.* **31:** 2053–2065.

157. Bartscherer, K., N. Pelte, D. Ingelfinger & M. Boutros. 2006. Secretion of Wnt ligands requires Evi, a conserved transmembrane protein. *Cell* **125:** 523–533.

Publikation II

Affinity Proteomics Identifies Interaction Partners and Defines Novel Insights into the Function of the Adhesion GPCR VLGR1/ADGRV1

Barbara Knapp [1], Jens Roedig [1], Heiko Roedig [1], Jacek Krzysko [1], Nicola Horn [2], Baran E. Güler [1], Deva Krupakar Kusuluri [1], Adem Yildirim [1], Karsten Boldt [2], Marius Ueffing [2], Ines Liebscher [3] and Uwe Wolfrum [1,*]

[1] Institute of Molecular Physiology (ImP), Molecular Cell Biology, Johannes Gutenberg University Mainz, 55128 Mainz, Germany; bknapp@web.de (B.K.); jens.roedig@live.de (J.R.); heiko.roedig@live.de (H.R.); jkrzysko@uni-mainz.de (J.K.); bgueler@uni-mainz.de (B.E.G.); deva.kusuluri@unige.ch (D.K.K.); yildadem@uni-mainz.de (A.Y.)

[2] Core Facility for Medical Bioanalytics, Institute for Ophthalmic Research, University of Tuebingen, 72076 Tuebingen, Germany; nicola.horn@medizin.uni-tuebingen.de (N.H.); karsten.boldt@uni-tuebingen.de (K.B.); marius.ueffing@uni-tuebingen.de (M.U.)

[3] Rudolf Schönheimer Institute of Biochemistry, Faculty of Medicine, Leipzig University, 04103 Leipzig, Germany; ines.liebscher@medizin.uni-leipzig.de

* Correspondence: wolfrum@uni-mainz.de

Abstract: The very large G-protein-coupled receptor 1 (VLGR1/ADGRV1) is the largest member of the adhesion G-protein-coupled receptor (ADGR) family. Mutations in VLGR1/ADGRV1 cause human Usher syndrome (USH), a form of hereditary deaf-blindness, and have been additionally linked to epilepsy. In the absence of tangible knowledge of the molecular function and signaling of VLGR1, the pathomechanisms underlying the development of these diseases are still unknown. Our study aimed to identify novel, previously unknown protein networks associated with VLGR1 in order to describe new functional cellular modules of this receptor. Using affinity proteomics, we have identified numerous new potential binding partners and ligands of VLGR1. Tandem affinity purification hits were functionally grouped based on their Gene Ontology terms and associated with functional cellular modules indicative of functions of VLGR1 in transcriptional regulation, splicing, cell cycle regulation, ciliogenesis, cell adhesion, neuronal development, and retinal maintenance. In addition, we validated the identified protein interactions and pathways in vitro and in situ. Our data provided new insights into possible functions of VLGR1, related to the development of USH and epilepsy, and also suggest a possible role in the development of other neuronal diseases such as Alzheimer's disease.

Keywords: adhesions GPCR; Usher syndrome; affinity proteomics; protein networks

1. Introduction

The longest isoform 1b of the very large G-protein-coupled receptor 1 (VLGR1/ADGRV1), also known as GPR98, MASS1, or FEB4, is the largest adhesion G-protein-coupled receptor (ADGR) in the human body (Figure 1a) [1–3]. Mutations in *VLGR1/ADGRV1* can manifest in two disease phenotypes. Most VLGR1 mutations are causative for the human Usher syndrome type 2C (USH2C) [4]. Usher syndrome (USH) is a severe genetically heterogenous autosomal recessive disorder and the most common cause of hereditary deaf-blindness [5,6]. There is growing evidence for a relation of haploinsufficiency of VLGR1 to epilepsy in humans [7–10]. This association with epilepsy is consistent with the audiogenic seizure phenotype in VLGR1 mutant mice [11–13].
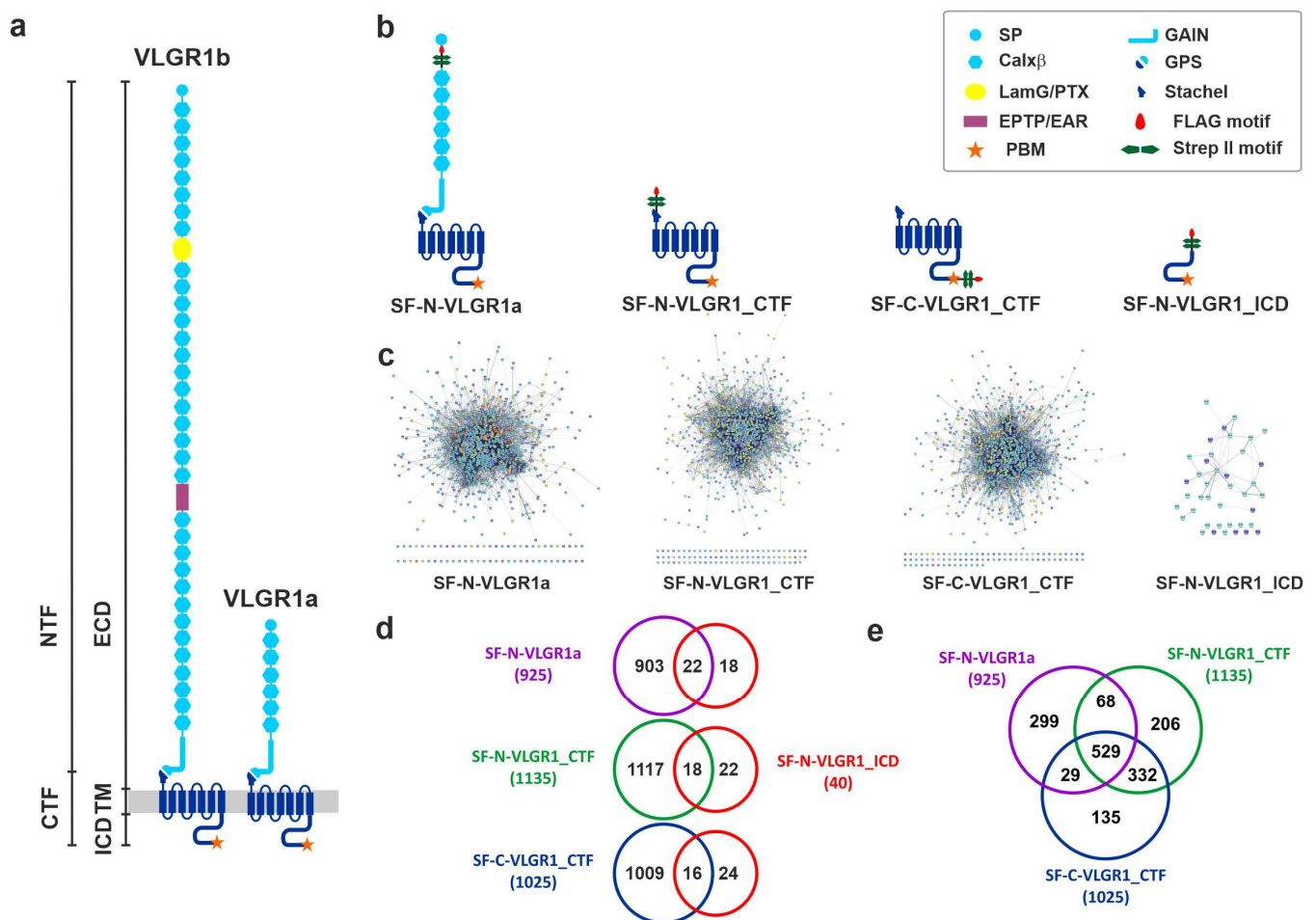
Figure 1. VLGR1 domain structures and VLGR1-associated protein networks. (**a**) The two long iso-forms of VLGR1, the full-length protein VLGR1b, and the shorter isoform VLGR1a can be autocleaved at the GPS (G-protein-coupled receptor proteolytic site) into the following fragments: N-terminal fragment (NTF) and the C-terminal fragment (CTF), which are composed of a short intracellular domain (ICD), the seven transmembrane domain (TM), and the long extracellular domain (ECD). (**b**) N- or C-terminally Strep II- FLAG (SF)-tagged VLGR1 constructs were used as baits. (**c**) Protein networks of prey identified with SF-N-VLGR1a (863 out of 925 prey proteins are interconnected, based on the STRING database (https://string-db.org/, accessed on 10 September 2017), SF-N-VLGR1_CTF (1054 out of 1135 prey proteins are interconnected), SF-C-VLGR1_CTF (939 of 1025 prey proteins are interconnected), and SF-N-VLGR1_ICD (29 out of 40 prey proteins are interconnected). (**d**,**e**) Venn diagrams of VLGR1 prey revealing overlaps between the interactomes found for the VLGR1 constructs.

VLGR1 is mainly expressed in the nervous system, with a strong expression in the eye and the inner ear [5,12,14–16]. In both sensory organs, the VLGR1 protein is found at the synapses of the sensory cells [17,18]. In inner ear hair cells, VLGR1 is an essential component of the ankle links, which connect neighboring stereocilia, and thereby stabilizes the nascent hair bundles of the cochlear during differentiation [14,16,19]. In the retinal photoreceptor cells, VLGR1 is also associated with fibrous connectors [20]. Here, the extremely long adhesive extracellular domain of VLGR1 spans between the membranes of the apical inner segment and of the connecting cilium of photoreceptor cells. In mice, defects in VLGR1 cause the disruption of the fibrous links and the membrane–membrane adhesion in both sensory cell types [14,20].

Similar to other ADGRs, VLGR1 possesses a unique structure (Figure 1a) characterized by the N-terminal extracellular domains (ECD) that mediate cell–cell or cell–matrix adhe-

sion, combined with a secretin-like GPCR moiety [3] that includes a seven transmembrane (7TM) domain and a cytoplasmic region. It is the N-terminus that mainly contributes to the enormous size of VLGR1, which can undergo alternative splicing, thus yielding also shorter variants such as VLGR1a (Figure 1) [2]. An important feature of ADGRs is their capability to be self-cleaved at the so-called G-protein-coupled receptor proteolysis site (GPS) [21], located close to the first of the seven transmembrane (7TM) domain and embedded in the GPCR autoproteolysis-inducing domain (GAIN) [22]. The two resulting fragments, an N-terminal (NTF) and a C-terminal fragment (CTF), mostly stay associated as a dimer. However, there is increasing evidence that the NTF and CTF can execute independent functions [23,24]. In particular, the expression of the NTF mediates a signal independent from the coupled G protein, while the CTF alone results in the increased activation of downstream signaling pathways compared to the full-length protein [25–28]. This is due to a tethered internal agonist that comprises the first 5–10 amino acids of the CTF, the so-called *Stachel* [29]. For some ADGRs, there is evidence that the release of the NTF triggers the binding of the *Stachel* peptide to the exoplasmic face of the ADGRs and, in consequence, induces the conformational changes, which allows the binding of ADGR effector proteins. In addition, there is also evidence for several ways of *Stachel*-independent receptor stimulation, proving that ADGR activation is complex and far away from being fully understood [30].

In any case, the active and inactive receptors most probably associate with different protein complexes enrolled in diverse functional modules. Previous analyses of the protein–protein interaction revealed that the cytoplasmic tail of VLGR1 binds through its PDZ-binding motive to the PDZ domains of USH-related scaffold proteins, namely whirlin (USH2D), harmonin (USH1C), and the USH genetic modifier PDZD7 [13]. These interactions also mediate the integration of VLGR1 into the USH-protein networks associated with membrane adhesion complexes. More recently, it became evident that defects in USH molecules lead to dysfunctions in primary cilia, which are regarded as the sensory antennae and signaling hub of the cell [31–34]. However, nothing is known about VLGR1 signaling in primary cilia [35]. In addition, two studies addressing VLGR1 signaling pathways reported contradictory pathways via $G\alpha_s/G\alpha_q$ and $G\alpha_i$, respectively [36,37].

Here, we aimed to identify novel proteins interacting with VLGR1 and thereby define signaling pathways, protein networks, and functional cell modules related to VLGR1. For this, we applied tandem affinity purifications (TAPs) coupled to mass spectrometry analysis using different fragments of VLGR1 as bait. We identified numerous putative novel complex partners, that we analyzed by bioinformatics tools to group the identified prey according to their GO terms, and preliminarily validated some of the interactions. Our analysis identifies VLGR1-related cell modules which shed light on possible cellular functions of VLGR1 including neural development, gene and cell cycle regulation, cell adhesion, and photoreceptor function.

2. Results and Discussion

2.1. Identification of Novel VLGR1 Protein Complex Partners by Tandem Affinity Purification (TAP)

To identify novel interactors of VLGR1 we applied affinity proteomics using TAPs [38]. We fused the tandem Strep II-FLAG (SF)-tag to the N-terminus of a full-length VLGR1a isoform, the N- and/or C-terminus of the C-terminal fragment (VLGR1_CTF), and the end of the C-terminus of the intracellular domain of VLGR1 (VLGR1_ICD) (Figure 1b). These SF-tagged baits were expressed in HEK293T cells and TAPs were performed. Eluted protein complexes were separated by liquid chromatography and their peptide content determined with tandem mass spectrometry (LC-MS/MS). To identify interacting proteins, we searched the raw spectra against SwissProt databases and verified the results applying the Scaffold program. All prey identified for the four different VLGR1 constructs as baits are listed in the Supplementary Table S1.

We identified ~1000 novel putative interacting partners of VLGR1 in TAPs with both VLGR1_CTFs and VLGR1a as baits. In contrast, only 40 hits were found in VLGR1_ICD CT

TAPs (Figure 1c). Half of the molecules identified in VLGR1_ICD TAPs were also found in TAPs with the longer constructs VLGR1_CTFs and VLGR1a (Figure 1d). Comparisons among TAP data sets between the two VLGR1_CTFs and VLGR1a revealed an intersection of over 500 (Figure 1e). However, our analyses also revealed high diversity in prey found in the different TAPs. The putative interaction partners belong to very heterogeneous protein groups and families that exert functions in diverse cellular compartments. This may reflect diverse functions of VLGR1 in different cellular contexts and/or may also depend on the activation state of VLGR1. This section may be divided by subheadings. It should provide a concise and precise description of the experimental results, their interpretation, as well as the experimental conclusions that can be drawn.

2.1.1. Specificity of TAP Hits

In order to gauge the reliability of the identified interaction partners, we compared our datasets to the *Contaminant Repository for Affinity Purifications*, short CRAPome, which contains a collection of common contaminants in affinity proteomics data sets [39]. About half of the identified VLGR1 prey occur in less than 5% of all protein listed in the CRAPome (corresponding to a cutout $\leq$20), which indicates a high degree of specificity.

A comparison of TAP hits with previously identified VLGR1 binding partners [35] confirmed the two USH scaffold proteins whirlin (DFNB31/USH2D) and harmonin (USH1C) as the binary binding partners of VLGR1 in VLGR1_ICD TAPs (Supplementary Table S1). We have also previously shown that VLGR1 directly binds with its PDZ-binding motif (PBM) in the C-terminal end of the VLGR1_ICD to one of the PDZ domains of the two scaffold proteins [15,17]. Although there is no doubt that we have also identified some false-positive interactors, our validation proves the specificity of selected interactions and confirms the suitability of our affinity capture approach for the identification of novel interactors of transmembrane receptor proteins, such as VLGR1.

2.1.2. Grouping and Categorizing of TAP Hits

We grouped and categorized TAP hits by Gene Ontology (GO) term enrichment analyses, applying the Cytoscape (http://www.cytoscape.org, accessed on 10 September 2017) plugin ClueGO [40] for all three GO term categories, *Biological Process, Cellular Component, and Molecular Function,* and, in addition, for *KEGG (Kyoto Encyclopedia of Genes and Genomes) pathways* (Supplementary Tables S2–S5). In our data sets, we found multiple, often unexpected, links to different cellular processes. Some of the most interesting connections are examined and discussed in the following.

2.2. VLGR1 G Protein Coupling Switches between $G\alpha_s$/$G\alpha_q$ and $G\alpha_i$

As expected for a GPCR, we identified in our VLGR1 TAPs several subunits of heterotrimeric G-proteins, namely Gβ1 (GNB1), Gβ2 (GNB2), Gαi3 (GNAI3), and Gαs (GNAS). Interestingly, we found the association of a full-length VLGR1a with Gαi and Gαs, respectively, whereas the VLGR1_CTFs only interacted with Gαi, which primarily inhibits the cAMP dependent pathway by inhibiting adenylyl cyclase activity, decreasing the production of cAMP and resulting in decreased activity of the cAMP-dependent protein kinase. To analyze the Gα coupling of VLGR1 in more depth, we first measured the concentration of the second messenger cAMP in HEK293T cells expressing VLGR1a (Figure 2a). Overexpressing VLGR1a revealed a dose-dependent increase of cAMP, indicating the coupling of VLGR1 to Gαs. We also found a significant increase of cAMP upon the co-expression of VLGR1a with a Gαsq chimera, suggesting an activation of Gαq (Figure 2b). Based on the assumption that the CTF mutant represents the active conformation of VLGR1, we expected to see an increase in cAMP levels (Gs pathway) as well as IP levels (Gq pathway) when comparing CTF to full length constructs (Figure 2c). The proper surface and total expression of the full-length and CTF mutant was controlled using ELISA assays (Figure 2d). Surprisingly, constitutive activity of the CTF was seemingly only confirmed for Gq-mediated IP accumulation, while Gs-mediated cAMP levels were reduced. However,

cAMP reduction can also be caused by activation of Gi proteins. Indeed, utilizing a Gqi chimera, this activation could be shown for the CTF mutant. These findings are consistent with previous results from independent groups reporting signaling of VLGR1 via Gαs/Gαq and Gαi [36,37]. Shin et al. (2013) used a shortened version of VLGR1 that contained an artificial NTF comprising the PTX domain, the EAR domain, and five Calxα domains. This VLGR1 version appeared to be essential for Gαs signaling, which is in line with our data observed with VLGR1a (Figure 2b). In contrast, Hu and coworkers (2014) used the VLGR1_CTF for their measurements and found the coupling to Gαi. In accordance with these previous results, we observed a stronger activation of Gαi with VLGR1_CTF, compared to VLGR1a (Figure 2c). For Gαs, we did not detect significant differences between both constructs in their basal activity levels. However, the association of Gαs with VLGR1a, but not VLGR1_CTF in our TAPs, and the dose-dependent increase of basal activity upon VLGR1a overexpression (Figure 2a), all indicate a preferred coupling of Gαs to full-length VLGR1a, compared to VLGR1_CTF, which in turn favors Gi-coupling. A signaling switch from basal Gs to active Gi has been previously shown for ADGRG3/GPR97 [41]. Interestingly, switches between Gα coupling are not restricted to ADGRs, but were previously also reported for other GPCRs [42]. A physiological role for these signaling switches in VLGR1 remains to be determined. Interestingly, the activation of the Gq protein is utilized by the receptor in its full-length as well as in its CTF version (Figure 2b,c). The same Gq-preferred activation can be found when screening for potential *Stachel*-derived agonistic peptides in a cAMP assay. We found that peptides of 10 and 11 amino acids of the respective tethered agonist region could significantly activate VLGR1 when adding a Gsq chimera (Figure 2e). As in other ADGRs, the release of the NTF from VLGR1 may trigger the binding of this 11-amino-acids *Stachel* peptide to the exoplasmic face of the VLGR1_CTF. The resulting conformational changes in the receptor may induce the switch from Gαs- to Gαi-mediated signaling of VLGR1, as indicated in the TAPs for VLGR1a and VLGR1_CTF.

2.3. TAP Data Analysis Indicates Coupling of VLGR1 to Various Downstream Signaling Pathways

Enrichment analyses of VLGR1 TAP data sets in the categories of the KEGG pathway and Biological Process displayed the participation of VLGR1 at 13 different signaling pathways. However, the number of prey identified with three different VLGR1 baits for these pathway categories obviously differs. Based on these differences we were able to predict how VLGR1 molecules are connected to the specific pathway. KEGG pathway analysis revealed, for VLGR1_ICD prey proteins, two mitogen-activated protein kinases, MAPK1 and MAPK3, categorized to the mTOR-pathway, which is involved in the cellular response to energy levels and nutritional or environmental cues [43]. An enrichment of prey related to mTOR-signaling was also found for SF-N-VLGR1a but not for VLGR1_CTF TAPs.

Categorized pathways assigned by the identified prey proteins identified in TAPs with the VLGR1a and VLGR1_CTF as baits are listed in Table 1. For both, full-length VLGR1a and the VLGR1_CTFs, we found proteins which participate in the AMP-activated protein kinase (AMPK) pathway, MAPK signaling, the neurotrophin pathway, and Wnt signaling. Prey proteins connected to Hypoxia-inducible factor 1 (HIF-1) signaling were enriched for VLGR1a as bait. This suggests that the less active full-length VLGR1a participates in the HIF-1 pathway and regulations related to hypoxia [44]. In contrast, protein prey related to the Notch signaling pathway, the insulin receptor-mediated pathway, and Ephrin signaling or the sphingolipid pathway were almost exclusively identified in TAPs performed with VLGR1_CTFs. The interaction of these pathways with VLGR1 probably only occurs in the active receptor stage.

Interestingly, protein prey categorized to integrin signaling was mainly associated with SF-C-VLGR1_CTF, but not with SF-N-VLGR1_CTF. The N-terminal tags at VLGR1_CTF most probably may hinder receptor activation by the tethered *Stachel* agonist [29,45]. Thus, our data favor that *Stachel*-mediated activation of VLGR1 is essential for downstream integrin signaling. In contrast, proteins involved in Wnt and Sonic Hedgehog (Shh) signaling, namely Smoothened (SMO), Frizzled 7 (FZD7), and protein tyrosine kinase 7 (PTK7), were

only found in TAPs with the N-terminally tagged VLGR1_CTF. This indicates that a free, untagged C-terminus of VLGR1 is important to interact with these proteins. Notably, VLGR1, SMO, and FZD7 all contain C-terminal class I PDZ-binding motifs (PBMs). The binding of PBMs to PDZ domain scaffolding proteins likely mediates the interaction of the proteins and their clustering at the membranes. Moreover, we found 30 proteins related to the ER-associated protein degradation (ERAD) pathway that is activated by misfolded proteins [46]. This might be due to overexpression of the aGPCR bait. We also noticed that VLGR1_CTFs interacted with several proteins associated with apoptotic pathways. However, we did not observe an apoptotic effect upon the overexpression of these molecules in HEK293T cells.
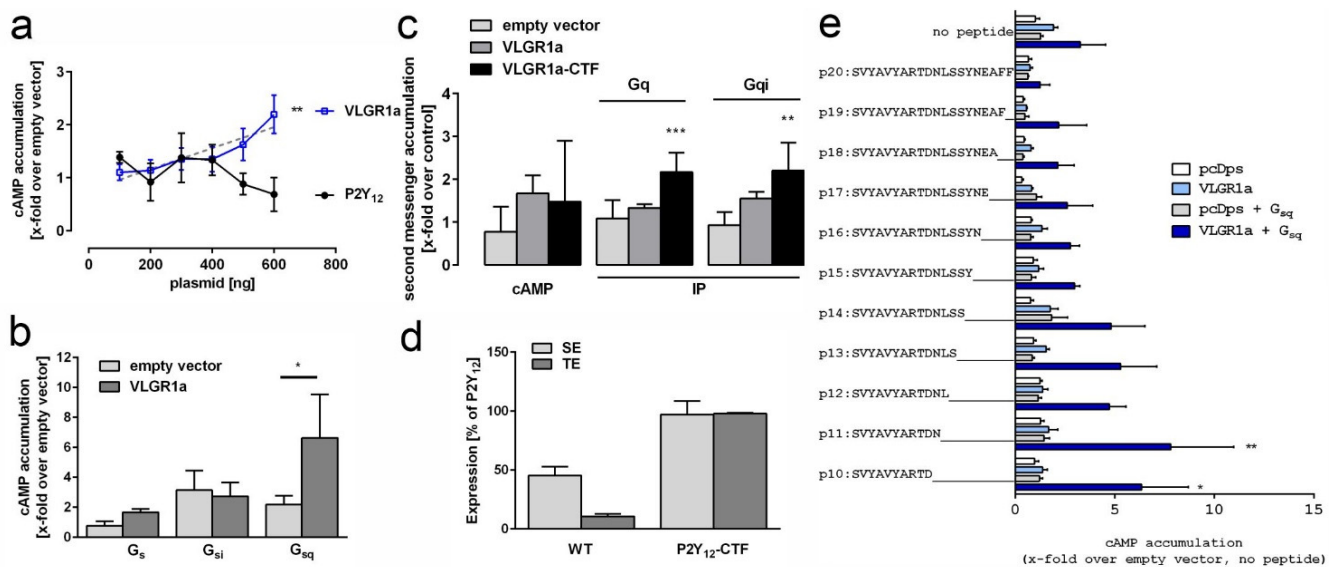
Figure 2. Signal transduction and activation of VLGR1. (**a**) HEK293T cells were transfected with increasing amounts (100–600 ng/well) of plasmids encoding either human VLGR1 or human P2Y12. VLGR1, but not P2Y12, a known Gi coupling receptor, caused a dose-dependent increase of cAMP. Statistics displayed significant linear regression for VLGR1. (**b**) Coupling analysis of VLGR1a using chimeric G proteins in cAMP accumulation assay revealed significant 2nd messenger accumulation with a chimera that couples to a Gq-binding receptor. (**c**) Comparison of basal 2nd messenger production of full length and CTF, where the NTF was replaced with the N-terminus of P2Y12 to ensure proper surface expression of the mutant. Constitutive activity of the CTF is observed in IP accumulation assay with and without a Gqi chimeric protein, indicating coupling to Gq and Gi. (**d**) Cell surface (SE) and total cell expression (TE) of full length and CTF mutant constructs of VLGR1 in relation to P2Y12 (100%), which served as positive control. (**e**) Screening for VLGR1 *Stachel*-mimicking peptides. A *Stachel*-derived peptide library of VLGR1 was tested in cAMP with and without the addition of a Gsq chimeric G protein. Peptides 10 and 11 amino acids long were found to significantly activate VLGR1 in comparison to pcDps when the Gsq chimera was added. (**a–e**): Data are given as means ± S.D. of three independent experiments each performed in triplicate. (**b**,**c**): Statistics was performed using one-way ANOVA with Bonferroni as post-hoc test and (**d**) utilized one-way ANOVA with Sidak's multiple comparison test. p-values in b, c and e: * $p \leq 0.05$, ** $p \leq 0.01$, *** $p \leq 0.001$.

2.4. VLGR1 Participates in Signaling at Focal Adhesions

Beside their signaling function, ADGRs possess adhesive properties. In VLGR1 TAPs with HEK293T cell lysates, we identified 96 proteins that are assigned to the GO term focal adhesion, of which 25 have a CRAPome value 20 (Figure 3a). The high number of focal adhesions (FA)-associated prey is consistent with data from RPE1 cells performed in a parallel study [47]. Figure 3b shows the localization of VLGR1 in FAs of primary mouse brain astrocytes, concordant with data of the latter study [47]. FAs are macromolecular

assemblies at contact sites of cell membranes with the extracellular matrix (ECM) [48]. There they act as hubs for bidirectional signaling, the "inside-out" transmission of intracellular forces to the ECM, and the "outside-in" signal transmission of shear forces between the cell and the ECM from the environment to the cell interior [49]. While no FA protein was found in the VLGR1_ICD TAPs, the prey for SF-N-VLGR1a, SF-N-VLGR1_CTF, and SF-C-VLGR1_CTF contained several FA core proteins. Being proteins directly associated with integrins, the core FA adhesion molecules were mostly restricted to both VLGR1_CTF TAPs. This suggests that the interaction with integrin complexes depends on the activity level of VLGR1. All in all, these data further support our recent findings that VLGR1 functions as a metabotropic mechanosensor in FAs that is critical for cell spreading and cell migration [47].

Table 1. VLGR1 is connected to several cellular signaling pathways (selection is based on KEGG pathway and Biological Process enrichment analysis, see also Supplementary Tables S1–S4). Prey proteins with CRAPome values ≤ 20 are shown. Baits: SF-N-VLGR1a (full-length VLGR1a), SF-N-VLGR1_CTF (N-CTF), and SF-C-VLGR1_CTF (C-CTF).

Pathways	Prey Proteins	VLGR1a	Baits N-CTF	C-CTF	Prey Proteins	VLGR1a	Baits N-CTF	C-CTF
AMPK pathway: *coordinates cell growth, autophagy and metabolism*	CPT1A	+	+	+	PIK3R2	+		
	G6PC3		+	+	PRKAG1		+	
	HMGCR		+	+	SCD	+	+	+
	IGF1R	+	+	+	SCD5	+		+
	PCK2	+						
Ephrin signaling: *development*	ADAM10			+	NCSTN	+	+	+
	APH1A	+	+	+	PSEN2			+
	EFNB1		+	+				
FoxO pathway: *regulation of cell cycle, apoptosis and metabolism*	FOXG1	+			PCK2	+		
	G6PC3		+		PRKAG1		+	
	IGF1R	+	+		RAF1	+	+	
	PIK3R2	+			TGFBR1	+	+	
HIF 1 pathway: *regulates hypoxia inducible genes under hypoxic conditions*	CUL2	+			IGF1R	+	+	+
	EIF4E	+			PIK3R2	+		
	HK2	+	+	+	TCEB1	+		
	HMOX1		+		TCEB2	+		
Insulin receptor pathway: *controls critical energy functions such as glucose and lipid metabolism, connected to FoxO signaling pathway*	ATP6AP1	+	+	+	LAMTOR3			+
	ATP6V0A1		+	+	NCAM1			+
	ATP6V0A2		+	+	PIGU		+	+
	ATP6V0D1		+	+	PIK3R2	+		
	ATP6V1F		+	+	PIK3R4		+	+
	ATP6V1H		+	+	PRKAG1		+	
	EIF4E	+			RAF1	+	+	+
	IGF1R	+	+	+	SPNS1	+	+	+
	LAMTOR1		+	+				
Integrin signaling: *development, tissue maintenance and repair*	ADAM10			+	ITGA5			+
	ADAMTS	+			ITGA6			
	CD47			+	SPNS1	+	+	+

Table 1. *Cont.*

Pathways	Prey Proteins	VLGR1a	Baits N-CTF	C-CTF	Prey Proteins	VLGR1a	Baits N-CTF	C-CTF
MAPK pathway: *involved in proliferation, differentiation, motility, stress response, apoptosis and survival*	ARL6IP5		+	+	LEMD2	+	+	+
	ATP6AP1	+	+	+	MAP2K7	+		
	ATP6AP2		+	+	MTCH1		+	+
	CD81			+	NCAM1			+
	CDK5RAP3			+	NPTN			+
	FN1	+			PIGU		+	+
	FZD7		+		PPM1L		+	
	GDF15	+			PSEN1		+	+
	HMGCR		+		RAF1	+	+	+
	IGF1R	+	+	+	RHBDD3		+	+
	ILK		+		SPNS1	+	+	+
	INHBE	+			SYNJ2BP	+	+	+
	IRAK1	+	+	+	TAB2	+		
	LAMTOR1		+	+	TGFBR1	+	+	
	LAMTOR3			+	VRK2		+	
mTOR pathway: *senses and integrates nutritional and environmental cues*	EIF4E	+			K3R2	+		
	LAMTOR1		+	+	RICTOR	+		
	LAMTOR3P			+				
Neurotrophin pathway: *regulates survival, development and function of neurons*	ADAM17		+		PIK3R2	+		
	APH1A	+	+	+	PSEN2			+
	IRAK1	+	+	+	RAF1	+	+	+
	LAMTOR3			+	RICTOR	+		
	NCAM1			+	SMPD2		+	
	NCSTN	+	+	+	SORT1	+	+	+
	PIGU		+	+	SPNS1	+	+	+
Notch pathway: *regulates cell fate determination during development and maintains adult tissue homeostasis*	ADAM10			+	NCSTN	+	+	+
	ADAM17		+		PSEN1		+	+
	APH1A	+	+	+	PSEN2			+
	APP		+		SEL1L		+	+
	GALNT11			+	SYNJ2BP		+	+
	GOLT1B		+	+	TSPAN15		+	+
	MAGEA1		+					
SMAD pathway: *regulates cell growth, differentiation & development*	GDF15	+			NCEH1			+
	INHBE	+			SLC33A1	+	+	+
	LNPEP		+	+	STOML1		+	
Sphingolipid pathway: *regulate cellular responses to stress*	ABCC1		+	+	PLCB4		+	
	BAX		+		PLD2			+
	CERS1	+	+	+	RAF1	+	+	+
	CERS2	+	+	+	SGPL1	+	+	+
	CERS4		+	+	SGPP1		+	+
	CERS5		+	+	SMPD2		+	
	CERS6		+	+	SPTLC1	+	+	+
	DEGS1			+	SPTLC2	+	+	+
	PIK3R2	+						
Wnt pathway: *regulates cell migration, cell polarity, neural patterning and organogenesis*	ATP6AP2		+	+	PSEN1		+	+
	FZD7		+		PTK7		+	+
	GPC6	+			SMO		+	
	ILK		+		SPNS1	+	+	+
	LRP1			+	UBR5			+
	MESDC2	+			WLS	+	+	+
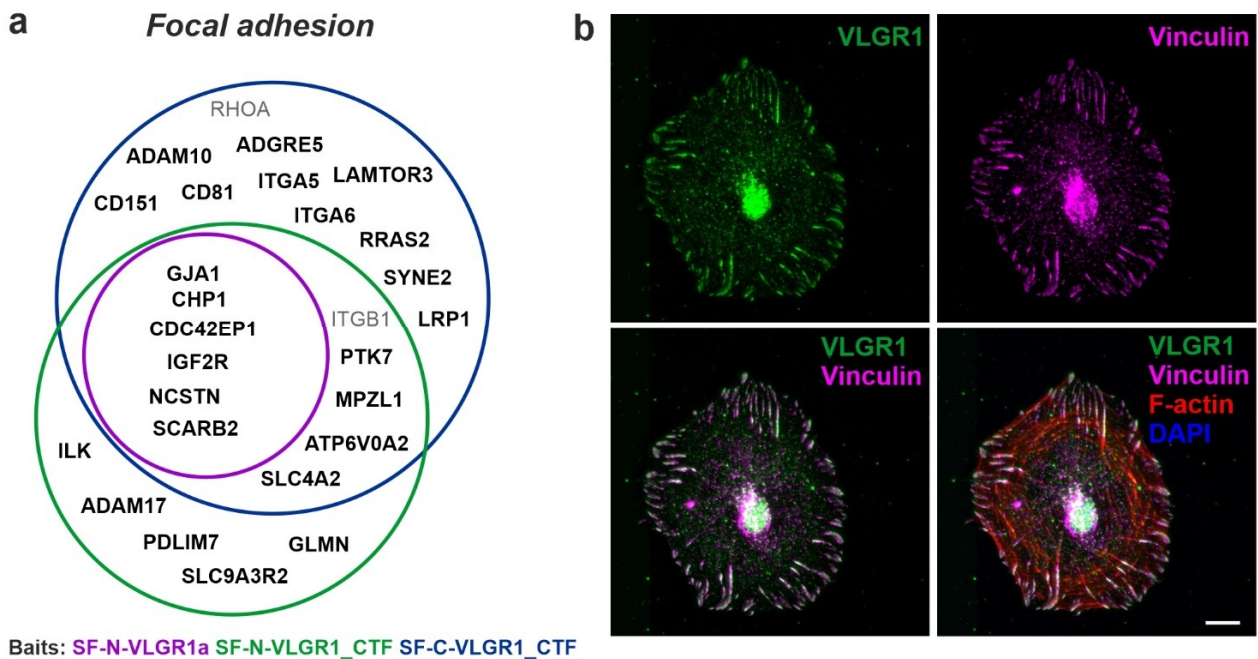
Figure 3. Association of VLGR1 with focal adhesions. (**a**) Venn diagram of VLGR1 prey assigned to the GO term *focal adhesion* in the category *Cellular Component*. Black font: CRAPome value ≤ 20; Grey font: CRAPome value > 20. (**b**) VLGR1 is expressed at focal adhesions (FA) in primary astrocytes derived from murine brain, where it co-localizes with the FA marker Vinculin and actin stress fibers. Scale bar: 10 μm.

2.5. VLGR1 Partners Participate in Cell Cycle Regulation, Cell Division, and Ciliogenesis

Our TAP data showed a high enrichment for proteins attributed with the GO term cell cycle (over 100 prey). VLGR1 interaction partners with a CRAPome value ≤ 20 could be further grouped into positive cell cycle regulators, negative cell cycle regulators, and other proteins (Figure 4a). It is worth noting that APP and other Alzheimer's disease-related proteins, such as APBB1 and ADAM17, are part of these categories. In addition, we identified the checkpoint kinases, cell division cycle 6 (CDC6), CDC7, and CDC45, which regulate G1/S transition [50–52].
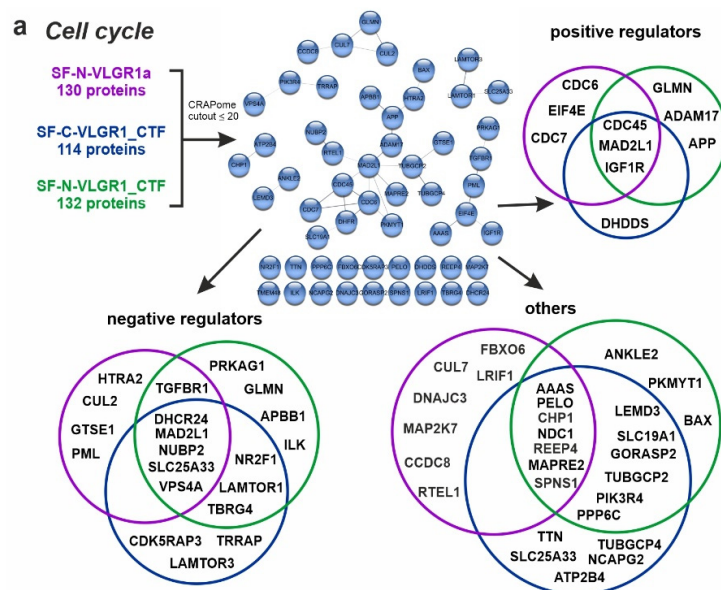
Figure 4. *Cont.*
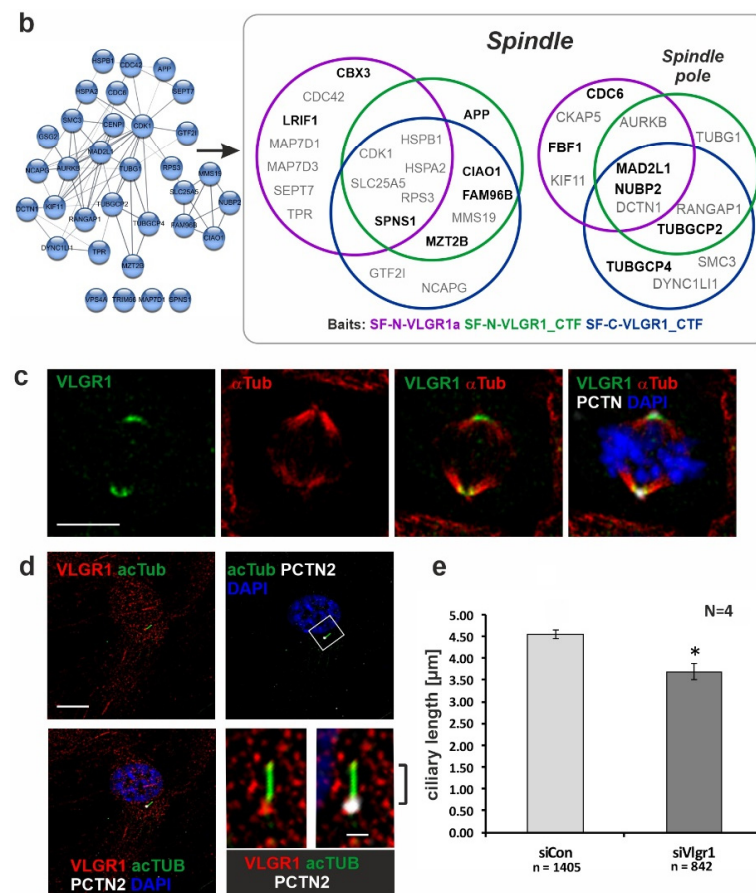
Figure 4. Association of VLGR1 with cell cycle regulators, mitotic spindle components, and primary cilia. (**a**) Venn diagrams of VLGR1 prey involved in cell cycle regulation. Interactions between these regulators are visualized in a STRING (https://string-db.org/, accessed on 10 September 2017) network. (**b**) VLGR1 prey that are assigned to the GO terms spindle and spindle pole in the category Cellular Component. Black font: CRAPome value ≤ 20; Grey font: CRAPome value > 20. (**c**) Triple immunofluorescence staining of VLGR1 (green), the spindle microtubules by α-tubulin (α-Tub, red), and the centriole/spindle pole marker protein pericentrin-2 (PCTN, white) in RPE1 cells reveals the localization of VLGR1 at spindle poles. Chromosomal DNA is stained by DAPI (blue). (**d**) Triple immunofluorescence staining revealed VLGR1 (red) co-localization with PCTN2 at the base of primary cilia in RPE1 cells. (**e**) siRNA-mediated knock-down of VLGR1 in RPE1 cells results in decrease of the ciliary length. Scale bars: 10 μm and 2 μm (magnified primary cilium). siCon, control siRNA (non-targeting); siVlgr1, siRNA directed against VLGR1; * $p < 0.05$.

We also observed that over 30 proteins were additionally assigned with the GO terms spindle, and, more specifically, the spindle pole (Figure 4b). The interaction partners for the full-length VLGR1a and VLGR1_CTF partially differed in these categories, suggesting different roles of the full-length protein and its C-terminal fragment in this cellular context. The association of VLGR1 with the spindle apparatus was confirmed by the immunocytochemical staining of spindle poles by antibodies raised against the C-terminal part of VLGR1 in dividing RPE1 cells (Figure 4c). In contrast, VLGR1 was localized to the base of primary cilia in quiescent cells (Figure 4d), which is in line with the localization of VLGR1 at the periciliary membrane complex of photoreceptor cells [20]. The SiRNA-mediated knock-down of VLGR1 revealed a significant reduction in cilia length when compared to the non-targeting control (NTC) knock-down (Figure 4e). This fits to our finding that various novel identified interaction partners of VLGR1, such as nucleotide binding protein 2 (NUBP2), the IQ motif containing B1 (IQCB1/NPHP5 (nephrocystin-5)), the actin-binding protein Filamin A (FLNA), and Fas binding factor 1 (FBF1), participate in ciliogenesis [53–56].

FBF1 and Filamin A both play a role in the modification, positioning, and anchoring of the mother centriole at the plasma membrane during ciliogenesis, and IQCB1/NPHP5 is thought to additionally regulate the ciliary import at the ciliary base of the cilium where VLGR1 is found [54,57].

Furthermore, we identified proteins which have been previously associated with non- and syndromic retinal ciliopathies: the Retinitis pigmentosa 1 protein (RP1), localized in the axoneme of photoreceptor cilia [33,58], and the Kinesin family member KIF11, which is found in the periciliary region at the base of the photoreceptor cilium [59], but interestingly, also at the spindle poles of dividing cells [60]. In summary, we found evidence for the involvement of VLGR1 in cell cycle regulation and ciliogenesis. The molecular background of these functions remains to be determined.

2.6. VLGR1 Is Part of Protein Networks in the ER and Nucleus

Our TAP datasets contain over 400 proteins, which are assigned to the Cellular Component GO term nucleus. The vast majority of these proteins also belong to the GO term category of the nuclear outer membrane–endoplasmic reticulum membrane network. About 196 proteins are part of the latter group, including 124 proteins with a CRAPome value ≤ 20, which suggests a high specificity. For the GO term category "endoplasmic reticulum", a large number of prey were found for SF-C-VLGR1_CTF (334), SF-N-VLGR1_CTF (348), and VLGR1a (259). In contrast, in SF-N-VLGR1_ICD TAPs, only two proteins were categorized to the ER. The association of VLGR1 with the nucleus suggested by the GO terms of the prey proteins were confirmed by the immunocytochemistry in the primary astrocytes derived from a murine brain. Immunostaining demonstrated the localization of VLGR1 in the plasma membrane (arrowhead), nucleus, focal adhesions (arrow), and in the perinuclear cytoplasm (asterisk) (Figure 5a). The association of VLGR1 with the ER suggested by the GO terms was verified by immunostaining VLGR1 and the ER component CLIMP63 in HeLa cells (Figure 5b). The staining of VLGR1 overlapped not only with the nuclear marker DAPI, but also with the ER marker CLIMP63, indicating the presence of VLGR1 in the ER. There, as with other transmembrane receptors, the aGPCRs are properly folded by chaperones present in the ER to be transported to the site of their activity. In addition, there is also evidence from our TAPs that VLGR1 may well play a role in ER function. In several TAPs, the prey were assigned to mitochondria-associated membranes (MAMs), a compartment that is formed by the adhesion of the ER membrane to the outer mitochondrial membrane [61]. This is in line with the localization of VLGR1 in this ER–mitochondria junction complex, as perilously shown [62]. In a parallel study, we have demonstrated that VLGR1 is part of a protein complex which is essential for the proper release of Ca^{2+} from the ER of the MAM, thereby controlling the Ca^{2+} homeostasis (Krzysko et al., in prep).

The identified prey of the nuclear categories participate in nuclear-specific functions, such as gene regulation, pre-RNA splicing, and transcription. We found 20 proteins that fall into the transcriptional factors and regulators category, and which have a CRAPome value ≤ 20 (Figure 5c). These include the ligand-dependent nuclear receptor interacting factor 1 (LRIF1), a repressor of retinoic acid receptor alpha (RARA) transcriptional activity [63]. Further, we identified transcriptional regulators that are involved in brain and inner ear development (FOXG1) [64,65], and the differentiation of progenitor cells in the retina (NR2F1) [66]. Moreover, amyloid beta precursor protein binding family B member 1 (APBB1) was included in this dataset, which forms a transcription complex with the intracellular domain of the amyloid precursor protein (APP) (APP_ICD) [67]. Both Notch_ICD and APP_ICD are products of γ-secretase cleavage. Strikingly, we also found four different subunits of the γ-secretase complex in our VLGR1 TAPs (see below), indicating that VLGR1 is a target for γ-secretase cleavage. In a parallel study, we obtained evidence that VLGR1_ICD is also cleaved and appears in the nucleus [62]. Since there is no obvious nuclear localization sequence in VLGR1 predicted by in silico analysis applying NLStradamus [68], it is probably co-shuttled with one of their binding proteins into the nucleus for fulfilling its nuclear function.
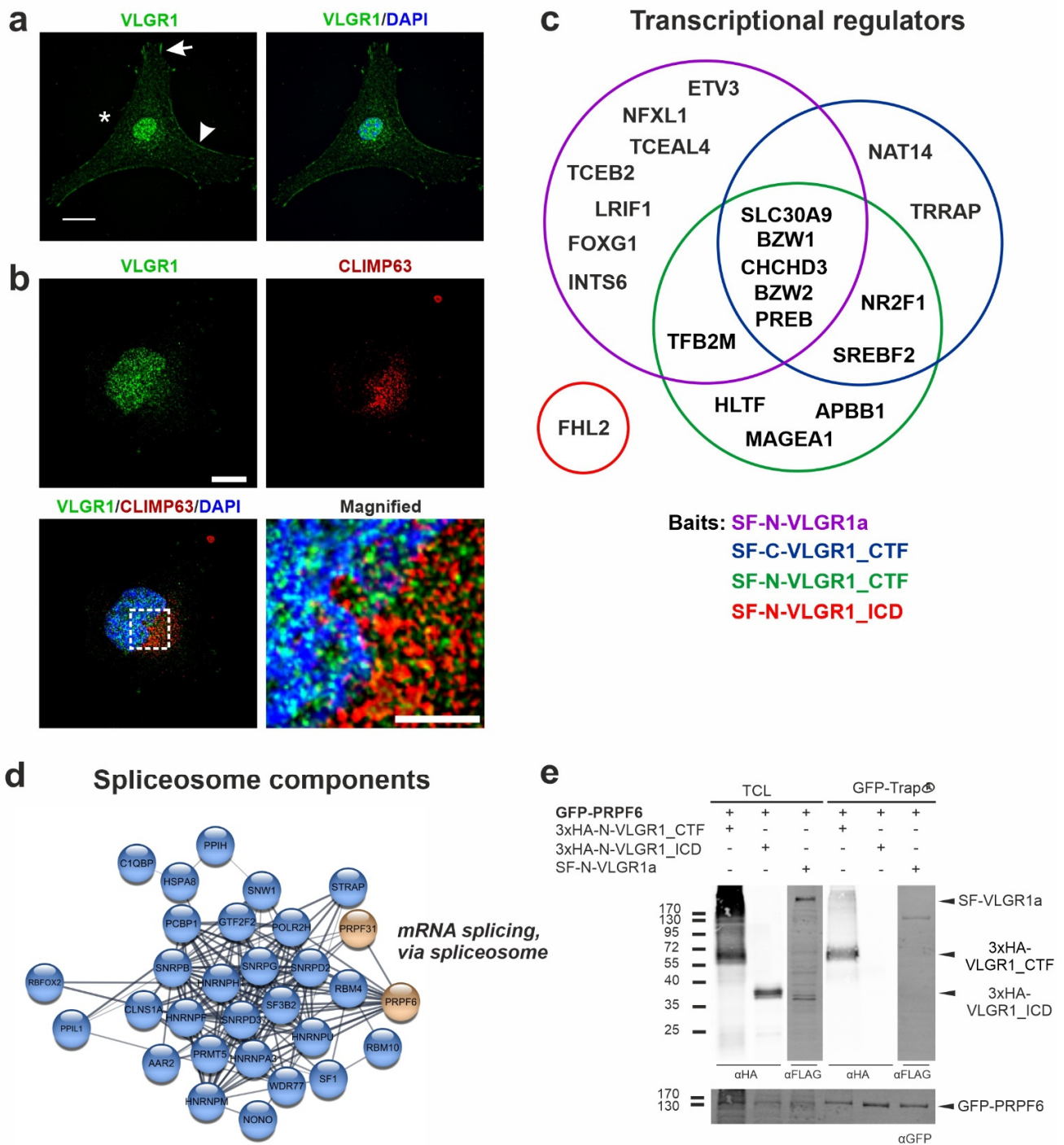
Figure 5. VLGR1 nuclear localization and its interaction with transcriptional regulators and components of the spliceosome. (**a**) Indirect immunofluorescence of VLGR1 counter stained for the nucleus by DAPI (blue) in astrocytes derived from mouse brains. VLGR1 (green) is localized in the plasma membrane (*arrowhead*) in the cytoplasm, in focal adhesions (*arrow*), and in the nucleoplasm of the nucleus (*asterisk*). (**b**) Double immunofluorescence of VLGR1 (green) and the ER marker CLIMP63 (red), counter stained for nuclear DNA by DAPI (blue) in HeLa cells demonstrating prominent VLGR1 localization in the ER. (**c**) Venn diagram of VLGR1 prey with a function in transcriptional regulation (CRAPome value ≤ 20). (**d**) STRING network of VLGR1 TAP prey assigned to the GO term *mRNA splicing*, via *spliceosome*. (**e**) Validation of the interaction of VLGR1 with the spliceosome component PRPF6. GFP-PRPF6 pulled down VLGR1_CTF in a GFP-Trap® assay. TCL: total cell lysate, CTF: C-terminal fragment, ICD; intracellular domain, SF: Strep II-FLAG. Scale bars in (**a**,**b**): 10 μm.

In addition, we identified several proteins that are known to participate in roles regarding pre-mRNA splicing catalyzed by the spliceosome (Figure 5d), a compositionally dynamic complex assembled stepwise on pre-mRNA [69]. We identified the RNA-binding protein Fox-1 homolog 2 (RBFOX2) as a highly reliable interactor (CRAPome value 14) which serves as an important regulator of alternative exon splicing, particularly in the nervous system [70]. In addition, we found the SNW domain containing 1 protein (SNW1), which is proposed to recruit peptidylprolyl isomerase-like 1 (PPIL1), an additional high-fidelity prey (CRAPome value 19), to the spliceosome [71,72]. To test whether VLGR1 is part of the spliceosomal core, we analyzed its interaction with the pre-mRNA-processing factors PRPF6 by pull down assays (Figure 5e). We observed the binding of HA-N-VLGR1_CTF to GFP-PRPF6 in contrast to GFP in GFP-Trap® pull-downs. This exemplifies the interaction of VLGR1 with spliceosome components, as suggested by the TAP results.

Taken together, we identified VLGR1 in association with the protein networks of the functional modules of the ER, MAMs, and nucleus, suggesting multiple roles of VLGR1 in gene regulation, pre-RNA splicing, transcriptional control, and balancing Ca^{2+} homeostasis.

2.7. VLGR1 Is Associated with the γ-Secretase Complex

We found several subunits of the γ-secretase complex in our TAP, namely nicastrin (NCSTN), the two presenilins, PSEN1 and PSEN2, and APH1a [73], as well as the occasional subunit of the γ-secretase Basigin (BSG) [74]. Although the γ-secretase complex is best known for its proteolytic action on APP, resulting in amyloid β-peptide (Aβ) accumulation, it also conducts to the intramembranous proteolytic excision of numerous other single and multiple transmembrane proteins [75]. γ-secretase cleavage of the multi-spanning transmembrane protein polycystin 1 (PKD1) results in the release of its intracellular C-terminus, which acts as a transcriptional regulator [76–79]. There are several lines of evidence that VLGR1 is a substrate of γ-secretase, such as positively charged residues at the junction of transmembrane helix 7, which are known primary determinants of the substrate binding of the secretase, and the general presence of released VLGR1_ICD in cells [62]. In addition, the nuclear localization and prey identified in VLGR1 TAPs include various transcriptional regulators as putative targets for the ICD of VLGR1 in the nucleus [62] (Figure 5a). Therefore, it is reasonable to speculate that VLGR1 regulates transcription by a mechanism similar to the transcriptional regulation by PKD1. However, a direct experimental proof for this hypothesis is still lacking. In addition, beside γ-secretase itself, VLGR1 TAPs also contain validated substrates of the γ-secretase, such as the ephrin beta 1 (EFNB1), the insulin-like growth factor 1 receptor (IGF1R), the LDL receptor-related protein 1 (LRP1), and the amyloid precursor protein (APP). Accordingly, it would also be possible that VLGR1 is indirectly linked to the γ-secretase via the interaction of these receptors, or it may act as a regulatory component of the proteolytic cleavage of these substrates.

2.8. VLGR1 Interacts with Proteins Involved in Neurogenesis

In VLGR1 TAPs we found 161 proteins in total assigned to the GO term neurogenesis, which is in line with the high expression of VLGR1 in the developing brain [2]. These hits were reduced to 69 proteins by filtering against the CRAPome dataset (cutout ≤ 20) (Figure 6a). Fourteen of them were categorized to the GO term neuron projection guidance, which includes the Alzheimer disease-related proteins APP, three subunits of the γ-secretase (NCSTN, PSEN2, APH1A), and Slit guidance ligand 2 (SLIT2) (Figure 6a). SLIT2 acts as a guidance cue for retinal ganglion cells [80,81]. Interestingly, SLIT2 is related to the fibronectin leucine-rich transmembrane protein 3 (FLRT3) [82], a ligand of the ADGR Latrophilin 2 (LPHN2, ADGRL2) [83], which we also identified in VLGR1a TAPs (Supplementary Table S1). The APP-binding protein APBB1 and the protein tyrosine kinase 7 (PTK7), an inactive kinase known to participate in Wnt signaling [84], were categorized to the category positive regulators of neuron projection. In accordance with the role of VLGR1, in the outgrowth of neuron projections is our finding that the overexpression of VLGR1_CTFs and myristoyl-palmitoyl-tagged VLGR1_ICD induces the formation of long

"axon-like" cell projections (Figure 6b). Nevertheless, other prey were categorized to negative regulators of neurogenesis, which includes APP, PSEN1, and the integral membrane protein 2C (ITM2C), a regulator of APP [85].
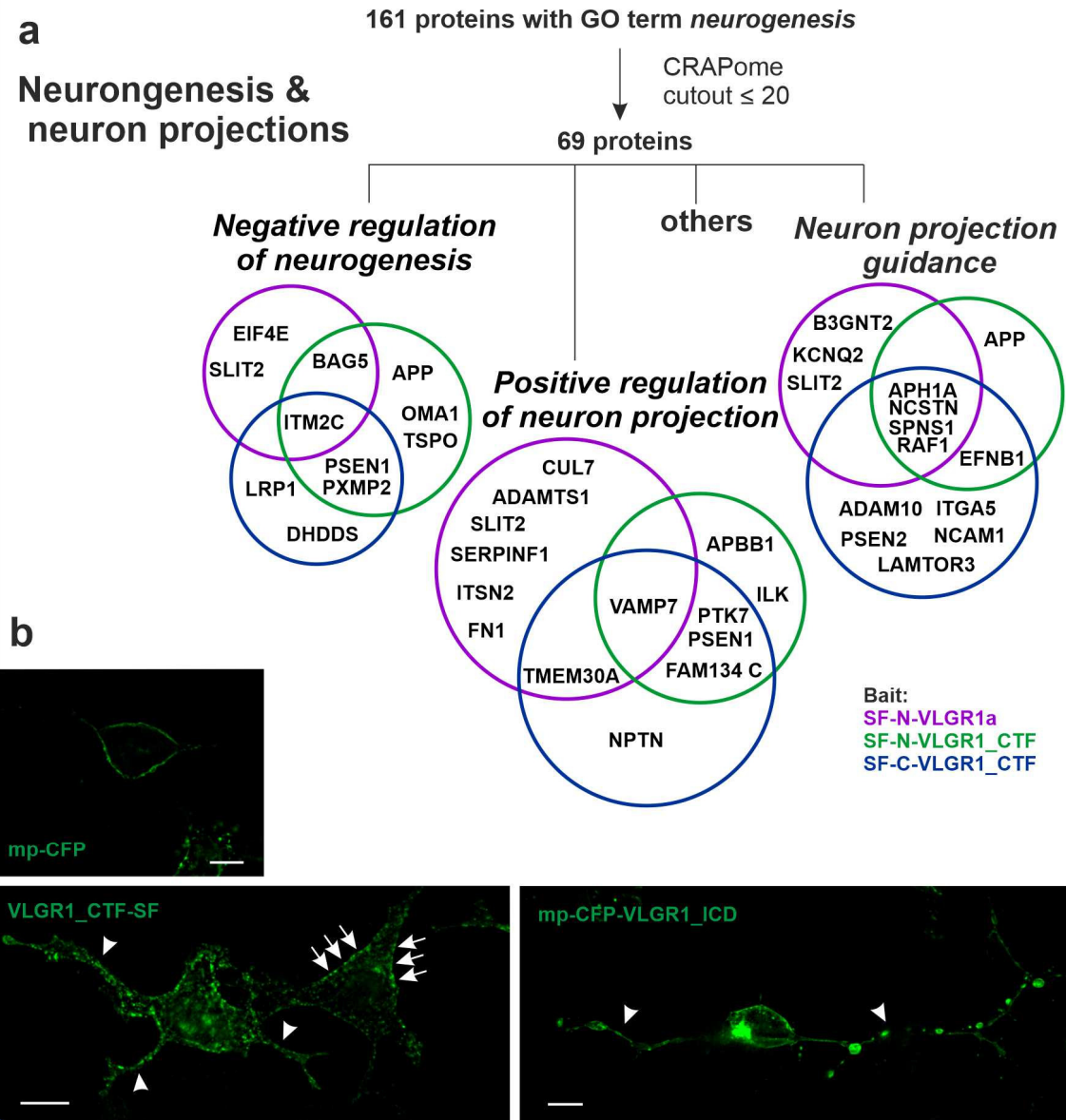

Figure 6. VLGR1 associates with neurogenesis. (**a**) Venn diagrams of VLGR1 prey that are assigned to the GO term neurogenesis in the category Biological Process. (**b**) Overexpression of VLGR1_CTF-SF and myristoyl-palmitoyl-(mp) VLGR1_ICD induces "axon-like outgrowth" (arrowheads) which are not found in myristoyl-palmitoyl-CFP transfected HEK293T cells. Note that VLGR1_CTF-SF is also localized at the plasma membrane (*arrows*). Scale bars: 10 μm.

GO term categorization also showed that several prey of VLGR1 TAPs play a role in the development of the neuronal retina. These include Sidekick 2 (SDK2), which is essential for the establishment of the well-defined characteristic layers of the neuronal retina [86]. Similar to VLGR1, SDK2 harbors a C-terminal type 1 PBM responsible for binding to PDZ domains in scaffold proteins. This is also essential for SDK2 localization to synapses [87]. Evidence suggests that SDK2 and VLGR1 bind to MAGI proteins (membrane-associated guanylate kinase (MAGUK) with a reversed arrangement of protein–protein interaction domains) and the postsynaptic density protein 95 (PSD95), respectively, thereby, in this manner, clustering at the membrane of the postsynaptic terminal [87].

TAP prey also point to a role of VLGR1 in retinoid acid receptor-mediated signaling, which essential for the development of retinal photoreceptors determining the ratio of rod and cone photoreceptors in the retina [88]. We identified in VLGR1 TAPs the ligand-dependent nuclear receptor interacting factor 1 (LRIF1), which regulates the retinoic acid receptor alpha (RARA) transcription [63] and SNW1, which binds to RXR receptors, probably together with the nuclear receptor coactivator 1 (NCOA1) [89]. The interplay of VLGR1 with RAX and NCOA1 is supported by own unpublished findings from yeast-2-hybrid screens that indicated a direct interaction of VLGR1 with NCOA1. Interestingly, both SNW1 and VLGR1 have also been shown to be part of protein interactomes associated with pre-RNA splicing (see above) [90].

In summary, our data indicate that VLGR1 plays a role in neurogenesis, particularly during the development of the neuronal retina, and is implicated in axon guidance, synapse formation, and related signaling pathways.

2.9. VLGR1 TAPs Confirm and Specify Roles in the Function of the Mature Retina and Photoreceptor Cells

VLGR1 is highly expressed in the neuronal retina of vertebrates, mainly localized to specialized adhesion complexes such as the periciliary membrane complex at the base of the photoreceptor cilium, the retinal ribbon synapses of photoreceptor cells [5,20]. Accordingly, in VLGR1 TAPs we have identified several proteins that are attributed to the *Cellular Component* GO terms, the *photoreceptor outer segment, axoneme, photoreceptor connecting cilium, photoreceptor inner segment*, and *neuronal postsynaptic density* (Figure 7a,b). Among the enriched GO terms in the *Biological Process* category, we found several terms connected to retinal or ciliary function. These are, for example, *cilium organization, visual perception, retina development in the camera-type eye, retina homeostasis, phototransduction, neurotransmitter secretion*, and the *regulation of the synapse structure or activity* (Figure 7c). Data analysis with the cytoscape plugin *stringApp* (http://apps.cytoscape.org/apps/stringapp, accessed on 10 September 2017) demonstrated that the interconnection of about half of these proteins is supported by STRING data (https://string-db.org/, accessed on 10 September 2017). Notably, TAP prey assigned with GO terms related to the *photoreceptor outer segment, connecting cilium, cilium organization*, and *visual perception* were exclusively found in the dataset of the full-length protein VLGR1a. Prey assigned to the *inner segment, phototransduction*, and *retinal development* were identified in all three datasets, the full-length VLGR1a and the two VLGR1_CTFs, whereas prey assigned to the *neuronal post-synaptic density* and *regulation of the synaptic structure or activity* were mainly found with the VLGR1_CTFs.

These data indicate an important role of VLGR1 in retinal photoreceptor cell function. This is further strengthened by the fact that mutations in the VLGR1 gene cause USH2C, which is also characterized by a strong ocular component leading to vision loss [4]. As already discussed above, VLGR1 TAPs indicate the interaction with proteins associated with syndromic and non-syndromic retinal ciliopathies, such as KIF11 [91], Nephrocystin 5 (IQCB1/NPHP5), associated with Senior-Løken syndrome [92], and Retinitis pigmentosa 1 (RP1), the product of the autosomal dominant Retinitis pigmentosa *RP1* gene [93,94]. Furthermore, VLGR1 TAPs contain Wolframin (WFS1) which is highly expressed in the human retina [95] and it is, similar to VLGR1, part of the photoreceptor ciliome [96]. In addition, as in VLGR1, mutations in *WFS1* can cause deafness [97].

2.10. TAP Data Support a Role of VLGR1 Associated with Epilepsy

VLGR1 is highly expressed in the central nervous system [2]. VLGR1 mutant mice are prone to audiogenic seizures and so considered as models for epilepsy [11–13]. In addition, there is increasing evidence that the haploinsufficiency of VLGR1 and epilepsy are related in humans [7,9,10,98]. This prompted us to screen our TAP data for candidate molecules related to the different forms of epilepsy. Previous studies indicated that defects in the *CHRNA4* gene, which encodes a subunit of the high-affinity nicotinic acetylcholine receptor (nAChR), lead to autosomal dominant nocturnal frontal lobe epilepsy (ADNFLE) [99].

Interestingly, in our VLGR1_CTF TAP data, CHRNA5, another subunit of the nAChR, which has not been associated with ADNFLE so far, was present. However, in these VLGR1_CTF TAPs, we additionally found the voltage-gated Cl- channels, CLCN1, CLCN3, and CLCN7. Missense variants in *CLCN7* are enriched in epilepsy patients, making them candidates for the disease [100]. Furthermore, we found NIPA2 (non-imprinted in the Prader-Willi/Angelman syndrome region protein 2) in all VLGR1_CTF TAPs. NIPA2 is a highly selective Mg^{2+} transporter and *NIPA2* mutations were previously described within a population of patients with childhood absence epilepsy [101]. Taken together, our findings are in line with a role of VLGR1 in the pathogenesis in epilepsy.
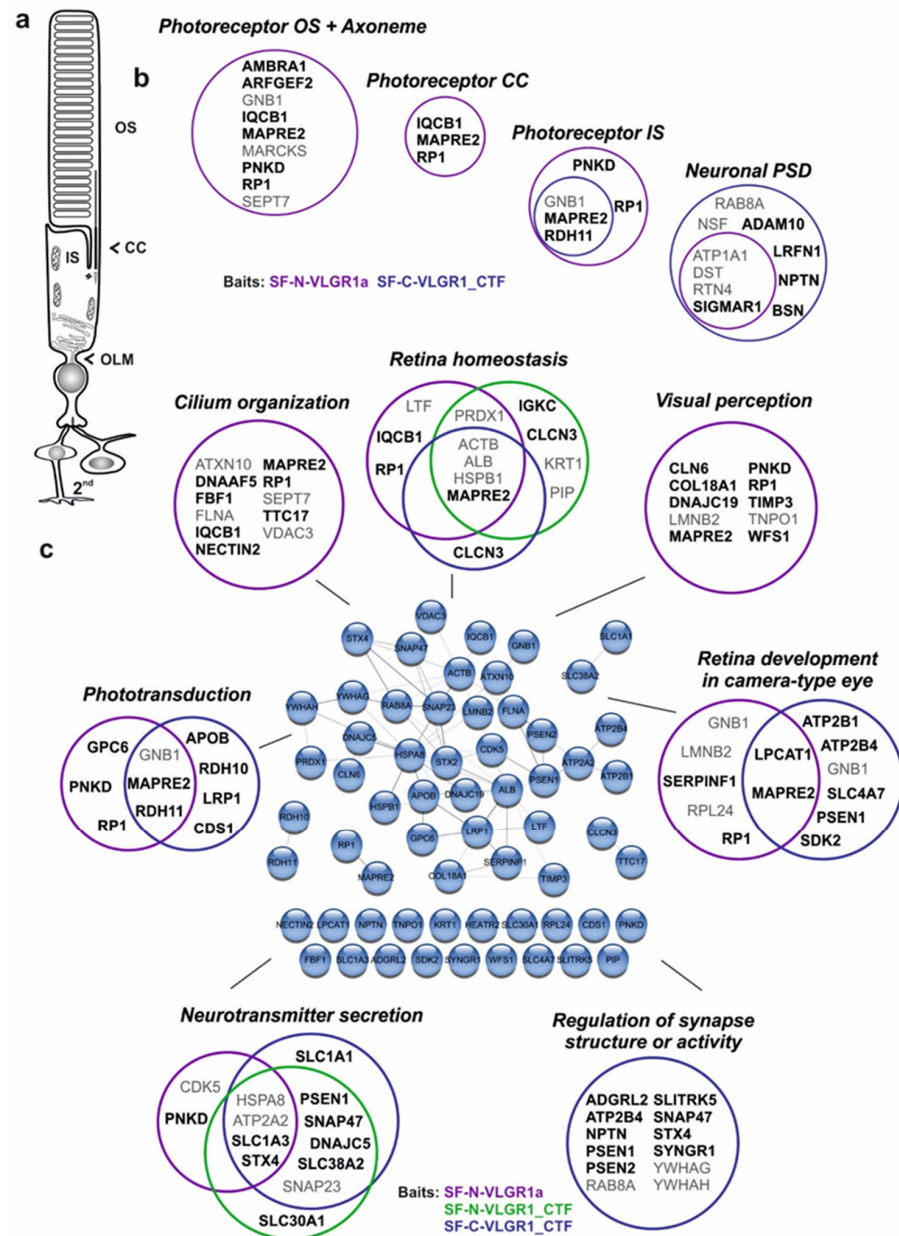
Figure 7. VLGR1 prey associates with molecules related to photoreceptors and retinal functions. (**a**) Scheme of a rod photoreceptor cell, (**b**) VLGR1 prey assigned with GO terms in the Cellular Component category that are related to photoreceptor cells and cell synapses. OS, outer segment; CC, connecting cilium; IS, inner segment; OLM, outer limiting membrane; PSD, postsynaptic density; Ax, axoneme. Black font: CRAPome value ≤ 20; Grey font: CRAPome value > 20. (**c**) Relation of VLGR1 prey to retinal function. Venn diagrams of VLGR1 prey that are assigned to retina-related GO terms in the Biological Process category. Black font: CRAPome value ≤ 20; Grey font: CRAPome value > 20.

2.11. VLGR1 Protein Networks Are Linked to Neuron Death and Degenerative Diseases of the Central Nervous System

In line with a role in neuronal degeneration, TAP prey were assigned to the GO term *neuron death* (Figure 8). After filtering against the CRAPome (cutout ≤ 20) 24 proteins remained that belong to this category. These include, e.g., 24-Dehydrocholesterol reductase (DHCR24), Sigma non-opioid intracellular receptor 1 (SIGMAR1), and Wolframin (WFS1), which have cell protective functions. Mutations in these proteins are associated with severe diseases, such as Alzheimer's disease, Amyotrophic lateral sclerosis (ALS), and Wolfram syndrome [102–104].
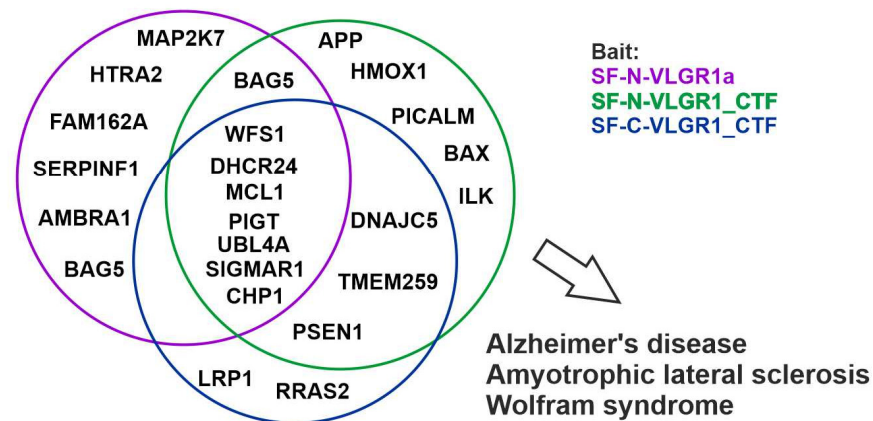
Figure 8. VLGR1 associates with neuron death. VLGR1 prey are associated with neuron integrity. Venn diagram of VLGR1 prey assigned with the GO term *neuron death*. Some of these proteins are related to neurodegenerative diseases such as Alzheimer's disease, Amyotrophic lateral sclerosis, and Wolfram syndrome.

2.12. VLGR1 Is Found in Alzheimer's Disease-Related Protein Complexes

In VLGR1 TAPs, we identified several molecules in whose genes mutations cause early-onset familial Alzheimer's disease (AD). An amyloid precursor protein (APP) occurred as a prey in one of our TAPs with SF-N-VLGR1_CTF. Mutations in the APP are related to AD, whereby APP processing by secretases plays a critical role in the Alzheimer's disease's progression [105]. In addition to the γ-secretase discussed above, we also found additional proteins that are involved in APP processing, regulation, and/or signaling. We identified, for example, the metalloproteases ADAM10 and ADAM17 that both cleave APP in the extracellular domain, preceding γ-secretase cleavage in the non-amyloidogenic pathway [106,107]. Another regulator of APP found in the VLGR1 TAPs is LRP1 which is involved in endocytosis of the released APP770 fragment, and its protein expression is decreased in Alzheimer's patients [108]. Furthermore, we found the amyloid beta precursor protein-binding family B member 1 (APBB1) that binds to the intracellular fragment of APP (APP_ICD). Both LRP1 and APBB1 act together in gene expression [109,110]. APBB1 also co-localizes with APP in the ER and/or Golgi and, presumably, in endosomes, where it regulates the APP metabolism [111]. Interestingly, the above-mentioned TAP prey and γ-secretase substrate LRP1 modulates APBB1/APP-mediated gene activation [112,113].

The TAP prey DHCR24 (24-Dehydrocholesterol reductase) is also related to Alezheimer's disease and plays a role in the cholesterol metabolic pathway [114]. It has a protective effect against Aβ-induced toxicity and is downregulated in Alzheimer's patients [108]. Last but not least, we found the protein four and a half LIM domains 2 (FHL2), which binds to both ADAM17 [115] and PSEN2 [116], and thereby could indirectly regulate APP cleavage.

In summary, we identified a whole set of VLGR1 interactors that are related to APP metabolism. Whether VLGR1 is itself processed by γ-secretase and/or metallopro-

teases, or whether it is implicated in APP-mediated pathways in a different way, remains to be elucidated [102–104].

3. Materials and Methods

3.1. Plasmids

Plasmids used for tandem affinity purifications were coded for Strep II-FLAG (SF)-tagged human VLGR1a (Uni-Prot ID Q8WXG9-2, aa 1- 1967), VLGR1_CTF (Uniprot ID Q8WXG9-1, aa 5891-6306), and VLGR1_ICD (Uniprot ID Q8WXG9-1, aa 6155-6306). The SF-tag was inserted between aa 66 and 67 in the VLGR1a construct, N-terminally and C-terminally fused in VLGR1_CTF, and N-terminally fused in VLGR1_ICD. For myristoyl-palmitoyl-tagged VLGR1_ICD, VLGR1_ICD was subcloned into the MyrPalm-eCFP vector (plasmid 14867, Addgene, Cambridge, MA, USA). For 3xHA-tagged VLGR1 constructs, VLGR1_CTF and VLGR1_ICD were subcloned into the p3xHA/DEST vector. Receptors for second messenger assays were sublconed into pcDps vector and HA- and Flag-tagged at the N- and C-terminus, respectively. Truncated CTF receptor version was fused to the N-terminus of P2Y12 to ensure proper membrane expression, as described in Liebscher et al. [29].

3.2. Cell Culture

HEK293T, HeLa, and hTERT-RPE1 cells were cultured in Dulbecco's modified Eagle's medium (DMEM and DMEM-F12, respectively) containing 10% heat-inactivated fetal calf serum (FCS). Primary astrocytes were isolated from mouse brains and cultured, as described in [117]. Cells were transfected with GeneJuice® (Merck Millipore, Darmstadt, Germany) according to manufacturer's instructions, if not indicated differently.

3.3. Tandem Affinity Purification (TAP)

The tandem affinity purification (TAP) was performed as described in [118]. Four TAPs were performed for VLGR1a, three TAPs for each VLGR1_CTF construct and two TAPs for VLGR1_ICD. In brief, SF-tagged proteins were overexpressed in HEK293T cells for 48 h. Mock treated cells were used as a control. The cells were lysed and the lysate was cleared by centrifugation. The supernatant was then subjected to a two-step purification on Strep-Tactin®Superflow® beads (IBA, Göttingen, Germany) and anti-FLAG M2 agarose beads (Sigma-Aldrich, Hamburg, Germany). Competitive elution was achieved by desbiothin (IBA, Göttingen, Germany) in the first step and FLAG® peptide (Sigma-Aldrich, Hamburg, Germany) in the second step. The eluate was precipitated by methanol–chloroform and then subjected to mass spectrometric analysis.

3.4. Mass Spectrometry

Mass spectrometry was performed as previously described by [38]. In brief, SF-TAP-purified protein complexes were solubilized before subjecting to trypsin cleavage. Resulting peptides were desalted and purified using stage tips before separation on a Dionex RSLC system. Eluted peptides were directly ionized by Nano spray ionization and detected by a LTQ Orbitrap Velos mass spectrometer (Thermo Fisher Scientific, Waltham, MA, USA). We searched the raw spectra against the human SwissProt database using Mascot, and verified the results by Scaffold (version Scaffold 4.02.01, Proteome Software Inc., Portland, OR, USA) to validate MS/MS-based peptide and protein identifications.

3.5. Data Processing

Mass spectrometry data of the different VLGR1 fragments were compared to the according data for mock-transfected cells. Proteins that occurred in the mock dataset were not considered for subsequent analysis. Datasets of identical VLGR1 fragments were combined for further analysis. Gene names (according to HGNC) of VLGR1 prey were used as input for the Cytoscape plugins, STRING and ClueGO. The parameter confidence (score) cutout was set to 0.40 and the parameter maximum number of interactors was set to

0 for STRING analysis. ClueGO v2.3.3 was used for Gene Ontology (GO) term enrichment analysis. Network specificity was set to default (medium).

3.6. Antibodies

The following antibodies were used: rabbit anti-VLGR1 [20], mouse anti-Vinculin (Merck KGaA, Darmstadt, Germany, clone hVIN-1), mouse anti-CLIMP63 (Enzo Life Sciences, Lörrach, Germany, G1/296), rat anti-HA (Roche, clone 3F10), mouse anti-FLAG M2 (Merck KGaA, clone M2), rabbit anti-GFP (kind gift from Dr. Clay Smith, University of Florida), mouse anti-α-Tubulin (Abcam, Cambridge, UK, clone DM1A), and goat anti-Pericentrin 2 (Santa Cruz Biotechnology, Dallas, TX, USA, clone C-16). Secondary antibodies conjugated to Alexa 488, Alexa 568, or Alexa 647 were purchased from Molecular Probes (Life Technologies, Darmstadt, Germany) or from Rockland Inc. (Gilbertsville, PA, USA). Nuclear DNA was stained with DAPI (1 mg/mL) (Merck KGaA).

3.7. Immunocytochemistry

Cells were fixed and permeabilized in ice cold methanol for 10 min and washed with PBS. After washing, the cells were covered with blocking solution and incubated overnight with the primary antibody at 4 °C. Cells were washed and then incubated with the secondary antibody in blocking solution containing DAPI for 1.5 h at room temperature. After washing, sections were mounted in Mowiol (Roth). Specimens were analyzed on a Leica DM6000B microscope, and images were processed with Leica imaging software and Adobe Photoshop CS (intensity adjustment).

3.8. siRNA Knock Down

For VLGR1 knock-down, hTERT-RPE1 cells (1×105) were seeded on 6-well plates. After 18 h, cells were transfected with 100 μmol of a siRNA pool targeted against VLGR1 (L-005656-00-0005, Dharmacon, Lafayette, CO, USA) and non-targeting siRNA (D-001810-10-05), respectively, using Lipofectamin® RNAiMAX (Life Technologies, Darmstadt, Germany), according to the manufacturer's protocol. Concomitant with siRNA knock-down, cells were starved for 72 h in OptiMEM® to induce cilia formation.

3.9. GFP-Trap®

GFP-fused proteins were immobilized on nanobody GFP-Trap® agarose beads (ChromoTek, Planegg-Martinsried, Germany) and used for co-precipitation assays according to the manufacturer's protocol. Briefly, cell lysates from co-transfected HEK293T cells (GFP-tagged proteins with HA-tagged proteins) were suspended in lysis buffer, spun down, and the supernatant was diluted to 1 mL dilution buffer. Next, 50 μm were separated as input (total cell lysate) and samples were added to equilibrated beads for 2 h at 4 °C under constant shaking. After washing, precipitated protein complexes were eluted with SDS-sample buffer and subjected to SDS–PAGE and Western blotting.

3.10. Immunoprecipitation

For co-IP, HA-PRPF31 was co-expressed with SF-N-VLGR1_ICD in HEK293T cells and lysed in Triton-X-100 lysis buffer containing PI-mix. Co-IP was performed using anti-HA affinity gel (Biotool, Munich, Germany), according to the manufacturer's protocol. Briefly, cell lysates were incubated with equilibrated HA-affinity beads for 2 h at 4 °C. After three washing steps, samples were eluted with SDS-sample buffer and subjected to SDS-page and Western blot analysis.

3.11. Second Messenger Assays

Measurements of cAMP and IP were performed as described previously [119]. In brief, HEK293T cells were split into 12-well plates (IP assay) and 48-well plates (cAMP assay) and transfected with LipofectamineTM2000 (Invitrogen, Paisley, UK), according to the manufacturer's protocol. For the IP assay, cells were incubated with 2 μCi/mL myo-

[3H]inositol (18.6 Ci/mmol, PerkinElmer Life Sciences, Waltham, MA, USA) for 24 h. After washing with 10 mM LiCl in serum-free DMEM, cells were incubated with 10 mM LiCl for 1 h at 37 °C. Intracellular IP levels were determined by anion-exchange chromatography, as described in [120]. IP accumulation data were analyzed using GraphPad Prism version 4.0 for Windows (GraphPad Software, San Diego, CA, USA). For the cAMP assay, transfected cells were incubated with 3-isobutyl-methyl-xanthine (1 mM)-containing medium for 1 h. Cells were lysed in LI buffer (PerkinElmer Life Sciences, Monza, Italy) and frozen at −20 °C until measurement. The cAMP concentration was determined with the Alpha Screen cAMP assay kit (PerkinElmer Life Sciences), according to the manufacturer's protocol, and measured with the Fusion AlphaScreen multilabel reader (PerkinElmer Life Sciences). The surface expression of the HA-tagged receptors was determined by an indirect cellular enzyme-linked immunosorbent assay (ELISA), as described in [121]. Peptide synthesis was performed, as described in [122].

4. Conclusions

Our results, obtained by systematic affinity proteomics, point to diverse roles of VLGR1, depending on its cellular localization and structural or state of activation (Figure 9). We provide evidence that VLGR1 harbors a tethered agonist sequence, which mediates a switch in Gα-mediated signaling. Our data also suggest that VLGR1 is active in functional modules of the cell that include cellular Ca^{2+} homeostasis, transcriptional regulation, pre-mRNA splicing, cell differentiation, and primary cilia integrity. In addition, our study provides evidence for the role of VLGR1 in the maintenance of sensory-neuronal systems, and the identified interactions with disease molecules support previously found associations with diseases such as Usher syndrome and epilepsy, but also suggest links to other neuronal disorders, such as Alzheimer's disease. Whether these functions are mediated via the activation of signaling cascades, the adhesive function of VLGR1, or a combination of both will need to be elucidated in future detailed studies.
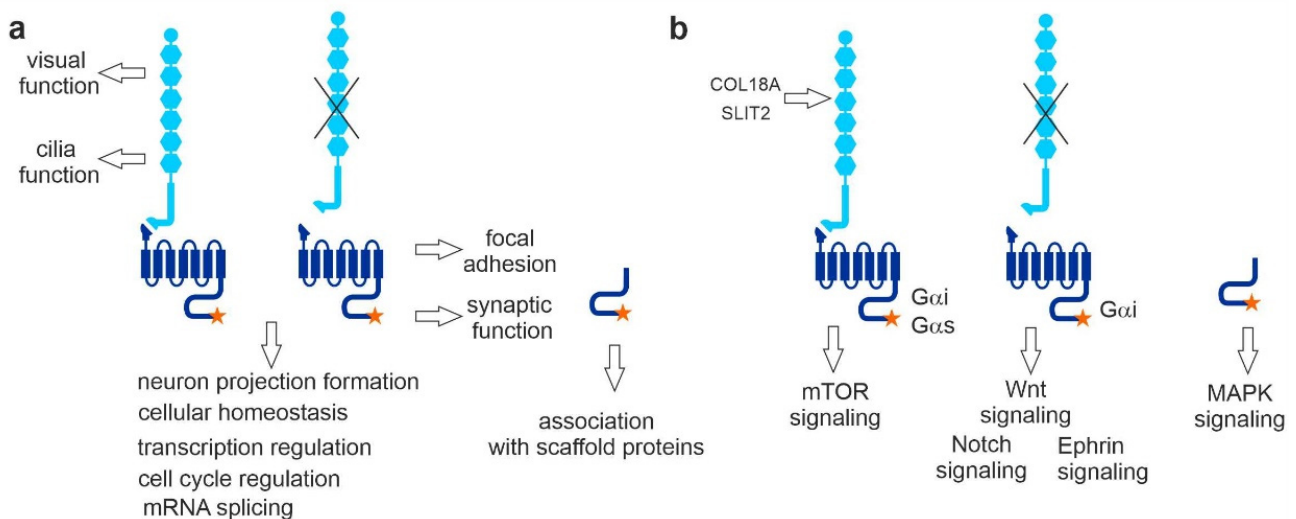
Figure 9. Summary and conclusions from the present affinity capture approach to VLGR1 function and for VLGR1 signaling pathways. (**a**) TAP prey related to ciliary and retinal function were mainly found with full-length VLGR1a. VLGR1_CTF was sufficient for focal adhesion and synaptic protein binding. Both full-length and VLGR1_CTF interact with proteins involved in neuron projection formation, cellular homeostasis, transcription regulation, cell cycle regulation, and pre-mRNA splicing. VLGR1_ICD binds to PDZ domain-containing scaffold proteins. (**b**) COL18A1 and SLIT2 are potential extracellular ligands for VLGR1, interacting with its NTF. VLGR1 full-length was linked to HIF-1 signaling coupled to Gαi and Gαs. VLGR1_CTF is coupled to Gαi and linked to Wnt, Notch, and Ephrin signaling; VLGR1_ICD seems to be linked to MAPK signaling.

References

1. McMillan, D.R.; Kayes-Wandover, K.M.; Richardson, J.A.; White, P.C. Very Large G Protein-coupled Receptor-1, the Largest Known Cell Surface Protein, Is Highly Expressed in the Developing Central Nervous System. *J. Biol. Chem.* **2002**, *277*, 785–792. [CrossRef] [PubMed]
2. McMillan, D.R.; White, P.C. Studies on the Very Large G Protein-Coupled Receptor: From Initial Discovery to Determining its Role in Sensorineural Deafness in Higher Animals. *Adhes.-Gpcrs Struct. Funct.* **2010**, *706*, 76–86. [CrossRef]
3. Hamann, J.; Aust, G.; Araç, D.; Engel, F.; Formstone, C.; Fredriksson, R.; Hall, R.; Harty, B.L.; Kirchhoff, C.; Knapp, B.; et al. International Union of Basic and Clinical Pharmacology. XCIV. Adhesion G Protein–Coupled Receptors. *Pharmacol. Rev.* **2015**, *67*, 338–367. [CrossRef] [PubMed]
4. Stemerdink, M.; García-Bohórquez, B.; Schellens, R.; Garcia-Garcia, G.; Van Wijk, E.; Millan, J.M. Genetics, pathogenesis and therapeutic developments for Usher syndrome type 2. *Hum. Genet.* **2021**, *141*, 737–758. [CrossRef]
5. Reiners, J.; Nagel-Wolfrum, K.; Jürgens, K.; Märker, T.; Wolfrum, U. Molecular basis of human Usher syndrome: Deciphering the meshes of the Usher protein network provides insights into the pathomechanisms of the Usher disease. *Exp. Eye Res.* **2006**, *83*, 97–119. [CrossRef]
6. Wolfrum, U. Protein networks related to the Usher syndrome gain insights in the molecular basis of the disease. In *Usher Syndrome: Pathogenesis, Diagnosis and Therapy*; Satpal, A., Ed.; Nova Science Publishers: New York, NY, USA, 2011; pp. 51–73.
7. Nakayama, J.; Fu, Y.-H.; Clark, A.M.; Nakahara, S.; Hamano, K.; Iwasaki, N.; Matsui, A.; Arinami, T.; Ptacek, L.J. A nonsense mutation of the MASS1 gene in a family with febrile and afebrile seizures. *Ann. Neurol.* **2002**, *52*, 654–657. [CrossRef]
8. Wang, Y.; Fan, X.; Zhang, W.; Zhang, C.; Wang, J.; Jiang, T.; Wang, L. Deficiency of very large G-protein-coupled receptor-1 is a risk factor of tumor-related epilepsy: A whole transcriptome sequencing analysis. *J. Neuro-Oncol.* **2015**, *121*, 609–616. [CrossRef]
9. Zhou, X.-W.; Wang, X.; Yang, Y.; Luo, J.-W.; Dong, H.; Liu, Y.-H.; Mao, Q. Biomarkers related with seizure risk in glioma patients: A systematic review. *Clin. Neurol. Neurosurg.* **2016**, *151*, 113–119. [CrossRef]
10. Myers, K.A.; Nasioulas, S.; Boys, A.; McMahon, J.M.; Slater, H.; Lockhart, P.; du Sart, D.; Scheffer, I.E. *ADGRV1* is implicated in myoclonic epilepsy. *Epilepsia* **2018**, *59*, 381–388. [CrossRef]
11. Skradski, S.L.; Clark, A.M.; Jiang, H.; White, H.S.; Fu, Y.-H.; Ptáček, L.J. A Novel Gene Causing a Mendelian Audiogenic Mouse Epilepsy. *Neuron* **2001**, *31*, 537–544. [CrossRef]
12. McMillan, D.R.; White, P.C. Loss of the transmembrane and cytoplasmic domains of the very large G-protein-coupled receptor-1 (VLGR1 or Mass1) causes audiogenic seizures in mice. *Mol. Cell. Neurosci.* **2004**, *26*, 322–329. [CrossRef] [PubMed]
13. Yagi, H.; Takamura, Y.; Yoneda, T.; Konno, D.; Akagi, Y.; Yoshida, K.; Sato, M. Vlgr1 knockout mice show audiogenic seizure susceptibility. *J. Neurochem.* **2005**, *92*, 191–202. [CrossRef] [PubMed]

14. McGee, J.; Goodyear, R.J.; McMillan, D.R.; Stauffer, E.A.; Holt, J.R.; Locke, K.G.; Birch, D.G.; Legan, P.K.; White, P.C.; Walsh, E.J.; et al. The Very Large G-Protein-Coupled Receptor VLGR1: A Component of the Ankle Link Complex Required for the Normal Development of Auditory Hair Bundles. *J. Neurosci.* **2006**, *26*, 6543–6553. [CrossRef] [PubMed]

15. van Wijk, E.; van der Zwaag, B.; Peters, T.; Zimmermann, U.; Brinke, H.T.; Kersten, F.F.; Märker, T.; Aller, E.; Hoefsloot, L.H.; Cremers, C.W.; et al. The DFNB31 gene product whirlin connects to the Usher protein network in the cochlea and retina by direct association with USH2A and VLGR1. *Hum. Mol. Genet.* **2006**, *15*, 751–765. [CrossRef] [PubMed]

16. Michalski, N.; Michel, V.; Bahloul, A.; Lefèvre, G.; Barral, J.; Yagi, H.; Chardenoux, S.; Weil, D.; Martin, P.; Hardelin, J.-P.; et al. Molecular Characterization of the Ankle-Link Complex in Cochlear Hair Cells and Its Role in the Hair Bundle Functioning. *J. Neurosci.* **2007**, *27*, 6478–6488. [CrossRef]

17. Reiners, J.; Van Wijk, E.; Märker, T.; Zimmermann, U.; Jürgens, K.; Brinke, H.T.; Overlack, N.; Roepman, R.; Knipper, M.; Kremer, H.; et al. Scaffold protein harmonin (USH1C) provides molecular links between Usher syndrome type 1 and type 2. *Hum. Mol. Genet.* **2005**, *14*, 3933–3943. [CrossRef]

18. Specht, D.; Wu, S.-B.; Turner, P.; Dearden, P.; Koentgen, F.; Wolfrum, U.; Maw, M.; Brandstätter, J.H.; Dieck, S.T. Effects of Presynaptic Mutations on a Postsynaptic Cacna1s Calcium Channel Colocalized with mGluR6 at Mouse Photoreceptor Ribbon Synapses. *Investig. Opthalmology Vis. Sci.* **2009**, *50*, 505–515. [CrossRef]

19. Yagi, H.; Tokano, H.; Maeda, M.; Takabayashi, T.; Nagano, T.; Kiyama, H.; Fujieda, S.; Kitamura, K.; Sato, M. Vlgr1 is required for proper stereocilia maturation of cochlear hair cells. *Genes Cells* **2007**, *12*, 235–250. [CrossRef]

20. Maerker, T.; Van Wijk, E.; Overlack, N.; Kersten, F.F.; McGee, J.; Goldmann, T.; Sehn, E.; Roepman, R.; Walsh, E.J.; Kremer, H.; et al. A novel Usher protein network at the periciliary reloading point between molecular transport machineries in vertebrate photoreceptor cells. *Hum. Mol. Genet.* **2008**, *17*, 71–86. [CrossRef]

21. Lin, H.-H.; Chang, G.-W.; Davies, J.Q.; Stacey, M.; Harris, J.; Gordon, S. Autocatalytic Cleavage of the EMR2 Receptor Occurs at a Conserved G Protein-coupled Receptor Proteolytic Site Motif. *J. Biol. Chem.* **2004**, *279*, 31823–31832. [CrossRef]

22. Araç, D.; Boucard, A.A.; Bolliger, M.F.; Nguyen, J.; Soltis, S.M.; Südhof, T.C.; Brunger, A.T. A novel evolutionarily conserved domain of cell-adhesion GPCRs mediates autoproteolysis. *EMBO J.* **2012**, *31*, 1364–1378. [CrossRef] [PubMed]

23. Prömel, S.; Frickenhaus, M.; Hughes, S.; Mestek, L.; Staunton, D.; Woollard, A.; Vakonakis, I.; Schöneberg, T.; Schnabel, R.; Russ, A.P.; et al. The GPS Motif Is a Molecular Switch for Bimodal Activities of Adhesion Class G Protein-Coupled Receptors. *Cell Rep.* **2012**, *2*, 321–331. [CrossRef] [PubMed]

24. Patra, C.; van Amerongen, M.J.; Ghosh, S.; Ricciardi, F.; Sajjad, A.; Novoyatleva, T.; Mogha, A.; Monk, K.R.; Mühlfeld, C.; Engel, F.B. Organ-specific function of adhesion G protein-coupled receptor GPR126 is domain-dependent. *Proc. Natl. Acad. Sci. USA* **2013**, *110*, 16898–16903. [CrossRef] [PubMed]

25. Okajima, D.; Kudo, G.; Yokota, H. Brain-specific angiogenesis inhibitor 2 (BAI2) may be activated by proteolytic processing. *J. Recept. Signal Transduct.* **2010**, *30*, 143–153. [CrossRef]

26. Paavola, K.J.; Stephenson, J.; Ritter, S.L.; Alter, S.P.; Hall, R.A. The N Terminus of the Adhesion G Protein-coupled Receptor GPR56 Controls Receptor Signaling Activity. *J. Biol. Chem.* **2011**, *286*, 28914–28921. [CrossRef]

27. Ward, Y.; Lake, R.; Yin, J.J.; Heger, C.D.; Raffeld, M.; Goldsmith, P.K.; Merino, M.; Kelly, K. LPA Receptor Heterodimerizes with CD97 to Amplify LPA-Initiated RHO-Dependent Signaling and Invasion in Prostate Cancer Cells. *Cancer Res.* **2011**, *71*, 7301–7311. [CrossRef]

28. Stephenson, J.; Paavola, K.J.; Schaefer, S.A.; Kaur, B.; Van Meir, E.G.; Hall, R.A. Brain-specific Angiogenesis Inhibitor-1 Signaling, Regulation, and Enrichment in the Postsynaptic Density. *J. Biol. Chem.* **2013**, *288*, 22248–22256. [CrossRef]

29. Liebscher, I.; Schöneberg, T. Tethered Agonism: A Common Activation Mechanism of Adhesion GPCRs. In *Handbook of Experimental Pharmacology*; Springer: Cham, Switzerland, 2016; Volume 234, pp. 111–125. [CrossRef]

30. Purcell, R.H.; Hall, R.A. Adhesion G Protein–Coupled Receptors as Drug Targets. *Annu. Rev. Pharmacol. Toxicol.* **2018**, *58*, 429–449. [CrossRef]

31. Braun, D.A.; Hildebrandt, F. Ciliopathies. *Cold Spring Harb. Perspect. Biol.* **2017**, *9*, a028191. [CrossRef]

32. Bujakowska, K.; Liu, Q.; Pierce, E.A. Photoreceptor Cilia and Retinal Ciliopathies. *Cold Spring Harb. Perspect. Biol.* **2017**, *9*, a028274. [CrossRef]

33. May-Simera, H.; Nagel-Wolfrum, K.; Wolfrum, U. Cilia—The sensory antennae in the eye. *Prog. Retin. Eye Res.* **2017**, *60*, 144–180. [CrossRef] [PubMed]

34. Satir, P. CILIA: Before and after. *Cilia* **2017**, *6*, 1. [CrossRef] [PubMed]

35. Knapp, B.; Wolfrum, U. Adhesion GPCR-Related Protein Networks. In *Handbook of Experimental Pharmacology*; Springer: Cham, Switzerland, 2016; Volume 234, pp. 147–178. [CrossRef]

36. Shin, D.; Lin, S.-T.; Fu, Y.-H.; Ptáček, L.J. Very large G protein-coupled receptor 1 regulates myelin-associated glycoprotein via $G_{\alpha s}$/$G_{\alpha q}$-mediated protein kinases A/C. *Proc. Natl. Acad. Sci. USA* **2013**, *110*, 19101–19106. [CrossRef] [PubMed]

37. Hu, Q.-X.; Dong, J.-H.; Du, H.-B.; Zhang, D.-L.; Ren, H.-Z.; Ma, M.-L.; Cai, Y.; Zhao, T.-C.; Yin, X.-L.; Yu, X.; et al. Constitutive Gαi Coupling Activity of Very Large G Protein-coupled Receptor 1 (VLGR1) and Its Regulation by PDZD7 Protein. *J. Biol. Chem.* **2014**, *289*, 24215–24225. [CrossRef]

38. Boldt, K.; Van Reeuwijk, J.; Lu, Q.; Koutroumpas, K.; Nguyen, T.-M.T.; Texier, Y.; Van Beersum, S.E.C.; Horn, N.; Willer, J.R.; Mans, D.A.; et al. An organelle-specific protein landscape identifies novel diseases and molecular mechanisms. *Nat. Commun.* **2016**, *7*, 11491. [CrossRef]

39. Mellacheruvu, D.; Wright, Z.; Couzens, A.L.; Lambert, J.-P.; St-Denis, N.A.; Li, T.; Miteva, Y.V.; Hauri, S.; Sardiu, M.E.; Low, T.Y.; et al. The CRAPome: A contaminant repository for affinity purification—Mass spectrometry data. *Nat. Methods* **2013**, *10*, 730–736. [CrossRef]

40. Bindea, G.; Mlecnik, B.; Hackl, H.; Charoentong, P.; Tosolini, M.; Kirilovsky, A.; Fridman, W.-H.; Pagès, F.; Trajanoski, Z.; Galon, J. ClueGO: A Cytoscape plug-in to decipher functionally grouped gene ontology and pathway annotation networks. *Bioinformatics* **2009**, *25*, 1091–1093. [CrossRef]

41. Hsiao, C.-C.; Chu, T.-Y.; Wu, C.-J.; van den Biggelaar, M.; Pabst, C.; Hébert, J.; Kuijpers, T.W.; Scicluna, B.P.; I, K.-Y.; Chen, T.-C.; et al. The Adhesion G Protein-Coupled Receptor GPR97/ADGRG3 Is Expressed in Human Granulocytes and Triggers Antimicrobial Effector Functions. *Front. Immunol.* **2018**, *9*, 2830. [CrossRef]

42. Appert-Collin, A.; Baisamy, L.; Diviani, D. Regulation of G Protein-Coupled Receptor Signaling by A-Kinase Anchoring Proteins. *J. Recept. Signal Transduct.* **2006**, *26*, 631–646. [CrossRef]

43. Kennedy, B.; Lamming, D.W. The Mechanistic Target of Rapamycin: The Grand ConducTOR of Metabolism and Aging. *Cell Metab.* **2016**, *23*, 990–1003. [CrossRef]

44. Semenza, G.L. Hypoxia-Inducible Factor 1 (HIF-1) Pathway. *Sci. STKE* **2007**, *2007*, cm8. [CrossRef] [PubMed]

45. Liebscher, I.; Schön, J.; Petersen, S.; Fischer, L.; Auerbach, N.; Demberg, L.M.; Mogha, A.; Cöster, M.; Simon, K.-U.; Rothemund, S.; et al. A Tethered Agonist within the Ectodomain Activates the Adhesion G Protein-Coupled Receptors GPR126 and GPR133. *Cell Rep.* **2014**, *9*, 2018–2026. [CrossRef] [PubMed]

46. Pisoni, G.B.; Molinari, M. Five Questions (with their Answers) on ER-Associated Degradation. *Traffic* **2016**, *17*, 341–350. [CrossRef] [PubMed]

47. Kusuluri, D.K.; Güler, B.E.; Knapp, B.; Horn, N.; Boldt, K.; Ueffing, M.; Aust, G.; Wolfrum, U. Adhesion G protein-coupled receptor VLGR1/ADGRV1 regulates cell spreading and migration by mechanosensing at focal adhesions. *iScience* **2021**, *24*, 102283. [CrossRef] [PubMed]

48. Geiger, B.; Spatz, J.P.; Bershadsky, A.D. Environmental sensing through focal adhesions. *Nat. Rev. Mol. Cell Biol.* **2009**, *10*, 21–33. [CrossRef] [PubMed]

49. Sun, Z.; Guo, S.S.; Fässler, R. Integrin-mediated mechanotransduction. *J. Cell Biol.* **2016**, *215*, 445–456. [CrossRef] [PubMed]

50. Owens, J.C.; Detweiler, C.S.; Li, J.J. CDC45 is required in conjunction with CDC7/DBF4 to trigger the initiation of DNA replication. *Proc. Natl. Acad. Sci. USA* **1997**, *94*, 12521–12526. [CrossRef]

51. Kumagai, H.; Sato, N.; Yamada, M.; Mahony, D.; Seghezzi, W.; Lees, E.; Arai, K.; Masai, H. A novel growth- and cell cycle-regulated protein, ASK, activates human Cdc7-related kinase and is essential for G1/S transition in mammalian cells. *Mol. Cell. Biol.* **1999**, *19*, 5083–5095. [CrossRef]

52. Lunn, C.L.; Chrivia, J.C.; Baldassare, J.J. Activation of Cdk2/Cyclin E complexes is dependent on the origin of replication licensing factor Cdc6 in mammalian cells. *Cell Cycle* **2010**, *9*, 4533–4541. [CrossRef]

53. Adams, M.; Simms, R.J.; Abdelhamed, Z.; Dawe, H.R.; Szymanska, K.; Logan, C.; Wheway, G.; Pitt, E.; Gull, K.; Knowles, M.A.; et al. A meckelin–filamin A interaction mediates ciliogenesis. *Hum. Mol. Genet.* **2012**, *21*, 1272–1286. [CrossRef]

54. Wei, Q.; Xu, Q.; Zhang, Y.; Li, Y.; Zhang, Q.; Hu, Z.; Harris, P.C.; Torres, V.E.; Ling, K.; Hu, J. Transition fibre protein FBF1 is required for the ciliary entry of assembled intraflagellar transport complexes. *Nat. Commun.* **2013**, *4*, 2750. [CrossRef] [PubMed]

55. Kypri, E.; Christodoulou, A.; Maimaris, G.; Lethan, M.; Markaki, M.; Lysandrou, C.; Lederer, C.W.; Tavernarakis, N.; Geimer, S.; Pedersen, L.B.; et al. The nucleotide-binding proteins Nubp1 and Nubp2 are negative regulators of ciliogenesis. *Cell. Mol. Life Sci.* **2014**, *71*, 517–538. [CrossRef] [PubMed]

56. Ronquillo, C.C.; Hanke-Gogokhia, C.; Revelo, M.P.; Frederick, J.M.; Jiang, L.; Baehr, W. Ciliopathy-associated IQCB1/NPHP5 protein is required for mouse photoreceptor outer segment formation. *FASEB J.* **2016**, *30*, 3400–3412. [CrossRef] [PubMed]

57. Tanos, B.E.; Yang, H.-J.; Soni, R.; Wang, W.-J.; Macaluso, F.P.; Asara, J.M.; Tsou, M.-F.B. Centriole distal appendages promote membrane docking, leading to cilia initiation. *Genes Dev.* **2013**, *27*, 163–168. [CrossRef] [PubMed]

58. Liu, Q.; Zuo, J.; Pierce, E. The Retinitis Pigmentosa 1 Protein Is a Photoreceptor Microtubule-Associated Protein. *J. Neurosci.* **2004**, *24*, 6427–6436. [CrossRef] [PubMed]

59. Ostergaard, P.; Simpson, M.; Mendola, A.; Vasudevan, P.; Connell, F.C.; van Impel, A.; Moore, A.T.; Loeys, B.; Ghalamkarpour, A.; Onoufriadis, A.; et al. Mutations in KIF11 Cause Autosomal-Dominant Microcephaly Variably Associated with Congenital Lymphedema and Chorioretinopathy. *Am. J. Hum. Genet.* **2012**, *90*, 356–362. [CrossRef]

60. Blangy, A.; Lane, H.A.; D'Hérin, P.; Harper, M.; Kress, M.; Nigg, E. Phosphorylation by p34cdc2 regulates spindle association of human Eg5, a kinesin-related motor essential for bipolar spindle formation in vivo. *Cell* **1995**, *83*, 1159–1169. [CrossRef]

61. Vance, J.E. MAM (mitochondria-associated membranes) in mammalian cells: Lipids and beyond. *Biochim. Et Biophys. Acta* **2014**, *1841*, 595–609. [CrossRef]

62. Knapp, B.; Rödig, J.; Boldt, K.; Krzysko, J.; Horn, N.; Ueffing, M.; Wolfrum, U. Affinity proteomics identifies novel functional modules related to adhesion GPCRs. *Ann. N. Y. Acad. Sci.* **2019**, *1456*, 144–167. [CrossRef]

63. Li, H.J.; Haque, Z.K.; Chen, A.; Mendelsohn, M. RIF-1, a novel nuclear receptor corepressor that associates with the nuclear matrix. *J. Cell. Biochem.* **2007**, *102*, 1021–1035. [CrossRef]

64. Xuan, S.; Baptista, C.A.; Balas, G.; Tao, W.; Soares, V.C.; Lai, E. Winged helix transcription factor BF-1 is essential for the development of the cerebral hemispheres. *Neuron* **1995**, *14*, 1141–1152. [CrossRef]

65. Pauley, S.; Lai, E.; Fritzsch, B. Foxg1 is required for morphogenesis and histogenesis of the mammalian inner ear. *Dev. Dyn.* **2006**, *235*, 2470–2482. [CrossRef]

66. Inoue, M.; Iida, A.; Satoh, S.; Kodama, T.; Watanabe, S. COUP-TFI and -TFII nuclear receptors are expressed in amacrine cells and play roles in regulating the differentiation of retinal progenitor cells. *Exp. Eye Res.* **2010**, *90*, 49–56. [CrossRef]

67. Lau, K.-F.; Chan, W.-M.; Perkinton, M.S.; Tudor, E.L.; Chang, R.C.C.; Chan, H.-Y.E.; McLoughlin, D.M.; Miller, C.C.J. Dexras1 Interacts with FE65 to Regulate FE65-Amyloid Precursor Protein-dependent Transcription. *J. Biol. Chem.* **2008**, *283*, 34728–34737. [CrossRef]

68. Ba, A.N.N.; Pogoutse, A.; Provart, N.; Moses, A.M. NLStradamus: A simple Hidden Markov Model for nuclear localization signal prediction. *BMC Bioinform.* **2009**, *10*, 202. [CrossRef]

69. Papasaikas, P.; Valcárcel, J. The Spliceosome: The Ultimate RNA Chaperone and Sculptor. *Trends Biochem. Sci.* **2016**, *41*, 33–45. [CrossRef] [PubMed]

70. Underwood, J.G.; Boutz, P.L.; Dougherty, J.D.; Stoilov, P.; Black, D.L. Homologues of the *Caenorhabditis elegans* Fox-1 Protein Are Neuronal Splicing Regulators in Mammals. *Mol. Cell. Biol.* **2005**, *25*, 10005–10016. [CrossRef]

71. Folk, P.; Půta, F.; Skružný, M. Transcriptional coregulator SNW/SKIP: The concealed tie of dissimilar pathways. *Cell. Mol. Life Sci.* **2004**, *61*, 629–640. [CrossRef]

72. Bertram, K.; Agafonov, D.E.; Liu, W.-T.; Dybkov, O.; Will, C.L.; Hartmuth, K.; Urlaub, H.; Kastner, B.; Stark, H.; Lührmann, R. Cryo-EM structure of a human spliceosome activated for step 2 of splicing. *Nature* **2017**, *542*, 318–323. [CrossRef]

73. Wolfe, M.S. Structure and Function of the γ-Secretase Complex. *Biochemistry* **2019**, *58*, 2953–2966. [CrossRef]

74. Zhou, S.; Zhou, H.; Walian, P.J.; Jap, B.K. CD147 is a regulatory subunit of the γ-secretase complex in Alzheimer's disease amyloid β-peptide production. *Proc. Natl. Acad. Sci. USA* **2005**, *102*, 7499–7504. [CrossRef] [PubMed]

75. Zhang, X.; Li, Y.; Xu, H.; Zhang, Y.-W. The Î³-secretase complex: From structure to function. *Front. Cell. Neurosci.* **2014**, *8*, 427. [CrossRef] [PubMed]

76. Chauvet, V.; Tian, X.; Husson, H.; Grimm, D.H.; Wang, T.; Hieseberger, T.; Igarashi, P.; Bennett, A.M.; Ibraghimov-Beskrovnaya, O.; Somlo, S.; et al. Mechanical stimuli induce cleavage and nuclear translocation of the polycystin-1 C terminus. *J. Clin. Investig.* **2004**, *114*, 1433–1443. [CrossRef] [PubMed]

77. Low, S.H.; Vasanth, S.; Larson, C.H.; Mukherjee, S.; Sharma, N.; Kinter, M.; Kane, M.E.; Obara, T.; Weimbs, T. Polycystin-1, STAT6, and P100 Function in a Pathway that Transduces Ciliary Mechanosensation and Is Activated in Polycystic Kidney Disease. *Dev. Cell* **2006**, *10*, 57–69. [CrossRef]

78. Lal, M.; Song, X.; Pluznick, J.L.; Di Giovanni, V.; Merrick, D.M.; Rosenblum, N.D.; Chauvet, V.; Gottardi, C.J.; Pei, Y.; Caplan, M.J. Polycystin-1 C-terminal tail associates with β-catenin and inhibits canonical Wnt signaling. *Hum. Mol. Genet.* **2008**, *17*, 3105–3117. [CrossRef]

79. Merrick, D.; Chapin, H.; Baggs, J.E.; Yu, Z.; Somlo, S.; Sun, Z.; Hogenesch, J.B.; Caplan, M.J. The γ-Secretase Cleavage Product of Polycystin-1 Regulates TCF and CHOP-Mediated Transcriptional Activation through a p300-Dependent Mechanism. *Dev. Cell* **2012**, *22*, 197–210. [CrossRef]

80. Chalasani, S.H.; Sabol, A.; Xu, H.A.; Gyda, M.A.; Rasband, K.; Granato, M.; Chien, C.-B.; Raper, J.A. Stromal Cell-Derived Factor-1 Antagonizes Slit/Robo Signaling In Vivo. *J. Neurosci.* **2007**, *27*, 973–980. [CrossRef]

81. Bellon, A.; Iyer, A.; Bridi, S.; Lee, F.; Ovando-Vázquez, C.; Corradi, E.; Longhi, S.; Roccuzzo, M.; Strohbuecker, S.; Naik, S.; et al. miR-182 Regulates Slit2-Mediated Axon Guidance by Modulating the Local Translation of a Specific mRNA. *Cell Rep.* **2017**, *18*, 1171–1186. [CrossRef]

82. Leyva-Díaz, E.; del Toro, D.; Menal, M.J.; Cambray, S.; Susín, R.; Tessier-Lavigne, M.; Klein, R.; Egea, J.; López-Bendito, G. FLRT3 Is a Robo1-Interacting Protein that Determines Netrin-1 Attraction in Developing Axons. *Curr. Biol.* **2014**, *24*, 494–508. [CrossRef]

83. O'Sullivan, M.L.; de Wit, J.; Savas, J.N.; Comoletti, D.; Otto-Hitt, S.; Yates, J.R., 3rd; Ghosh, A. FLRT Proteins Are Endogenous Latrophilin Ligands and Regulate Excitatory Synapse Development. *Neuron* **2012**, *73*, 903–910. [CrossRef]

84. Puppo, F.; Thomé, V.; Lhoumeau, A.; Cibois, M.; Gangar, A.; Lembo, F.; Belotti, E.; Marchetto, S.; Lécine, P.; Prébet, T.; et al. Protein tyrosine kinase 7 has a conserved role in Wnt/β-catenin canonical signalling. *EMBO Rep.* **2011**, *12*, 43–49. [CrossRef] [PubMed]

85. Matsuda, S.; Matsuda, Y.; D'Adamio, L. BRI3 Inhibits Amyloid Precursor Protein Processing in a Mechanistically Distinct Manner from Its Homologue Dementia Gene BRI2. *J. Biol. Chem.* **2009**, *284*, 15815–15825. [CrossRef] [PubMed]

86. Yamagata, M.; Weiner, J.; Sanes, J.R. Sidekicks: Synaptic Adhesion Molecules that Promote Lamina-Specific Connectivity in the Retina. *Cell* **2002**, *110*, 649–660. [CrossRef]

87. Yamagata, M.; Sanes, J.R. Synaptic Localization and Function of Sidekick Recognition Molecules Require MAGI Scaffolding Proteins. *J. Neurosci.* **2010**, *30*, 3579–3588. [CrossRef] [PubMed]

88. Stevens, C.B.; Cameron, D.A.; Stenkamp, D.L. Plasticity of photoreceptor-generating retinal progenitors revealed by prolonged retinoic acid exposure. *BMC Dev. Biol.* **2011**, *11*, 51. [CrossRef]

89. Zhang, C.; Baudino, T.A.; Dowd, D.R.; Tokumaru, H.; Wang, W.; MacDonald, P.N. Ternary Complexes and Cooperative Interplay between NCoA-62/Ski-interacting Protein and Steroid Receptor Coactivators in Vitamin D Receptor-mediated Transcription. *J. Biol. Chem.* **2001**, *276*, 40614–40620. [CrossRef]

90. Carpio, R.V.-D.; Kaplan, F.M.; Weaver, K.L.; VanWye, J.D.; Alves-Guerra, M.-C.; Robbins, D.J.; Capobianco, A.J. Assembly of a Notch Transcriptional Activation Complex Requires Multimerization. *Mol. Cell. Biol.* **2011**, *31*, 1396–1408. [CrossRef]
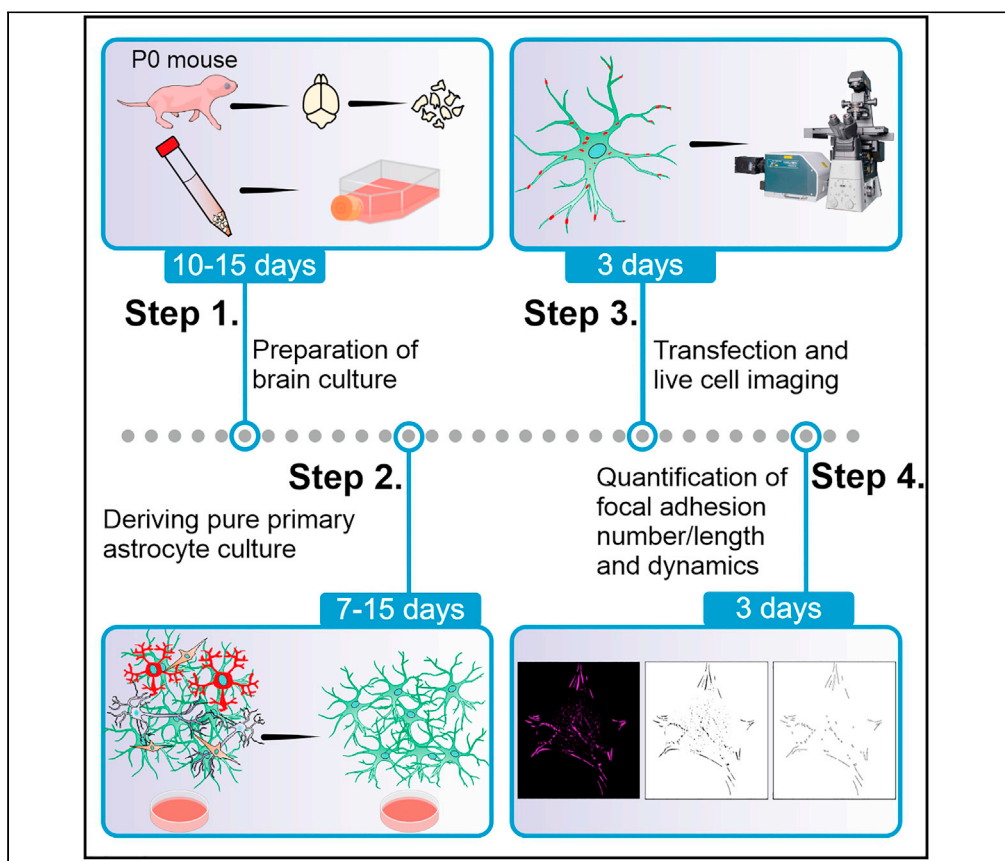
91. Birtel, J.; Gliem, M.; Mangold, E.; Tebbe, L.; Spier, I.; Müller, P.L.; Holz, F.G.; Neuhaus, C.; Wolfrum, U.; Bolz, H.J.; et al. Novel Insights into the Phenotypical Spectrum of *KIF11*-Associated Retinopathy, Including a New Form of Retinal Ciliopathy. *Investig. Opthalmology Vis. Sci.* **2017**, *58*, 3950–3959. [CrossRef]

92. Ronquillo, C.C.; Bernstein, P.S.; Baehr, W. Senior–Løken syndrome: A syndromic form of retinal dystrophy associated with nephronophthisis. *Vis. Res.* **2012**, *75*, 88–97. [CrossRef]

93. Gao, J.; Cheon, K.; Nusinowitz, S.; Liu, Q.; Bei, D.; Atkins, K.; Azimi, A.; Daiger, S.P.; Farber, D.B.; Heckenlively, J.R.; et al. Progressive photoreceptor degeneration, outer segment dysplasia, and rhodopsin mislocalization in mice with targeted disruption of the retinitis pigmentosa-1 (*Rp1*) gene. *Proc. Natl. Acad. Sci. USA* **2002**, *99*, 5698–5703. [CrossRef]

94. Liu, Q.; Lyubarsky, A.; Skalet, J.H.; Pugh, E.N., Jr.; Pierce, E.A. RP1 Is Required for the Correct Stacking of Outer Segment Discs. *Investig. Opthalmology Vis. Sci.* **2003**, *44*, 4171–4183. [CrossRef] [PubMed]

95. Schmidt-Kastner, R.; Kreczmanski, P.; Preising, M.; Diederen, R.; Schmitz, C.; Reis, D.; Blanks, J.; Dorey, C.K. Expression of the diabetes risk gene wolframin (WFS1) in the human retina. *Exp. Eye Res.* **2009**, *89*, 568–574. [CrossRef] [PubMed]

96. Liu, Q.; Tan, G.; Levenkova, N.; Li, T.; Pugh, E.N., Jr.; Rux, J.J.; Speicher, D.W.; Pierce, E.A. The Proteome of the Mouse Photoreceptor Sensory Cilium Complex. *Mol. Cell. Proteom.* **2007**, *6*, 1299–1317. [CrossRef] [PubMed]

97. Tranebjaerg, L.; Barrett, T.; Rendtorff, N.D. WFS1-Related Disorders. In *GeneReviews (R)*; Pagon, R.A., Adam, M.P., Ardinger, H.H., Wallace, S.E., Amemiya, A., Bean, L.J.H., Bird, T.D., Ledbetter, N., Mefford, H.C., Smith, R.J.H., et al., Eds.; University of Washington: Seattle, WA, USA, 1993.

98. Wang, J.; Zhong, J.; Chen, G.; Li, M.; Wu, F.-X.; Pan, Y. ClusterViz: A Cytoscape APP for Cluster Analysis of Biological Network. *IEEE/ACM Trans. Comput. Biol. Bioinform.* **2015**, *12*, 815–822. [CrossRef]

99. Raggenbass, M.; Bertrand, D. Nicotinic receptors in circuit excitability and epilepsy. *J. Neurobiol.* **2002**, *53*, 580–589. [CrossRef]

100. Chen, T.T.; Klassen, T.L.; Goldman, A.M.; Marini, C.; Guerrini, R.; Noebels, J.L. Novel brain expression of ClC-1 chloride channels and enrichment of CLCN1 variants in epilepsy. *Neurology* **2013**, *80*, 1078–1085. [CrossRef]

101. Xie, H.; Zhang, Y.; Zhang, P.; Wang, J.; Wu, Y.; Wu, X.; Netoff, T.; Jiang, Y. Functional Study of NIPA2 Mutations Identified from the Patients with Childhood Absence Epilepsy. *PLoS ONE* **2014**, *9*, e109749. [CrossRef]

102. Greeve, I.; Hermans-Borgmeyer, I.; Brellinger, C.; Kasper, D.; Gomez-Isla, T.; Behl, C.; Levkau, B.; Nitsch, R.M. The human DIMINUTO/DWARF1 homolog seladin-1 confers resistance to Alzheimer's disease-associated neurodegeneration and oxidative stress. *J. Neurosci.* **2000**, *20*, 7345–7352. [CrossRef]

103. Khanim, F.; Kirk, J.; Latif, F.; Barrett, T. WFS1/wolframin mutations, Wolfram syndrome, and associated diseases. *Hum. Mutat.* **2001**, *17*, 357–367. [CrossRef]

104. Al-Saif, A.; Al-Mohanna, F.; Bohlega, S. A mutation in sigma-1 receptor causes juvenile amyotrophic lateral sclerosis. *Ann. Neurol.* **2011**, *70*, 913–919. [CrossRef]

105. O'Brien, R.J.; Wong, P.C. Amyloid Precursor Protein Processing and Alzheimer's Disease. *Annu. Rev. Neurosci.* **2011**, *34*, 185–204. [CrossRef] [PubMed]

106. Kojro, E.; Fahrenholz, F. The Non-Amyloidogenic Pathway: Structure and Function of α-Secretases. *Sub-Cell. Biochem.* **2005**, *38*, 105–127. [CrossRef]

107. Chow, V.W.; Mattson, M.P.; Wong, P.C.; Gleichmann, M. An Overview of APP Processing Enzymes and Products. *Neuromol. Med.* **2010**, *12*, 1–12. [CrossRef] [PubMed]

108. Kounnas, M.Z.; Moir, R.D.; Rebeck, G.W.; Bush, A.I.; Argraves, W.S.; Tanzi, R.E.; Hyman, B.T.; Strickland, D.K. LDL receptor-related protein, a multifunctional ApoE receptor, binds secreted beta-amyloid precursor protein and mediates its degradation. *Cell* **1995**, *82*, 331–340. [CrossRef]

109. Cao, X.; Südhof, T.C. A Transcriptively Active Complex of APP with Fe65 and Histone Acetyltransferase Tip60. *Science* **2001**, *293*, 115–120. [CrossRef]

110. Sumioka, A.; Nagaishi, S.; Yoshida, T.; Lin, A.; Miura, M.; Suzuki, T. Role of 14-3-3γ in FE65-dependent Gene Transactivation Mediated by the Amyloid β-Protein Precursor Cytoplasmic Fragment. *J. Biol. Chem.* **2005**, *280*, 42364–42374. [CrossRef]

111. Sabo, S.L.; Lanier, L.M.; Ikin, A.F.; Khorkova, O.; Sahasrabudhe, S.; Greengard, P.; Buxbaum, J.D. Regulation of beta-amyloid secretion by FE65, an amyloid protein precursor-binding protein. *J. Biol. Chem.* **1999**, *274*, 7952–7957. [CrossRef]

112. Klug, W.; Dietl, A.; Simon, B.; Sinning, I.; Wild, K. Phosphorylation of LRP1 regulates the interaction with Fe65. *FEBS Lett.* **2011**, *585*, 3229–3235. [CrossRef]

113. Malicki, J.J.; Johnson, C.A. The cilium: Cellular antenna and central processing unit. *Trends Cell Biol.* **2017**, *27*, 126–140. [CrossRef]

114. Waterham, H.R.; Koster, J.; Romeijn, G.J.; Hennekam, R.C.; Vreken, P.; Andersson, H.C.; FitzPatrick, D.R.; Kelley, R.I.; Wanders, R.J. Mutations in the 3β-Hydroxysterol Δ24-Reductase Gene Cause Desmosterolosis, an Autosomal Recessive Disorder of Cholesterol Biosynthesis. *Am. J. Hum. Genet.* **2001**, *69*, 685–694. [CrossRef]

115. Canault, M.; Tellier, E.; Bonardo, B.; Mas, E.; Aumailley, M.; Juhan-Vague, I.; Nalbone, G.; Peiretti, F. FHL2 interacts with both ADAM-17 and the cytoskeleton and regulates ADAM-17 localization and activity. *J. Cell. Physiol.* **2006**, *208*, 363–372. [CrossRef] [PubMed]

116. Tanahashi, H.; Tabira, T. Alzheimer's disease-associated presenilin 2 interacts with DRAL, an LIM-domain protein. *Hum. Mol. Genet.* **2000**, *9*, 2281–2289. [CrossRef] [PubMed]

117. Güler, B.E.; Krzysko, J.; Wolfrum, U. Isolation and culturing of primary mouse astrocytes for the analysis of focal adhesion dynamics. *STAR Protoc.* **2021**, *2*, 100954. [CrossRef] [PubMed]

118. Gloeckner, C.J.; Boldt, K.; Schumacher, A.; Roepman, R.; Ueffing, M. A novel tandem affinity purification strategy for the efficient isolation and characterisation of native protein complexes. *Proteomics* **2007**, *7*, 4228–4234. [CrossRef] [PubMed]

119. Bohnekamp, J.; Schöneberg, T. Cell Adhesion Receptor GPR133 Couples to Gs Protein. *J. Biol. Chem.* **2011**, *286*, 41912–41916. [CrossRef]

120. Berridge, M.J. Rapid accumulation of inositol trisphosphate reveals that agonists hydrolyse polyphosphoinositides instead of phosphatidylinositol. *Biochem. J.* **1983**, *212*, 849–858. [CrossRef]

121. Schoneberg, T.; Schulz, A.; Biebermann, H.; Gruters, A.; Grimm, T.; Hubschmann, K.; Filler, G.; Gudermann, T.; Schultz, G. V2 vasopressin receptor dysfunction in nephrogenic diabetes insipidus caused by different molecular mechanisms. *Hum. Mutat.* **1998**, *12*, 196–205. [CrossRef]

122. Wilde, C.; Fischer, L.; Lede, V.; Kirchberger, J.; Rothemund, S.; Schöneberg, T.; Liebscher, I. The constitutive activity of the adhesion GPCR GPR114/ADGRG5 is mediated by its tethered agonist. *FASEB J.* **2015**, *30*, 666–673. [CrossRef]

Publikation III

STAR Protocols

Protocol

Isolation and culturing of primary mouse astrocytes for the analysis of focal adhesion dynamics

Baran E. Güler,
Jacek Krzysko, Uwe
Wolfrum

wolfrum@uni-mainz.de

Highlights

High purity of primary
mouse astrocyte
isolation without
commercial kits

Isolated mouse
primary astrocytes
are functional for
downstream
applications

Quantitative analysis
of focal adhesion
properties in fixed
and living astrocytes

Primary astrocytes have gained attention as an important model for *in vitro* biological and biochemical research in the last decades. In this protocol, we describe a fast and cost-effective technique for isolating, culturing and maintaining primary mouse astrocytes at ∼ 80% purity levels, which can be used in *in vitro* studies for migration and focal adhesion dynamics. In addition, we present an optimized transfection and manual quantification approach for focal adhesion analysis in fixed and living cells.

Protocol

Isolation and culturing of primary mouse astrocytes for the analysis of focal adhesion dynamics

Baran E. Güler,[1,2] Jacek Krzysko,[1] and Uwe Wolfrum[1,2,3,*]

[1]Institute of Molecular Physiology, Molecular Cell Biology, Johannes Gutenberg University of Mainz, Hanns-Dieter-Hüsch-Weg 17, 55128 Mainz, Germany

[2]Technical contact

[3]Lead contact

*Correspondence: wolfrum@uni-mainz.de
https://doi.org/10.1016/j.xpro.2021.100954

SUMMARY

Primary astrocytes have gained attention as an important model for *in vitro* biological and biochemical research in the last decades. In this protocol, we describe a fast and cost-effective technique for isolating, culturing, and maintaining primary mouse astrocytes at ∼ 80% purity levels, which can be used in *in vitro* studies for migration and focal adhesion dynamics. In addition, we present an optimized transfection and manual quantification approach for focal adhesion analysis in fixed and living cells.
For complete details on the use and execution of this protocol, please refer to Kusuluri et al. (2021).

BEFORE YOU BEGIN

Dissection of mice and preparation of brain culture should be performed under sterile conditions. All equipment (Biosafety cabinet, forceps, scissors and plates, etc.) should be sterile to prevent any contamination. In this protocol, the isolation of primary astrocytes cells depends on the differential binding method which separates primary astrocytes, oligodendrocyte progenitor cells (OPCs) and microglia cells based on their different affinities for bacterial grade plastic dishes. Do not use plates that have been treated for animal cell culture because all cell types will attach to these plates with equal affinities. Primary astrocytes were isolated from brains of P0 C57BL/6J (wild type). This protocol was also successfully applied for two mouse models for Usher syndrome 2C namely *Vlgr1/del7TM* (McMillan and White, 2004) and *Drum B* mutated mice (Potter et al., 2016), bred on a C57BL/6J background and we did not observe any difference in protocol efficiency. All experiments described herein were performed in accordance with the guidelines provided by Association for Research in Vision and Ophthalmology.

Before starting the experiment several chemicals and surgical instruments should be prepared (For detailed information please see key resources table and materials and equipment section).

KEY RESOURCES TABLE

REAGENT or RESOURCE	SOURCE	IDENTIFIER
Antibodies		
Rabbit monoclonal anti-GFAP (Glial fibrillary acidic protein), working dilution 1 in 1000	DAKO-Agilent	Cat#ZO334
Mouse monoclonal anti-GFAP (Glial fibrillary acidic protein), working dilution 1 in 1000	Sigma-Aldrich	Cat#G3839

(Continued on next page)

Continued

REAGENT or RESOURCE	SOURCE	IDENTIFIER
Guineapig monoclonal anti-MAP2 (Microtubule associated protein), working dilution 1 in 1000	Synaptic systems	Cat#188004
Mouse monoclonal anti-Vinculin, working dilution 1 in 100	Sigma-Aldrich	Cat#V9131
Rabbit polyclonal anti- PDGFR-α, working dilution 1 in 200	Santa Cruz Biotechnology, Inc.	Cat#sc-338
Rat monoclonal anti-CD68, working dilution 1 in 200	Bio-Rad Laboratories	Cat#MCA1957
Chemicals, peptides, and recombinant proteins		
Alexa Fluor 488-conjugated goat anti-rabbit IgG, working dilution 1 in 400	Molecular Probes	Cat#A-11034
Alexa Fluor 568-conjugated goat anti-rat IgG, working dilution 1 in 400	Biotrend	Cat#20092-1
Alexa Fluor 640-conjugated goat anti-mouse IgG, working dilution 1 in 200	Biotrend	Cat#20177
Phalloidin-TRITC, working dilution 1 in 400	Sigma-Aldrich	Cat#P1951
Dulbecco's Modified Eagle Medium (DMEM)	Gibco™	Cat#31966-021
Fetal bovine serum (FBS)	Gibco™	Cat#16000044
Penicillin-streptomycin	Gibco™	Cat#15140122
10× Hanks' Balanced Salt Solution (HBSS)	Gibco™	Cat#14065-056
1 M HEPES solution	Gibco™	Cat#15630106
DNase I, recombinant, Grade II, from bovine pancreas	Merck	Cat#10104159001
0.01% Poly-L-Lysine solution	Sigma-Aldrich	Cat#25988-63-0
0.05% Trypsin-EDTA (1×)	Gibco™	Cat#25300-054
1×PBS	Gibco™	Cat#14190-094
Opti-MEM™ I Reduced Serum Medium	Thermo Fisher Scientific	Cat#31985062
GeneJuice® Transfection Reagent	Merck	Cat#70967-6
Fibronectin bovine plasma	Merck	Cat#F4759-5MG
Albumin crude from chicken egg = Ovalbumin	PanReac AppliChem	Cat#A4344
Gelatin From Cold Water Fish Skin, 40–50% in Water	Sigma-Aldrich	Cat#G7765-250ML
Deposited data		
Raw and analyzed data	This paper and Kusuluri et al. (2021)	N/A
Experimental models: organisms/strains		
Mouse: C57BL/6J (P0 age)	The Jackson Laboratory	Stock no: 000664
Mouse: *Vlgr1*/del7TM (P0 age)	Breed on a C57BL/6 background	McMillan and White (2004)
Mouse: *Drum* B (P0 age)	Breed on a C57BL/6 background	Potter et al. (2016) and Kusuluri et al. (2021)
Recombinant DNA		
RFP-Paxillin	Rudolf E. Leube, Rick Horwitz	Rudolf E. Leube, Rick Horwitz
Software and algorithms		
ImageJ software	National Institutes of Health (NIH)	http://imagej.nih.gov/ij/download.html
Focal adhesion analysis server	https://faas.bme.unc.edu	Berginski and Gomez (2013)
Other		
Stereomicroscope	Leica Microsystems	Leica WILD M3B
Cold light source	Leica Microsystems	Schott KL750
Inverted microscope	Nikon Instruments Inc.	Nikon Eclipse Ti2-E
Spinning disc unit	Yokogawa Electric Corporation	CSU-W1
Leica confocal microscope	Leica Microsystems	DM6000B
Centrifuge	Eppendorf	Centrifuge 5430 R
Medium-sized scissors	A. Dumont & Fils	Cat#T5074
Dumont #3 curved forceps	A. Dumont & Fils	Cat#T504
Dumont #4 standard tip forceps	A. Dumont & Fils	Cat#T505
Dumont #7 standard tip forceps	A. Dumont & Fils	Cat#T508
Vannas spring scissors	A. Dumont & Fils	Cat#T5322
100 mm petri dish (cell culture)	Greiner Bio-One	Cat#664160
100 mm bacterial grade petri dish	SARSTEDT AG & Co. KG	Cat#82.1472
T-75 culture flasks	Greiner Bio-One	Cat#658170
6-well culture plates	Greiner Bio-One	Cat#657160
15 mL Centrifuge Tubes	SARSTEDT AG & Co. KG	Cat#62.554.502

(Continued on next page)

Continued

REAGENT or RESOURCE	SOURCE	IDENTIFIER
10 mm glass coverslips	Carl Roth GmbH +Co. KG	Cat#YX02.1
0.22 μm filter	Carl Roth GmbH +Co. KG	Cat#KH541
0.45 μm filter	Carl Roth GmbH +Co. KG	Cat#CCX9.1
μ-Slide 4 Well chamber	Ibidi GmbH	Cat#80426

MATERIALS AND EQUIPMENT

Growth medium		
Reagent	Final concentration	Amount
Dulbecco's Modified Eagle Medium (DMEM)	n/a	450 mL
Fetal bovine serum (FBS)	10%	50 mL
Penicillin-streptomycin	2%	11 mL
Total	n/a	511 mL

⚠ CRITICAL: Final antibiotic concentration may be adjusted, since different antibiotic concentrations can affect cell proliferation and differentiation.

Note: Growth medium should be kept at +4°C for a maximum of 1 month. If there is a pH level change during storage which can be distinguished by a color change, new medium should be prepared.

1× HBSS for brain tissue storage during dissection		
Reagent	Final concentration	Amount
10× HBSS	1×	100 mL
1 M HEPES	0.01 M	10 mL
ddH$_2$O	n/a	890 mL
Total	n/a	1000 mL

⚠ CRITICAL: Adjust pH 7.0 of buffer using 1 N HCl or 1 N NaOH and sterile medium by passing through a 0.22 μm filter.

Note: Medium should be stored at +4°C for a maximum of 1 month. If there is a pH level change during storage which can be distinguished by the color change in medium, the new medium should be prepared.

DNase I solution		
Reagent	Final concentration	Amount
DNase I	0.05%	100 mg
1× HBSS	n/a	200 mL
Total	n/a	200 mL

⚠ CRITICAL: Do not dissolve the DNase I by using vortex as mechanical force may denaturate the enzyme which can cause decrease in the activity. The solution should be prepared by pipetting and sterilized by passing through a 0.22 μm filter. To prevent any freeze/thaw

cycles which may reduce activity, 1–5 mL aliquots can be prepared and kept at –20°C or –80°C for a maximum of 6 months.

Blocking solution		
Reagent	Final concentration	Amount
Ovalbumin	0.1%	0.1 g
40–50% Fish gelatin	0.5%	1.1 g
1× PBS	n/a	100 mL
Total	n/a	100 mL

Note: Mix the Ovalbumin and 40%–50% Fish gelatin in 100 mL PBS for 12–16 h. The day after, bring the temperature of the solution to 50°C. Centrifuge for 10 min at 3000 RCF to remove undissolved particles. Sterile medium by passing through a 0.45 µm filter. In order to prevent freeze/thaw cycles, prepare 1–2 mL aliquots and keep at −20°C for a maximum of 12 months.

STEP-BY-STEP METHOD DETAILS
Preparation of primary brain culture

⊘ Timing: 10–15 days

Before starting dissection of mice pups, place 10 mL of 1× HBSS (in a 15 mL Falcon tube), 1 mL of 0.05% DNase I and 1 mL of 0.05% trypsin on ice and arrange dissection tools, microscope, a cold light source and 70% ethanol under the dissection hood. This step includes dissection and preparation of primary brain cultures. To obtain a confluent layer of primary astrocytes cells, collect 3–4 pups' brains in a 15 mL tube containing 1× HBSS solution.

Preparation of brain tissue

⊘ Timing: 15–30 min

1. Before starting the dissection, gently hold the mice pup and spray the neck with 70% of ethanol to prevent contamination.
2. Decapitation of mice can be done by using sharp scissors in one cut.

   △ CRITICAL: Brain isolation can take time due to inexperience. In order to achieve high efficiency after the procedure and healthy brain culture, only one decapitation should be applied at a time and the remaining decapitation procedures should be carried out after step 14 is finished from the first mouse.

3. To keep the head fixed and stabile use anchoring forceps at orbital cavities (Figure 1A).
4. Make an incision of the skin at the hindbrain and follow along the midline to eye level where transverse cuts to the eye cavity will be made (Figure 1B).
5. Grasp the skin from both sides by using Dumont #5 forceps and pull it aside to reveal the skull (Figure 1C).
6. Carefully cut the cranium using a small scissors. The cut should start from the neck where the vertebral foramen is located and extended anteriorly to the nose. Make additional transverse cuts to the eye cavity.

   △ CRITICAL: While cutting the cranium be sure that no excess pressure is applied to the brain. This may cause deformation in brain tissue and bleeding, which can lower culture purity because of contamination with red blood cells and endothelial cells.
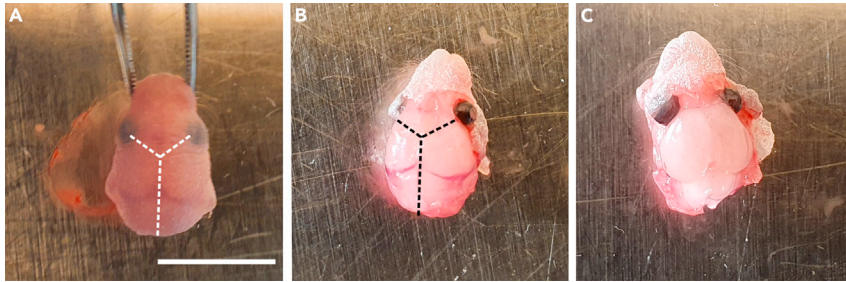
Figure 1. Dissection of the brain from PN0 mouse
(A and B) (A) Cut should be performed to remove the skin and (B) skull layers covering the brain. Dashed lines indicate the cuts using Vannas spring scissors. The cut starts from the neck where the vertebral foramen is located and extends anteriorly to the nose.
(C) Exposed brain. Scale bar: 5 mm.

7. Carefully pull apart the cranium using forceps to reveal the brain.
8. Take out the brain with the help of a small spatula. First, place the spatula under the cerebellum and gently push it towards the olfactory bulbs and scoop out by lifting. This will disconnect the brain from the skull base.
9. Transfer the brain to a 10 cm petri dish containing ice-cold 1× HBSS under sterile conditions. The brain should submerge completely in the liquid.
10. Remove olfactory bulbs in order to free the meninges. Meninges can be distinguished by their reddish color resulting from blood vessels (Figures 2A and 2B).
11. Reversing the brain and starting from the bottom side can help to remove meninges easily. Dissect the meninges from the surface of the cortical layer by using fine forceps.

   Note: We observed that keeping brain integrity during the process may reduce the risk of meningeal cells and fibroblast contamination and ensure full removal.

12. Flip the brain and continue meninges removal.
13. Carefully check whether there is any meninges residue and if not, cut the brain into 6–10 pieces using forceps or sharp blades in order to increase disassociation efficiency (Figure 2C).
14. Place the brain pieces into a 15 mL tubes that contain 10 mL 1× HBSS and keep on ice (Figure 3A).

   △ CRITICAL: Only 3–4 brains should be collected in 10 mL 1× HBSS. If more brain tissue is needed, use a 50 mL Falcon and increase the volume of 1× HBSS for 5 brains to 11 mL and for 12 brains 20 mL. If the brain pieces are not submerged completely, tap the bottom of the Falcon tube. This may help to submerge brain pieces that float on top.

   Note: After obtaining meninges-free brain, repeat the steps 1–14 for the rest of the mice. Doing only one brain at a time will ensure healthy cultures.

15. Under the sterile condition, add ice cold 0.05% DNase I into the tube and gently triturate brain tissue 10–15 times with a 10 mL and 2 mL pipette, respectively.
16. Afterwards, add 0.05% trypsin, mix by using 10 mL pipette 20–30 times and incubate at room temperature (22°C–25°C) for 20 min.

   △ CRITICAL: The amount of DNase I and trypsin can be adjusted depending on the number of brains in one tube. For 3–4 brains; 1 mL of DNase I and 1 mL of trypsin, for 5 brains; 1.5 mL of DNase I and 1.5 mL of trypsin, for 12 brains; 3 mL of DNase I and 3 mL of trypsin should be added.
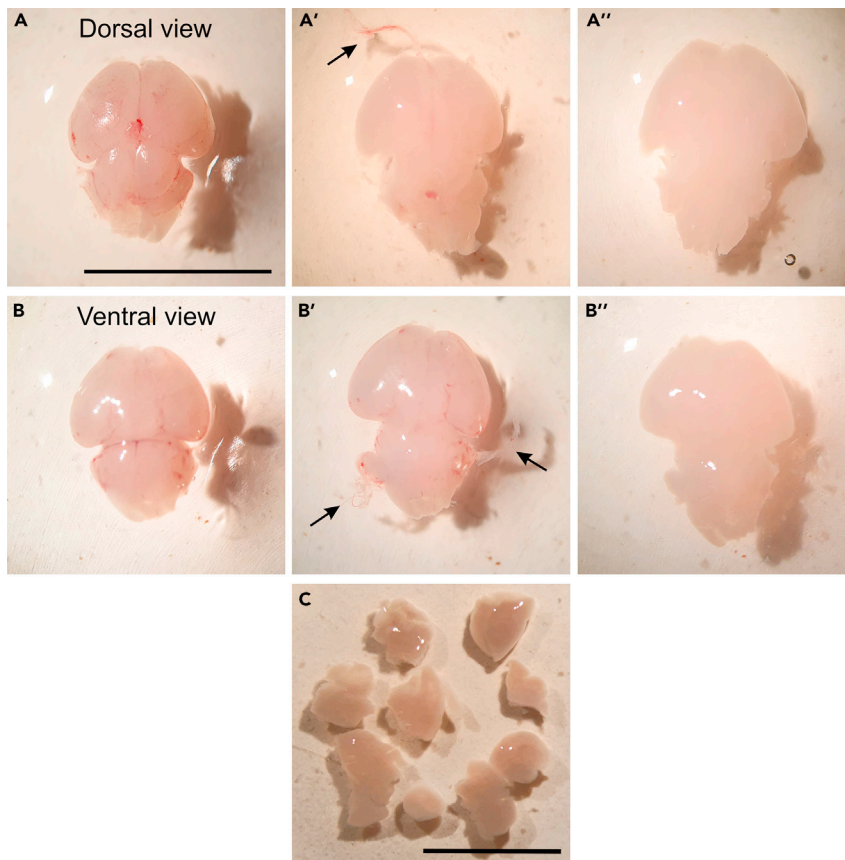
Figure 2. Dissection of mouse brain at P0
(A and B) Removing the meninges from mouse brain. (A) Dorsal view (B) and ventral view of isolated mouse brain. Meninges can be distinguished by reddish color in the cortex of the mouse brain. (A′ and B′) Meninges removal from the cortex of the mouse brain. Arrows indicate removed meninges from the cortex of the mouse brain. (A″ and B″) Dorsal and ventral view of completely meninges-free brain.
(C) Dissection of brain parts with a sharp razor blade or fine forceps. Scale bars: A and B: 10 mm; C: 5 mm.

17. During incubation time, prepare one T-75 flask for 3–4 brains and coat with 3 mL of 0.01% Poly-L-Lysine (PLL) for 20 min. Place the T-75 flask in the incubator.
18. 20 min after incubation of brain pieces mix the Falcon tube thoroughly (Figure 3B).
19. Centrifuge for 10 min at 150 RCF to the pellet brain tissue (Figure 3C).
20. After centrifugation, carefully aspirate the supernatant using a Pasteur pipette connected to a pump (Figure 3D).

    Note: If there is any meninges residue or blood vessel contamination, which can be distinguished by a reddish color on top of the pellet, also aspirate and discard this layer. Resuspend pellet with 2 mL of complete growth medium and repeat centrifugation step.

21. Resuspend cell pellet with 2–4 mL of DMEM with a 10 mL pipette and mix thoroughly 10–20 times in order to obtain a single-cell suspension (Figure 3E).
22. Aspirate PLL from the T-75 flask and rinse with 10 mL of DMEM to completely wash out any residue. Add 8–10 mL of pre-warmed 37°C DMEM supplemented with 10% FBS and 2% pen/strep.
23. Plate the resuspended cell pellet and incubate at 37°C with 5% CO_2 in an incubator.
24. Change the medium on day 1, day 2 and day 7 after plating the primary cells (Figure 7A).
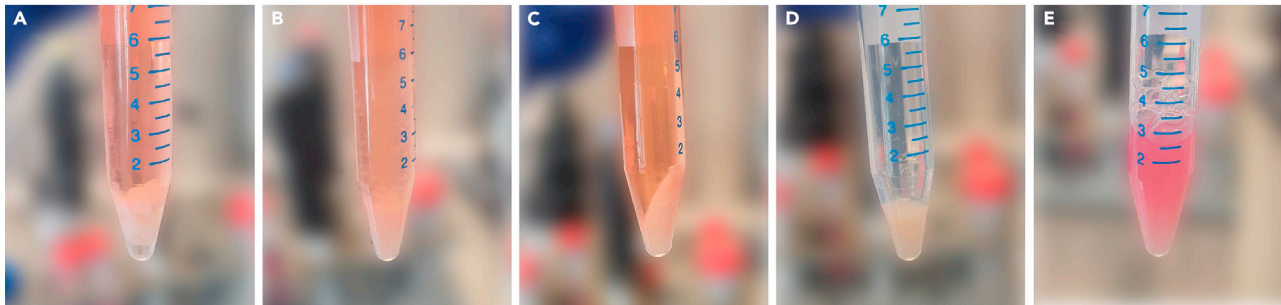
Figure 3. Dissociation of mouse brain tissue for primary cell cultivation
(A) Brain tissue dissected from wild type mice in 1× HBSS.
(B) Homogenized mouse brain tissue (MBT).
(C) MBT pellet after centrifugation.
(D) MBT pellet after removing supernatant.
(E) Resuspended MBT pellet in complete growth medium.

> *Note:* In order to remove unattached and death cells wash the plate by using 1× PBS, before adding fresh complete growth medium.

Deriving pure primary mouse astrocyte culture

⊙ Timing: 7–15 days

This step will be used for the separation of primary astrocytes cells from oligodendrocyte progenitor cells (OPCs), microglia and neurons. In confluence, their tight arrangement at the bottom of the culture flask can distinguish primary astrocytes cells from other cell types. Widefield microcopy distinguishes microglia cells from other brain-derived cells revealing a bright and small rounded cell morphology.

Removal of oligodendrocyte progenitor cells (OPCs)

⊙ Timing: 10–20 min

25. Mixed primary cell cultures which were obtained in steps 1 to 24 reach full confluency on days 10–15. When mixed cell culture reach confluency, gently tap the flask from both sides several times in order to detach the OPCs layer. After tapping the flask, check the cells under the microscope. Detach OPCs can be distinguished as floating cells in the plate (Figure 4).

> *Note:* In case of incomplete detachment repeat tapping several times. Tapping should be done gently so as not detach the astrocyte layer.

26. After the OPCs are released aspirate the medium completely to remove detached cells and rinse remaining cells carefully with 10 mL of complete growth medium.

> *Note:* To avoid any loosening or loss of astrocyte layer, medium aspiration and rinsing should be done carefully. A 10 mL pipette should be placed at the corner of the flask and the medium should be slowly added against the wall of the flask and not directly onto the attached cells.

27. After removing OPCs, add 10 mL of complete growth medium and ice cold 0.5 mL DNase I to loosen the remaining cell layer and incubate 5 min at 37°C with 5% CO_2 in an incubator.
28. After DNase I treatment, the remaining OPCs are released by horizontal shaking the T-75 Flask 20–30 times.
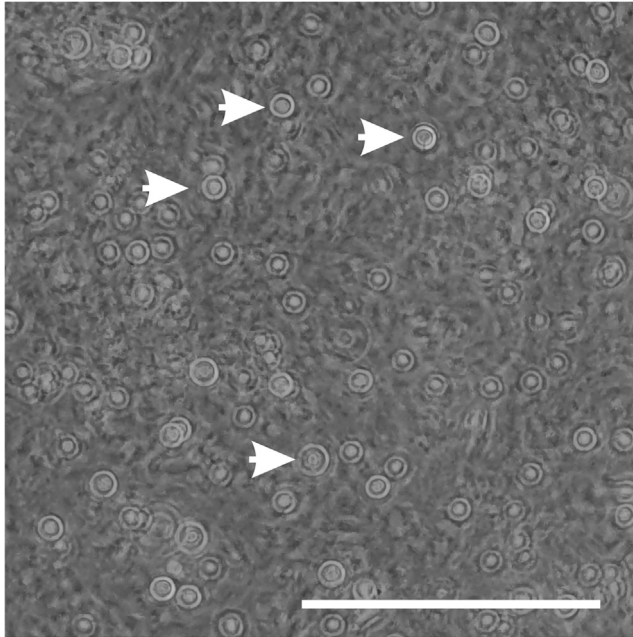
Figure 4. Detached oligodendrocyte progenitor cells after tapping the flask
OPCs are distinguished as floating cells above the monolayer of astrocytes and microglia. Arrow heads indicate round shaped floating OPCs. Scale bars: 100 μm.

Note: While too gentle shaking may cause insufficient OPCs removal, too intense shaking can damage the astrocyte layer. Shaking should be performed at a steady speed by hand.

⚠ CRITICAL: Shaking can cause foaming; therefore, the shaken flask should be held vertically for 30 s to allow the foam to float on the top.

Removal of microglia

⏱ Timing: 2–2.30 h

29. Aspirate the medium which may still contains OPCs, and wash the astrocytes and microglia layer with 3–4 mL PBS.
30. Add 3–4 mL of 0.05% trypsin and incubate 3–5 min at 37°C with 5% CO_2 in an incubator.

⚠ CRITICAL: Cells should not be incubated with trypsin for more than 5 min. Longer incubation time may harm primary astrocytes and results in an unhealthy culture.

31. After incubation, check the cells under the microscope. If there is incomplete detachment, tap the slide of the flask several times and check under the microscope again.
32. After trypsinization, add 6–7 mL of complete growth medium and resuspend the cells.
33. Transfer the suspension to a new 15 mL Falcon tube and pellet detached cells by centrifugation for 10 min at 150 rcf.
34. During centrifugation, prepare 4 sterile 10-cm bacterial grade plates. Add 2 mL of complete growth medium in each of 4 Petri dishes.
35. Aspirate the supernatant which you obtain after step 33 and resuspend cells with 4 mL of complete growth medium.
36. Add 1 mL of the cell suspension to each petri dish (Figure 5A) and incubate at 37°C with 5% CO_2 in the incubator for 20 min (Figure 5B).
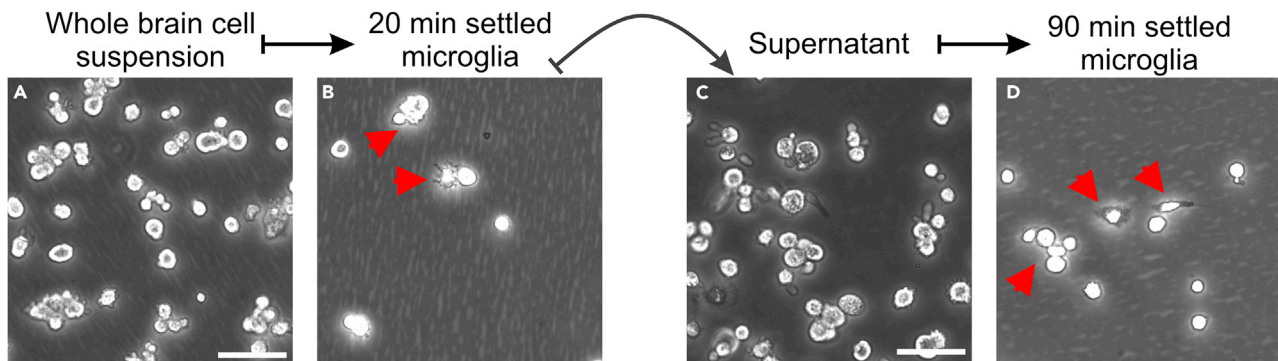
Figure 5. Differential surface binding of primary astrocytes from mouse brain
(A) Whole brain cell suspension which obtained in step 35.
(B) Red arrow heads indicate settled microglia after 20 min of incubation.
(C) Transferring the supernatant which obtained in step 37 to a new bacterial grade plate.
(D) Red arrows indicate settled microglia after 90 min of incubation. Scale bar: 50 μm.

Note: In this step, remaining microglia cells should adhere to the bacterial grade plate while primary astrocyte cells should not.

37. After incubation, collect all supernatants containing astrocytes of all 4 Petri dishes and pool them to a new 10-cm bacterial grade plate (Figure 5C).

⚠ CRITICAL: The transfer of supernatant should be performed carefully as shaking of the plate may result in loosening bound microglia. Gently tilt the plate and collect the supernatant from the side of the plate.

38. Incubate the supernatant (obtained in step 37) contains ∼10–12 mL medium at 37°C with 5% CO_2 in the incubator for 90 min (Figure 5D).

Note: After incubation, check the cells under the microscope. Microglia cells should completely adhere after this step and primary astrocytes can be distinguished as floating cells in the culture medium.

39. Transfer the supernatant containing primary astrocytes into a new T-75 flask.

Note: According to volume of the obtained supernatant, add additional amount of pre-warmed complete growth medium to the T-75 flask to fill up to 20 mL.

40. Incubate the primary astrocytes for 7–15 days at 37°C with 5% CO_2 in the incubator. Primary astrocytes are reaching confluency in between day 7–15 after isolation. After culture reach confluency, primary astrocytes can be used for downstream experiments (Figure 7B).

⚠ CRITICAL: Change the complete growth medium by aspirating half of the old medium (approx. 10 mL) and replacing it with a fresh, pre-warmed complete growth medium (approx. 10 mL) every 4 days during cultivation. This will provide you with a conditioned medium that will help maintain a healthy culture.

Transfection of isolated primary astrocytes and live-cell imaging

⏱ Timing: 3 days

In these steps, we describe how to transfect primary mouse astrocytes with a focal adhesion (FA) construct namely RFP-Paxillin and how to perform live imaging to investigate FA dynamics. For live-cell imaging, we use a μ-Slide 4 Well chamber (Ibidi, Munich, Germany) and for transfection, we use GeneJuice® transfection reagent (Merck, Darmstadt, Germany).

41. First, coat the μ-Slide 4 Well chamber with 300 μL of fibronectin 5 μg/mL dissolved in dH_2O for 1 h at 37°C.
42. Next, remove the fibronectin from the wells and wash the wells once with 500 μL of sterile 1× PBS or water. After the washing, place the chamber in the incubator in order to dry it.

   Note: Fibronectin solution can be used up to 3 times, therefore discarded fibronectin can be store at −20°C for further usage.

   ⚠ CRITICAL: If the purpose of the experiment is to study migration or focal adhesion dynamics, we strongly recommend the usage of fibronectin instead of poly-L-Lysine coating, since fibronectin may enhance cell adhesion and spreading (Blau 2013).

43. Wash the primary astrocytes when reach confluency which are cultured in T-75 flask with 1× PBS and add 3 mL of 0.05% trypsin for 5 min at 37°C to detach cells.
44. Collect the detached cells in a 15 mL tube and add 1–5 mL of growth media for preparing cell suspension. Count the number of cells and prepare 5×10^4 cell/mL suspension.
45. Add 700 μL (∼35,000 cells) of cell suspension into each well and incubate 1 day at 37°C with 5% CO_2 in the incubator.

   Note: Cell number can be adjusted based on chamber size used. Cells should be at least 50% confluent before transfection.

46. The day after incubation, change the medium to fresh 700 μL of complete growth medium.

   Note: Transfection reagent volumes and DNA amount can be scaled up if more than 4 wells are needed.

47. For the single transfection of focal adhesion construct, prepare 1 Eppendorf tube and add 100 μL of Opti-MEM^{TM} and add 6 μL of GeneJuice®. Vortex the solution thoroughly to mix it and incubate at room temperature for 5 min.
48. Add 2 μL of focal adhesion construct at a 1 μg/mL concentration into the serum-free/GeneJuice® mixture and mix it by tapping the tubes and incubate at room temperature for 15 min.

   ⚠ CRITICAL: Do not vortex the solution after adding the DNA construct, vigorous mixing can cause low transfection efficiency.

49. Drop-wisely add 27 μL of reagent/DNA mixture to the cells and rock the chamber to homogenize the solution in the complete growth medium.
50. After 24 h of transfection remove the old medium which contains transfection reagent and add pre-warmed complete growth medium and incubate the cells for additional 24 h at 37°C with 5% CO_2 in the incubator.
51. Before starting live-cell imaging, turn on the temperature and CO_2 controller of Nikon Eclipse Ti2-E/Yokogawa CSU-W1 Spinning disk microscope and wait till the condition stabilizes for usage.
52. Acquire the movies at 1 frame/3–5 min with 20 z-stacks at 0.5 μm step size for 1.25 h to 3-h time course (Methods video S1).

Note: Time interval between frames and z-stacks size and steps can be adjusted based on your experimental setup. After determining the parameter, all movies should be acquired using the same settings in order to provide experimental consistence.

53. Apply maximum projections to the movies and analyze focal adhesion assembly/ disassembly rates by using Focal Adhesion Analysis Server (FAAS) (Figure 10) (Berginski and Gomez 2013).

Note: Microtubule induced focal adhesion disassembly experiment can be used as a control experiment in order to establish the protocol (Ezratty et al., 2005).

Immunostaining of focal adhesion molecules in fixed primary astrocytes

⏱ Timing: 4 days

We used a Leica DM6000B microscope (Leica, Bensheim, Germany) for imaging of specimens.

54. Prepare 10 mm glass coverslips in 6-well plates and coat with fibronectin as described in step 41–42.
55. Seed 1–1.5 × 10^5 cells in each well and incubate the primary astrocytes cells for 48 h at 37°C with 5% CO_2 in the incubator.
56. After the 48 h incubation, carefully remove the growth medium and wash one time rapidly with 1× PBS and do second time washing using 1× PBS for 10 min in room temperature.
57. Prepare a parafilm sheet and place it a wet chamber for keeping humidity during incubation times. Take the coverslips out from wells, place onto parafilm sheet and fix the cells by using 50 μL of 2% of PFA in 1× PBS for each coverslip for 10 min at room temperature.
58. Wash the cells 2 times for 10 min with 1× PBS to remove any remaining PFA.
59. Permeabilize the cells with 50 μL of 0.2% Triton-X-100 in PBS solution.
60. Remove the permeabilization solution and wash cells with 50 μL of 50 mM NH_4Cl in PBS for 5 min in room temperature.
61. Incubate the cells with 50 μL of blocking solution (0.1% Ovalbumin and 0.5% Fish gelatin in 1× PBS) for 60 min in room temperature.
62. After incubation, treat the cells with 50 μL of primary antibodies 12–16 h at 4°C. We used rabbit anti-GFAP (1:400 dilution) and mouse anti-vinculin (1:200 dilution) prepared in blocking solution.

Note: Primary antibodies can be incubated at room temperature for 2–3 h.

63. After primary antibody incubation, wash the cells with 1× PBS one time rapidly and two additional times for 10 min.
64. Apply the 50 μL of secondary antibodies for each coverslip. Alexa Flour 488-conjugated goat anti-rabbit 488 IgG antibody (1:400 diluted in blocking solution), Alexa Fluor 640-conjugated goat anti-mouse IgG antibody (1:400 diluted in blocking solution) and the dyes TRITC-phalloidin (1:400 diluted in blocking solution) for labeling actin filaments (F-actin) and 4′,6-Diamidino-2-Phenylindole (DAPI) (1:400 diluted in blocking solution) for counterstaining of nucleus were prepared in a 1.5 mL tube. Incubate the cells with antibodies at room temperature for 60–75 min in room temperature.
65. Wash the cells with 1× PBS one time rapidly and three times for 10 min.
66. Mount the coverslips with Mowiol.

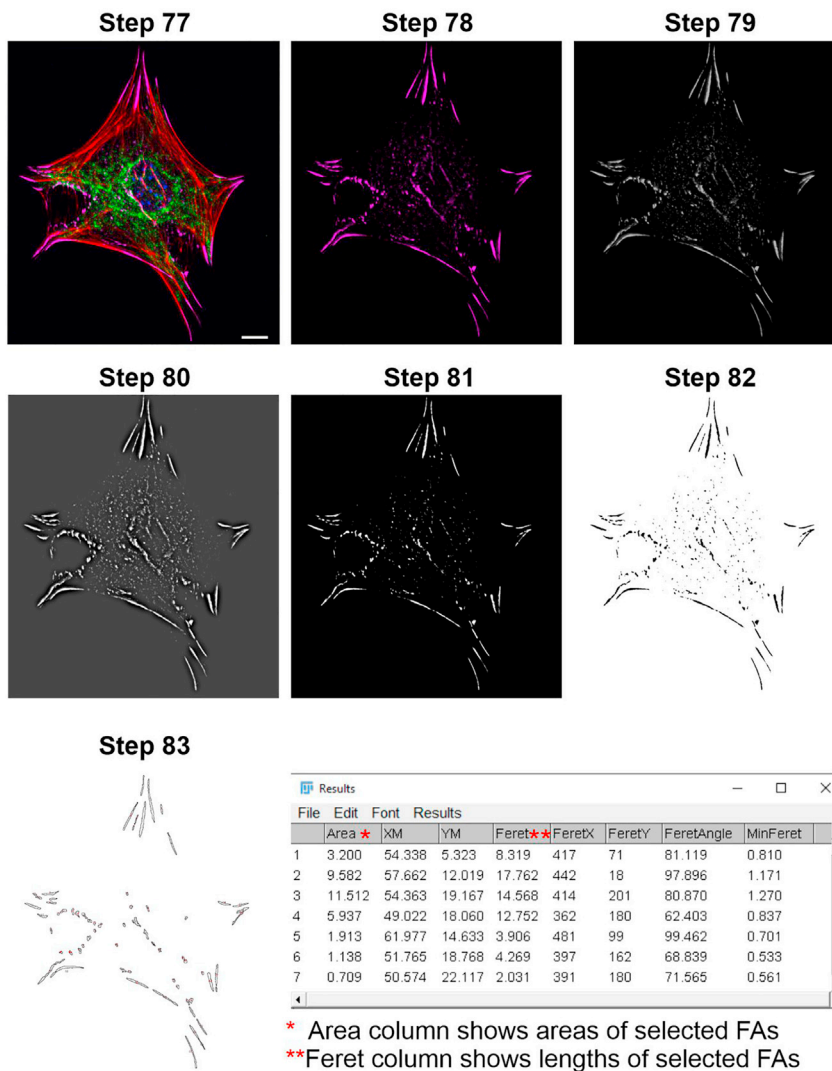△ CRITICAL: Step 63–66 should be conducted in subdued lighting to prevent bleaching of the fluorescent probes.

Figure 6. Step by step quantification of focal adhesion (FA) numbers and lengths

Step 77: Representative image shows merged image of primary mouse astrocytes which co-labeled with vinculin marker (magenta), actin filaments (red), GFAP (green) and for nuclear staining DAPI (blue). **Step 78:** After splitting channels, only vinculin staining is shown. **Step 79:** 8-bit image. **Step 80:** FFT Bandpass filter applied image. **Step 81–83:** Subtracting background and detecting FAs in the cell. Scale bar: 10 μm.

Quantification of number and length of focal adhesion molecules in the primary astrocyte cells

⏱ Timing: 1–2 days

Images were acquired on Leica DM6000B microscope (Leica, Bensheim, Germany) with a 63× objective and 20 cells for each condition were used for quantification. The number and length of focal adhesion molecules were quantified by using Fiji (Figure 6). For this, we modified a protocol which previously described (Horzum et al., 2014).

67. Open the images using ImageJ software.
68. If Z-projection is not created
    a. Go to Image-Stacks-Z Project-Maximum Projection.

    b. Save the processed image in the folder.
69. Pick an exported and processed image from the images folder.
70. To set the scale: First, draw a straight line on the image scale bar.
    a. Go to Analyze-Set scale
    b. And mark as global.
71. Verify the scale by drawing a line on the scale bar.
72. Make a duplicate image named DUP1 for the RGB image (for comparison).
73. Draw a scale bar in the image near to the cell to be cropped.
    a. Analyze-Tools-Scale bar
74. Now, select the Rectangle box symbol from the imageJ toolbar and draw around the cell.
75. Then right-click within the drawn box and press duplicate.
    a. Go to Image-Adjust-Brightness and contrast for adjustments and then save the image in the folder.
76. Again, go to 1st duplicate RGB image and again right-click within yellow box for the FFT image.
77. Separate the merged imaged
    a. Go to Image-Color-Split channels
    b. And pick the channels which contain focal adhesion staining
78. To acquire the FFT image, change the RGB image to an 8-bit image.
    a. Image-Type 8-bit
79. In order to subtract background
    a. Process-FFT Bandpass filter
    b. Set pixel size for large structure to 20 pixels and small 1 pixel.
    c. Adjust tolerance of direction to 5%
    d. Select Autoscale after filtering
    e. Select Saturate image when autoscaling
    f. And press OK
80. Go to Image-Adjust-Brightness
    a. Adjust brightness till getting black background and save the Min/Max values for applying to other images.
    b. Adjust maximum & then minimum.
81. Save the FFT filtered image.
    a. Duplicate image.
    b. Image-Type-RGB color as in this step you cannot save 8-bit image.
    c. Close RGB image.
82. Go to Image-Adjust-Threshold
    a. Select Dark Background.
    b. In first drop-down box select-Huang.
    c. In the second drop-down box select-B&W.
    d. Then apply.
83. Run analyze particles.
    a. Set the parameter for size: 40-Infinity and for circularity 0.00–0.99.
    b. Select pixel units and show the outlines option.
    c. Select display results, clear results, summarize & include holes.
84. Quantification of focal adhesion numbers per cell area
    a. Open the image with F-actin staining.
    b. Draw a line around the cell body using the freehand tool in imageJ tool bar.
    c. Press control+M, this will give the area of the cell body.
    d. Save the results.
    e. Transfer the data to an Excel file.
    f. Count the number of focal adhesions and divide it by the total cell area.
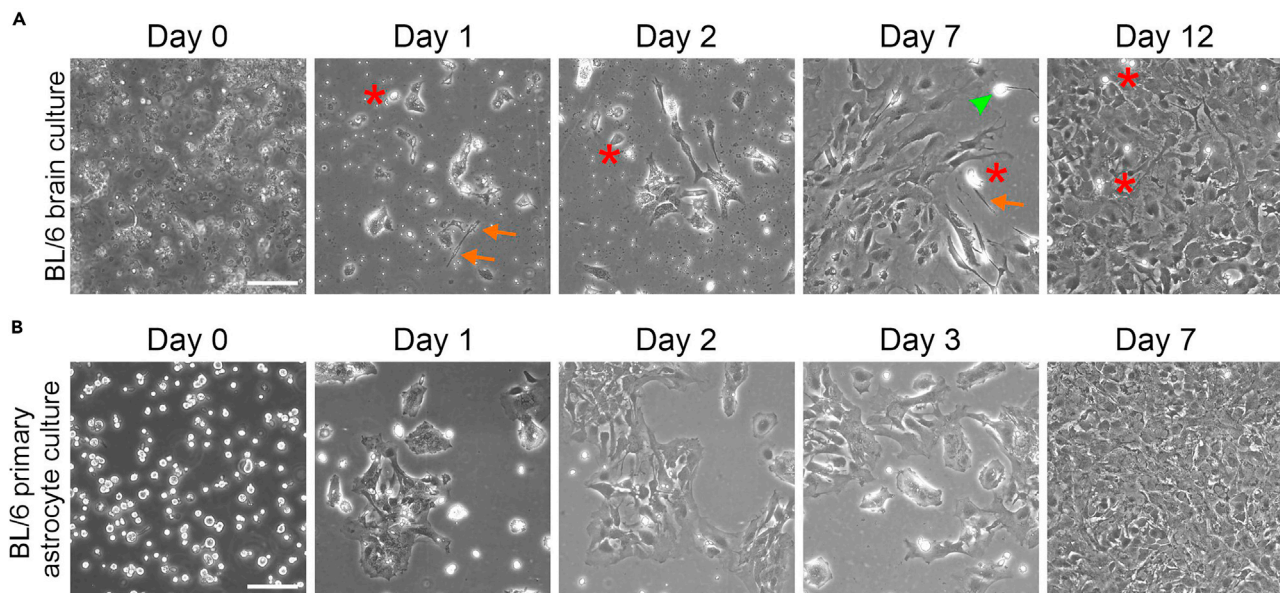85. Use Mann-Whitney-Wilcoxon Test for the significant test.

Figure 7. Growth of BL/6 mouse primary astrocyte cells in mixed brain culture and pure culture
(A) Representative differential interference contrast (DIC) images show growth of different cell types during culturing days before applying the differential binding method.
(B) Primary astrocytes in culture after applying the differential binding method. After differential binding method primary astrocytes reached the confluency. Red asterisks indicate microglia cells, arrows indicate fibroblast cells and green arrowhead indicates a neuron. Scale bars: 100 μm.

EXPECTED OUTCOMES

In this protocol, we provide a cost-efficient, reproducible isolation of primary astrocytes from P0 BL/6 mice without the requirement of commercial kits or special equipment. Applying our protocol, a healthy and easy to maintain primary astrocyte culture can be obtained from wild type or mutant mice strains (Figure 7). Furthermore, and most importantly, the purity of the primary astrocyte cell culture is suitable for studying several astrocytes dependent or related physiological processes. Isolated primary astrocytes can be identified by indirect immunofluorescence using antibodies against the glial fibrillary acidic protein (GFAP). In addition, we applied immunofluorescence staining of microtubule-associated protein (MAP2), PDGRF-alpha and CD68 as marker, respectively, for the identification primary neurons, OPC and microglia, to confirm the purity of astrocyte culture (Figure 8).

We applied our isolation protocol described above for the analysis of focal adhesion dynamics in murine isolated primary astrocytes (Figure 9). Focal adhesions (FAs) are highly dynamic molecules which serve as bi-directional signaling hub in the cell by sensing environmental (outside-in) and intracellular cues (inside-out) (Shen et al., 2012; Sun et al., 2016). With this unique bi-directional signaling feature FA molecules play essential roles in the migration and spreading (Kim et al., 2012; Kim and Wirtz 2013). Namely, size and turnover of FAs are highly important for the migration capacity of the cell. We recently showed that the adhesion G protein coupled receptor (GPCR) ADGRV1/VLGR1 (very large G protein coupled-receptor-1) is a component of FAs and mutations in *VLGR1* cause defects in FA growth and maturation processes (Kusuluri et al., 2021). In the latter study, we used isolated primary BL/6 wild-type astrocytes, *Vlgr1/*del7TM mice lacking the seven transmembrane domains (7TM) and the intracellular domain (ICD) of *Vlgr1* (McMillan and White, 2004), and mutant Drum B mice in which only a small portion of the N-terminal fragment is present and the entire C-terminal fragment is missing (Potter et al., 2016; Kusuluri et al., 2021). A significant decrease in the number and length of FAs was observed in both *Vlgr1* mutant mice compared with primary BL/6 wild-type astrocytes (Figure 10) (Kusuluri et al., 2021). For the quantifications, we applied
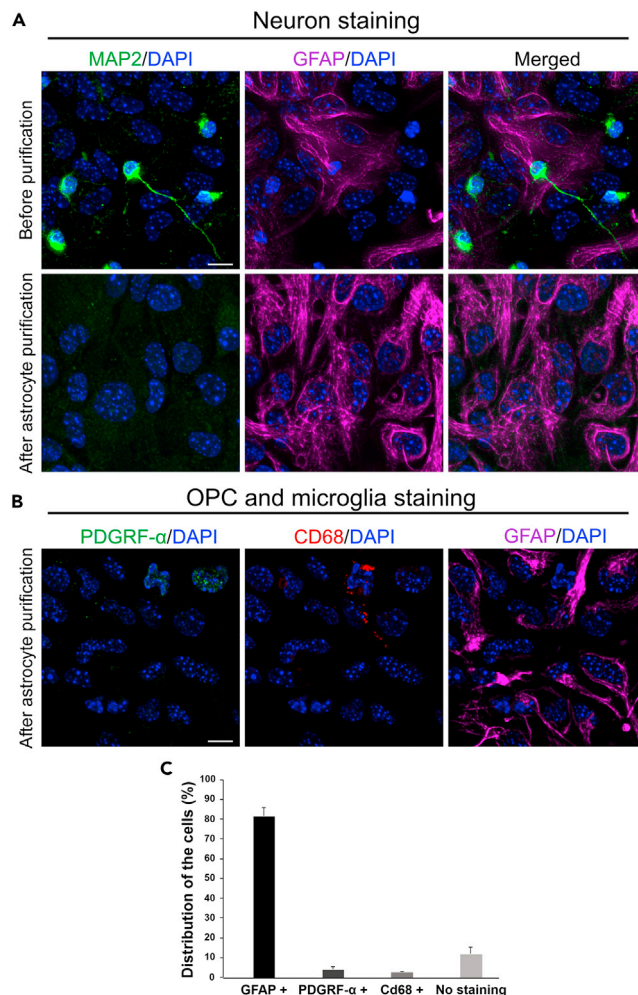
Figure 8. Representative indirect immunostaining of BL/6 mouse brain primary cell cultures

(A) Indirect immunofluorescence double staining of MAP2 (green) and primary astrocyte marker GFAP (magenta), as common markers for primary neurons and primary astrocytes, counterstained by DAPI (blue) for nuclear DNA, before and after the purification of astrocytes.

(B) Immunofluorescence staining of a primary astrocyte culture after primary astrocyte purification. OPC, microglia and primary astrocytes cells were stained by antibodies against PDGRF-α, CD68 and GFAP, respectively.

(C) Quantification of the number of GFAP, PDGRF-α and CD68-stained positive cells after astrocyte purifications demonstrates that primary astrocytes are the most prominent cell type (~80%). N = 360–490 cells per condition, 3 independent experiments. Scale bar: 10 μm.

the ImageJ protocol described above in step 67 to 85. Moreover, our study demonstrated that VLGR1 is metabotropic mechanosensor at FAs and provided novel insights into the pathomechanisms underlying VLGR1-associated diseases, such as human Usher syndrome (Reiners and Wolfrum 2006) and epilepsy (Wang et al., 2015; Myers et al., 2018).

LIMITATIONS

This protocol is designed for isolation of primary astrocytes from P0 mice and all isolation steps are optimized for this age. Nevertheless, our protocol can be adjusted for different aged mice brain culture. It might be taken under consideration that precursor and adult primary astrocyte can show different transcriptional profile which may affect experimental outcome (Zhang et al., 2016; Clarke et al., 2018; Bronzuoli et al., 2019). In addition, there might be species-specific differences between species that primary astrocyte derived may show differences in transcriptomic and protein
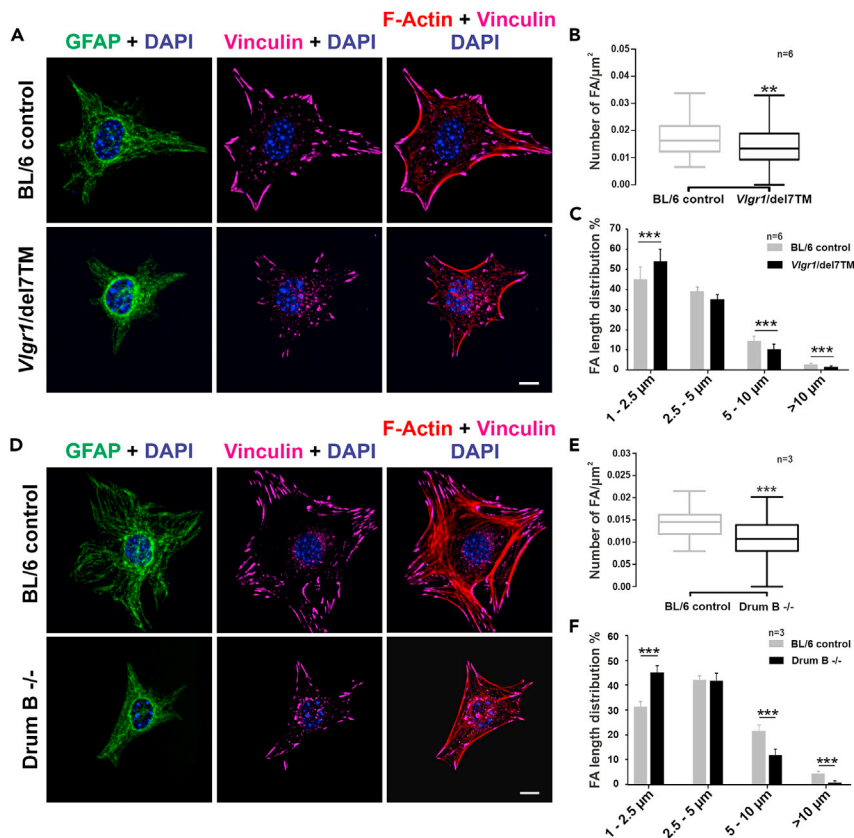
Figure 9. VLGR1 deficiency alters FA morphology

Representative images of FAs in *VLGR1*-deficient mouse primary astrocytes.

(A and D) FAs were stained for vinculin (magenta), F-actin with TRITC-phalloidin (red), and nuclei with DAPI (blue); GFAP (green) was used as an astrocyte marker. FA number and length were reduced after *VLGR1*-depletion in primary astrocytes of both *Vlgr1* mutant mouse lines.

(B and C) (B) 20 cells per condition, (C) ∼1300–1700 FAs per category for control and ∼200–1000 FAs for mutant astrocytes.

(E and F) (E) 20 cells per condition, (F) ∼950–1250 FAs per condition for control and ∼410–510 FAs for mutant astrocytes. Scale bars: (A and D) 10 µm. Data are represented in B and E are shown as box plot and statistical analyses were done using two-tailed Mann-Whitney U test. Data in C and F are represented as mean ± SD. Statistical analyses were done using Sidak's multiple comparison test; *p ≤ 0.05, **p ≤ 0.01, ***p ≤ 0.001.

(A–F). Figure is acquired and adapted from Figures 3D–3H in Kusuluri et al. (2021) with the permission of Elsevier.

interaction level. In human and mice astrocytes, it has been reported that metabolism and mitochondria related protein network was higher in mice astrocyte whereas defensive response and extracellular space related proteins were higher in human astrocytes (Li et al., 2021). In rat and mouse astrocytes, significant differences in GFAP expression level, cell proliferation and morphology has been also shown (Puschmann et al., 2010). We observed that primary astrocytes can only be sub-passaged up to 3 times. As more than 3 sub passaging cause astrocyte marker (GFAP) expression loss and unhealthy cell phenotype such as poor cell growth, reduce in cell migration capacity and changes in cell morphology, we highly recommend that experiments should be planned in advance and passage 1 and passage 2 should be used. Astrocytes are one of the main parts of active information transport in central nervous system by interacting with neurons. Neuron-astrocyte interaction through messenger and signaling molecules such as Ca²⁺ and glutamate, is highly important in the CNS for function, development and pathology of the brain (Wilhelm et al., 2004; Benarroch 2005; Nimmerjahn 2009). Therefore, it should be taken under consideration that pure primary astrocyte culture may not always reflect in-vivo physiology in the absence of different cell types.
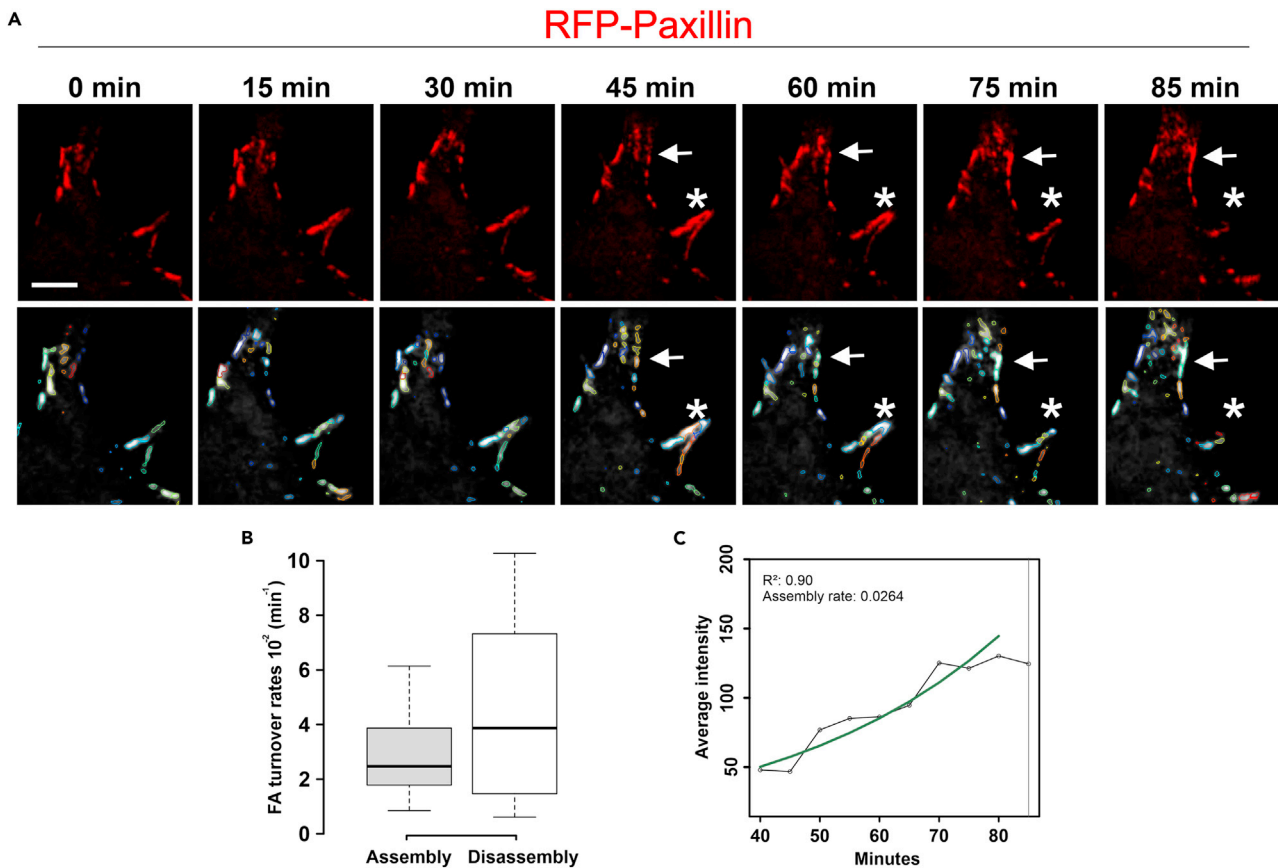
Figure 10. Analysis of assembly and disassembly of focal adhesions by life cell imaging in RFP-Paxillin transfected BL/6 mouse primary astrocytes
(A) Tracking of RFP-Paxillin molecules in focal adhesions (FAs) by live cell imaging. Images were acquired for 85 min with 3 min time intervals. Arrows point to an individual FA which assembles and asterisk indicated a FA which disassembles during the time course of imaging. Lower panel shows color coded individual FAs identified and analyzed via the Focal adhesion analysis server (FAAS) (Berginski and Gomez 2013).
(B) Assembly and disassembly rates of FAs in a single BL/6 primary mouse astrocyte.
(C) Automated intensity analysis of RFP-paxillin in an individual FAs during assembly by FAAS. Green line in the intensity plot indicates the trend line of assembling FA. Scale bar: 10 μm.

TROUBLESHOOTING

Problem 1
Contamination of fibroblast and endothelial cells in the primary cultures (step 10).

Potential solution
Fibroblast and endothelial cells are the two major cell types present in meninges. Poor handling in meningeal removing increases the contamination level in culture. These two cell types can reach confluency very rapidly which may cause a reduced number of astrocytes and purity of cultures. Meninges should peel away using fine forceps. Be sure that meninges are removed in one piece, if not there can be patches of meninges left which may cause contamination.

Problem 2
Insufficient dissociation of brain tissue (step 21).

Potential solution
When performing dissociation of brain tissue, be sure to use freshly thawed ice-cold DNase I solution as DNase I is enzymatically helping dissociation of brain tissue. Due to environmental and mechanical stress during the dissociation process DNA can leak as a result of cell damage. Released DNA is

often the cause of cell clumps that affects efficiency of dissociation. Start the resuspension of cell pellet with a 10 mL pipette and continue with 5 mL and 2 mL pipettes, respectively. Using a smaller pipette size can increase dissociation efficiency and reduce aggregation levels.

Problem 3
Cell viability is not sufficient after plating (step 24).

Potential solution
This problem may occur because of excessive Poly-L-Lysine (PLL) residue in flask. Therefore, wash the plates coated with PLL thoroughly before plating single-cell suspension. After plating single-cell suspension, cellular growth should be observed on day 1, day 2, day 7 and day 14. Differential binding should be performed when cultures reach full confluency, as insufficient cell numbers may affect the cell viability.

Problem 4
OPCs contamination in isolated astrocyte cultures (step 25).

Potential solution
After 7–15 days of culturing, primary astrocytes reach confluency. It is important to keep the astrocyte layer attached to the flask surface during the OPCs. While too gentle shaking of flask may cause lower yield of OPCs removal, too intense shanking may damage the astrocyte layer. Therefore, shaking should be done carefully.

Problem 5
Microglia contamination after differential binding (step 29).

Potential solution
After trypsinization, transfer medium containing astrocytes and potential microglia cells to the bacterial grade plates. Microglia cells are attached to the surface of bacterial grade plates whereas primary astrocytes do not. After 20 min of transferring to bacterial grade plate, check the cells, primary astrocytes can be distinguished easily as they float in the medium. Collect the medium containing primary astrocytes and repeat the step carefully for another 90 min. When collecting medium, be careful not to shake the plate or the microglia may become detached.

Problem 6
Low transfection rate (step 41).

Potential solution
An efficient transfection rate is very important for successful experiment. We have observed that transfection efficiency in primary astrocyte was the range of 15%–30%. To optimize transfection efficiency for your gene/protein of interest, you may try different transfection methods, such as transfection by electroporation or transfection by liposomes. Transfection efficiency may depend on several factors, such as DNA:transfection reagent ratio, purity and composition of the DNA, the degree of confluency of the culture and transfection method. Therefore, to achieve sufficient number of transfected cells and transfection protocol must be optimized. Plasmid DNA should be prepared by using Endotoxin-free isolation kit, as residue of bacterial toxin may lower the efficiency. After obtaining endotoxin-free DNA, different transfection reagent:DNA ratios should be tested to optimize transfection.

Problem 7
Poor migration speed during live-cell imaging (step 52).

Potential solution

Extracellular matrix is vital for migration of cells in vitro and in vivo. Primary astrocytes produce and secrete extracellular matrix (ECM) proteins such as laminin in vitro condition to provide growth and spreading condition (Chiu et al., 1991). However, in low cell density such as single cell migration study, migration speed can reduce dramatically due to lack of sufficient ECM. A potential solution to this problem is to coating the surface using fibronectin at a 5 µg/mL. Since, different ECM concentrations have an effect on migration speed and migrating cell numbers (Desban and Duband 1997; Millon-Fremillon et al., 2008), effective fibronectin concentration from 1 µg/mL to 10 µg/mL may be tested before starting the experiment. Also, providing conditioned astrocyte medium can enhance the migration speed of primary astrocyte cells as it contains ECM molecules.

RESOURCE AVAILABILITY

Lead contact

Further information and requests for resources and reagents should be directed to and will be fulfilled by the lead contact, Uwe Wolfrum (wolfrum@uni-mainz.de).

Materials availability

Reagents and resources used in this study are commercially available with the exception of RFP-paxillin plasmid which was kindly provided by Drs. Leube and Hortwitz. Nevertheless, requests for resources and reagents can be directed to and will be fulfilled by the lead contact.

Data and code availability

This study did not generate new data sets.

SUPPLEMENTAL INFORMATION

Supplemental information can be found online at https://doi.org/10.1016/j.xpro.2021.100954.

AUTHOR CONTRIBUTIONS

Conceptualization, B.E.G. and U.W.; investigation, B.E.G. and J.K.; writing – original draft, B.E.G. and U.W.; writing – review & editing, B.E.G., J.K. and U.W.

DECLARATION OF INTERESTS

The authors declare no competing interests.

REFERENCES

Benarroch, E.E. (2005). Neuron-astrocyte interactions: partnership for normal function and disease in the central nervous system. Mayo Clin. Proc. *80*, 1326–1338.

Berginski, M.E., and Gomez, S.M. (2013). The Focal Adhesion Analysis Server: a web tool for analyzing focal adhesion dynamics. F1000Res *2*, 68.

Blau, A. (2013). Cell adhesion promotion strategies for signal transduction enhancement in microelectrode array in vitro electrophysiology: an introductory overview and critical discussion. Curr. Opin. Colloid Interface Sci. *18*, 481–492.

Bronzuoli, M.R., Facchinetti, R., Valenza, M., Cassano, T., Steardo, L., and Scuderi, C. (2019). Astrocyte function is affected by aging and not Alzheimer's disease: a preliminary investigation in hippocampi of 3xTg-AD mice. Front. Pharmacol. *10*, 644.

Chiu, A.Y., Espinosa De Los Monteros, A., Cole, R.A., Loera, S., and De Vellis, J. (1991). Laminin and s-laminin are produced and released by astrocytes, Schwann cells, and schwannomas in culture. Glia *4*, 11–24.

Clarke, L.E., Liddelow, S.A., Chakraborty, C., Munch, A.E., Heiman, M., and Barres, B.A. (2018). Normal aging induces A1-like astrocyte reactivity. Proc. Natl. Acad. Sci. U S A *115*, E1896–E1905.

Desban, N., and Duband, J.L. (1997). Avian neural crest cell migration on laminin: interaction of the alpha1beta1 integrin with distinct laminin-1 domains mediates different adhesive responses. J. Cell Sci. *110*, 2729–2744.

Ezratty, E.J., Partridge, M.A., and Gundersen, G.G. (2005). Microtubule-induced focal adhesion disassembly is mediated by dynamin and focal adhesion kinase. Nat. Cell Biol. *7*, 581–590.

Horzum, U., Ozdil, B., and Pesen-Okvur, D. (2014). Step-by-step quantitative analysis of focal adhesions. MethodsX *1*, 56–59.

Kim, D.H., and Wirtz, D. (2013). Focal adhesion size uniquely predicts cell migration. FASEB J. *27*, 1351–1361.

Kim, M.C., Kim, C., Wood, L., Neal, D., Kamm, R.D., and Asada, H.H. (2012). Integrating focal adhesion dynamics, cytoskeleton remodeling, and actin motor activity for predicting cell migration on 3D curved surfaces of the extracellular matrix. Integr. Biol. *4*, 1386–1397.

Kusuluri, D.K., Guler, B.E., Knapp, B., Horn, N., Boldt, K., Ueffing, M., Aust, G., and Wolfrum, U. (2021). Adhesion G protein-coupled receptor VLGR1/ADGRV1 regulates cell spreading and migration by mechanosensing at focal adhesions. iScience *24*, 102283.

Li, J., Pan, L., Pembroke, W.G., Rexach, J.E., Godoy, M.I., Condro, M.C., Alvarado, A.G., Harteni, M., Chen, Y.W., Stiles, L., et al. (2021). Conservation and divergence of vulnerability and responses to stressors between human and mouse astrocytes. Nat. Commun. *12*, 3958.

McMillan, D.R., and White, P.C. (2004). Loss of the transmembrane and cytoplasmic domains of the very large G-protein-coupled receptor-1 (VLGR1 or Mass1) causes audiogenic seizures in mice. Mol. Cell Neurosci. *26*, 322–329.

Millon-Fremillon, A., Bouvard, D., Grichine, A., Manet-Dupe, S., Block, M.R., and Albiges-Rizo, C. (2008). Cell adaptive response to extracellular matrix density is controlled by ICAP-1-dependent beta1-integrin affinity. J. Cell Biol. *180*, 427–441.

Myers, K.A., Nasioulas, S., Boys, A., Mcmahon, J.M., Slater, H., Lockhart, P., Sart, D.D., and Scheffer, I.E. (2018). ADGRV1 is implicated in myoclonic epilepsy. Epilepsia *59*, 381–388.

Nimmerjahn, A. (2009). Astrocytes going live: advances and challenges. J. Physiol. *587*, 1639–1647.

Potter, P.K., Bowl, M.R., Jeyarajan, P., Wisby, L., Blease, A., Goldsworthy, M.E., Simon, M.M., Greenaway, S., Michel, V., Barnard, A., et al. (2016). Novel gene function revealed by mouse mutagenesis screens for models of age-related disease. Nat. Commun. *7*, 12444.

Puschmann, T.B., Dixon, K.J., and Turnley, A.M. (2010). Species differences in reactivity of mouse and rat astrocytes in vitro. Neurosignals *18*, 152–163.

Reiners, J., and Wolfrum, U. (2006). Molecular analysis of the supramolecular usher protein complex in the retina. Harmonin as the key protein of the Usher syndrome. Adv. Exp. Med. Biol. *572*, 349–353.

Shen, B., Delaney, M.K., and Du, X. (2012). Inside-out, outside-in, and inside-outside-in: G protein signaling in integrin-mediated cell adhesion, spreading, and retraction. Curr. Opin. Cell Biol. *24*, 600–606.

Sun, Z., Guo, S.S., and Fassler, R. (2016). Integrin-mediated mechanotransduction. J. Cell Biol. *215*, 445–456.

Wang, Y., Fan, X., Zhang, W., Zhang, C., Wang, J., Jiang, T., and Wang, L. (2015). Deficiency of very large G-protein-coupled receptor-1 is a risk factor of tumor-related epilepsy: a whole transcriptome sequencing analysis. J. Neurooncol. *121*, 609–616.

Wilhelm, A., Volknandt, W., Langer, D., Nolte, C., Kettenmann, H., and Zimmermann, H. (2004). Localization of SNARE proteins and secretory organelle proteins in astrocytes in vitro and in situ. Neurosci. Res. *48*, 249–257.

Zhang, Y., Sloan, S.A., Clarke, L.E., Caneda, C., Plaza, C.A., Blumenthal, P.D., Vogel, H., Steinberg, G.K., Edwards, M.S., Li, G., et al. (2016). Purification and characterization of progenitor and mature human astrocytes reveals transcriptional and functional differences with mouse. Neuron *89*, 37–53.

Publikation IV

Article

The Adhesion GPCR VLGR1/ADGRV1 Regulates the Ca^{2+} Homeostasis at Mitochondria-Associated ER Membranes

Jacek Krzysko [1], Filip Maciag [2], Anna Mertens [1], Baran Enes Güler [1], Joshua Linnert [1], Karsten Boldt [3], Marius Ueffing [3], Kerstin Nagel-Wolfrum [1], Martin Heine [2] and Uwe Wolfrum [1,*

[1] Institute of Molecular Physiology (imP), Molecular Cell Biology, Johannes Gutenberg University Mainz, 55128 Mainz, Germany
[2] Institute for Developmental Biology and Neurobiology (IDN), Functional Neurobiology, Johannes Gutenberg University Mainz, 55128 Mainz, Germany
[3] Institute for Ophthalmic Research, University of Tuebingen, 72076 Tuebingen, Germany
[*] Correspondence: wolfrum@uni-mainz.de; Tel.: +49-6131-39-25148

Abstract: The very large G protein-coupled receptor (VLGR1, ADGRV1) is the largest member of the adhesion GPCR family. Mutations in VLGR1 have been associated with the human Usher syndrome (USH), the most common form of inherited deaf-blindness as well as childhood absence epilepsy. VLGR1 was previously found as membrane–membrane adhesion complexes and focal adhesions. Affinity proteomics revealed that in the interactome of VLGR1, molecules are enriched that are associated with both the ER and mitochondria, as well as mitochondria-associated ER membranes (MAMs), a compartment at the contact sites of both organelles. We confirmed the interaction of VLGR1 with key proteins of MAMs by pull-down assays in vitro complemented by in situ proximity ligation assays in cells. Immunocytochemistry by light and electron microscopy demonstrated the localization of VLGR1 in MAMs. The absence of VLGR1 in tissues and cells derived from VLGR1-deficient mouse models resulted in alterations in the MAM architecture and in the dysregulation of the Ca^{2+} transient from ER to mitochondria. Our data demonstrate the molecular and functional interaction of VLGR1 with components in MAMs and point to an essential role of VLGR1 in the regulation of Ca^{2+} homeostasis, one of the key functions of MAMs.

Keywords: adhesion GPCR; mitochondria-associated ER membranes (MAM); mitochondria-endoplasmic reticulum contact sites (MERCS); Ca^{2+} transient at ER and mitochondria; Ca^{2+} homeostasis

1. Introduction

VLGR1 (very large G protein-coupled receptor-1), also known as ADGRV1, GPR98, and MASS, has a molecular weight of up to 700 kDa, making it the largest member of the 33 adhesive G protein-coupled receptors (ADGRs), a unique subfamily of the GPCR superfamily [1]. The molecular architecture of ADGRs is characterized by an extended large extracellular domain (ECD), a seven-span transmembrane domain (7TM) and a short intracellular domain (ICD) (Figure 1A). Autoproteolysis at the highly conserved GPCR proteolytic site (GPS) in the GAIN (autoproteolysis-inducing) domain positioned next to the 7TM results in a bipartite receptor molecule [2]. The resulting molecules consist of the N-terminal fragment (NTF), which contains characteristic cell-adhesive protein motifs and the G protein signaling 7TM-containing C-terminal fragment (CTF).

VLGR1 is expressed almost ubiquitously in humans and mice with high expression levels in the nervous system [4]. In humans, mutations of the VLGR1 gene cause Usher syndrome (USH), the most common form of hereditary deaf-blindness [5]. Haploinsufficiency in VLGR1/ADGRV1 has been associated with childhood absence epilepsy [4,6,7]. In mice, defects in Vlgr1 lead to audiogenic seizures [4,6,7].
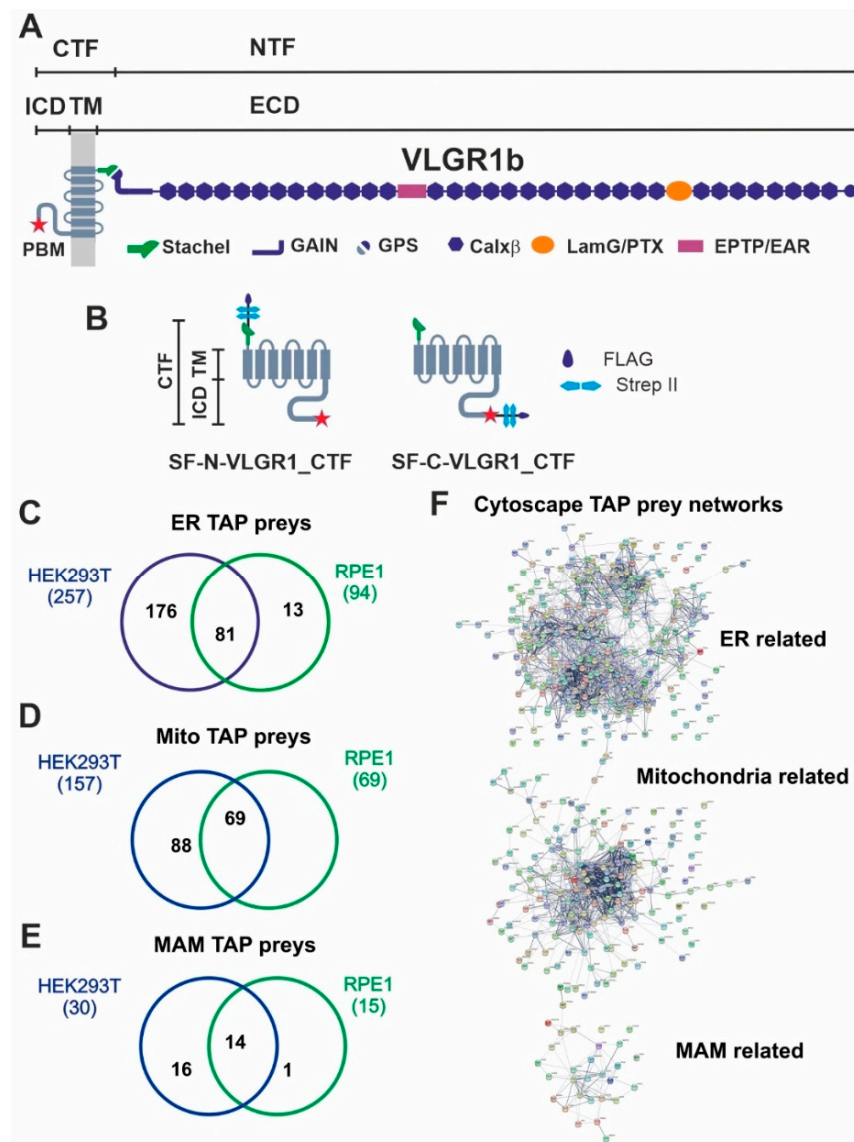
Figure 1. VLGR1 protein domain composition, VLGR1_CTF constructs for TAPs and overlap of proteins associated to ER, mitochondria and MAM identified in VLGR1_CTF TAPs. (**A**) VLGR1 protein domain composition: VLGR1 molecules consist of a C-terminal fragment (CTF) and a N-terminal fragment (NTF) which result from the cleavage at the highly conserved GPCR proteolytic site (GPS) in the GAIN (autoproteolysis-inducing) domain positioned next to the seven-span transmembrane domain (TM). After autoproteolytic cleavage the first 11 amino acids of VLGR1_CTF, the so-called Stachel peptide, can act as a tethered internal agonist for receptor activation [3]. The extracellular domain (ECD) of VLGR1b contains numerous Ca^{2+} binding calcium exchanger β motifs (Calx-β), seven epilepsy-associated/Epitemptin-like (EAR/EPTP) repeats and a pentaxin/laminin G-like domain (LamG/PTX). The intracellular domain (ICD) ends with a class-1 PDZ binding motif (PBM). (**B**) VLGR1_CTF, N- or C-terminal tagged with Strep II/FLAG (SF)-tag used as baits in TAPs. (**C**) Venn diagram shows an overlap of 81 proteins of ER-related TAP prey for polled VLGR1_CTF N-and C-terminal tagged TAPs from HEK293T and hTERT-RPE1 cells. (**D**) Mitochondria-related prey proteins from VLGR1_CTF N-and C-terminal tagged TAPs in HEK293T and hTERT-RPE1 cells, compared in a Venn diagram with an overlap of 69 proteins. (**E**) 14 common MAM prey proteins are identified in TAPs from HEK293T and hTERT-RPE1 cells. (**F**) Protein networks of ER, mitochondria and MAM-related proteins, illustrated by Cytoscape analysis of preys identified in VLGR1_CTF N-and C-terminal tagged TAPs.

We have previously shown that VLGR1 is a part of membrane–membrane adhesion complexes associated with the photoreceptor primary cilium and the ankle-links of stereocilia of the developing hair cells [8]. In addition, VLGR1 functions as a metabotropic mechanoreceptor in focal adhesions [9]. More recently, our affinity proteomics-based studies provided the first evidence that VLGR1 associates with molecules of intracellular membrane networks, namely of the endoplasmic reticulum (ER) and the mitochondria-associated ER membranes (MAMs) [3,8].

MAMs, also named MERCs (mitochondria-ER contacts), are specialized subcellular compartments that are shaped by specific subdomains of the ER surface juxtaposed to the outer mitochondria membrane. MAMs are composed of a characteristic set of molecules which guarantees the juxtaposition between these organelles and determines several intracellular processes, such as Ca^{2+} and lipid homeostasis, immune response or autophagy [10]. The MAM contact sites are dynamic and the dysfunction of MAMs has been associated with various neurodegenerative disorders, such as Alzheimer's or Parkinson's disease [11,12].

Here, we demonstrate the localization and functions of an aGPCR in the ER, particularly in the MAM complex. We show that VLGR1 contributes to the arrangement of a protein complex that is crucial for regulating Ca^{2+} flux from the ER into the MAM interface and the uptake through the outer mitochondria membrane. We demonstrate that the arrangement of the MAMs is altered in Vlgr1-deficient neurons. Further, live cell imaging of Ca^{2+} shows that the Ca^{2+} fluxes from the ER and into mitochondria are severely impaired in primary astrocytes from Vlgr1-deficient *Vlgr1*del7TM. The morphological changes and disrupted Ca^{2+} homeostasis observed in the absence of VLGR1 from the MAM possibly contribute to the pathophysiology of the disorders caused by defects in VLGR1 in USH2 and childhood absence epilepsy patients.

2. Materials and Methods

2.1. Animals

All experiments were performed in compliance with guidelines established by Association for Research in Vision and Ophthalmology. Mice were kept under 12/12 h light/dark cycles, food and water ad libitum. *Vlgr1*del7TM mice harbor a nonsense mutation in Vlgr1, V2250X, which results in loss of Vlgr1's transmembrane and cytoplasmic domain [13]. Breeding background of *Vlgr1*del7TM mice was the C57BL/6 strain. The use of mice in research was approved by District administration Mainz-Bingen, 41a/177-5865-§11 ZVTE, 30.04.2014. Zebrafish were obtained from the Institute of Molecular Biology (IMB). Porcine eyes were obtained from the local slaughterhouse.

2.2. Antibodies

The following primary antibodies were used: rabbit anti-Nogo-A/RTN4 (AHP1799, Biorad, Feldkirchen, Germany), mouse anti-TOM20 (Santa Cruz, CA, USA, sc-17764), mouse anti-SIGMA1R (Santa Cruz, sc-137075), rat anti-SIGMA1R (Merck, Darmstadt, Germany, ICR-SIG1R-A), mouse anti-ACSL4 (Santa Cruz, sc-365230), mouse anti-Myc (Cell Signaling, Danvers, MA, USA, 2276), rabbit anti-HA (Sigma-Aldrich, St. Louis, MO, USA, H6908), rat anti-HA (Roche, Basel, Switzerland, 3F10), rabbit anti-VLGR1, raised against the against the C-terminus of murine VLGR1 (amino acids 6198–6307) and previously characterized in [9,14], rabbit anti-α-Tubulin (Abcam, Cambridge, UK, DM1A), rabbit anit-COX IV (NEB, Ipswich, MA, USA, 3E11), rabbit anti-GFAP (Dako Agilent, Santa Clara, CA, USA, Z0334), rat anti-RFP (Chromotek, Planegg, Germany, 5F8), mouse anti-CLIMP63, (Enzo Life Sciences, G1/296), goat anti-Pericentrin 2 (Santa Cruz, C-16), mouse anti-Arl13b (Abcam, Cambridge, UK, ab136648), goat anti-Centrin 2 [15]. Secondary antibodies conjugated Alexa 488, Alexa 555, Alexa 568 or Alexa 647 were purchased from Molecular Probes (Life Technologies, Darmstadt, Germany) or Rockland Inc. (Gilbertsville, PA, USA). Nuclear DNA was stained with DAPI (4′,6-diamidino-2-phenylindole, 1 mg/mL: Sigma-Aldrich).

2.3. Cell Lines

We used the following cell lines: HEK293T cells constitutively expressing Simian virus 40 (SV40) large T antigen isolated from human embryonic kidney tissue were mainly used as highly transfectable cells in assays, such as tandem affinity purifications (TAPs, Section 2.6). hTERT-RPE-1 are human telomerase reverse transcriptase (hTERT)-immortalizeretinal cells from the retinal pigment epithelium (RPE) of the human eye [8]. The genetically stable, nearly diploid hTERT-RPE1 cells have been previously used in studies on VLGR1 and were used here in additional complementary TAPs [9]. HeLa cells, epithelial cells isolated from cervical carcinoma were used for the analysis of the ER-mitochondria interface. All cell lines were initially purchased from American Type Culture Collection (ATCC).

2.4. Cell Culture

HEK293T and HeLa were cultured in Dulbecco's modified Eagle's medium (DMEM), and hTERT-RPE1 cells were cultured in DMEM-F12, respectively, all supplemented with 10% fetal bovine serum (FBS) (ThermoFisher Scientific, Waltham, MA, USA). Cells were transfected with GeneJuice® (Merck Millipore, Darmstadt, Germany) according to manufacturer's instructions. Primary astrocyte cultures were prepared from cerebral cortices of C57BL/6 WT, Vlgr1/del7TM mice, as previously described [16]. In brief, mouse pups from C57BL/6 WT, Vlgr1/del7TM were dissected postnatal day 0 (PN0), and cerebral cortices were collected in 1x HBSS (ThermoFisher Scientific, Waltham, MA, USA) medium contains Dnase/trypsin (Merck, Darmstadt, Germany) for enzymatic dissociation. Additionally collected cortices were mechanically dissociated by 10 mL and 5 mL pipettes, respectively. Single cell suspensions were cultured in DMEM/10% FBS/2% penicillin/streptomycin (ThermoFisher Scientific, Waltham, MA, USA) and growth medium was changed on day 1, day 2, and day 7. Upon confluency, oligodendrocytes and neurons were removed by shaking the plates. To remove microglia cells, trypsin and DNase were added to dishes and cells were passed over successive bacterial grade dishes. Primary astrocytes were cultured for 14 days in complete growth medium and used for downstream experiments.

2.5. DNA Constructs

VLGR1_CTF (Uniprot ID Q8WXG9-1, aa 5891-6306) sequence was used for VLGR1 constructs. For tandem affinity purifications, Strep II-FLAG (SF)-tagged human VLGR1_CTF was used. The SF-tag was N-terminally and C-terminally fused in VLGR1_CTF. For HA-and RFP-tagged constructs, VLGR1_CTF was subcloned into a HA/DEST vector (pDEST520; Invitrogen, Waltham, MA, USA) and an RFP/DEST vector (pDEST733; Invitrogen). The SIGMA1R-Myc (S1R-Myc) construct was a kind gift from Christian Behl (University Medical Center Mainz). Indicators for calcium imaging were pCMV CEPIA2mt and pCMV G-CEPIA1er [17].

2.6. Tandem Affinity Purification (TAP) and Mass Spectrometry

The tandem affinity purification (TAP) and mass spectrometry (LC-MS/MS) analysis were performed as previously described [8,18]. The two Strep II/FLAG-(SF)-tagged VLGR1_CTF (Figure 1B) were expressed in HEK293T cells or hTERT-RPE1 cells, respectively for 48 h, lysed and cleared by centrifugation. Mock-treated cells were used as controls. Subsequently supernatants were subjected to a two-step purification on Strep-Tactin® Superflow® beads (IBA, Göttingen, Germany) and anti-FLAG M2 agarose beads (Merck). In these steps competitive elutions were achieved by desbiothin (IBA) and FLAG® peptide (Merck), respectively. Methanol-chloroform precipitated eluates were subjected to liquid chromatography coupled with tandem mass spectrometry (LC-MS/MS).

2.7. Data Processing

Obtained raw MS spectra were searched against the human SwissProt database using Mascot and results were verified by Scaffold (version Scaffold 4.02.01, Proteome Software Inc., Portland, OR, USA) for the validation of MS/MS-based peptide and polopeptide iden-

tifications. Mass spectrometry results for the tow VLGR1_CTF fragment were compared to the according data for mock-transfected cells and to common control TAPs of the RAF1-protein [18]. Proteins in mock and RAF1 datasets were excluded for subsequent analysis. VLGR1_CFT preys were used as input for the Cytoscape plugins STRING, ClueGO and the STRAP software according to their gene names based on HGNC. Confidence (score) cutout 0.40 and maximum number of interactors 0 were set as parameters for STRING analysis. Gene Ontology (GO) term enrichment analysis was performed by ClueGO v2.3.3. Network specificity was set to default (medium).

2.8. RFP-Trap®/Myc-Trap®

Nanobody RFP-Trap®/Myc-Trap® agarose beads (ChromoTek) were used for precipitation assays according to the manufacturer's protocol. Briefly, RFP/Myc-tagged proteins were expressed in HEK293T cells (24 h). For cell lysis, Triton X-100 lysis buffer (50 mM Tris–HCl pH 7.5, 150 mM NaCl, and 0.5% Triton X-100) containing protease inhibitor cocktail (PI mix; Roche) was used. 10% of total cell lysates were separated for input. Remaining lysates were incubated on equilibrated beads for 2 h at 4 °C under constant rotation. After washing the beads with dilution buffer (10 mM Tris-HCl pH 7.5, 150 mM NaCl, 0.5 mM EDTA, precipitated proteins were eluted with SDS buffer. Samples were analyzed by SDS-PAGE and western blotting.

2.9. Immunocytochemistry and Fluorescence Microscopy

Cells were fixed with 4% paraformaldehyde in PBS for 10 min at RT, washed with PBS, permeabilized with PBST (0.1% Triton-X100 (Roth, Karlsruhe, Germany)) 5 min at RT and blocked with 0.1% ovalbumin, 0.5% fish gelatine in PBS for 45 min at RT. Primary antibodies were incubated overnight at 4 °C, followed by washing with PBS and secondary antibody incubations 1 h at RT. After a final washing cycle (3 × 10 min), cells were mounted with Mowiol 4.88 (Hoechst) and analyzed with a Leica DM6000B microscope (Leica, Wetzlar, Germany). Images were acquired by sCMOS K5 camera (Leica-microsystems GmbH) with a Leica HCX PL 63x/1.32 objective and processed using the Leica Application Suit X, Adobe Photoshop CS® (Adobe Systems, San Jose, CA, USA), and Image J.

2.10. Isolation of Mitochondria-Associated Membrane Fraction

MAMs were isolated from HEK293T cells transfected with VLGR1_CTF_HA according to the protocol by Wieckowski et al. [19]. The workflow of the isolation of MAMs are illustrated in the Figure S1. In brief, 48 h after transfection cells were harvested and homogenized in IBcells1 buffer (225 mM D-Mannitol, 75 mM sucrose and 30 mM-Tris-HCl and 0.1 mM EGTA, pH 7.4) using a Dounce homogenizer (B. Braun Melsungen, Melsungen, Germany). To remove unbroken cells, plasma membranes and nuclei a centrifugation step applied at $700\times g$ for 5 min using an Eppendorf Centrifuge 5430 R. Supernatants were carefully collected and additional centrifugation step at $7000\times g$ for 10 min were carried out to obtain the supernatants for cytosolic fractions containing ER, lysosomes, and microsomes (Mic), and the pellet for crude mitochondria fraction. In a 1st step, supernatants were transferred to new centrifugation tubes and centrifugated at $20,000\times g$ for 30 min in an Eppendorf Centfigure 5910 R (Eppendorf FA-6 × 50 rotor) to separate the ER and microsomes. Pure ER pellets were obtained with further ultra-centrifugation at $100,000\times g$ for 1 h (Beckman Coulter OptimaTLX, SW 40 Ti Swinging-Bucket Rotor, Brea, CA, USA) and resuspended in MRB buffer (250 mM D-Mannitol, 25 mM HEPES, 1 mM EGTA). In a 2nd step, pellets for crude mitochondria fractionation were resuspended in IBcells-2 buffer (225 mM D-Mannitol, 75 mM sucrose, 30 mM Tris-HCl) and centrifugated at $7000\times g$ for 5 min in two rounds to remove contaminants. The obtained pellets of crude the mitochondrial fraction were then resuspended in MRB buffer and added on 8 mL cushion of 30% Percoll in 225 mM D-Mannitol, 25 mM HEPES, 1 mM EGTA for the subfractionation of MAMs and pure mitochondria. After ultra-centrifugation at $95,000\times g$ for 30 min, MAM and mitochondria fractions could be distinguished as two separated bands in the tubes.

Mitochondria fractions were collected from the band localizing close the bottom of the tube and MAM fractions were collected from the band above. Collected mitochondria fractions were resuspended in buffer and centrifuged for 10 min at $7000 \times g$ to remove potential MAM contaminants. Supernatants were discarded and pellets resuspended in MRB buffer as the pure mitochondria. Finally, MAM fractions from previous steps were centrifuged at $100,000 \times g$ for 30 min to remove mitochondria contaminants. Supernatants were removed and pellets resuspended in MRB buffer as pure MAM fractions. All obtained fractions were analyzed by Western blot applying markers of the different subcellular fractions.

2.11. Co-Localization Analysis

Pearson correlation coefficient (R) was used to determine the degree of colocalization between VLGR1_CTF_RFP and ER-mitochondrial interface in cells [20]. The correlation value has a range from +1 to −1. A value of 0 indicates no association, greater than 0 indicates a positive association and less than 0 indicates a negative association between the two variables. The Pearson coefficient was calculated using the Coloc 2 plugin of ImageJ (https://imagej.nih.gov/ij/ (accessed on 19 December 2019)). To determine the localization of the interface of mitochondria and ER the immunofluorescences staining for TOM20 and Nogo-A/RTN4 [21] were subtracted by applying "subtract function" in Adobe Photoshop® CS5 V5 (AP) (Adobe Systems). For this, immunofluorescence signals for the ER marker Noga-A and the mitochondria marker TOM20 in the whole image were screened via AP function: screen and subtracted via AP function: subtract, leaving only the signals with an overlap (Noga-A/TOM20 co-staining), which allowed us to demonstrate the Noga-A and TOM20 signal interface of ER and mitochondria, roughly representing the MAM compartment. We additionally validated the co-localization of immunostained molecules by fluorescence intensity line plots. For this, lines were drawn across to the region of interest (ROI) and pixel intensities were analyzed using Leica Application Suit X (Leica-microsystems). The co-localization of VLGR1_CTF_RFP with ER-mitochondrial markers were determined by the peak values of the signals in fluorescence intensity plots.

2.12. Transmission Electron Microscopy (TEM)

For conventional TEM dissected eyeballs and brains were pre-fixed for 2 h in buffered 2.5% glutaraldehyde containing sucrose and post-fixed in buffered 2% OsO4 as previously described [22]. For the pre-embedding labeling of VLGR1 in adult zebrafish retinas and porcine retinas, the antibody against the C-terminal of murine VLGR1 (see Section 2.2. Antibodies) was used in our previously published protocol of pre-embedding labeling for TEM [23]. In brief, perforated fish eyes and eye cups of porcine eyes were pre-fixed in buffered 4% paraformaldehyde, dissected, infiltrated with 30% buffered sucrose, and cracked by several freezing-thawing cycles. After embedding in buffered 2% Agar (Sigma-Aldrich) agar blocks were sliced with a Leica VT1000S vibratome. Endogenous peroxidase activities of vibratome sections were suppressed by incubation with H_2O_2. Vibratome sections were incubated with primary antibodies against VLGR1 for 96 h and overnight with anti-rabbit biotinylated secondary antibody, which were visualized by a Vectastain ABC-Kit (Vector Laboratories, Newark, CA, USA). Retina sections were then postfixed sequentially in buffered 2.5% glutaraldehyde and 0.5% OsO_4. Dehydrated specimens were flatmounted between ACLAR®-films (Ted Pella Inc., Redding, CA, USA) in Renlam® M-1 resin (Sigma-Aldrich). After heat-polymerization, flatmounts were and clued on top of empty Araldit blocks for ultrathin sectioning. Specimens were ultrthin-sectioned with an Ultracut S ultramicrotome (Leica) and collected on Formvar-coated copper or nickel grids. Sections were counter stained with heavy metals before analyzed and imaged in a Tecna12 BioTwin TEM (FEI) equipped with a SIS Mega-View3 CCD camera (Surface Imaging Systems) was used. Images were acquired with a charge-coupled camera (SIS Megaview3; Olympus Soft Imaging Solutions GmbH, Muenster, Germany), archived by analSIS (Olympus Soft Imaging Solutions GmbH), and processed with Adobe Photoshop CS® (Adobe Systems, San Jose, CA, USA).

2.13. Proximity Ligation Assay (PLA)

In situ proximity ligation assays (PLA) were performed using the Duolink® In Situ Red Starter Kit Mouse/Rabbit (Sigma-Aldrich), according to the manufacturer's protocol. Primary antibodies were incubated overnight at 4 °C. Anti-rabbit PLUS and anti-mouse MINUS secondary PLA probes were applied. The two complementary oligonucleotides were then hybridized, ligated and amplified by rolling circle amplification. Targeted proteins with a proximity under 40 nm result in a fluorescence signal.

2.14. Ca^{2+} Imaging

For imaging the Ca^{2+} signals in the ER and mitochondria, pCMV G-CEPIA1er and pCMV CEPIA2mt were expressed in the cells, respectively [17]. Images were acquired with an eclipse Ti microscope (Nikon, Tokyo, Japan) equipped with a 63xApo TIRF oil objective (1.49 NA; Nikon). Dyes were excited with a 488 nm laser (Coherent; MPB communications Inc., Pointe-Claire, QC, Canada). The exposure time was 25 ms. Images were captured by a sCMOS camera (Orca-Flash 4.0 Hamamatsu Photonics, Herrsching, Germany) controlled by NIS-Elements Advanced Research acquisition software (Nikon). Experiments were performed at 35 °C. Extracellular solution contained, in mM: NaCl, 145; KCl, 2.5; glucose, 24; HEPES, 10; MgCl2, 2, CaCl2, 2; the pH was 7.3–7.4. Ca^{2+} transients were evoked by the addition of 10 μM ATP. Data were analyzed using Fiji, Prism (GraphPad, San Diego, CA, USA) and Microsoft Excel. The fluorescence values were normalized to the first 10 s of the measurement F/F0 = F(t)/F(t0 − 10s).

3. Results

3.1. Affinity Proteomics Identified Interactions of VLGR1 with Proteins of MAMs

To identify novel interaction proteins of VLGR1, we applied tandem affinity purification (TAP) [18,24]. We performed standard TAPs in highly transfectable HEK293T kidney cells and confirmed them in hTERT-RPE1 cells derived from the retinal pigment epithelium of the human eye. Both cell types were transfected with VLGR1_CTF constructs tagged with Strep II/FLAG (SF) (Figure 1B). Since tags can interfere with the interaction of molecules especially in the region of the tags and we aimed to identify proteins interacting with the N- and the C-terminal end of the VLGR1 molecule, we used N- and C- terminal tagged VLGR1_CTFs for our TAPs. After SF-TAPs eluted protein complexes were separated by liquid chromatography coupled with tandem mass spectrometry (LC-MS/MS) to determine their peptide contents. The raw spectra were searched against SwissProt databases to identify interacting proteins and results were verified in the Scaffold program. Next, proteomic data sets were analyzed by Software Tool for Researching Annotations of Proteins (STRAP) [25] and prey proteins were grouped according to their Gene Ontology (GO) terms by using a Cytoscape (http://www.cytoscape.org/) plugin (ClueGO; accessed on 10 September 2017) and STRING data (https://string-db.org/) (STRING; accessed on 20 March 2022) [26]. Our analysis revealed GO terms' enrichments of proteins related to the endoplasmic reticulum (ER) and mitochondria for both cell types used (Figure 1C–E) (Table S1). 257 proteins for VLGR1_CTF baits in HEK293T cells and 94 in hTERT-RPE1 cells, with an overlap of 81 proteins were identified. As mitochondria-related proteins we found 157 preys in HEK293T and 69 in hTERT-RPE1 cells, all of them were also present in the HEK293T pool (Figure 1C,D). Interestingly, we identified 30 TAP preys in HEK293T and 19 in hTERT-RPE1 cells, which associate to MAMs (Figure 1E) (Table 1). Among them are core MAM molecules related to the structural arrangement and formation of MAMs (5 proteins), such as the reticulon 4 protein (RTNA4, neurite outgrowth inhibitor or Nogo-A) and the vesicle-associated membrane protein-associated protein B (VAPB), which both are known to participate in ER-mitochondria tethering [21,27]. Other MAM-related prey proteins are known to be engaged in important MAM functions, namely the regulation of lipid metabolism (8 proteins) and/or Ca^{2+} homeostasis (9 proteins) or are implicated in tethering the membranes of the ER and mitochondria at MAMs (Table 1). Examples of identified molecules associated with lipid metabolism are long-chain fatty acid CoA

ligase 4 (ACSL4), SLC27A4, or the two phosphatidylserine synthases PTDSS1 and PTDSS2. VLGR1 TAP preys associated with Ca^{2+} homeostasis are the sigma-1 receptor (S1R), which regulates the inositol trisphosphate receptor (IP3R) that mediates Ca^{2+} release from the ER upon stimulation. The two voltage-gated anion channels VADC1 and VADC2 in the outer mitochondrial membrane are responsible for the Ca^{2+} uptake of the mitochondria [28]. Cytoscape analysis demonstrated that the prey proteins identified in the VLGR1 TAPs related to the ER, mitochondria, and MAM cluster in specific protein networks (Figure 1E).

Table 1. MAM related proteins identified by VLGR1 TAPs in HEK293T and hTERT-RPE1 cells proteins associated with: Ca^{2+} homeostasis, orange ; lipid metabolism, yellow , MAM structure, gray .

Gene	Protein	Protein Function	Reference	HEK	RPE1
ACSL4	Long-chain-fatty-acid—CoA ligase 4	lipid biosynthesis & fatty acid degradation	[29]	+	−
AIFM1	Mitochondrial apoptosis-inducing factor 1	apoptosis, mito. morphology	[30]	+	−
AMFR	Autocrine motility factor receptor	ubiquitination	[31]	+	−
BCAP31	B-cell receptor-associated protein 31	apoptosis	[32]	+	−
BSG	Basigin	regulatory component of γ-secretase	[33]	+	+
CANX	Calnexin	calcium pump	[34]	+	+
CISD2	CDGSH iron sulfur domain 2	calcium homeostasis	[35]	+	−
ERLIN2	Erlin-2	targets IP3Rs for degradation	[36]	+	+
ERP44	ER resident protein 44	ER protein retention	[37]	+	−
G6PC3	Glucose-6-phosphatase 3	gluconeogenesis	[38]	+	−
HSPA5	Heat shock protein 5	chaperone, ER stress	[39]	+	+
HSPA9	Mitochondrial heat shock protein 9	chaperone, binds VDAC	[40]	+	+
LCLAT1	Lysocardiolipin acyltransferase 1	chardolipin acyl chain remodeling	[41]	+	−
LMAN1	ERGIC-53	mannose-specific lectin	[42]	+	−
MAVS	Mito. antiviral-signaling protein	activation of NF-kb/IRF3	[43]	+	+
P4HB	Protein disulfide-isomerase	ER protein retention	[44]	+	+
PIGN	Phosphatidylinositol glycan anchor biosynthesis, class N	glycolipid, GPI syntheses	[41]	+	−
PSEN1	Presenilin-1	component of γ-secretase	[45]	+	−
PSEN2	Presenilin-2	component of γ-secretase	[45]	+	−
PTDSS1	Phosphatidylserine synthase 1	phospholipid metabolism	[46]	+	−
PTDSS2	Phosphatidylserine synthase 1	phospholipid metabolism	[46]	+	−
RHOT1	Mitochondrial Rho GTPase 1	mitochondrial trafficking	[47]	+	−
RTN2	Reticulon-2	formation of tubular ER	[48]	+	+
RTN4	Reticulon 4, neurite outgrowth inhibitor, Nogo-A	ER-mitochondria tethering, membrane trafficking	[21]	+	+
SCD	Stearoyl-CoA desaturase	fatty acid transport	[49]	+	+
SIGMAR1	Sigma-1 receptor, SR1	chaperone, lipid transport , Ca^{2+} signaling	[39]	+	+
SLC27A4	Long-chain fatty acid transport protein 4	fatty acid transport	[50]	+	+
SOAT1	Sterol O-acyltransferase 1	cholesterol metabolism	[42]	+	+
VAPB	VAMP-associated protein	ER-mitochondria tethering	[27]	+	−
VDAC1	Voltage-dependent anion-channel 1	ion exchange, Ca^{2+} transport	[40]	+	+
VDAC2	Voltage-dependent anion-channel 2	ion exchange, Ca^{2+} transport	[51]	−	+
WSF1	Wolframin, ER, transmembrane	Ca^{2+} transport, ER stress	[52]	+	−

3.2. VLGR1 Interacts with MAM-Associated Proteins

Next, we validated the interaction of VLGR1_CTF with the MAM core proteins, namely ACSL4 and the S1R, previously described as ER residents [12,53], and the mitochondrial import receptor subunit TOM20, a component of the mitochondrial outer membrane [54]. In RFP-Trap® immunoprecipitations of mRFP-tagged VLGR1_CTF expressed in HEK293T cells endogenous S1R, ACSL4 and TOM20 were recovered confirming their interaction with VLGR1 (Figure 2A,C,D). However, S1R was not recovered by mRFP-tagged VLGR1_ICD, indicating an interaction of the transmembrane or loop domains of VLGR1 with S1R (Figure S2). None of the MAM-associated proteins was co-precipitated with mRFP. Reciprocal Myc-Trap® immunoprecipitation of Myc-tagged S1R and mRFP-tagged VLGR1_CTF co-expressed in HEK293T cells, confirmed the interaction of S1R and VLGR1_CTF (Figure 2B).
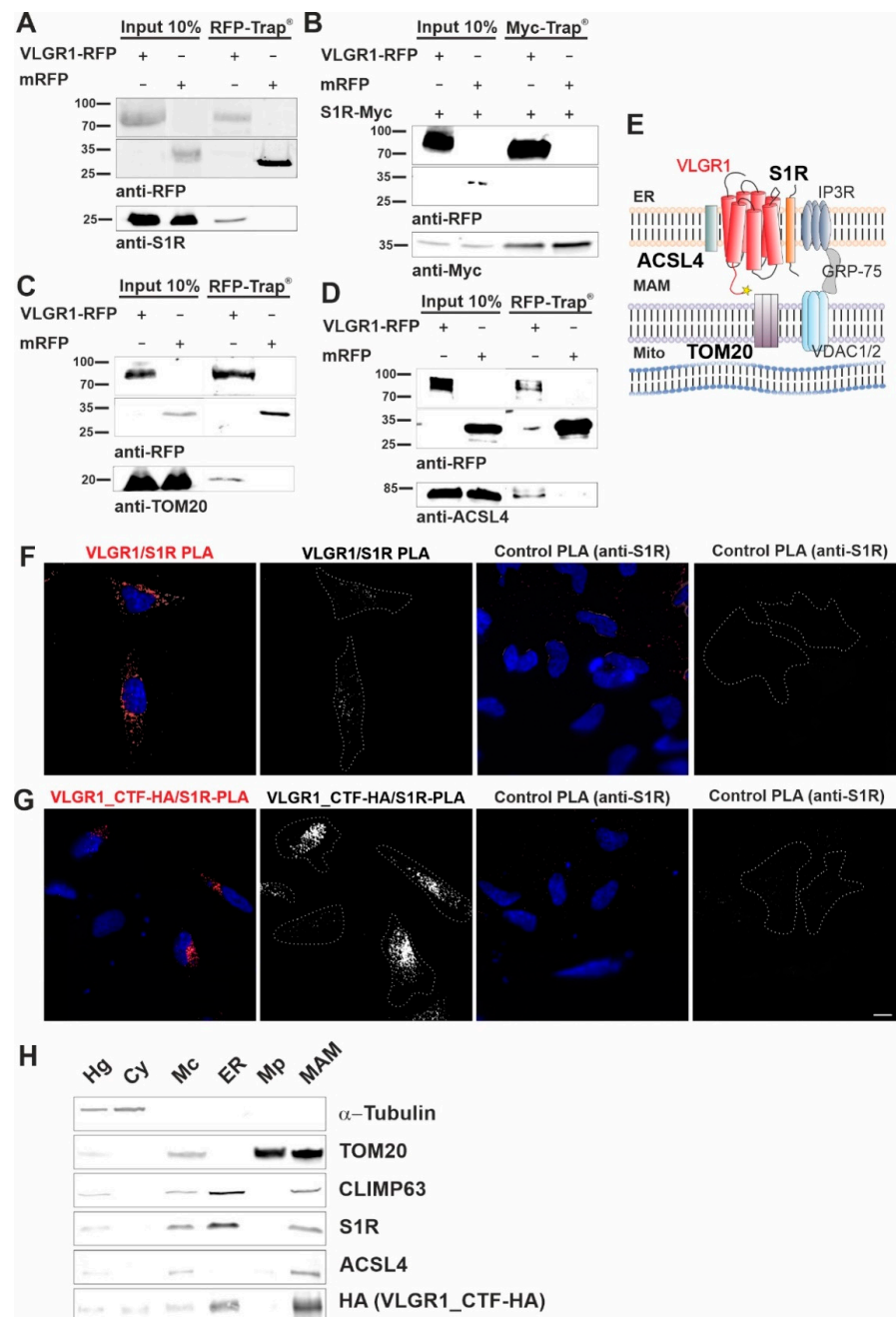
Figure 2. VLGR1_CTF interacts with S1R, ACSL4, TOM20 and is present in the purified MAM compartment. (**A–C**) Western blot analysis of RFP-Trap® from lysates of HEK293T cells expressing

VLGR1_CTF-mRFP or mRFP. Endogenous S1R (sigma-1 receptor), ACSL4 (long-chain fatty acid CoA ligase 4) and TOM20 are precipitated by VLGR1_CTF-mRFP. (**D**) Western blot of Myc-Trap®️ from HEK293T cells coexpressing VLGR1_CTF-mRFP or mRFP and S1R-Myc. VLGR1_CTF-mRFP binds to S1R-Myc. (**E**) Schematic illustration of interactions complex of VLGR1 at the MAM site: pull-downs show that VLGR1 interacts with the ER membrane molecules ACSL4 and S1R. S1R binds to IP3R (inositol trisphosphate receptor), regulating the Ca^{2+} effluxes through the receptor. IP3R is in turn connected via GRP75 to voltage-gated anion channels VDAC1/2 in the outer mitochondrial membrane, where they are associated with the mitochondrial importer subunit TOM20 which also interact with VLGR1. Mito, mitochondria. (**F**) Proximity ligation assay (PLA) for endogenous VLGR1 and S1R in HEK293T cells. White PLA signals represent colocalization of both proteins. Both, anti-S1R and anti-VLGR1 (not shown) only were probed with both PLA (rabbit, rb and mouse, ms) secondary antibodies including PLUS and MINUS complementary sequences and used as negative control. (**G**) PLA assay for VLGR1_CTF-HA and S1R in VLGR1_CTF-HA transfected HEK293T cells. Protein-protein interaction is indicated by white PLA signals. Anti-S1R and anti-VLGR1 (not shown) with PLA (rabbit, rb and mouse, ms) secondary antibodies including PLUS and MINUS complementary sequences were used as negative control, no signal was observed in the control. All images of the respective replicates were acquired using the same light exposure and intensity settings. Nuclei were stained with DAPI (blue). Scale bar, 10 μm. (**H**) Representative Western blot analysis of fractions obtained in MAM isolation assay with VLGR1_CTF-HA transfected HEK293T cells. Purity of cellular fractions was validated by marker proteins, namely α-Tubulin for the cytoplasm, CLIMP63 for the ER. TOM20 as markers for the inner and outer mitochondrial membrane, respectively, and sigma-1 receptor (S1R) and ACSL4 as the MAM component [12]. VLGR1_CTF is present in isolated/crude mitochondria (Mc), ER and MAM fractions. Cell homogenate (Hg), crude mitochondria (Mc), endoplasmic reticulum (ER), pure mitochondrial fraction (Mp), mitochondria-associated membranes (MAM) and cytosolic (Cy). A total of ~30 μg of protein was loaded for each fraction. The pulldown experiments shown in (**A**–**C**) and the PLAs shown in (**F**,**G**) were each performed three times. The fractionations for MAM isolation analyzed in (**H**) were carried out five times.

Next, we validated the interaction between overexpressed VLGR1_CTF and endogenous VLGR1 with S1R in HEK293T cells by in situ proximity ligation assays (PLA) (Figure 2E–G). We observed positive PLA signals and close proximity of VLGR1 and S1R in both scenarios, confirming the interaction of the two proteins in cells. No signals were observed in either control PLA. The interaction of VLGR1 and S1R observed in HEK293T cells was confirmed in Hela cells (Figure S3). Taken together, these findings strongly support the molecular interaction of VLGR1 with MAM core proteins.

3.3. VLGR1 Is Enriched in ER and MAM Fractions

We next wanted to verify the presence of VLGR1 in the MAM compartment by applying a cell fractionation assay modified from Wieckowski et al. [19] (Figures S1 and 2H). HA-tagged VLGR1-CTF transfected HEK293T cells were fractionated and the obtained fractions were validated by Western blots for specific marker proteins [19,55]. The MAM marker S1R was detected in the enriched MAM fraction [12]. As expected, S1R was additionally found in the whole cell lysate and in the fraction of crude mitochondria, which was also positive for the mitochondria marker TOM20 and in the ER fraction specified by the presence of the ER-resident protein CLIMP63 [56]. VLGR1_CTF was detected together with the MAM core proteins S1R and ACSL4 in crude mitochondria fraction, the ER and more importantly also in the fraction enriched for MAMs. This finding supports that VLGR1 is a component of the ER and the MAM.

3.4. VLGR1 Is Localized at the ER-Mitochondria Interface

Next, we aimed to validate the presence of VLGR1 in the MAM compartment by immunocytochemistry. For this, we immunostained the ER-resident protein Nogo-A/RTN4 and the outer mitochondrial membrane protein TOM20 which were both present in the

VLGR1_CTF TAPs as prey, in HeLa cells expressing VLGR1_CTF_HA (Figure 3A). Immunofluorescence microscopy showed the co-staining of VLGR1 with the ER marker Nogo-A, confirmed by a positive Pearson correlation coefficient value (R = 0.70) and an overlapping staining with the outer mitochondrial membrane marker TOM20 with a positive but lower Pearson correlation coefficient (R = 0.33). Next, we determined the localization of the ER-mitochondria interface in HeLa cells by applying the "subtract function" tool in Adobe Photoshop® subtracting the immunofluorescences signal of TOM20 and Nogo-A (Figure 3A). Merging the immunofluorescence of VLGR1 with the fluorescence subtraction result revealed the co-localization of VLGR1 with the ER-mitochondrial interface, which was also confirmed by the Pearson correlation coefficient (R = 0.40). The higher magnification of the zoom-ins of the merged images (Figure 3A, bottom panel) and the common peaks in the fluorescence intensity plots of the three channels of the region of interest (Figure 3B) further support these results. These findings indicate that VLGR1 is localized in ER membranes associated with ER-mitochondria interface of the MAM compartment illustrated in Figure 3C. The localization of VLGR1 at the interface of MAMs was confirmed by immunoelectron microscopy in sections through the inner segments of retinal photoreceptor cells of two different vertebrate species, namely the domestic pig (Sus scrofa) and zebrafish (Danio rerio) (Figure 3D).
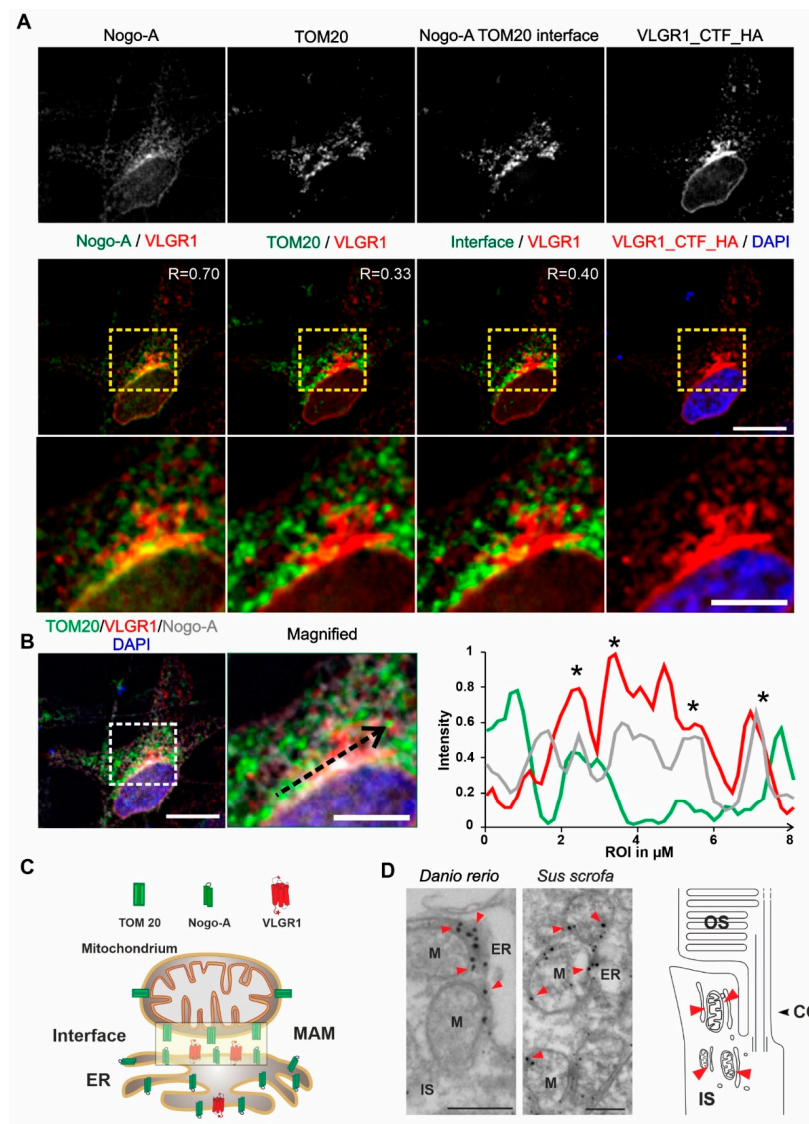

Figure 3. VLGR1_CFT localizes at the ER-mitochondria interface and is present at mitochondrial membranes in photoreceptor cells. (**A**) Immunocytochemical localization analysis of VLGR1_CTF

at the ER-mitochondria interface in HeLa cells. Noga-A and TOM20 were used as markers for the ER and for the outer membrane of mitochondria, respectively. ER-mitochondria interface is visualized by the overlay of Nogo-A and TOM20 signals and subtraction of all individual Nogo-A and TOM20 signals. VLGR1_CTF-HA single staining and merged with DAPI (blue). VLGR1_CTF (red) is localized at the ER-mitochondria interface (Pearson coefficient 0.40). VLGR1_CTF is also localized at the ER with a Pearson coefficient of 0.70 and at mitochondria with a Pearson coefficient of 0.33. Pearson coefficients were calculated for 50 cells in three independents experiments. (**B**) Triple immunofluorescence of VLGR1_CTF-HA (red), TOM20 (green), and Nogo-A (grey), counterstained with DAPI (blue) for nuclear localization. Normalized intensity plot of the tree channels of region of interest (ROI) indicated by the black dashed arrow in the magnified image. Shared intensity peaks (asterisks) indicate the co-localization of VLGR1_CTF-HA with TOM20 and Nogo-A. (**C**) Schematic representation of Nogo-A and TOM20 distribution in ER and mitochondria and along the interface of the two organelles. VLGR1 localization is indicated at the ER-mitochondrial interface. (**D**) Immunoelectron microscopy of the inner segment (IS) of retinal photoreceptor cells from a zebrafish (*Danio rerio*) and a domestic pig (*Sus scrofa*) showing localization of VLGR1 along the membranes of mitochondria (M) (red arrowheads) in close proximity to the ER. Cartoon of a rod photoreceptor cell demonstrating the localization of mitochondria-ER interfaces (red arrowheads). Connecting cilium (CC) and the outer segment (OS) are indicated. Scale bars: (**A**) 10 μm, 5 μm; (**B**) 10 μm, 5 μm; (**C**) 400 nm.

3.5. VLGR1 Deficiency Alters the Structure of the ER-Mitochondria Interface

Characteristic changes in the MAM structure have been described in several diseases whose pathophysiology is associated with a MAM perturbation [11,57,58]. To determine whether VLGR1 deficiency also affects MAM structure, we focused on cerebral neurons and photoreceptor cells, both neurons whose dysfunction has been linked to neurologic disorders, such as epilepsy [59] as well as USH [11,57], respectively. To evaluate whether the deficiency of VLGR1 also affects the MAM structure, we examined MAMs in neurons of wild-type (WT) and *Vlgr1*delta7TM mice lacking the Vlgr1_CTF by transmission electron microscopy (Figure 4 and Figure S4). It has been previously highlighted that the contact point distances at the ER-mitochondrial interface are a key structural parameter related to MAM functions [57]. We measured the latter parameter in ultrathin sections through neurons of the cerebellum and the inner segment of retinal photoreceptor cells (Figures 4A and S4A). Quantitative morphometric analyses revealed that the contact point distances at the ER-mitochondrial interface were significantly enlarged in both cerebellar neurons and photoreceptor cells of *Vlgr1*del7TM mice when compared to wild-type controls.

Furthermore, we morphometrically analyzed two additional structural parameters of MAMs, namely the mitochondrial surface coverage by the ER and the mitochondrial perimeter in both cerebellar neurons and photoreceptor cells (Figures 4B,C and S4B,C). While the mitochondrial surface coverage by the ER was increased in both types of neurons, the mitochondrial perimeter was only increased in cerebellar neurons and not in photoreceptor cells of *Vlgr1*del7TM mice when compared to wild-type controls.

3.6. Ca^{2+} Transients at ER-Mitochondria Contact Sites Are Impaired by VLGR1 Deficiency

The MAMs represent a critical platform for the Ca^{2+} transfer from ER to mitochondria [60,61]. To monitor the Ca^{2+} flux in the two organelles, we made use of genetically encoded Ca^{2+} indicators targeted to ER, (G-CEPIA1er) and mitochondria (CEPIA2mt) [17]. We previously showed that primary astrocytes from mouse brain are well suited for studies of VLGR1 in cells [3,9]. Both Ca^{2+} indicators were transfected into primary brain astrocytes, derived from *Vlgr1*del7TM or wild-type control mice. To trigger the release of Ca^{2+} from the ER and to promote the mitochondrial Ca^{2+} uptake at the ER-mitochondria interface, we applied adenosine triphosphate (ATP) to the culture medium of the astrocytes. ATP stimulates purinergic receptor P2Y receptors, which activate phospholipase C (PLC), leading to

hydrolysis of phosphatidylinositol 4,5-bisphosphate (PIP2) to diacylglycerol (DAG) and inositol triphosphate (IP3). Binding of IP3 to IP3 receptor (IP3R) on the ER membrane triggers the release of Ca^{2+} from the ER [62,63]. We monitored the dynamics of Ca^{2+} fluxes in the ER and the mitochondria in response to ATP in G-CEPIA1er- and CEPIA2mt-expressing astrocytes of *Vlgr1*del7TM and WT by live-cell imaging (Figure 5 and Figure S5A). We quantified the time course of Ca^{2+} release from the ER (Figure 5A) by calculating the amplitude and the kinetics of the G-CEPIA1er signal, respectively (Figure 5B,C). The experiments showed significantly decreased Ca^{2+} release from the ER (Figure 5B), which was accompanied by an almost significant slowing of Ca^{2+} efflux in *Vlgr1*del7 TM astrocytes compared with wild-type control astrocytes (Figure 5C). Further, the measurement of CEPIA2mt signals showed a significant decrease of mitochondrial Ca^{2+} uptake in *Vlgr1*del7TM astrocytes (Figures 5D,E and S5B). In conclusion, our data demonstrate that VLGR1 is necessary for the proper regulation of Ca^{2+} homeostasis at MAMs and absence of VLGR1 results in dysregulated Ca^{2+} homeostasis at MAMs, as illustrated in Figure 5F.
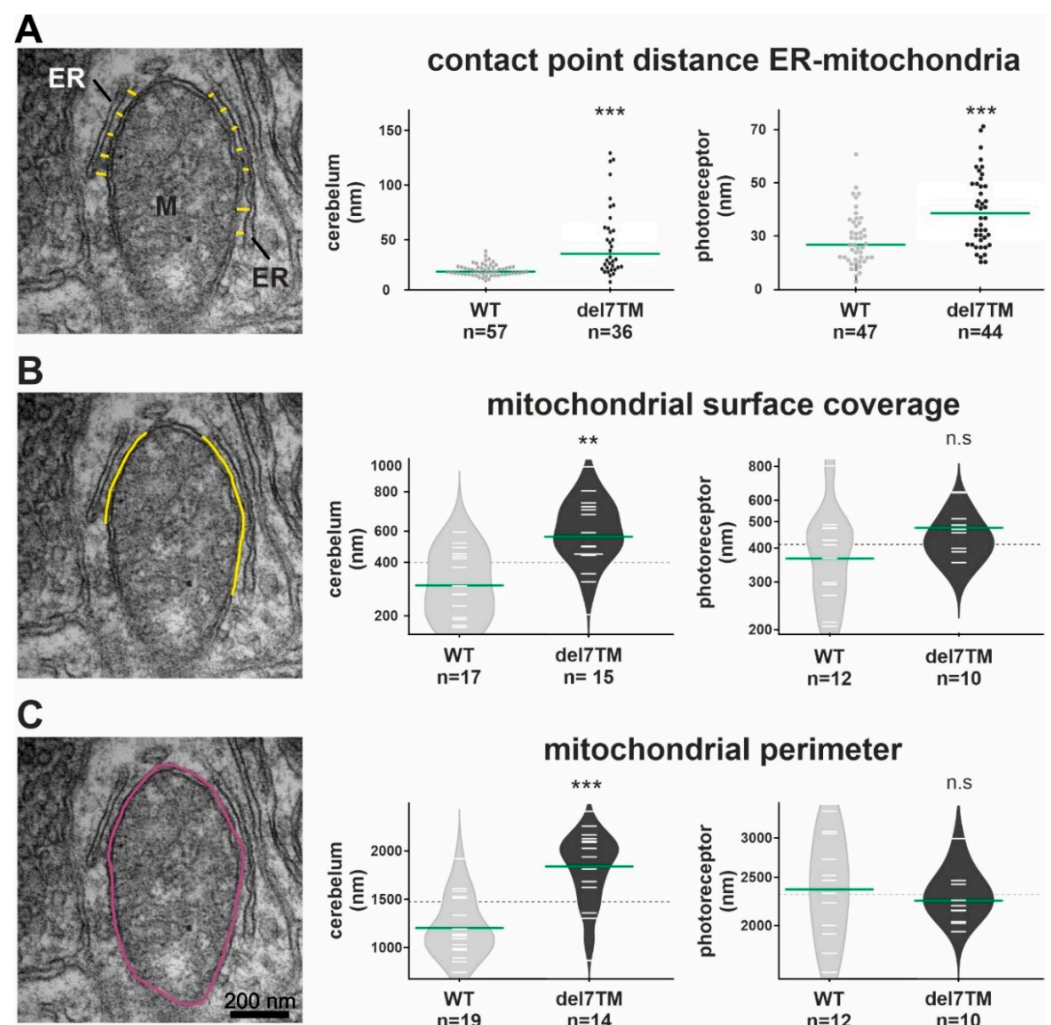

Figure 4. Electron microscopy analysis of the ER-mitochondria interface in murine cerebellum neurons and retinal photoreceptors and S1R abundance at the ER. (**A**) Representative TEM image for the measurement of contact point distance at the ER-mitochondrial interface (WT mice). Mitochondria (M) and the ER (yellow spacer lines) are indicated. Calculation of contact point distance at the ER-mitochondrial interface in WT control and *Vlgr1*del7TM cerebellar neurons and photoreceptor cells. (**B**) The mitochondrial surface coverage by ER is indicated by yellow lines in the representative TEM image. Measurements of mitochondrial surface coverage in WT control and *Vlgr1*del7TM cerebellum

neurons and photoreceptor cells. (**C**) The mitochondrial perimeter indicated in purple in the representative TEM image was measured in WT control and *Vlgr1*del7TM cerebellum neurons and photoreceptors. Three independent samples of mature mice of both genotypes and sexes at the age of 4 to 6 months were analyzed. Student's t-test for statistical significance: ** $p < 0.01$, *** $p < 0.001$, n.s. no significance.
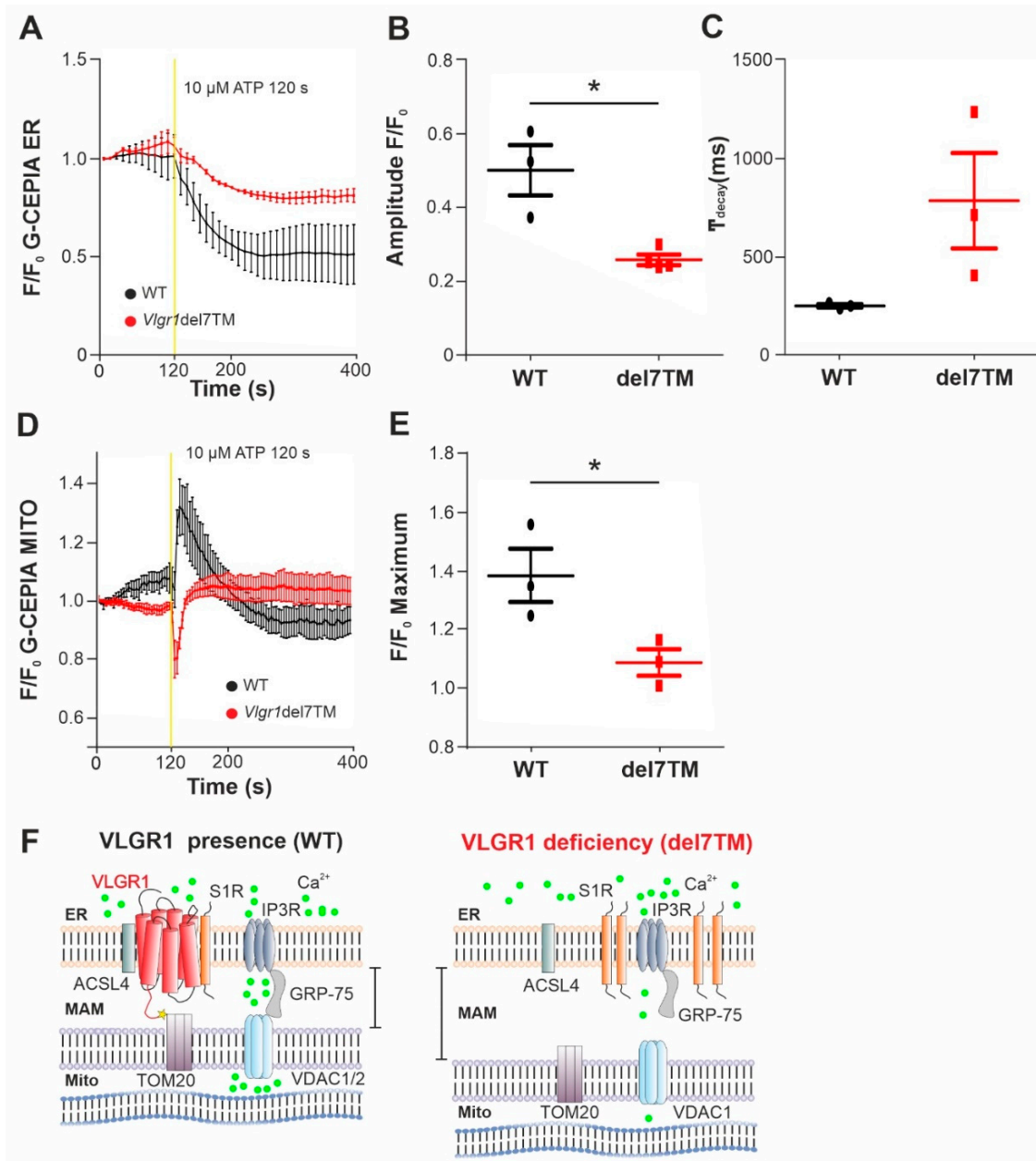

Figure 5. VLGR1 deficiency decreases the Ca^{2+} release from ER and uptake to mitochondria in astrocytes. (**A**) Averaged time-course of the ER Ca^{2+} signal in response to ATP stimulation at 120 s, monitored by G-CEPIA1er, in WT control (black) and *Vlgr1*del7TM *(red)* astrocytes. (**B**) Quantification of G-CEPIA1er signal amplitude, $p = 0.0056$. WT: $n = 3$ individual experiments; *Vlgr1*del7TM: $n = 3$ individual experiments. (**C**) Quantification of time constant (τ) of the G-CEPIA1er signal decay (fitting by single exponential function), $p = 0.2814$. (**D**) Mitochondrial Ca^{2+} signals were measured using CEPIA2mt after stimulation with ATP at 120 s in WT control and *Vlgr1*del7TM astrocytes. (**E**) Amplitude of signals for mitochondrial Ca^{2+} response after ATP stimulus; $p = 0.0438$. WT: $n = 3$ individual experiments; *Vlgr1*del7TM: $n = 4$ individual experiments. Yellow line indicates application of 10 μM ATP at 120 s. Error bars represent SEM. Student's t-test for statistical significance: * $p < 0.05$

(**F**) Schematic illustration of Ca^{2+} release (green dots) from the ER through and mitochondrial uptake of Ca^{2+} by the Ca^{2+} shuttling complex of MAMs in the presence and absence/deficiency of VLGR1. VLGR1 interacting partners identified TAPs and confirmed in pull-downs: ACSL4, long-chain fatty acid CoA ligase 4; S1R, Sigma-1 receptor; TOM2, mitochondrial import receptor. IP3R (inositol trisphosphate receptor) is regulated by S1R and bridged by GRP75 to the voltage-dependent anion channels VDAC1 and 2, both also present as prey in VLGR1_CTF TAPs.

4. Discussion

We identified the adhesion GPCR (aGPCR) VLGR1 in internal membranes of the cell, namely at the ER membrane and at mitochondria-associated ER membranes (MAMs), a specialized compartment at the interface between the membranes of the ER and mitochondria. MAMs provide platforms for several cellular processes and signaling pathways, such as ER stress signaling, metabolism, autophagy, apoptosis, inflammation, and Ca^{2+} homeostasis [10]. VLGR1 functions have been previously related to cell membrane adhesion, such as the ankle-links between the stereocilia of mechanosensitive hair cells in the inner ear and the periciliary membrane complex at the base of the cilium of photoreceptor cells or as a metabotropic mechanoreceptor at focal adhesions, the adhesion sites of the cell membrane to the substrate [9,14,64]. However, hitherto it has not been associated with functions at internal membrane contact sites of the cell, where opposing organelles are tethered facilitating the communication between organelles [65]. Here, we provide evidence that the aGPCR VLGR1 is a component of a protein complex that is crucial for regulating Ca^{2+} flux from the ER into the MAM interface to mitochondria and thus for the Ca^{2+} homeostasis.

We identified several MAM core proteins as interaction partners of VLRG1 by affinity proteomics capture approaches performed in two different human cell lines. All MAM protein hits that we discovered in hTERT-RPE1 were also present in the HEK293T dataset, providing evidence that VLGR1 is closely associated with MAMs. We confirmed the putative interactions with several MAM components of both the ER part and the outer mitochondrial membrane using complementary protein-protein interaction assays, such as in vitro co-IPs and in situ PLAs. In addition, our observed subcellular localization of VLGR1 in the ER membrane and its enrichment in the intersections between the ER and mitochondria further supports that VLGR1 is a component of MAMs. All in all, our data demonstrate the molecular association of VLGR1 with MAMs and its localization in the mitochondria-ER contacts of MAMs in the membrane of the ER.

MAMs play pivotal roles in cellular physiology by regulating intracellular Ca^{2+} homeostasis driven by a tightly balanced interplay between the Ca^{2+} release from the ER and the Ca^{2+} uptake through the juxtaposed outer mitochondrial membrane [60,61,66]. To this end, MAMs harbor a channel complex for Ca^{2+}, mainly composed of the inositol 1,4,5-trisphosphate receptors (IP3Rs) in the ER membrane, bridged by the chaperone GPR-75 to the voltage-dependent anion channel 1 (VDAC1) in the outer mitochondrial membrane [67], which channels Ca^{2+} to the mitochondrial Ca^{2+} uniporter (MCU), and the Na$^+$-dependent mitochondrial Ca^{2+} efflux transporter (NCLX), both of the inner mitochondrial membrane [28]. In the present study, we provide evidence that VLGR1 is closely associated with this Ca^{2+} delivery system at MAMs by interacting with several of its components. We demonstrate that VLGR1 physically interacts with the sigma-1 receptor (S1R), the Ca^{2+}-sensitive and ligand-operated receptor chaperone which regulates the Ca^{2+} out-flux via IP3Rs from the ER at MAMs [39]. In addition, we show the interaction of VLGR1 with TOM20, a peripheral subunit of the mitochondrial outer membrane translocase essential of mitochondrial protein import. It has been recently shown that TOM20 forms a complex with the VDAC1 and cooperates in channeling Ca^{2+} ions into mitochondria [68]. It is worth noting that both voltage-dependent anion channels VDAC1 and VDAC2 were also found to be hits in the VLGR1 TAPs (see Table 1), so they also represent potential binding partners of VLGR1 in a protein complex related to VLGR1 in the MAM compartment (see cartoon, Figure 2E).

In addition to these physical molecular interactions of VLGR1, we observed a functional interaction of VLGR1 with the Ca^{2+} signaling between the ER and mitochondria at MAMs. In the absence of VLGR1, both the Ca^{2+} release from the ER through IP3Rs in response to ATP and the subsequent Ca^{2+} uptake by mitochondria were significantly reduced. We assume that the reduced outflow of Ca^{2+} from the ER into the cleft at the MAM interface does not provide a sufficiently large pool of local Ca^{2+} available for uptake by mitochondria. The result is that the absence of VLGR1 leads to reduced uptake of Ca^{2+} into the mitochondria. This is consistent with the altered mitochondrial Ca^{2+} dynamics observed after siRNA-mediated knockdown of S1R and IP3R3, respectively [39]. Even without direct measurements of the Ca^{2+} release from the ER, the authors of the latter study assumed that the measured reduced Ca^{2+} uptake by mitochondria was also caused by a disturbed Ca^{2+} supply from the neighboring ER Ca^{2+} store. Overall, our results suggest that VLGR1 participates in the regulation of IP3Rs in the ER membrane of MAMs, directly or through its interaction with the membrane chaperonin S1R which controls the functions of IP3Rs.

Under normal physiological conditions, the membranes between the ER and the mitochondrial membranes are approximately 10–30 nm apart at the MAM interfaces [69,70]. This close arrangement is required to ensure proper flow of Ca^{2+} and normal exchange of phospholipids between the two organelles. Several ER-mitochondria tethering protein complexes consisting of proteins located on the opposing membranes have been reported to establish and maintain this distance. Measuring the contact point distances at the ER-mitochondrial interface in cerebellar neurons and photoreceptor cells revealed a significant increase in the distances between the ER and mitochondria in the absence of VLGR1 in both neurons and photoreceptor cells (Figure 4A). This might be due to a direct association of VLGR1 with the tethering complexes, which is supported by the identification of ER and mitochondrial tethering molecules as interaction partners of VLGR1, namely VDAC1, the VAMP-associated protein (VAPB) or reticulon 4 (RTN4, Nogo-A) both are present in our VLGR1 TAPs (Table 1) [21,27,70]. The wider distance between the membranes of both organelles at MAMs in VLGR1 deficient cells could be, however, also due to reduced Ca^{2+} release from the ER and the resulting decrease of the local Ca^{2+} concentration in the cleft. Because of many molecular links, the assembly by the tethering molecules is Ca^{2+}-dependent [71].

Several diseases have been associated with alterations in the ER-mitochondrial junctions as a phenotype. Alterations in the connections between the ER and the mitochondria have been described as a pathological feature underlying the pathomechanisms of many neurodegenerative diseases, such as Alzheimer's disease, Parkinson's disease, and amyotrophic lateral sclerosis with associated frontotemporal dementia [70]. Here, we show that the absence of VLGR1 leads to a comparable phenotype at MAMs. Thus, the pathophysiological pathways of neurodegenerative diseases and the two diseases associated with VLGR1 defects, Usher syndrome type 2 and childhood absence epilepsy [4,6,7], may open the avenue for common therapeutic targets and therapy options.

One obvious pathway that is disrupted in these diseases is the bioenergetics of cells. Due to the reduced Ca^{2+} influx, the Ca^{2+} level in the mitochondria decreases, which impairs the activity of mitochondrial enzymes, such as the pyruvate, isocitrate, and α-ketoglutarate dehydrogenases, and thereby the bioenergetics of the cells [72,73]. This is in line with previous findings indicating that the pathology in Alzheimer's and retinal degeneration are accompanied by effects on the mitochondrial energetics [74,75].

5. Conclusions

We identified and validated VLGR1 as the first aGPCR in MAMs. We show that VLGR1 is a vital component for the correct architecture of MAMs. In addition, we demonstrate that VLGR1 is crucial for balancing the Ca^{2+} homeostasis of MAMs, mitochondria and thereby the entire cell. Our findings also provide novel insights that help to explain

the pathomechanisms underlying VLGR1-associated diseases, namely the human Usher syndrome type 2C and childhood absence epilepsy.

References

1. Hamann, J.; Aust, G.; Arac, D.; Engel, F.B.; Formstone, C.; Fredriksson, R.; Hall, R.A.; Harty, B.L.; Kirchhoff, C.; Knapp, B.; et al. International Union of Basic and Clinical Pharmacology. XCIV. Adhesion G protein-coupled receptors. *Pharmacol. Rev.* **2015**, *67*, 338–367. [CrossRef]
2. Arac, D.; Boucard, A.A.; Bolliger, M.F.; Nguyen, J.; Soltis, S.M.; Sudhof, T.C.; Brunger, A.T. A novel evolutionarily conserved domain of cell-adhesion GPCRs mediates autoproteolysis. *EMBO J.* **2012**, *31*, 1364–1378. [CrossRef]
3. Knapp, B.; Roedig, J.; Roedig, H.; Krzysko, J.; Horn, N.; Guler, B.E.; Kusuluri, D.K.; Yildirim, A.; Boldt, K.; Ueffing, M.; et al. Affinity Proteomics Identifies Interaction Partners and Defines Novel Insights into the Function of the Adhesion GPCR VLGR1/ADGRV1. *Molecules* **2022**, *27*, 3108. [CrossRef] [PubMed]
4. McMillan, D.R.; White, P.C. Studies on the Very Large G Protein-Coupled Receptor: From Initial Discovery to Determining its Role in Sensorineural Deafness in Higher Animals. In *Adhesion-GPCRs: Structure to Function*; Springer: Boston, MA, USA, 2010; Volume 706, pp. 76–86. [CrossRef]
5. Reiners, J.; Nagel-Wolfrum, K.; Jurgens, K.; Marker, T.; Wolfrum, U. Molecular basis of human Usher syndrome: Deciphering the meshes of the Usher protein network provides insights into the pathomechanisms of the Usher disease. *Exp. Eye Res.* **2006**, *83*, 97–119. [CrossRef] [PubMed]
6. Skradski, S.L.; Clark, A.M.; Jiang, H.; White, H.S.; Fu, Y.H.; Ptacek, L.J. A novel gene causing a mendelian audiogenic mouse epilepsy. *Neuron* **2001**, *31*, 537–544. [CrossRef]

7. Yagi, H.; Noguchi, Y.; Kitamura, K.; Sato, M. Deficiency of Vlgr1 resulted in deafness and susceptibility to audiogenic seizures while the degree of hearing impairment was not correlated with seizure severity in C57BL/6- and 129-backcrossed lines of Vlgr1 knockout mice. *Neurosci. Lett.* **2009**, *461*, 190–195. [CrossRef]

8. Knapp, B.; Roedig, J.; Boldt, K.; Krzysko, J.; Horn, N.; Ueffing, M.; Wolfrum, U. Affinity proteomics identifies novel functional modules related to adhesion GPCRs. *Ann. N. Y. Acad. Sci.* **2019**, *1456*, 144–167. [CrossRef] [PubMed]

9. Kusuluri, D.K.; Guler, B.E.; Knapp, B.; Horn, N.; Boldt, K.; Ueffing, M.; Aust, G.; Wolfrum, U. Adhesion G protein-coupled receptor VLGR1/ADGRV1 regulates cell spreading and migration by mechanosensing at focal adhesions. *iScience* **2021**, *24*, 102283. [CrossRef] [PubMed]

10. Ilacqua, N.; Sanchez-Alvarez, M.; Bachmann, M.; Costiniti, V.; Del Pozo, M.A.; Giacomello, M. Protein Localization at Mitochondria-ER Contact Sites in Basal and Stress Conditions. *Front. Cell Dev. Biol.* **2017**, *5*, 107. [CrossRef] [PubMed]

11. Hedskog, L.; Pinho, C.M.; Filadi, R.; Ronnback, A.; Hertwig, L.; Wiehager, B.; Larssen, P.; Gellhaar, S.; Sandebring, A.; Westerlund, M.; et al. Modulation of the endoplasmic reticulum-mitochondria interface in Alzheimer's disease and related models. *Proc. Natl. Acad. Sci. USA* **2013**, *110*, 7916–7921. [CrossRef]

12. Lewis, A.; Tsai, S.Y.; Su, T.P. Detection of Isolated Mitochondria-Associated ER Membranes Using the Sigma-1 Receptor. *Methods Mol. Biol.* **2016**, *1376*, 133–140. [CrossRef] [PubMed]

13. McMillan, D.R.; White, P.C. Loss of the transmembrane and cytoplasmic domains of the very large G-protein-coupled receptor-1 (VLGR1 or Mass1) causes audiogenic seizures in mice. *Mol. Cell Neurosci.* **2004**, *26*, 322–329. [CrossRef] [PubMed]

14. Maerker, T.; van Wijk, E.; Overlack, N.; Kersten, F.F.; McGee, J.; Goldmann, T.; Sehn, E.; Roepman, R.; Walsh, E.J.; Kremer, H.; et al. A novel Usher protein network at the periciliary reloading point between molecular transport machineries in vertebrate photoreceptor cells. *Hum. Mol. Genet.* **2008**, *17*, 71–86. [CrossRef]

15. Trojan, P.; Krauss, N.; Choe, H.W.; Giessl, A.; Pulvermuller, A.; Wolfrum, U. Centrins in retinal photoreceptor cells: Regulators in the connecting cilium. *Prog. Retin. Eye Res.* **2008**, *27*, 237–259. [CrossRef]

16. Guler, B.E.; Krzysko, J.; Wolfrum, U. Isolation and culturing of primary mouse astrocytes for the analysis of focal adhesion dynamics. *STAR Protoc.* **2021**, *2*, 100954. [CrossRef]

17. Suzuki, J.; Kanemaru, K.; Ishii, K.; Ohkura, M.; Okubo, Y.; Iino, M. Imaging intraorganellar Ca^{2+} at subcellular resolution using CEPIA. *Nat. Commun.* **2014**, *5*, 4153. [CrossRef] [PubMed]

18. Boldt, K.; van Reeuwijk, J.; Lu, Q.; Koutroumpas, K.; Nguyen, T.M.; Texier, Y.; van Beersum, S.E.; Horn, N.; Willer, J.R.; Mans, D.A.; et al. An organelle-specific protein landscape identifies novel diseases and molecular mechanisms. *Nat. Commun.* **2016**, *7*, 11491. [CrossRef] [PubMed]

19. Wieckowski, M.R.; Giorgi, C.; Lebiedzinska, M.; Duszynski, J.; Pinton, P. Isolation of mitochondria-associated membranes and mitochondria from animal tissues and cells. *Nat. Protoc.* **2009**, *4*, 1582–1590. [CrossRef] [PubMed]

20. Adler, J.; Parmryd, I. Quantifying colocalization by correlation: The Pearson correlation coefficient is superior to the Mander's overlap coefficient. *Cytometry A* **2010**, *77*, 733–742. [CrossRef] [PubMed]

21. Sutendra, G.; Dromparis, P.; Wright, P.; Bonnet, S.; Haromy, A.; Hao, Z.; McMurtry, M.S.; Michalak, M.; Vance, J.E.; Sessa, W.C.; et al. The Role of Nogo and the Mitochondria-Endoplasmic Reticulum Unit in Pulmonary Hypertension. *Sci. Transl. Med.* **2011**, *3*, 88ra55. [CrossRef] [PubMed]

22. Karlstetter, M.; Sorusch, N.; Caramoy, A.; Dannhausen, K.; Aslanidis, A.; Fauser, S.; Boesl, M.R.; Nagel-Wolfrum, K.; Tamm, E.R.; Jagle, H.; et al. Disruption of the retinitis pigmentosa 28 gene Fam161a in mice affects photoreceptor ciliary structure and leads to progressive retinal degeneration. *Hum. Mol. Genet.* **2014**, *23*, 5197–5210. [CrossRef] [PubMed]

23. Sedmak, T.; Wolfrum, U. Intraflagellar transport molecules in ciliary and nonciliary cells of the retina. *J. Cell Biol.* **2010**, *189*, 171–186. [CrossRef] [PubMed]

24. Gloeckner, C.J.; Boldt, K.; Schumacher, A.; Roepman, R.; Ueffing, M. A novel tandem affinity purification strategy for the efficient isolation and characterisation of native protein complexes. *Proteomics* **2007**, *7*, 4228–4234. [CrossRef] [PubMed]

25. Bhatia, V.N.; Perlman, D.H.; Costello, C.E.; McComb, M.E. Software tool for researching annotations of proteins: Open-source protein annotation software with data visualization. *Anal. Chem.* **2009**, *81*, 9819–9823. [CrossRef]

26. Bindea, G.; Mlecnik, B.; Hackl, H.; Charoentong, P.; Tosolini, M.; Kirilovsky, A.; Fridman, W.H.; Pages, F.; Trajanoski, Z.; Galon, J. ClueGO: A Cytoscape plug-in to decipher functionally grouped gene ontology and pathway annotation networks. *Bioinformatics* **2009**, *25*, 1091–1093. [CrossRef]

27. Stoica, R.; Paillusson, S.; Gomez-Suaga, P.; Mitchell, J.C.; Lau, D.H.; Gray, E.H.; Sancho, R.M.; Vizcay-Barrena, G.; De Vos, K.J.; Shaw, C.E.; et al. ALS/FTD-associated FUS activates GSK-3beta to disrupt the VAPB-PTPIP51 interaction and ER-mitochondria associations. *EMBO Rep.* **2016**, *17*, 1326–1342. [CrossRef] [PubMed]

28. Shoshan-Barmatz, V.; De, S. Mitochondrial VDAC, the Na$^+$/Ca^{2+} Exchanger, and the Ca^{2+} Uniporter in Ca^{2+} Dynamics and Signaling. *Adv. Exp. Med. Biol.* **2017**, *981*, 323–347. [CrossRef] [PubMed]

29. Lewin, T.M.; Van Horn, C.G.; Krisans, S.K.; Coleman, R.A. Rat liver acyl-CoA synthetase 4 is a peripheral-membrane protein located in two distinct subcellular organelles, peroxisomes, and mitochondrial-associated membrane. *Arch. Biochem. Biophys.* **2002**, *404*, 263–270. [CrossRef]

30. Chiang, S.F.; Huang, C.Y.; Lin, T.Y.; Chiou, S.H.; Chow, K.C. An alternative import pathway of AIF to the mitochondria. *Int. J. Mol. Med.* **2012**, *29*, 365–372. [CrossRef]

31. Goetz, J.G.; Genty, H.; St-Pierre, P.; Dang, T.; Joshi, B.; Sauve, R.; Vogl, W.; Nabi, I.R. Reversible interactions between smooth domains of the endoplasmic reticulum and mitochondria are regulated by physiological cytosolic Ca^{2+} levels. *J. Cell Sci.* **2007**, *120*, 3553–3564. [CrossRef] [PubMed]

32. Iwasawa, R.; Mahul-Mellier, A.L.; Datler, C.; Pazarentzos, E.; Grimm, S. Fis1 and Bap31 bridge the mitochondria-ER interface to establish a platform for apoptosis induction. *EMBO J.* **2011**, *30*, 556–568. [CrossRef] [PubMed]

33. Hashimoto, T.; Hussien, R.; Brooks, G.A. Colocalization of MCT1, CD147, and LDH in mitochondrial inner membrane of L6 muscle cells: Evidence of a mitochondrial lactate oxidation complex. *Am. J. Physiol. Endocrinol. Metab.* **2006**, *290*, E1237–E1244. [CrossRef] [PubMed]

34. Myhill, N.; Lynes, E.M.; Nanji, J.A.; Blagoveshchenskaya, A.D.; Fei, H.; Carmine Simmen, K.; Cooper, T.J.; Thomas, G.; Simmen, T. The subcellular distribution of calnexin is mediated by PACS-2. *Mol. Biol. Cell* **2008**, *19*, 2777–2788. [CrossRef] [PubMed]

35. Wang, C.H.; Chen, Y.F.; Wu, C.Y.; Wu, P.C.; Huang, Y.L.; Kao, C.H.; Lin, C.H.; Kao, L.S.; Tsai, T.F.; Wei, Y.H. Cisd2 modulates the differentiation and functioning of adipocytes by regulating intracellular Ca^{2+} homeostasis. *Hum. Mol. Genet.* **2014**, *23*, 4770–4785. [CrossRef] [PubMed]

36. Browman, D.T.; Resek, M.E.; Zajchowski, L.D.; Robbins, S.M. Erlin-1 and erlin-2 are novel members of the prohibitin family of proteins that define lipid-raft-like domains of the ER. *J. Cell Sci.* **2006**, *119*, 3149–3160. [CrossRef]

37. Gilady, S.Y.; Bui, M.; Lynes, E.M.; Benson, M.D.; Watts, R.; Vance, J.E.; Simmen, T. Ero1alpha requires oxidizing and normoxic conditions to localize to the mitochondria-associated membrane (MAM). *Cell Stress Chaperones* **2010**, *15*, 619–629. [CrossRef] [PubMed]

38. Bionda, C.; Portoukalian, J.; Schmitt, D.; Rodriguez-Lafrasse, C.; Ardail, D. Subcellular compartmentalization of ceramide metabolism: MAM (mitochondria-associated membrane) and/or mitochondria? *Biochem. J.* **2004**, *382*, 527–533. [CrossRef]

39. Hayashi, T.; Su, T.P. Sigma-1 receptor chaperones at the ER-mitochondrion interface regulate Ca^{2+} signaling and cell survival. *Cell* **2007**, *131*, 596–610. [CrossRef]

40. Szabadkai, G.; Bianchi, K.; Varnai, P.; De Stefani, D.; Wieckowski, M.R.; Cavagna, D.; Nagy, A.I.; Balla, T.; Rizzuto, R. Chaperone-mediated coupling of endoplasmic reticulum and mitochondrial Ca^{2+} channels. *J. Cell Biol.* **2006**, *175*, 901–911. [CrossRef] [PubMed]

41. Kinoshita, T.; Inoue, N. Dissecting and manipulating the pathway for glycosylphos-phatidylinositol-anchor biosynthesis. *Curr. Opin. Chem. Biol.* **2000**, *4*, 632–638. [CrossRef]

42. Rusinol, A.E.; Cui, Z.; Chen, M.H.; Vance, J.E. A unique mitochondria-associated membrane fraction from rat liver has a high capacity for lipid synthesis and contains pre-Golgi secretory proteins including nascent lipoproteins. *J. Biol. Chem.* **1994**, *269*, 27494–27502. [CrossRef]

43. Horner, S.M.; Liu, H.M.; Park, H.S.; Briley, J.; Gale, M., Jr. Mitochondrial-associated endoplasmic reticulum membranes (MAM) form innate immune synapses and are targeted by hepatitis C virus. *Proc. Natl. Acad. Sci. USA* **2011**, *108*, 14590–14595. [CrossRef] [PubMed]

44. Hoffstrom, B.G.; Kaplan, A.; Letso, R.; Schmid, R.S.; Turmel, G.J.; Lo, D.C.; Stockwell, B.R. Inhibitors of protein disulfide isomerase suppress apoptosis induced by misfolded proteins. *Nat. Chem. Biol.* **2010**, *6*, 900–906. [CrossRef] [PubMed]

45. Area-Gomez, E.; de Groof, A.J.; Boldogh, I.; Bird, T.D.; Gibson, G.E.; Koehler, C.M.; Yu, W.H.; Duff, K.E.; Yaffe, M.P.; Pon, L.A.; et al. Presenilins are enriched in endoplasmic reticulum membranes associated with mitochondria. *Am. J. Pathol.* **2009**, *175*, 1810–1816. [CrossRef] [PubMed]

46. Stone, S.J.; Vance, J.E. Phosphatidylserine synthase-1 and -2 are localized to mitochondria-associated membranes. *J. Biol. Chem.* **2000**, *275*, 34534–34540. [CrossRef] [PubMed]

47. Saotome, M.; Safiulina, D.; Szabadkai, G.; Das, S.; Fransson, A.; Aspenstrom, P.; Rizzuto, R.; Hajnoczky, G. Bidirectional Ca^{2+}-dependent control of mitochondrial dynamics by the Miro GTPase. *Proc. Natl. Acad. Sci. USA* **2008**, *105*, 20728–20733. [CrossRef] [PubMed]

48. Hubner, C.A.; Kurth, I. Membrane-shaping disorders: A common pathway in axon degeneration. *Brain* **2014**, *137*, 3109–3121. [CrossRef]

49. Man, W.C.; Miyazaki, M.; Chu, K.; Ntambi, J. Colocalization of SCD1 and DGAT2: Implying preference for endogenous monounsaturated fatty acids in triglyceride synthesis. *J. Lipid Res.* **2006**, *47*, 1928–1939. [CrossRef] [PubMed]

50. Jia, Z.; Pei, Z.; Maiguel, D.; Toomer, C.J.; Watkins, P.A. The fatty acid transport protein (FATP) family: Very long chain acyl-CoA synthetases or solute carriers? *J. Mol. Neurosci.* **2007**, *33*, 25–31. [CrossRef] [PubMed]

51. Subedi, K.P.; Kim, J.C.; Kang, M.; Son, M.J.; Kim, Y.S.; Woo, S.H. Voltage-dependent anion channel 2 modulates resting Ca^{2+} sparks, but not action potential-induced Ca^{2+} signaling in cardiac myocytes. *Cell Calcium* **2011**, *49*, 136–143. [CrossRef] [PubMed]

52. Delprat, B.; Maurice, T.; Delettre, C. Wolfram syndrome: MAMs' connection? *Cell Death Dis.* **2018**, *9*, 364. [CrossRef]

53. Smith, M.E.; Saraceno, G.E.; Capani, F.; Castilla, R. Long-chain acyl-CoA synthetase 4 is regulated by phosphorylation. *Biochem. Biophys. Res. Commun.* **2013**, *430*, 272–277. [CrossRef] [PubMed]

54. Meisinger, C.; Ryan, M.T.; Hill, K.; Model, K.; Lim, J.H.; Sickmann, A.; Muller, H.; Meyer, H.E.; Wagner, R.; Pfanner, N. Protein import channel of the outer mitochondrial membrane: A highly stable Tom40-Tom22 core structure differentially interacts with preproteins, small tom proteins, and import receptors. *Mol. Cell Biol.* **2001**, *21*, 2337–2348. [CrossRef] [PubMed]

55. Sala-Vila, A.; Navarro-Lerida, I.; Sanchez-Alvarez, M.; Bosch, M.; Calvo, C.; Lopez, J.A.; Calvo, E.; Ferguson, C.; Giacomello, M.; Serafini, A.; et al. Interplay between hepatic mitochondria-associated membranes, lipid metabolism and caveolin-1 in mice. *Sci. Rep.* **2016**, *6*, 27351. [CrossRef]

56. Klopfenstein, D.R.; Klumperman, J.; Lustig, A.; Kammerer, R.A.; Oorschot, V.; Hauri, H.P. Subdomain-specific localization of CLIMP-63 (p63) in the endoplasmic reticulum is mediated by its luminal alpha-helical segment. *J. Cell Biol.* **2001**, *153*, 1287–1300. [CrossRef]

57. Giacomello, M.; Pellegrini, L. The coming of age of the mitochondria-ER contact: A matter of thickness. *Cell Death Differ.* **2016**, *23*, 1417–1427. [CrossRef] [PubMed]

58. De Mario, A.; Quintana-Cabrera, R.; Martinvalet, D.; Giacomello, M. (Neuro)degenerated Mitochondria-ER contacts. *Biochem. Biophys. Res. Commun.* **2017**, *483*, 1096–1109. [CrossRef] [PubMed]

59. Streng, M.L.; Krook-Magnuson, E. The cerebellum and epilepsy. *Epilepsy Behav.* **2021**, *121*, 106909. [CrossRef]

60. Kuo, I.Y.; Brill, A.L.; Lemos, F.O.; Jiang, J.Y.; Falcone, J.L.; Kimmerling, E.P.; Cai, Y.; Dong, K.; Kaplan, D.L.; Wallace, D.P.; et al. Polycystin 2 regulates mitochondrial Ca^{2+} signaling, bioenergetics, and dynamics through mitofusin 2. *Sci. Signal.* **2019**, *12*, eaat7397. [CrossRef] [PubMed]

61. Hirabayashi, Y.; Kwon, S.K.; Paek, H.; Pernice, W.M.; Paul, M.A.; Lee, J.; Erfani, P.; Raczkowski, A.; Petrey, D.S.; Pon, L.A.; et al. ER-mitochondria tethering by PDZD8 regulates Ca^{2+} dynamics in mammalian neurons. *Science* **2017**, *358*, 623–630. [CrossRef]

62. Salter, M.W.; Hicks, J.L. ATP causes release of intracellular Ca2+ via the phospholipase C beta/IP3 pathway in astrocytes from the dorsal spinal cord. *J. Neurosci.* **1995**, *15*, 2961–2971. [CrossRef] [PubMed]

63. Dubyak, G.R.; El-Moatassim, C. Signal transduction via P2-purinergic receptors for extracellular ATP and other nucleotides. *Am. J. Physiol.* **1993**, *265*, C577–C606. [CrossRef] [PubMed]

64. Lefevre, G.; Michel, V.; Weil, D.; Lepelletier, L.; Bizard, E.; Wolfrum, U.; Hardelin, J.P.; Petit, C. A core cochlear phenotype in USH1 mouse mutants implicates fibrous links of the hair bundle in its cohesion, orientation and differential growth. *Development* **2008**, *135*, 1427–1437. [CrossRef]

65. Wu, H.; Carvalho, P.; Voeltz, G.K. Here, there, and everywhere: The importance of ER membrane contact sites. *Science* **2018**, *361*, eaan5835. [CrossRef]

66. Rizzuto, R.; Pinton, P.; Carrington, W.; Fay, F.S.; Fogarty, K.E.; Lifshitz, L.M.; Tuft, R.A.; Pozzan, T. Close contacts with the endoplasmic reticulum as determinants of mitochondrial Ca^{2+} responses. *Science* **1998**, *280*, 1763–1766. [CrossRef]

67. Szabadkai, G.; Simoni, A.M.; Bianchi, K.; De Stefani, D.; Leo, S.; Wieckowski, M.R.; Rizzuto, R. Mitochondrial dynamics and Ca2+ signaling. *Biochim. Biophys. Acta* **2006**, *1763*, 442–449. [CrossRef] [PubMed]

68. Bhagawati, M.; Arroum, T.; Webeling, N.; Montoro, A.G.; Mootz, H.D.; Busch, K.B. The receptor subunit Tom20 is dynamically associated with the TOM complex in mitochondria of human cells. *Mol. Biol. Cell* **2021**, *32*, br1. [CrossRef]

69. Lee, K.S.; Huh, S.; Lee, S.; Wu, Z.; Kim, A.K.; Kang, H.Y.; Lu, B. Altered ER-mitochondria contact impacts mitochondria calcium homeostasis and contributes to neurodegeneration *in vivo* in disease models. *Proc. Natl. Acad. Sci. USA* **2018**, *115*, E8844–E8853. [CrossRef]

70. Paillusson, S.; Stoica, R.; Gomez-Suaga, P.; Lau, D.H.; Mueller, S.; Miller, T.; Miller, C.C. There's Something Wrong with my MAM; the ER-Mitochondria Axis and Neurodegenerative Diseases. *Trends Neurosci.* **2016**, *39*, 146–157. [CrossRef]

71. Idevall-Hagren, O.; Lu, A.; Xie, B.; De Camilli, P. Triggered Ca^{2+} influx is required for extended synaptotagmin 1-induced ER-plasma membrane tethering. *EMBO J.* **2015**, *34*, 2291–2305. [CrossRef] [PubMed]

72. Denton, R.M.; Richards, D.A.; Chin, J.G. Calcium ions and the regulation of NAD+-linked isocitrate dehydrogenase from the mitochondria of rat heart and other tissues. *Biochem. J.* **1978**, *176*, 899–906. [CrossRef] [PubMed]

73. Cardenas, C.; Miller, R.A.; Smith, I.; Bui, T.; Molgo, J.; Muller, M.; Vais, H.; Cheung, K.H.; Yang, J.; Parker, I.; et al. Essential regulation of cell bioenergetics by constitutive InsP3 receptor Ca2+ transfer to mitochondria. *Cell* **2010**, *142*, 270–283. [CrossRef] [PubMed]

74. Yao, J.; Irwin, R.W.; Zhao, L.; Nilsen, J.; Hamilton, R.T.; Brinton, R.D. Mitochondrial bioenergetic deficit precedes Alzheimer's pathology in female mouse model of Alzheimer's disease. *Proc. Natl. Acad. Sci. USA* **2009**, *106*, 14670–14675. [CrossRef] [PubMed]

75. Eckmiller, M.S. Energy depletion hypothesis for retinitis pigmentosa. *Adv. Exp. Med. Biol.* **2003**, *533*, 277–285. [CrossRef] [PubMed]

Erratum

Errata zur Publikation IV. Krzysko J, Maciag F, Mertens A, Güler B, Linnert J, Knapp B, Boldt K, Ueffing M, Nagel-Wolfrum K, Heine M, and Wolfrum U (2022). The Adhesion GPCR VLGR1/ADGRV1 Regulates the Ca^{2+} Homeostasis at Mitochondria-Associated ER Membranes. Cells 2022, 11, 2790.

Auf Seite 1 befindet sich bedauerlicherweise ein Zitierfehler. Die zitierten Publikationen „4 (McMillan and White, 2010), 6 (Skradski et al. 2001) und 7 (Yagi et al. 2009)" müssen durch Zitieren der Publikationen „Wang et al. 2015a, Zhou et al. 2016, Myers et al. 2018, Han et al. 2020, Dahawi et al. 2021 und Liu et al. 2022" ersetzt werden. Die zu zitirenden Publikationen sind im Anhang dieser Arbeit unter Referenzen gelistet.

Auf Seite 13 befindet sich bedauerlicherweise ein Schreibfehler. In der Legende zu Abbildung 4. Muss es statt „Electron microscopy analysis of the ER-mitochondria interface in murine cerebellum neurons and retinal photoreceptors a and S1R abundance at the ER" korrekt lauten "Electron microscopy analysis of the ER-mitochondria interface in murine cerebellum neurons and retinal photoreceptors"

3. Zusammenfassung der Ergebnisse und Diskussion

Die Grundlage der vorliegenden Arbeit basiert auf den identifizierten Proteinnetzwerken des humanen Usher Syndrom (USH1C) Proteins VLGR1. Hierzu wurden affinity capture approaches mittels Affinity Proteomics durchgeführt (Publikation I & II). Der Kern dieser Arbeit befasst sich mit der Fortführung dieser Erkenntnisse und im Fokus mit der Validierung von VLGR1, als ersten und bislang einzigen Vertreter der Adhäsions G-Protein gekoppelten Rezeptoren (ADGRs) im subzellulären Kompartiment der Mitochondrien-assoziierten Membranen (MAMs). Über die Validierung von VLGR1 als MAM-residentes Protein und der Interaktion sowie der Co-Lokalisation mit MAM-Schlüsselproteinen hinaus, konnte eine strukturgebende Beteiligung an der MAM-Komposition, sowie ein funktioneller Einfluss auf die Regulation der Ca^{2+}-Homöostase zwischen ER und Mitochondrium nachgewiesen werden (Publikation VI). Fehlfunktionen am MAM-Kompartiment werden mit neurodegenerativen Krankheiten wie Alzheimer, Parkinson oder Epilepsie assoziiert und die hier gewonnen neuen Erkenntnisse über die Beteiligung von VLGR1 in diesem speziellen Bereich zwischen den beiden Organellen, leisten einen Beitrag zum Verständnis und Aufklärung der pathogenen Mechanismen auch zur Genese von USH. Des Weiteren wurde eine Methode etabliert, die *in vivo* Untersuchungen in murinen Astrozyten effizient und hoher Qualität gewährleistet (Publikation III).

3.1 Proteinnetzwerke von VLGR1 und weiteren ADGRs

Das USH1C Protein VLGR1 gehört zur Protein-Familie der ADGRs, welche sich in neun Untergruppen unterteilt. Als Grundlage für weiterführende Charakterisierungen und somit einem tieferen Verständnis der molekularen Funktion der ADGRs und im speziellen VLGR1, dienten die Interaktionsanalysen, welche zur Modellierung von Proteinnetzwerke führten. In unseren Analysen konnten wir bereits beschriebene Proteininteraktionen, sowie zahlreiche neue putative Interaktionspartner, mittels TAPs zusammen mit Massenspektrometrie, identifizieren. Diese Ergebnisse lieferten neue Erkenntnisse, an welchen physiologischen Prozessen und welchen in zellulären Kompartimenten, VLGR1 als Teil der ADGRs Familie beteiligt ist (**Publikation I und II**).

3.1.1 ADGRs interagieren mit Gerüstproteinen, dem γ-Sekretase Komplex und sind integraler Bestandteil synaptischer Proteinnetzwerke

Die TAP-Daten unserer Studien zeigten zahlreiche Interaktionen von ADGRs mit Gerüstproteinen. Alle identifizierten Gerüstproteine verfügen über PDZ-Domänen und alle in der vorliegenden Studie untersuchten ADGRs enthalten ein PBM an ihrem C-terminalen Ende,

welche die Bindung an PDZ-Domänen ermöglicht. Die Interaktion wird höchstwahrscheinlich über die Bindung der PBM der ADGRs an den PDZ-Domänen hergestellt. Dies wird auch durch frühere experimentelle Daten bestätigt. Wir haben bereits beschrieben, dass VLGR1 direkt mit zwei weiteren USH Proteinen (Harmonin (USH1C) und Whirlin (USH2D)) interagiert. Beide Proteine haben die Funktion als zytoplasmatischer Anker im Membrankomplex in Haarsinneszellen und Photorezeptorzellen (Reiners et al. 2005, Reiners et al. 2006, van Wijk et al. 2006). Des Weiteren geht aus unseren TAP-Daten hervor, dass ADGRs der Gruppe I (Latrophiline), Gruppe III (GPR123, GPR124 und GPR125) und der Gruppe VII (BAIs) mit denselben Gerüstproteinen interagieren. Interaktionen mit Gerüstproteinen haben vermutlich eine regulatorische Wirkung auf die Aktivität von ADGRs (Stephenson et al. 2014, Stephenson et al. 2013, Hu et al. 2014), inwiefern und ob ADGRs jedoch in Proteinnetzwerke und Signalketten eingebunden sind, welche von Gerüstproteinen in Zellen und Gewebe organisiert werden, bedarf weiterer Untersuchungen.

Obwohl die identifizierten Gerüstproteine ubiquitär exprimiert werden, sind sie wesentliche Komponenten der Proteinnetzwerke von Synapsen, insbesondere der postsynaptischen Dichte von Neuronen (Langenhan et al. 2016). Vertreter dieser Gerüstproteine gehören hauptsächlich der Gruppe der *Membrane-associated guanylate kinase (MAGUK)* an, welche an der Bildung und Aufrechterhaltung der Zellpolarität und der dynamischen Anordnung von Rezeptoren und Kanälen an synaptischen Membranen beteiligt sind (Stephenson et al. 2013, Wu et al. 2000, Stephenson et al. 2014). Zusätzlich konnten wir mehrere Proteine als Interaktionspartner identifizieren, die an der Membranfusion synaptischer Vesikel beteiligt sind. SNAP23 zum Beispiel, interagiert mit allen ADGR_CTFs. Dieses Protein ist in den dendritischen Dornen angereichert. Dort kolokalisiert es mit Komponenten der postsynaptischen Dichte (Suh et al. 2010) und ist an der Regulation der Exocytose von Glutamat-Rezeptoren beteiligt (Washbourne et al. 2004). Unsere Ergebnisse decken sich mit bereits validierten Daten, die eine Anreicherung von ADGRs wie VLGR1, Latrophiline und BAIs an postsynaptischen Dendriten (Reiners et al. 2006, Silva et al. 2011, Specht et al. 2009) und der Regulation der synaptischen Plastizität zeigen (Stephenson et al. 2014, Duman et al. 2013, Sando et al. 2017, Kreienkamp et al. 2000).

Interaktionspartner von ADGRs sind sowohl post- wie auch präsynaptisch lokalisiert. Dies deutet auf eine Integration dieser Rezeptoren in Proteinnetzwerke auf beiden Seiten von Synapsen hin und ist konsistent mit Beobachtungen vorangegangener Arbeiten (Rahman et al. 1999, Kreienkamp et al. 2000, Tobaben et al. 2000, Boucard et al. 2012).

Neben Interaktionen mit Gerüst- und synaptischen Proteinen, deuten die TAP-Daten auf eine enge Verknüpfung von ADGRs mit dem γ-Sekretase Komplex hin. Mit Ausnahme von BAI2, konnten wir Untereinheiten des γ-Sekretase Komplex in allen ADGRs TAP-Daten finden. Der Intramembrane γ-Sekretase Komplex ist für die sequentielle proteolytische Spaltung von APP (Amyloid precursor protein) verantwortlich, bei der auch das β-Amyloid entsteht, welches bei der Entwicklung von Alzheimer eine wesentliche Rolle spielt (O'Brien and Wong 2011). Neben APP wurden auch verschieden integrale Membranproteine, darunter auch Rezeptoren als Substrate der γ-Sekretase identifiziert, die in Signalwegen für die Regulation der Transkription eine Rolle spielen (Haapasalo and Kovacs 2011). Dabei wird die intrazelluläre Domäne der Substrate abgespalten und fungiert als Transkriptionsfaktor im Zellkern. Wir konnten bei einigen ADGRs konservierte Aminosäurensequenzen analysieren, die putative γ-Sekretase Schnittstellen darstellen. Darüber hinaus haben wir in mehreren Zelllinien Fragmente in der kalkulierten Größe von ICDs mehrerer ADGRs nachweisen können, sowie eine Lokalisation der ADGR-Fragmente im Zellkern. Einige ADGRs ICDs weisen eine sogenannte Kernlokalisierungssequenz oder auch NLS (nuclear localization sequence) auf, diese wenige Aminosäuren umfassende Signalsequenzen sind für den aktiven Import des Proteins oder Proteinfragments in den Zellkern nötig (Makkerh et al. 1996). All diese Beobachtung liefern Hinweise, dass ADGRs in einem von der γ-Sekretase initiierten Signalweg eingebunden sind, ähnlich dem Szenario für Polycystin 1 (PKD1) (Merrick et al. 2012). PKD1 weist hohe Strukturähnlichkeiten zu ADGRs auf, es besteht aus mehreren Transmembrandomänen und unterliegt einer auto-proteolytischen Spaltung am GPS, analog zu ADGRs (Qian et al. 2002, Yu et al. 2007). Aufgrund Prozessierung durch die γ-Sekretase entsteht PKD1_ICD Fragment, welches abgespalten und in den Zellkern dirigiert wird (Chauvet et al. 2004, Low et al. 2006). Eingeleitet wird dieser Vorgang der Fragmentierung und Abspaltung des PKD1_ICD vermutlich durch einen mechanischen Stimulus (Chauvet et al. 2004), dieser Aktivierungsmechanismus wird auch für ADGRs diskutiert (Luo et al. 2011, Karpus et al. 2013, Scholz et al. 2015). Ob und wie die γ-Sekretase bei der Fragmentierung von ADGRs beteiligt ist, konnten wir im Rahmen dieser Arbeit nicht abschließend klären. Jedoch ergibt sich aus unseren Daten neben der Substrat-Hypothese ein weiterer Ansatz zur Funktionsweise von ADGRs und dem γ-Sekretase Komplex. So konnten wir neben den γ-Sekretase Untereinheiten auch regulatorische Faktoren der γ-Sekretase in unseren TAPs identifizieren. Darunter finden sich für LPHN2, CD97 und VLGR1 CTFs Interaktionspartner wie Basigin (BSG), das als weitere potentielle regulatorische Untereinheit der γ-Sekretase beschrieben wurde (Zhou et al. 2005). Das Transmembrane Emp24-Like Trafficking Protein 10 (TMED10) wurde in allen

ADGR TAPs, mit Ausnahme von BAI2 gefunden. Als Teil des Präsenilin-Komplexes reguliert TMED10 die Aktivität der γ-Sekretase (Chen et al. 2006). Eine andere wichtige regulatorische Komponente stelle das Minor histocompatibility antigen H13 (HM13) dar. HM13 wurde in allen ADGR TAPs identifiziert und ist als Aktivator von Präsenilin1 (PSEN1) wesentlich an der Spaltaktivität des γ-Sekretase-Komplexes beteiligt (Moliaka et al. 2004). Diese Daten legen nahe, dass ADGRs alternativ auch eine Rolle bei der Rekrutierung, Positionierung und Zusammenbau des γ-Sekretase-Komplexes in Membrandomänen spielen können oder auch an der Regulation der Aktivität beteiligt sind. Zusammengefasst liefern unsere Daten robuste Hinweise auf eine Beteiligung von ADGRs an der Aktivität und in Signalwegen, die der γ-Sekretase unterliegen. In diesem Zusammenhang ist es interessant festzuhalten, dass der γ-Sekretase Komplex nicht nur an Plasmamembranen lokalisiert, sondern vielmehr an intrazellulären Subkompartimenten wie den Mitochondrien-assoziierten Membranen (MAMs) oder dem ER (Pinho et al. 2014, Schreiner et al. 2015, Leal et al. 2016).

3.1.2 ADGRs sind mit MAMs assoziiert

In unseren TAP-Daten konnten wir viele potentielle Interaktionspartner identifizieren, die an speziellen intrazellulären Organellen wie dem ER oder Mitochondrien lokalisiert sind. Die hohe Anzahl, dieser an bestimmten subzellulären Kompartimenten beteiligten Proteine, lässt auf neue Funktionen von ADGRs als Netzwerkkomponenten schließen, die bislang nicht bekannt waren. Unsere Analysen ergaben, dass Proteine, die am MAM-Komplex beteiligt sind, in allen untersuchten ADGR TAPs gefunden wurden, jedoch für VLGR1 mit Abstand die meisten. Der MAM-Komplex stellt die Schnittstelle zwischen dem ER und den Mitochondrien dar und dient einer Vielzahl von molekularen Prozessen als Plattform. Die Interaktion mit MAM assoziierten Proteinen könnte auf eine Funktion oder Beteiligung der AGDRs in Adhäsionskomplexen zwischen intrazellulären Membranen oder bei der Signalübermittlung zwischen Zellorganellen hindeuten.

3.2 Isolierte Astrozyten als robuste in vitro Modele

Um Studien möglichst nahe an der biologischen Wirklichkeit, sprich der *in vivo* Situation, durchführen zu können, jedoch eine Reduktion der Komplexität z.B. von Gewebestrukturen, Organen oder ganzer Organismen für die Analysen bestimmter Prozesse notwendig ist, eignen sich primäre Zellkulturen besonders. Bei direkt aus dem Zielgewebe isolierten Zellen, bleiben die physiologischen und metabolischen Kapazitäten und Prozesse des Ursprungsgewebes weitestgehend erhalten. In der vorliegenden Arbeit lag der Fokus auf der Charakterisierung von VLGR1 am MAM-Komplex, welcher in Verbindung mit verschiedenen neurodegenerativen

Erkrankungen steht (Hedskog et al. 2013, Lewis et al. 2016). Hier ist es uns gelungen, eine effiziente Methode zu etablieren, welche uns ein robustes Modell in Form von isolierten Astrozyten für Untersuchung an Zellen des Nervensystems liefert. Astrozyten bilden den Hauptbestandteilen des aktiven Informations-transports im zentralen Nervensystem durch Interaktion mit Neuronen. Der Austausch und das Zusammenspiel zwischen Neuronen und Astrozyten von und über Botenstoffe und Signalmoleküle wie Ca^{2+} und Glutamat ist im ZNS für Funktion, Entwicklung und Pathologie des Gehirns von großer Bedeutung (Nimmerjahn et al. 2009, Benarroch 2005). Ausgehend von Vlgr1 defizienten und WT Mäusen, konnten wir für unsere Untersuchungen ein robustes *in vitro* Model gewinnen, welches uns erlaubt, physiologische Szenarien nahe den Bedingungen des Ursprungsgewebes zu simulieren.

3.3 VLGR1 am subzellulären MAM-Komplex

Der Fokus dieser Arbeit lag auf der Validierung und funktionellen Beschreibung des USH2C-Proteins VLGR1, an dem speziellen subzellulären Kompartiment zwischen ER und Mitochondrien, dem sogenannten MAM-Komplex. Wir haben VLGR1 als eine Komponente des MAM-Kompartiments identifiziert, einen dynamischen und spezialisierten Bereich zwischen den Membranen des ER und der Mitochondrien. Der MAM-Komplex stellt eine Plattform für verschiedene zelluläre Prozesse wie ER-Stress Antwort, Autophagie, Apoptose, und Ca^{2+}- Homöostase dar (Ilacqua et al. 2017). Hier konnten wir zeigen, dass VLGR1 als erster Vertreter der ADGR Familie ein Teil des MAM-Komplexes ist, an der Strukturbildung dieses Kompartiments mitwirkt und an der Regulation des Ca^{2+}-Austauschs zwischen ER und Mitochondrien an der MAM-Schnittstelle beteiligt ist.

3.3.1 VLGR1 interagiert mit MAM-Proteinen und ist an den Schnittstellen von ER und Mitochondrien lokalisiert

Nachdem wir mehrere MAM-Proteine als putative Interaktionspartner von VLGR1 mittels TAP-Analysen in Kombination mit LC-MS/MS identifiziert haben (**Publikation II**), konnten wir VLGR1 als Teil des MAM-Komplexes mit verschiedenen Ansätzen validieren. Wir konzentrierten uns insbesondere auf die VLGR1_CTF Domäne, da die in den TAP-Analyse identifizierten MAM-assoziierten Proteine für dieses VLGR1-Fragment am häufigsten gefunden wurden. Zudem stellt das CTF die bei der Signalübertragung relevante Struktur des Rezeptors dar, während das NTF mit der Adhäsionsfunktion des Rezeptors in Verbindung steht. Die Interaktion mit gut beschriebenen MAM-Schlüsselproteinen und Proteinen, die an der MAM-Funktion beteiligt sind, insbesondere mit S1R, ACSL4 und TOM20 (Lalier et al. 2021, Lewis et al. 2016, Smith et al. 2013, Wieckowski et al. 2009), wurde durch Trap®-Co-

Immunopräzipitationen und *in situ* PLA Daten validiert. Zusätzlich konnten wir zeigen, dass VLGR1 in biochemisch hoch aufgereinigten MAM-Fraktionen vorhanden ist. Schließlich liefert Lokalisierungsanalyse an der ER-Mitochondrien Schnittstelle starke Hinweise auf die Präsenz von VLGR1 im MAM-Kompartiment.

Neben den bekannten Funktionen des Rezeptors als Bestandteil des „ankle link complex" in der Cochlea und der Stereozilien Genese von Cochlea Haarsinneszellen (McGee et al. 2006, Yagi et al. 2007) fanden wir immer mehr Hinweise für die Beteiligung von VLGR1 an verschiedenen zellulären Prozessen (**Publikation II**). Kürzlich wurde VLGR1 als Regulator der Zellmigration an den „focal adhesions" beschrieben (Kusuluri et al. 2021). Bislang wurden nur ein G-Protein-gekoppelter Rezeptor, nämlich GPR37, und ein ADGR, LPHN3, durch Proteom Analysen als Bestandteil des MAM-Proteinnetzwerks bestätigt. Grundsätzlich ist anzumerken, dass die Proteom Analysen des MAM-Komplex eine große Diskrepanz bei den identifizierten Proteinen aufweisen. Es kann nicht ausgeschlossen werden, dass de facto MAM-Proteine in diesen Datensätzen nicht identifiziert werden (Ma et al. 2017). Nichtsdestotrotz untermauern unsere Ergebnisse die Daten und die Hypothese, dass VLGR1 an mehreren zellulären Funktionen neben den bekannten und beschriebenen beteiligt ist, speziell im MAM-Kompartiment.

3.3.2 VLGR1 Defizienz vergrößert den Abstand an der Schnittstelle zwischen ER und Mitochondrien und verändert die MAM-Komposition

Um den Einfluss oder die Beteiligung von VLGR1 am oder im MAM-Komplex zu untersuchen und zu beschreiben, war es entscheidend zu analysieren, ob VLGR1 in einer Beziehung zu den charakteristischsten Strukturparametern dieses Kompartiments steht. Einer dieser Parameter ist die Entfernung zwischen beiden Organellen an ihren Schnittstellen (Giacomello and Pellegrini 2016). Dafür untersuchten wir den Abstand zwischen der äußeren Mitochondrienmembran und der ER-Membran. Zusammen mit weiteren Parametern, wie der Oberfläche der Mitochondrien, die in Kontakt zum ER stehen und dem Mitochondrien Umfang, kann ein ER-Mitochondrien-Kontaktkoeffizient bestimmt werden, der als strukturelles Merkmal des MAM-Komplexes gilt und seine Funktion beeinflusst (Giacomello and Pellegrini 2016, Naon et al. 2016). Wir konnten zeigen, wie Vlgr1-Defizienz, insbesondere der Verlust des CTF in *Vlgr1*del7TM Mäusen, die gesamte MAM-Struktur im Kleinhirn verändert und den „Spalt" zwischen ER und Mitochondrium in der Retina vergrößert. Höchstwahrscheinlich ist VLGR1 allein nicht an der direkten Verbindung zwischen ER und Mitochondrien beteiligt, also an der Bildung von Adhäsionskomplexen zwischen den intrazellulären Membranen, wie es das Anker-Protein

Mitofusin 2 (MFN2) beschrieben ist (Larrea et al. 2019). Die kurze ICD von VLGR1 ist nicht lang genug, um die Distanz zwischen dem ER und den Mitochondrien zu überbrücken. Das sehr große extrazelluläre NTF wäre tatsächlich lang genug den Abstand beider Organellen im MAM-Komplex zu überbrücken, jedoch wird dieses Fragment in *Vlgr1*del7TM Mäusen immer noch exprimiert, und die Ausrichtung des Rezeptors ist mit der ICD in den zytosolischen Teil am ER gerichtet. Unsere Ergebnisse deuten eher darauf hin, dass VLGR1 mit Proteinen interagiert und Proteinkomplexe bildet, welche an der MAM-Zusammensetzung beteiligt sind und diese definieren. Veränderungen in der MAM-Struktur werden unter verschiedenen pathogenen Bedingungen und in neurodegenerativen Erkrankungen (Alzheimer, Parkinson, Epilepsie) beobachtet (Giacomello et al. 2013, Hedskog et al. 2013, Lewis et al. 2016). In unseren Untersuchungen haben wir uns auf die Regionen konzentriert, in denen die pathogenen VLGR1 Phänotypen (audiogen induzierte Anfälle und Retinadegeneration (USH)) höchstwahrscheinlich ihren Ursprung haben. Interessanterweise mehren sich in jüngsten Studien Hinweise darauf, dass Haploinsuffizienz von VLGR1 Epilepsie verursacht, wobei der zugrunde liegende Mechanismus unklar bleibt (Myers et al. 2018, Wang et al. 2015a). Unsere Beobachtung können zum Verständnis der molekularen Prozesse und ihrer lokalen Genese in der Zelle im Zusammenhang mit VLGR1-Fehlfunktionen beitragen.

3.3.3 VLGR1 beeinflusst den Ca^{2+}-Fluss zwischen ER und Mitochondrien

Wie beschrieben stellt der MAM-Komplex eine besondere Plattform für viele biologische Prozesse dar. Ca^{2+}-Homöostase ist einer der wichtigsten Prozesse, die an diesem Kompartiment zwischen ER und Mitochondrien stattfinden (Hirabayashi et al. 2017, Kuo et al. 2019). Der Ca^{2+}-Fluss zwischen ER und Mitochondrien wird durch Signalkaskaden und metabolische Prozesse reguliert (Kornmann 2013). Das ER fungiert hierbei als intrazellulärer Ca^{2+}-Speicher und der Ca^{2+}-Strom wird u. a. durch IP3R3 und VDAC vom ER zu den Mitochondrien am MAM-Komplex vermittelt. Dieser Ca^{2+}-Übergang zwischen diesen beiden Organellen ist unter VLGR1 Knockdown Bedingungen und in Vlgr1-defiziente Mausmodellen beeinträchtigt und der Ca^{2+}-Ausstrom aus dem ER im Vergleich zu WT Bedingungen reduziert. Der Inositol-1,4,5-Trisphosphat-Rezeptor (IP3R) ist ER resident und für den Ausfluss von Ca^{2+} aus dem ER verantwortlich. Die Aktivität des IP3R als Ca^{2+}-Kanal ist cAMP abhängig, da er von der cAMP regulierten Proteinkinase (PKA) phosphoryliert wird. Die Phosphorylierung verstärkt die durch IP3 evozierte Ca^{2+}-Freisetzung durch IP3R (Taylor 2017). VLGR1 interagiert mit mehreren Untereinheiten von heterotrimeren G-Proteinen. Interessanterweise interagiert VLGR1_CTF nur mit $G\alpha_i$ (Knapp et al. 2022) das den cAMP abhängigen Signalweg durch Hemmung der

Adenylylzyklase Aktivität reguliert. Dies führt zu einer verringerten cAMP-Produktion und zu einer verminderten cAMP abhängigen Proteinkinaseaktivität. Es ist spekulativ, aber naheliegend, dass VLGR1 die IP3R3-Aktivität durch G-Protein-Kopplung und den cAMP-Signalweg regulieren kann. Mit der verringerten Freisetzung von Ca^{2+} aus dem ER, geht auch eine reduzierte Ca^{2+}-Aufnahme in den Mitochondrien einher. Dies beeinträchtigt die Aktivität mitochondrialer Enzyme wie der Pyruvat-, Isocitrat- und α-Ketoglutarat-Dehydrogenasen und damit die Bioenergetik der Zellen (Denton et al. 1978, Cardenas et al. 2010). Diese Beobachtungen stehen im Einklang mit früheren Erkenntnissen, die darauf hindeuten, dass die Pathologie neurodegenerativer Dysfunktionen wie der Alzheimer-Krankheit und der Netzhautdegeneration von Auswirkungen auf die mitochondriale Energetik begleitet wird (Yao et al. 2009, Eckmiller 2003). Unsere Ergebnisse deuten darauf hin, dass VLGR1 wesentliche an der Modellierung am MAM-Komplex beteiligt ist und somit auch einen Einfluss auf den Ca^{2+}-Strom zwischen dem ER und Mitochondrien hat. Ebenso könnte VLGR1 als Regulator an der IP3R Aktivität durch cAMP- Signalweg beteiligt sein. Ob VLGR1 eine direkte Rolle bei Prozessen am MAM-Kompartiment spielt oder ob es als Modulator anderer Proteine in Proteinkomplexen fungiert, bedarf weiterer Untersuchungen.

4. Ausblick

Die Basis der vorliegenden Arbeit bilden affinity capture approaches mittels Affinity Proteomics. Interaktionsstudien zu ADGRs und im Speziellen zu VLGR1. Diese TAP-Daten, lieferten uns nach bioinformatischer Auswertung, Informationen zu möglichen Interaktionspartnern, sowie zu Integration in Proteinnetzwerke. Ausgehend von diesen Daten, ergaben sich Hinweise, dass VLGR1 in verschiedenen zellulären und molekularen Prozessen involviert ist. Im Fokus dieser Arbeit stand die Validierung und Charakterisierung von VLGR1 am subzellulären Kompartiment der Mitochondrien-assoziierten ER Membranen (MAMs). Es gelang die Interaktion von VLGR1 mit mehreren bekannten MAM-Proteinen zu validieren. Um ein umfassenderes Bild von VLGR1 in dem MAM-Proteinnetzwerk zu zeichnen, könnten die Interaktionsanalysen auf weitere bekannte MAM-Proteine ausgeweitet werden. Aus der Funktion dieser bereits gut charakterisierten MAM-Proteine, wie z. B. IP3R, VDAC oder GRP75 (Giacomello et al. 2013, Patron et al. 2014), könnten sich weitere Rückschlüsse auf die Rolle von VLGR1 an den MAMs ergeben. Für diese Interaktionsstudien könnten Konstrukte der zu untersuchenden Proteine sowie valide Antikörper generiert werden.

Die in dieser Arbeit gezeigten Lokalisations- und Zellfraktionierungsanalysen, deuten primär auf eine Lokalisation von VLGR1 am ER hin. Um diese Beobachtungen zu vertiefen, wäre eine Analyse mittels Elektronenmikroskopie mit Antikörpern gegen VLGR1 unter Fokussierung auf die Bereiche der Mitochondrien und ER Schnittstellen erforderlich. MAMs stellen eine sehr dynamische Form intrazellulärer Membran-Membran Kontakte dar (Ilacqua et al. 2017), was bedeutet, dass diese Verbindungen ständigen Bildungs- und Umbildungsprozessen unterliegen. Um die Beteiligung von VLGR1 an diesen Vorgängen zu untersuchen, könnten Beobachtungen aus der Live Cell Imaging Mikroskopie weitere Erkenntnisse liefern. Hierfür könnten geeignete VLGR1 sowie Mitochondrien und ER Marker eingesetzt werden und die Lokalisation von VLGR1 im Zuge der Dynamik zu untersuchen.

Neben der Validierung von VLGR1 als MAM-Protein, konnten wir zeigen, dass VLGR1-Defizienz zu morphologischen Veränderungen der MAM-Komposition führt. Da VLGR1 besonders in neuronalen Geweben exprimiert wird (McMillan and White 2004) und mit dem humanen Usher Syndrom sowie Epilepsie assoziiert ist (Reiners et al. 2006, Wang et al. 2005, McMillan and White 2010, Zhou et al. 2016), war es naheliegende zuerst Strukturen im Gehirn und der Retina zu untersuchen. Dysfunktionen der MAMs können jedoch weitreichendere Folgen in verschiedenen Organen haben, so könnten diese Studien auf andere Gewebe ausgedehnt werden, um auch dort mögliche VLGR1 bedingte Veränderungen zu untersuchen.

Ein weiterer Aspekt für zukünftige Arbeiten könnten Expressionsanalysen des MAM-Proteoms in WT und VLGR1-defizienten Proben sein. Dafür müsste eine Methode etabliert werden, die neben der qualitativen Aufreinigung des MAM-Komplexes auch quantitativ ausreichende Mengen an MAMs, für Expressionsanalysen liefert. Diese würden weitere Aufschlüsse erlauben, welche Rolle VLGR1 bei der Zusammensetzung der Proteinnetzwerke in den MAMs einnimmt. Hierbei ist auch darauf zu achten, dass die Szenarien je nach Zell- und Gewebetyp unterschiedlich sein können und einer differenzierten Analyse bedürfen.

Messungen des Ca^{2+}-Stroms zwischen dem ER und Mitochondrien bestätigten eine funktionelle Einbindung von VLGR1 an der Ca^{2+}-Homöostase zwischen diesen zwei Organellen, welche vorrangig an den MAMs stattfindet (Wang et al. 2015b). Neben der Ca^{2+}-Homöostase stellen MAMs auch eine kritische Plattform für andere wichtige biologische Prozesse wie Autophagie, Apoptose, Entzündungsregulation, ER-Stress Antwort oder den Lipid-Metabolismus dar (Ilacqua et al. 2017). Mögliche Funktion von VLGR1 in weiteren MAM-assoziierten Prozessen, speziell bei der Autophagie, werden zurzeit in unserer Arbeitsgruppe erforscht. Dabei werden in ersten Schritten die Expression von Autophagie-Markern in verschieden VLGR1-defizienten Modellen untersucht. Grundsätzlich stellen die Erkenntnisse aus der vorliegenden Arbeit solide und weitreichende Untersuchungen zu VLGR1 an den MAMs dar. Diese Ergebnisse dienen der Aufschlüsselung und dem Verständnis der Genese von pathologischen Auswirkungen von VLGR1-Dysfunktionen.

Durch die Einführung einer effizienten und robusten Methode zur Isolierung von primären Astrozyten aus Mausmodellen, konnten wir ein *in vitro* Modelle etablieren, welches uns die Untersuchungen an VLGR1-defizienten und WT Zellen ermöglichte. Für zukünftige Studien ist die Etablierung mehrere VLGR1 KO-Zelllinien von Bedeutung, da diese im Gegensatz zu primären Zelllinien länger und einfacher kultivierbar sind. Da unser Fokus auf neuronalen Gewebestrukturen lag waren und sind Astrozyten ein valides Modell, um die Untersuchungen jedoch zu erweitern und auf andere Gewebe zu übertragen, sollten weitere VLGR1 KO-Zelllinien generiert werden.

5. Zusammenfassung

Gegenstand der vorliegenden Arbeit war es die Präsenz des USH2C-Proteins VLGR1 in dem subzellulären Kompartiment der Mitochondrien-assoziierten ER-Membranen (MAMs) zu validieren und dessen Rolle bei der Funktion der MAMs aufzuklären. VLGR1 gehört zur Gruppe der Adhäsions-G-Protein gekoppelten Rezeptoren (aGPCRs oder ADGRs) und stellt innerhalb dieser Gruppe den größten Rezeptor dar. Funktionen von VLGR1 stehen in Verbindung zum humanen Usher-Syndrom (USH), der häufigsten Form kombinierter Taub-Blindheit. Zudem gibt es mehr und mehr Hinweise darauf, dass Dysfunktionen von VLGR1 beim Manschen auch zur Ausbildung von Epilepsie führen. Die Grundlage dieser Untersuchungen bilden die Identifikation von potenziellen VLGR1-Interaktionspartnern und dessen Einbindung in Proteinnetzwerke.

In den **Publikationen I und II** wurden Tandem-Affinitäts-Aufreinigungen (TAPs) mit verschieden Proteinfragmenten von VLGR1 durchgeführt. Daten aus diesen Analysen wurden auf Basis von Gene Ontology (GO) Termen bioinformatisch gegliedert und ausgewertet. Neben bekannten VLGR1-Proteininteraktionsclustern, welche bereits beschriebene Funktionen des Rezeptors bestätigten, konnten auch Proteine als putative Interaktionspartner identifiziert werden, die auf bislang nicht beschriebene Funktionen von VLGR1 hinweisen. Dazu zählen auch Proteine, die insbesondere in den internen Membranen der Zelle am ER, den Mitochondrien und speziell an Mitochondrien-ER-Kontakten (MAMs) lokalisiert sind.

Publikation III beschreibt die Einführung einer effizienten und robusten Methode zur Isolierung von primären Astrozyten aus dem Gehirn von Mausmodellen. Diese Arbeit lieferte ein robustes Zellmodel zum Studium von VLGR1 und eine der Grundlagen für unsere Untersuchungen.

In Publikation IV konnte ich die Interaktionen von VLGR1 mit den MAM-Proteinen S1R, ACSL4 und TOM20 bestätigt. Des Weiteren bestätigte ich mittels immunhistologischen sowie biochemischen Zellfraktionierungen VLGR1 im MAM-Kompartiment. Elektronenmikroskopische Analysen der MAM-Strukturen zeigten eine Veränderung der MAM-Komposition in Neuronen der Retina und des Gehirns des Vlgr1-defizienten *Vlgr1*/del7TM Mausmodell im Vergleich zu Wild-Type-Mäusen. Abschließend konnte ich mittels Ca^{2+}-Imaging unter Einsatz von ER- und Mitochondrien-spezifischen Ca^{2+}-Sensoren zeigen, dass VLGR1 essential für die Aufrechterhaltung der Ca^{2+}-Homöostase in den MAMs ist. Das Fehlen von VLGR1 führt in Vlgr1-defizienten primären Astrozyten aus dem Gehirn

von *Vlgr1*/delTM-Mäusen im Vergleich zur Wild-Type-Kontrolle zu einem verringerten Ca^{2+}-Ausstrom aus dem ER und nachfolgen auch zu einem geringeren Einstrom von Ca^{2+} in die Mitochondrien.

Zusammengefasst leisten die erarbeiteten Ergebnisse und die daraus gezogenen Erkenntnisse der vorliegenden Arbeit einen entscheidenden Beitrag zur Aufschlüsselung der molekularen und zellulären Funktion des Adhäsions-GPCR VLGR1/ADGRV1 und liefern zudem auch wertvolle Hinweise auf die Pathogenese bei VLGR1-Dysfunktionen. Insbesondere die Aufklärung von VLGR1 als MAM-Komponente, kann zum Verständnis der USH und Epilepsie zugrundeliegenden Pathomechanismen beitragen.

6. Summary

The subject of the present work was to validate the presence of the USH2C protein VLGR1 in the subcellular compartment of mitochondria-associated ER membranes (MAMs) and to elucidate its role in MAM function. VLGR1 belongs to the group of adhesion G-protein coupled receptors (aGPCRs or ADGRs) and represents the largest receptor within this group. Functions of VLGR1 are associated with human Usher syndrome (USH), the most common form of combined deaf-blindness and epilepsy. In addition, there is increasing evidence that dysfunctions of VLGR1 in humans also lead to the development of epilepsy. These studies are based on the identification of potential VLGR1 interaction partners and their involvement in protein networks.

In **publications I and II**, tandem affinity purifications (TAPs) were performed with different protein fragments of VLGR1. Data from these analyses were bioinformatically parsed and analyzed based on Gene Ontology (GO). In addition to known VLGR1 protein interaction clusters, which confirmed previously described functions of the receptor, proteins were also identified as putative interaction partners indicating not described functions of VLGR1. These include proteins localized specifically to the ER, mitochondria, and specifically mitochondria-ER contacts (MAMs).

Publication III describes the introduction of an efficient and robust method to isolate primary astrocytes from brain of mouse models. This work provided a robust cell model for studying VLGR1 and one of the bases for our studies.

In **publication IV**, I was able to confirm the interactions of VLGR1 with the MAM proteins S1R, ACSL4, and TOM20. Furthermore, I confirmed VLGR1 as a MAM resident by

immunohistochemical as well as biochemical cell fractionation. Electron microscopic analysis of MAM structures, revealed a change in MAM composition in neurons of the retina and brain of the Vlgr1-deficient *Vlgr1*/delTM mouse model compared with wild-type mice. In conclusion, I demonstrated by Ca^{2+} imaging using ER- and mitochondria-specific Ca^{2+} sensors that VLGR1 is essential for maintaining Ca^{2+} homeostasis at MAMs. Absence of VLGR1 results in reduced Ca^{2+} efflux from the ER in Vlgr1-deficient primary astrocytes from the brain of *Vlgr1*/delTM mice compared with wild-type controls and, subsequently, in reduced Ca^{2+} influx into mitochondria

In summary, the elaborated results and the findings derived from the present work make a critical contribution to the unraveling of the molecular and cellular function of the adhesion GPCR VLGR1/ADGRV1 and also provide valuable information to the pathogenesis in VLGR1 dysfunctions . In particular, the elucidation of VLGR1 as a MAM component may contribute to the understanding of the pathomechanism underlying USH and epilepsy.

7. Anhang

7.1 Referenzen

Adato, A., Michel, V., Kikkawa, Y., Reiners, J., Alagramam, K. N., Weil, D., Yonekawa, H., Wolfrum, U., El-Amraoui, A. & Petit, C. 2005. Interactions in the network of Usher syndrome type 1 proteins. *Hum Mol Genet,* 14**,** 347-56.

Annunziata, I., Sano, R. & D'azzo, A. 2018. Mitochondria-associated ER membranes (MAMs) and lysosomal storage diseases. *Cell Death Dis,* 9**,** 328.

Arac, D., Boucard, A. A., Bolliger, M. F., Nguyen, J., Soltis, S. M., Sudhof, T. C. & Brunger, A. T. 2012. A novel evolutionarily conserved domain of cell-adhesion GPCRs mediates autoproteolysis. *EMBO Journal,* 31**,** 1364-78.

Area-Gomez, E., De Groof, A. J., Boldogh, I., Bird, T. D., Gibson, G. E., Koehler, C. M., Yu, W. H., Duff, K. E., Yaffe, M. P., Pon, L. A. & Schon, E. A. 2009. Presenilins are enriched in endoplasmic reticulum membranes associated with mitochondria. *American Journal of Pathology,* 175**,** 1810-6.

Area-Gomez, E., Del Carmen Lara Castillo, M., Tambini, M. D., Guardia-Laguarta, C., De Groof, A. J., Madra, M., Ikenouchi, J., Umeda, M., Bird, T. D., Sturley, S. L. & Schon, E. A. 2012. Upregulated function of mitochondria-associated ER membranes in Alzheimer disease. *EMBO J,* 31**,** 4106-23.

Bassilana, F., Nash, M. & Ludwig, M. G. 2019. Adhesion G protein-coupled receptors: opportunities for drug discovery. *Nat Rev Drug Discov,* 18**,** 869-884.

Baud, V., Chissoe, S. L., Viegas-Pequignot, E., Diriong, S., N'guyen, V. C., Roe, B. A. & Lipinski, M. 1995. EMR1, an unusual member in the family of hormone receptors with seven transmembrane segments. *Genomics,* 26**,** 334-44.

Benarroch, E. E. 2005. Neuron-astrocyte interactions: partnership for normal function and disease in the central nervous system. *Mayo Clin Proc,* 80**,** 1326-38.

Boldt, K., Van Reeuwijk, J., Lu, Q., Koutroumpas, K., Nguyen, T. M., Texier, Y., Van Beersum, S. E., Horn, N., Willer, J. R., Mans, D. A., Dougherty, G., Lamers, I. J., Coene, K. L., Arts, H. H., Betts, M. J., Beyer, T., Bolat, E., Gloeckner, C. J., Haidari, K., Hetterschijt, L., Iaconis, D., Jenkins, D., Klose, F., Knapp, B., Latour, B., Letteboer, S. J., Marcelis, C. L., Mitic, D., Morleo, M., Oud, M. M., Riemersma, M., Rix, S., Terhal, P. A., Toedt, G., Van Dam, T. J., De Vrieze, E., Wissinger, Y., Wu, K. M., Apic, G., Beales, P. L., Blacque, O. E., Gibson, T. J., Huynen, M. A., Katsanis, N., Kremer, H., Omran, H., Van Wijk, E., Wolfrum, U., Kepes, F., Davis, E. E., Franco, B., Giles, R. H., Ueffing, M., Russell, R. B., Roepman, R. & Group, U. K. R. D. 2016. An organelle-specific protein landscape identifies novel diseases and molecular mechanisms. *Nat Commun,* 7**,** 11491.

Bonnet, C., Riahi, Z., Chantot-Bastaraud, S., Smagghe, L., Letexier, M., Marcaillou, C., Lefevre, G. M., Hardelin, J. P., El-Amraoui, A., Singh-Estivalet, A., Mohand-Said, S., Kohl, S., Kurtenbach, A., Sliesoraityte, I., Zobor, D., Gherbi, S., Testa, F., Simonelli, F., Banfi, S., Fakin, A., Glavac, D., Jarc-Vidmar, M., Zupan, A., Battelino, S., Martorell Sampol, L., Claveria, M. A., Catala Mora, J., Dad, S., Moller, L. B., Rodriguez Jorge, J., Hawlina, M., Auricchio, A., Sahel, J. A., Marlin, S., Zrenner, E., Audo, I. & Petit, C. 2016. An innovative strategy for the molecular diagnosis of Usher syndrome identifies causal biallelic mutations in 93% of European patients. *European Journal of Human Genetics,* 24**,** 1730-1738.

Boucard, A. A., Ko, J. & Sudhof, T. C. 2012. High affinity neurexin binding to cell adhesion G-protein-coupled receptor CIRL1/latrophilin-1 produces an intercellular adhesion complex. *Journal of Biological Chemistry,* 287**,** 9399-413.

Cardenas, C., Miller, R. A., Smith, I., Bui, T., Molgo, J., Muller, M., Vais, H., Cheung, K. H., Yang, J., Parker, I., Thompson, C. B., Birnbaum, M. J., Hallows, K. R. & Foskett, J. K. 2010. Essential regulation of cell bioenergetics by constitutive InsP3 receptor Ca2+ transfer to mitochondria. *Cell,* 142**,** 270-83.

Chauvet, V., Tian, X., Husson, H., Grimm, D. H., Wang, T., Hiesberger, T., Igarashi, P., Bennett, A. M., Ibraghimov-Beskrovnaya, O., Somlo, S. & Caplan, M. J. 2004. Mechanical stimuli induce cleavage and nuclear translocation of the polycystin-1 C terminus. *Journal of Clinical Investigation,* 114**,** 1433-43.

Chen, F., Hasegawa, H., Schmitt-Ulms, G., Kawarai, T., Bohm, C., Katayama, T., Gu, Y., Sanjo, N., Glista, M., Rogaeva, E., Wakutani, Y., Pardossi-Piquard, R., Ruan, X., Tandon, A., Checler, F., Marambaud, P., Hansen, K., Westaway, D., St George-Hyslop, P. & Fraser, P. 2006. TMP21 is a presenilin complex component that modulates gamma-secretase but not epsilon-secretase activity. *Nature,* 440**,** 1208-12.

Dahawi M., Elmagzoub M. S., Ahmed E. A., Baldassari S., Achaz G. 2021. Involvement of gene in familial forms of genetic generalized epilepsy. *Front. Neurol.* 12, 738272. 10.3389/fneur.2021.738272

De Mario, A., Quintana-Cabrera, R., Martinvalet, D. & Giacomello, M. 2017. (Neuro)degenerated Mitochondria-ER contacts. *Biochemical and Biophysical Research Communications,* 483**,** 1096-1109.

Demberg, L. M., Rothemund, S., Schoneberg, T. & Liebscher, I. 2015. Identification of the tethered peptide agonist of the adhesion G protein-coupled receptor GPR64/ADGRG2. *Biochemical and Biophysical Research Communications,* 464**,** 743-7.

Denton, R. M., Richards, D. A. & Chin, J. G. 1978. Calcium ions and the regulation of NAD+-linked isocitrate dehydrogenase from the mitochondria of rat heart and other tissues. *Biochem J,* 176**,** 899-906.

Duman, J. G., Tzeng, C. P., Tu, Y. K., Munjal, T., Schwechter, B., Ho, T. S. & Tolias, K. F. 2013. The adhesion-GPCR BAI1 regulates synaptogenesis by controlling the recruitment of the Par3/Tiam1 polarity complex to synaptic sites. *Journal of Neuroscience,* 33**,** 6964-78.

Ebermann, I., Wiesen, M. H., Zrenner, E., Lopez, I., Pigeon, R., Kohl, S., Lowenheim, H., Koenekoop, R. K. & Bolz, H. J. 2009. GPR98 mutations cause Usher syndrome type 2 in males. *J Med Genet,* 46**,** 277-80.

Eckmiller, M. S. 2003. Energy depletion hypothesis for retinitis pigmentosa. *Adv Exp Med Biol,* 533**,** 277-85.

Favara, D. M., Banham, A. H. & Harris, A. L. 2014. A review of ELTD1, a pro-angiogenic adhesion GPCR. *Biochemical Society Transactions,* 42**,** 1658-64.

Gether, U. & Kobilka, B. K. 1998. G protein-coupled receptors. II. Mechanism of agonist activation. *Journal of Biological Chemistry,* 273**,** 17979-82.

Giacomello, M., Oliveros, J. C., Naranjo, J. R. & Carafoli, E. 2013. Neuronal Ca(2+) dyshomeostasis in Huntington disease. *Prion,* 7**,** 76-84.

Giacomello, M. & Pellegrini, L. 2016. The coming of age of the mitochondria-ER contact: a matter of thickness. *Cell Death Differ,* 23**,** 1417-27.

Gloeckner, C. J., Boldt, K., Schumacher, A., Roepman, R. & Ueffing, M. 2007. A novel tandem affinity purification strategy for the efficient isolation and characterisation of native protein complexes. *Proteomics,* 7**,** 4228-34.

Haapasalo, A. & Kovacs, D. M. 2011. The many substrates of presenilin/gamma-secretase. *J Alzheimers Dis,* 25**,** 3-28.

Hamann, J., Aust, G., Arac, D., Engel, F. B., Formstone, C., Fredriksson, R., Hall, R. A., Harty, B. L., Kirchhoff, C., Knapp, B., Krishnan, A., Liebscher, I., Lin, H. H., Martinelli, D. C., Monk, K. R., Peeters, M. C., Piao, X., Promel, S., Schoneberg, T., Schwartz, T. W., Singer, K., Stacey, M., Ushkaryov, Y. A., Vallon, M., Wolfrum, U., Wright, M. W., Xu, L., Langenhan, T. & Schioth, H. B. 2015. International Union of Basic and Clinical Pharmacology. XCIV. Adhesion G protein-coupled receptors. *Pharmacological Reviews,* 67**,** 338-67.

Hamann, J. & Petrenko, A. G. 2016. Introduction: History of the Adhesion GPCR Field. *Handb Exp Pharmacol,* 234**,** 1-11.

Hamasaki, M., Furuta, N., Matsuda, A., Nezu, A., Yamamoto, A., Fujita, N., Oomori, H., Noda, T., Haraguchi, T., Hiraoka, Y., Amano, A. & Yoshimori, T. 2013. Autophagosomes form at ER-mitochondria contact sites. *Nature,* 495**,** 389-93.

Hamm, H. E. 1998. The many faces of G protein signaling. *Journal of Biological Chemistry,* 273**,** 669-72.

Han J. Y., Lee H. J., Lee Y.-M., Park J. 2020. Identification of missense mutation as a candidate genetic cause of familial febrile seizure 4. *Children* (Basel, Switzerland) 7, 144. 10.3390/children7090144

Hayashi, T. & Fujimoto, M. 2010. Detergent-resistant microdomains determine the localization of sigma-1 receptors to the endoplasmic reticulum-mitochondria junction. *Mol Pharmacol,* 77**,** 517-28.

Hayashi, T. & Su, T. P. 2007. Sigma-1 receptor chaperones at the ER-mitochondrion interface regulate Ca(2+) signaling and cell survival. *Cell,* 131**,** 596-610.

Hedskog, L., Pinho, C. M., Filadi, R., Ronnback, A., Hertwig, L., Wiehager, B., Larssen, P., Gellhaar, S., Sandebring, A., Westerlund, M., Graff, C., Winblad, B., Galter, D., Behbahani, H., Pizzo, P., Glaser, E. & Ankarcrona, M. 2013. Modulation of the endoplasmic reticulum-mitochondria interface in Alzheimer's disease and related models. *Proceedings of the National Academy of Sciences of the United States of America,* 110**,** 7916-21.

Hirabayashi, Y., Kwon, S. K., Paek, H., Pernice, W. M., Paul, M. A., Lee, J., Erfani, P., Raczkowski, A., Petrey, D. S., Pon, L. A. & Polleux, F. 2017. ER-mitochondria tethering by PDZD8 regulates Ca(2+) dynamics in mammalian neurons. *Science,* 358**,** 623-630.

Hope, C. I., Bundey, S., Proops, D. & Fielder, A. R. 1997. Usher syndrome in the city of Birmingham--prevalence and clinical classification. *British Journal of Ophthalmology,* 81**,** 46-53.

Hu, Q. X., Dong, J. H., Du, H. B., Zhang, D. L., Ren, H. Z., Ma, M. L., Cai, Y., Zhao, T. C., Yin, X. L., Yu, X., Xue, T., Xu, Z. G. & Sun, J. P. 2014. Constitutive Galphai coupling activity of very large G protein-coupled receptor 1 (VLGR1) and its regulation by PDZD7 protein. *Journal of Biological Chemistry,* 289**,** 24215-25.

Ilacqua, N., Sanchez-Alvarez, M., Bachmann, M., Costiniti, V., Del Pozo, M. A. & Giacomello, M. 2017. Protein Localization at Mitochondria-ER Contact Sites in Basal and Stress Conditions. *Front Cell Dev Biol,* 5**,** 107.

Ji, T. H., Grossmann, M. & Ji, I. 1998. G protein-coupled receptors. I. Diversity of receptor-ligand interactions. *Journal of Biological Chemistry,* 273**,** 17299-302.

Karpus, O. N., Veninga, H., Hoek, R. M., Flierman, D., Van Buul, J. D., Vandenakker, C. C., Vanbavel, E., Medof, M. E., Van Lier, R. A., Reedquist, K. A. & Hamann, J. 2013. Shear stress-dependent downregulation of the adhesion-G protein-coupled receptor CD97 on circulating leukocytes upon contact with its ligand CD55. *Journal of Immunology,* 190**,** 3740-8.

Kimberling, W. J., Hildebrand, M. S., Shearer, A. E., Jensen, M. L., Halder, J. A., Trzupek, K., Cohn, E. S., Weleber, R. G., Stone, E. M. & Smith, R. J. 2010. Frequency of Usher

syndrome in two pediatric populations: Implications for genetic screening of deaf and hard of hearing children. *Genetics in Medicine,* 12**,** 512-6.

Kimberling, W. J. & Moller, C. 1995. Clinical and molecular genetics of Usher syndrome. *J Am Acad Audiol,* 6**,** 63-72.

Knapp, B., Roedig, J., Boldt, K., Krzysko, J., Horn, N., Ueffing, M. & Wolfrum, U. 2019. Affinity proteomics identifies novel functional modules related to adhesion GPCRs. *Ann N Y Acad Sci,* 1456**,** 144-167.

Knapp, B., Roedig, J., Roedig, H., Krzysko, J., Horn, N., Guler, B. E., Kusuluri, D. K., Yildirim, A., Boldt, K., Ueffing, M., Liebscher, I. & Wolfrum, U. 2022. Affinity Proteomics Identifies Interaction Partners and Defines Novel Insights into the Function of the Adhesion GPCR VLGR1/ADGRV1. *Molecules,* 27.

Knapp, B. & Wolfrum, U. 2016. Adhesion GPCR-Related Protein Networks. *Handb Exp Pharmacol,* 234**,** 147-178.

Kornmann, B. 2013. The molecular hug between the ER and the mitochondria. *Curr Opin Cell Biol,* 25**,** 443-8.

Kreienkamp, H. J., Zitzer, H., Gundelfinger, E. D., Richter, D. & Bockers, T. M. 2000. The calcium-independent receptor for alpha-latrotoxin from human and rodent brains interacts with members of the ProSAP/SSTRIP/Shank family of multidomain proteins. *Journal of Biological Chemistry,* 275**,** 32387-90.

Kuo, I. Y., Brill, A. L., Lemos, F. O., Jiang, J. Y., Falcone, J. L., Kimmerling, E. P., Cai, Y., Dong, K., Kaplan, D. L., Wallace, D. P., Hofer, A. M. & Ehrlich, B. E. 2019. Polycystin 2 regulates mitochondrial Ca(2+) signaling, bioenergetics, and dynamics through mitofusin 2. *Sci Signal,* 12.

Kusuluri, D. K., Guler, B. E., Knapp, B., Horn, N., Boldt, K., Ueffing, M., Aust, G. & Wolfrum, U. 2021. Adhesion G protein-coupled receptor VLGR1/ADGRV1 regulates cell spreading and migration by mechanosensing at focal adhesions. *iScience,* 24**,** 102283.

Lalier, L., Mignard, V., Joalland, M. P., Lanoe, D., Cartron, P. F., Manon, S. & Vallette, F. M. 2021. TOM20-mediated transfer of Bcl2 from ER to MAM and mitochondria upon induction of apoptosis. *Cell Death Dis,* 12**,** 182.

Langenhan, T. 2020. Adhesion G protein-coupled receptors-Candidate metabotropic mechanosensors and novel drug targets. *Basic Clin Pharmacol Toxicol,* 126 Suppl 6**,** 5-16.

Langenhan, T., Piao, X. & Monk, K. R. 2016. Adhesion G protein-coupled receptors in nervous system development and disease. *Nature Reviews: Neuroscience,* 17**,** 550-61.

Larrea, D., Pera, M., Gonnelli, A., Quintana-Cabrera, R., Akman, H. O., Guardia-Laguarta, C., Velasco, K. R., Area-Gomez, E., Dal Bello, F., De Stefani, D., Horvath, R., Shy, M. E., Schon, E. A. & Giacomello, M. 2019. MFN2 mutations in Charcot-Marie-Tooth disease alter mitochondria-associated ER membrane function but do not impair bioenergetics. *Hum Mol Genet,* 28**,** 1782-1800.

Leal, N. S., Schreiner, B., Pinho, C. M., Filadi, R., Wiehager, B., Karlstrom, H., Pizzo, P. & Ankarcrona, M. 2016. Mitofusin-2 knockdown increases ER-mitochondria contact and decreases amyloid beta-peptide production. *Journal of Cellular and Molecular Medicine,* 20**,** 1686-95.

Lee, K. S., Huh, S., Lee, S., Wu, Z., Kim, A. K., Kang, H. Y. & Lu, B. 2018. Altered ER-mitochondria contact impacts mitochondria calcium homeostasis and contributes to neurodegeneration in vivo in disease models. *Proc Natl Acad Sci U S A,* 115**,** E8844-E8853.

Lewis, A., Tsai, S. Y. & Su, T. P. 2016. Detection of Isolated Mitochondria-Associated ER Membranes Using the Sigma-1 Receptor. *Methods Mol Biol,* 1376**,** 133-40.

Liebscher, I., Schon, J., Petersen, S. C., Fischer, L., Auerbach, N., Demberg, L. M., Mogha, A., Coster, M., Simon, K. U., Rothemund, S., Monk, K. R. & Schoneberg, T. 2014. A tethered agonist within the ectodomain activates the adhesion G protein-coupled receptors GPR126 and GPR133. *Cell Rep, 9,* 2018-26.

Lin, H. H., Stacey, M., Yona, S. & Chang, G. W. 2010. GPS proteolytic cleavage of adhesion-GPCRs. *Advances in Experimental Medicine and Biology, 706,* 49-58.

Lingwood, D. & Simons, K. 2010. Lipid rafts as a membrane-organizing principle. *Science, 327,* 46-50.

Liu Z., Ye X., Zhang J., Wu B., Dong S., Gao P. 2022. Biallelic ADGRV1 variants are associated with Rolandic epilepsy. *Neurol. Sci.* 43, 1365–1374. 10.1007/s10072-021-05403-y

Low, S. H., Vasanth, S., Larson, C. H., Mukherjee, S., Sharma, N., Kinter, M. T., Kane, M. E., Obara, T. & Weimbs, T. 2006. Polycystin-1, STAT6, and P100 function in a pathway that transduces ciliary mechanosensation and is activated in polycystic kidney disease. *Developmental Cell, 10,* 57-69.

Luo, R., Jeong, S. J., Jin, Z., Strokes, N., Li, S. & Piao, X. 2011. G protein-coupled receptor 56 and collagen III, a receptor-ligand pair, regulates cortical development and lamination. *Proceedings of the National Academy of Sciences of the United States of America, 108,* 12925-30.

Ma, J. H., Shen, S., Wang, J. J., He, Z., Poon, A., Li, J., Qu, J. & Zhang, S. X. 2017. Comparative Proteomic Analysis of the Mitochondria-associated ER Membrane (MAM) in a Long-term Type 2 Diabetic Rodent Model. *Sci Rep, 7,* 2062.

Maerker, T., Van Wijk, E., Overlack, N., Kersten, F. F., Mcgee, J., Goldmann, T., Sehn, E., Roepman, R., Walsh, E. J., Kremer, H. & Wolfrum, U. 2008. A novel Usher protein network at the periciliary reloading point between molecular transport machineries in vertebrate photoreceptor cells. *Human Molecular Genetics, 17,* 71-86.

Makkerh, J. P., Dingwall, C. & Laskey, R. A. 1996. Comparative mutagenesis of nuclear localization signals reveals the importance of neutral and acidic amino acids. *Curr Biol, 6,* 1025-7.

Mcgee, J., Goodyear, R. J., Mcmillan, D. R., Stauffer, E. A., Holt, J. R., Locke, K. G., Birch, D. G., Legan, P. K., White, P. C., Walsh, E. J. & Richardson, G. P. 2006. The very large G-protein-coupled receptor VLGR1: a component of the ankle link complex required for the normal development of auditory hair bundles. *Journal of Neuroscience, 26,* 6543-53.

Mcmillan, D. R., Kayes-Wandover, K. M., Richardson, J. A. & White, P. C. 2002. Very large G protein-coupled receptor-1, the largest known cell surface protein, is highly expressed in the developing central nervous system. *The Journal of biological chemistry, 277,* 785-792.

Mcmillan, D. R. & White, P. C. 2004. Loss of the transmembrane and cytoplasmic domains of the very large G-protein-coupled receptor-1 (VLGR1 or Mass1) causes audiogenic seizures in mice. *Mol Cell Neurosci, 26,* 322-9.

Mcmillan, D. R. & White, P. C. 2010. STUDIES ON THE VERY LARGE G PROTEIN-COUPLED RECEPTOR: From Initial Discovery to Determining its Role in Sensorineural Deafness in Higher Animals. *Adhesion-Gpcrs: Structure to Function, 706,* 76-86.

Merrick, D., Chapin, H., Baggs, J. E., Yu, Z., Somlo, S., Sun, Z., Hogenesch, J. B. & Caplan, M. J. 2012. The gamma-secretase cleavage product of polycystin-1 regulates TCF and CHOP-mediated transcriptional activation through a p300-dependent mechanism. *Developmental Cell, 22,* 197-210.

Myers K. A., Nasioulas S., Boys A., McMahon J. M., Slater H., Lockhart P. 2018. ADGRV1 is implicated in myoclonic epilepsy. *Epilepsia* 59, 381–388. 10.1111/epi.13980

Michalski, N., Michel, V., Bahloul, A., Lefevre, G., Barral, J., Yagi, H., Chardenoux, S., Weil, D., Martin, P., Hardelin, J. P., Sato, M. & Petit, C. 2007. Molecular characterization of the ankle-link complex in cochlear hair cells and its role in the hair bundle functioning. *Journal of Neuroscience,* 27**,** 6478-88.

Millan, J. M., Aller, E., Jaijo, T., Blanco-Kelly, F., Gimenez-Pardo, A. & Ayuso, C. 2011. An update on the genetics of usher syndrome. *J Ophthalmol,* 2011**,** 417217.

Moliaka, Y. K., Grigorenko, A., Madera, D. & Rogaev, E. I. 2004. Impas 1 possesses endoproteolytic activity against multipass membrane protein substrate cleaving the presenilin 1 holoprotein. *FEBS Letters,* 557**,** 185-92.

Monnet, F. P. 2005. Sigma-1 receptor as regulator of neuronal intracellular Ca2+: clinical and therapeutic relevance. *Biol Cell,* 97**,** 873-83.

Myers, K. A., Nasioulas, S., Boys, A., Mcmahon, J. M., Slater, H., Lockhart, P., Sart, D. D. & Scheffer, I. E. 2018. ADGRV1 is implicated in myoclonic epilepsy. *Epilepsia,* 59**,** 381-388.

Nakayama, J., Fu, Y. H., Clark, A. M., Nakahara, S., Hamano, K., Iwasaki, N., Matsui, A., Arinami, T. & Ptacek, L. J. 2002. A nonsense mutation of the MASS1 gene in a family with febrile and afebrile seizures. *Annals of Neurology,* 52**,** 654-7.

Naon, D., Zaninello, M., Giacomello, M., Varanita, T., Grespi, F., Lakshminaranayan, S., Serafini, A., Semenzato, M., Herkenne, S., Hernandez-Alvarez, M. I., Zorzano, A., De Stefani, D., Dorn, G. W., 2nd & Scorrano, L. 2016. Critical reappraisal confirms that Mitofusin 2 is an endoplasmic reticulum-mitochondria tether. *Proc Natl Acad Sci U S A,* 113**,** 11249-11254.

Nikkila, H., Mcmillan, D. R., Nunez, B. S., Pascoe, L., Curnow, K. M. & White, P. C. 2000. Sequence similarities between a novel putative G protein-coupled receptor and Na+/Ca2+ exchangers define a cation binding domain. *Molecular Endocrinology,* 14**,** 1351-64.

Nimmerjahn, A., Mukamel, E. A. & Schnitzer, M. J. 2009. Motor behavior activates Bergmann glial networks. *Neuron,* 62**,** 400-12.

O'brien, R. J. & Wong, P. C. 2011. Amyloid precursor protein processing and Alzheimer's disease. *Annual Review of Neuroscience,* 34**,** 185-204.

Okajima, D., Kudo, G. & Yokota, H. 2010. Brain-specific angiogenesis inhibitor 2 (BAI2) may be activated by proteolytic processing. *Journal of Receptor and Signal Transduction Research,* 30**,** 143-53.

Paavola, K. J., Stephenson, J. R., Ritter, S. L., Alter, S. P. & Hall, R. A. 2011. The N terminus of the adhesion G protein-coupled receptor GPR56 controls receptor signaling activity. *Journal of Biological Chemistry,* 286**,** 28914-21.

Pakarinen, L., Karjalainen, S., Simola, K. O., Laippala, P. & Kaitalo, H. 1995. Usher's syndrome type 3 in Finland. *Laryngoscope,* 105**,** 613-7.

Patra, C., Van Amerongen, M. J., Ghosh, S., Ricciardi, F., Sajjad, A., Novoyatleva, T., Mogha, A., Monk, K. R., Muhlfeld, C. & Engel, F. B. 2013. Organ-specific function of adhesion G protein-coupled receptor GPR126 is domain-dependent. *Proceedings of the National Academy of Sciences of the United States of America,* 110**,** 16898-903.

Patron, M., Checchetto, V., Raffaello, A., Teardo, E., Vecellio Reane, D., Mantoan, M., Granatiero, V., Szabo, I., De Stefani, D. & Rizzuto, R. 2014. MICU1 and MICU2 finely tune the mitochondrial Ca2+ uniporter by exerting opposite effects on MCU activity. *Mol Cell,* 53**,** 726-37.

Paupe, V. & Prudent, J. 2018. New insights into the role of mitochondrial calcium homeostasis in cell migration. *Biochem Biophys Res Commun,* 500**,** 75-86.

Petit, C. 2001. Usher syndrome: from genetics to pathogenesis. *Annu Rev Genomics Hum Genet,* 2**,** 271-97.

Pimplikar, S. W. 2009. Reassessing the amyloid cascade hypothesis of Alzheimer's disease. *Int J Biochem Cell Biol,* 41**,** 1261-8.

Pinho, C. M., Teixeira, P. F. & Glaser, E. 2014. Mitochondrial import and degradation of amyloid-beta peptide. *Biochimica et Biophysica Acta,* 1837**,** 1069-74.

Potter, P. K., Bowl, M. R., Jeyarajan, P., Wisby, L., Blease, A., Goldsworthy, M. E., Simon, M. M., Greenaway, S., Michel, V., Barnard, A., Aguilar, C., Agnew, T., Banks, G., Blake, A., Chessum, L., Dorning, J., Falcone, S., Goosey, L., Harris, S., Haynes, A., Heise, I., Hillier, R., Hough, T., Hoslin, A., Hutchison, M., King, R., Kumar, S., Lad, H. V., Law, G., Maclaren, R. E., Morse, S., Nicol, T., Parker, A., Pickford, K., Sethi, S., Starbuck, B., Stelma, F., Cheeseman, M., Cross, S. H., Foster, R. G., Jackson, I. J., Peirson, S. N., Thakker, R. V., Vincent, T., Scudamore, C., Wells, S., El-Amraoui, A., Petit, C., Acevedo-Arozena, A., Nolan, P. M., Cox, R., Mallon, A. M. & Brown, S. D. 2016. Novel gene function revealed by mouse mutagenesis screens for models of age-related disease. *Nat Commun,* 7**,** 12444.

Promel, S., Waller-Evans, H., Dixon, J., Zahn, D., Colledge, W. H., Doran, J., Carlton, M. B., Grosse, J., Schoneberg, T., Russ, A. P. & Langenhan, T. 2012. Characterization and functional study of a cluster of four highly conserved orphan adhesion-GPCR in mouse. *Dev Dyn,* 241**,** 1591-602.

Qian, F., Boletta, A., Bhunia, A. K., Xu, H., Liu, L., Ahrabi, A. K., Watnick, T. J., Zhou, F. & Germino, G. G. 2002. Cleavage of polycystin-1 requires the receptor for egg jelly domain and is disrupted by human autosomal-dominant polycystic kidney disease 1-associated mutations. *Proceedings of the National Academy of Sciences of the United States of America,* 99**,** 16981-6.

Rahman, M. A., Ashton, A. C., Meunier, F. A., Davletov, B. A., Dolly, J. O. & Ushkaryov, Y. A. 1999. Norepinephrine exocytosis stimulated by alpha-latrotoxin requires both external and stored Ca2+ and is mediated by latrophilin, G proteins and phospholipase C. *Philosophical Transactions of the Royal Society of London B Biological Sciences,* 354**,** 379-86.

Reiners, J., Nagel-Wolfrum, K., Jurgens, K., Marker, T. & Wolfrum, U. 2006. Molecular basis of human Usher syndrome: deciphering the meshes of the Usher protein network provides insights into the pathomechanisms of the Usher disease. *Experimental Eye Research,* 83**,** 97-119.

Reiners, J., Van Wijk, E., Marker, T., Zimmermann, U., Jurgens, K., Te Brinke, H., Overlack, N., Roepman, R., Knipper, M., Kremer, H. & Wolfrum, U. 2005. Scaffold protein harmonin (USH1C) provides molecular links between Usher syndrome type 1 and type 2. *Human Molecular Genetics,* 14**,** 3933-43.

Rosenbaum, D. M., Rasmussen, S. G. & Kobilka, B. K. 2009. The structure and function of G-protein-coupled receptors. *Nature,* 459**,** 356-63.

Sando, R., Bushong, E., Zhu, Y., Huang, M., Considine, C., Phan, S., Ju, S., Uytiepo, M., Ellisman, M. & Maximov, A. 2017. Assembly of Excitatory Synapses in the Absence of Glutamatergic Neurotransmission. *Neuron,* 94**,** 312-321 e3.

Scholz, N., Gehring, J., Guan, C., Ljaschenko, D., Fischer, R., Lakshmanan, V., Kittel, R. J. & Langenhan, T. 2015. The adhesion GPCR latrophilin/CIRL shapes mechanosensation. *Cell Rep,* 11**,** 866-874.

Scholz, N., Monk, K. R., Kittel, R. J. & Langenhan, T. 2016. Adhesion GPCRs as a Putative Class of Metabotropic Mechanosensors. *Handb Exp Pharmacol,* 234**,** 221-247.

Schon, E. A. & Area-Gomez, E. 2013. Mitochondria-associated ER membranes in Alzheimer disease. *Molecular and Cellular Neurosciences,* 55**,** 26-36.

Schreiner, B., Hedskog, L., Wiehager, B. & Ankarcrona, M. 2015. Amyloid-beta peptides are generated in mitochondria-associated endoplasmic reticulum membranes. *J Alzheimers Dis,* 43**,** 369-74.

Shin, D., Lin, S. T., Fu, Y. H. & Ptacek, L. J. 2013. Very large G protein-coupled receptor 1 regulates myelin-associated glycoprotein via Galphas/Galphaq-mediated protein kinases A/C. *Proceedings of the National Academy of Sciences of the United States of America,* 110**,** 19101-6.

Silva, J. P., Lelianova, V. G., Ermolyuk, Y. S., Vysokov, N., Hitchen, P. G., Berninghausen, O., Rahman, M. A., Zangrandi, A., Fidalgo, S., Tonevitsky, A. G., Dell, A., Volynski, K. E. & Ushkaryov, Y. A. 2011. Latrophilin 1 and its endogenous ligand Lasso/teneurin-2 form a high-affinity transsynaptic receptor pair with signaling capabilities. *Proceedings of the National Academy of Sciences of the United States of America,* 108**,** 12113-8.

Simons, K. & Vaz, W. L. 2004. Model systems, lipid rafts, and cell membranes. *Annu Rev Biophys Biomol Struct,* 33**,** 269-95.

Skradski, S. L., Clark, A. M., Jiang, H., White, H. S., Fu, Y. H. & Ptacek, L. J. 2001. A novel gene causing a mendelian audiogenic mouse epilepsy. *Neuron,* 31**,** 537-44.

Smith, M. E., Saraceno, G. E., Capani, F. & Castilla, R. 2013. Long-chain acyl-CoA synthetase 4 is regulated by phosphorylation. *Biochem Biophys Res Commun,* 430**,** 272-7.

Specht, D., Wu, S. B., Turner, P., Dearden, P., Koentgen, F., Wolfrum, U., Maw, M., Brandstatter, J. H. & Tom Dieck, S. 2009. Effects of presynaptic mutations on a postsynaptic Cacna1s calcium channel colocalized with mGluR6 at mouse photoreceptor ribbon synapses. *Investigative Ophthalmology and Visual Science,* 50**,** 505-15.

Stephenson, J. R., Paavola, K. J., Schaefer, S. A., Kaur, B., Van Meir, E. G. & Hall, R. A. 2013. Brain-specific angiogenesis inhibitor-1 signaling, regulation, and enrichment in the postsynaptic density. *Journal of Biological Chemistry,* 288**,** 22248-56.

Stephenson, J. R., Purcell, R. H. & Hall, R. A. 2014. The BAI subfamily of adhesion GPCRs: synaptic regulation and beyond. *Trends in Pharmacological Sciences,* 35**,** 208-15.

Stoveken, H. M., Hajduczok, A. G., Xu, L. & Tall, G. G. 2015. Adhesion G protein-coupled receptors are activated by exposure of a cryptic tethered agonist. *Proceedings of the National Academy of Sciences of America,* 112**,** 6194-9.

Suh, Y. H., Terashima, A., Petralia, R. S., Wenthold, R. J., Isaac, J. T., Roche, K. W. & Roche, P. A. 2010. A neuronal role for SNAP-23 in postsynaptic glutamate receptor trafficking. *Nature Neuroscience,* 13**,** 338-43.

Taylor, C. W. 2017. Regulation of IP3 receptors by cyclic AMP. *Cell Calcium,* 63**,** 48-52.

Tobaben, S., Sudhof, T. C. & Stahl, B. 2000. The G protein-coupled receptor CL1 interacts directly with proteins of the Shank family. *Journal of Biological Chemistry,* 275**,** 36204-10.

Urano, T., Shiraki, M., Yagi, H., Ito, M., Sasaki, N., Sato, M., Ouchi, Y. & Inoue, S. 2012. GPR98/Gpr98 gene is involved in the regulation of human and mouse bone mineral density. *Journal of Clinical Endocrinology and Metabolism,* 97**,** E565-74.

Van Wijk, E., Van Der Zwaag, B., Peters, T., Zimmermann, U., Te Brinke, H., Kersten, F. F., Marker, T., Aller, E., Hoefsloot, L. H., Cremers, C. W., Cremers, F. P., Wolfrum, U., Knipper, M., Roepman, R. & Kremer, H. 2006. The DFNB31 gene product whirlin connects to the Usher protein network in the cochlea and retina by direct association with USH2A and VLGR1. *Human Molecular Genetics,* 15**,** 751-65.

Vance, J. E. 2014. MAM (mitochondria-associated membranes) in mammalian cells: lipids and beyond. *Biochimica et Biophysica Acta,* 1841**,** 595-609.

Wang, J., Zhong, J., Chen, G., Li, M., Wu, F. X. & Pan, Y. 2015a. ClusterViz: A Cytoscape APP for Cluster Analysis of Biological Network. *IEEE/ACM Trans Comput Biol Bioinform,* 12**,** 815-22.

Wang, T., Ward, Y., Tian, L., Lake, R., Guedez, L., Stetler-Stevenson, W. G. & Kelly, K. 2005. CD97, an adhesion receptor on inflammatory cells, stimulates angiogenesis through binding integrin counterreceptors on endothelial cells. *Blood,* 105**,** 2836-44.

Wang, Y., Fan, X., Zhang, W., Zhang, C., Wang, J., Jiang, T. & Wang, L. 2015b. Deficiency of very large G-protein-coupled receptor-1 is a risk factor of tumor-related epilepsy: a whole transcriptome sequencing analysis. *Journal of Neuro-Oncology,* 121**,** 609-16.

Ward, Y., Lake, R., Yin, J. J., Heger, C. D., Raffeld, M., Goldsmith, P. K., Merino, M. & Kelly, K. 2011. LPA receptor heterodimerizes with CD97 to amplify LPA-initiated RHO-dependent signaling and invasion in prostate cancer cells. *Cancer Research,* 71**,** 7301-11.

Washbourne, P., Liu, X. B., Jones, E. G. & Mcallister, A. K. 2004. Cycling of NMDA receptors during trafficking in neurons before synapse formation. *Journal of Neuroscience,* 24**,** 8253-64.

Wieckowski, M. R., Giorgi, C., Lebiedzinska, M., Duszynski, J. & Pinton, P. 2009. Isolation of mitochondria-associated membranes and mitochondria from animal tissues and cells. *Nat Protoc,* 4**,** 1582-90.

Wilde, C., Fischer, L., Lede, V., Kirchberger, J., Rothemund, S., Schoneberg, T. & Liebscher, I. 2016. The constitutive activity of the adhesion GPCR GPR114/ADGRG5 is mediated by its tethered agonist. *FASEB Journal,* 30**,** 666-73.

Wolfrum, U. 2011. Protein networks related to the Usher syndrome gain insights in the molecular basis of the disease. *In:* SATPAL, A. (ed.) *Usher Syndrome: Pathogenesis, Diagnosis and Therapy.* . Nova Science Publishers.

Wu, H., Reissner, C., Kuhlendahl, S., Coblentz, B., Reuver, S., Kindler, S., Gundelfinger, E. D. & Garner, C. C. 2000. Intramolecular interactions regulate SAP97 binding to GKAP. *EMBO Journal,* 19**,** 5740-51.

Yagi, H., Noguchi, Y., Kitamura, K. & Sato, M. 2009. Deficiency of Vlgr1 resulted in deafness and susceptibility to audiogenic seizures while the degree of hearing impairment was not correlated with seizure severity in C57BL/6- and 129-backcrossed lines of Vlgr1 knockout mice. *Neuroscience Letters,* 461**,** 190-5.

Yagi, H., Takamura, Y., Yoneda, T., Konno, D., Akagi, Y., Yoshida, K. & Sato, M. 2005. Vlgr1 knockout mice show audiogenic seizure susceptibility. *Journal of Neurochemistry,* 92**,** 191-202.

Yagi, H., Tokano, H., Maeda, M., Takabayashi, T., Nagano, T., Kiyama, H., Fujieda, S., Kitamura, K. & Sato, M. 2007. Vlgr1 is required for proper stereocilia maturation of cochlear hair cells. *Genes to Cells,* 12**,** 235-50.

Yao, J., Irwin, R. W., Zhao, L., Nilsen, J., Hamilton, R. T. & Brinton, R. D. 2009. Mitochondrial bioenergetic deficit precedes Alzheimer's pathology in female mouse model of Alzheimer's disease. *Proc Natl Acad Sci U S A,* 106**,** 14670-5.

Yu, S., Hackmann, K., Gao, J., He, X., Piontek, K., Garcia-Gonzalez, M. A., Menezes, L. F., Xu, H., Germino, G. G., Zuo, J. & Qian, F. 2007. Essential role of cleavage of Polycystin-1 at G protein-coupled receptor proteolytic site for kidney tubular structure. *Proceedings of the National Academy of Sciences of the United States of America,* 104**,** 18688-93.

Zhou, S., Zhou, H., Walian, P. J. & Jap, B. K. 2005. CD147 is a regulatory subunit of the gamma-secretase complex in Alzheimer's disease amyloid beta-peptide production. *Proceedings of the National Academy of Sciences of the United States of America,* 102**,** 7499-504.

Zhou, X. W., Wang, X., Yang, Y., Luo, J. W., Dong, H., Liu, Y. H. & Mao, Q. 2016. Biomarkers related with seizure risk in glioma patients: A systematic review. *Clinical Neurology and Neurosurgery,* 151**,** 113-119.

7.2 Zuordnung der geleisteten Beiträge zu den einzelnen Publikationen

Meine kumulative Dissertation setzt sich aus insgesamt vier Publikationen zusammen. Zu denen haben außer mir noch weitere Kolleginnen und Kollegen Beiträge geleistet. Im folgenden Abschnitt möchte ich meine Beiträge zu den einzelnen Arbeiten aufzeigen.

In Publikation IV, Krzysko et al. 2022, habe ich die bioinformatische Analyse der TAP-Daten durchgeführt und die Proteinnetzwerke erstellt (Pub. IV, Figure 1). Die Rohdaten der TAP-Analysen wurden von B. K. in den Publikationen I, II und IV generiert. Versuche zur Interaktion von VLGR1 mit S1R, ACSL4 und TOM20 mittels RFP-Traps bzw. Myc-Trap, sowie Zellfraktionierungen und PLA Assays (Pub. IV, Abb. 2) wurden von mir und unter meiner Anleitung von A. M. im Rahmen ihrer Bachelorarbeit durchgeführt. Die Lokalisation von VLGR1 am MAM-Komplex konnte ich mit Immunfluoreszenzmikroskopie zeigen. Die elektronenmikroskopischen Aufnahmen wurden durch E. S. angefertigt (Pub. IV, Abb.3). Die Analyse der MAM-Morphologie (Pub. IV, Abb.4) wurde von mir durchgeführt, die Vorbereitung der Proben für die Elektronenmikroskopie wurde von mir zusammen mit E. S. durchgeführt. Die unterschiedliche Kinetik bei Ca^{2+}-Ausstrom aus dem ER und Einstrom von Ca^{2+} in Mitochondrien konnte ich in Vlgr1-defizienten und WT Astrozyten zeigen (Abb.5). Bei der Durchführung der Messungen, der Auswertung der Daten, sowie der Disskusion wurde ich von F. M. unterstützt.

In Publikation I, Knapp et al. 2019, konnte ich die Kolokalisation von VLGR1 und dem zentralen MAM-Protein S1R in HeLa Zellen zeigen (Pub I, Abb. 3C). Dieser Nachweis gelang mittels Immunfluoreszenzmikroskopie. Ich führte die Analyse der einzelnen γ-Sekretase Untereinheiten als putative Interaktionspartner der jeweiligen ADGRs durch (Pub I, Abb. 4B). Dazu wertete ich Daten aus den TAPs aus und erstellte die Tabelle. Das Alignment der Aminosäurensequenzen verschiedener Rezeptoren an den konservierten γ-Sekretase Schnittstellen wurde durch mich angefertigt. Dabei verwendete ich ClustalX und verglich Gemeinsamkeiten in den relevanten Sequenzabschnitten (Pub I, Abb. 4C).

In Publikation II, Knapp et al. 2022, habe ich die Lokalisation von VLGR1 in aus Mausgehirnen isolierten und kultivierten Astrozyten, mittels Immunfluoreszenzmikroskopie, gezeigt (Pub.II Abb. 5a). Ebenso führte ich das Experiment zur fluoreszenzmikroskopische Analyse von VLGR1 und dem ER-Marker CLIMP63 in murinen Astrozyten durch (Pub.II Abb. 5b).

In Publikation III, Güler et al. 2021, bin ich mit Herr Güler Co-Autor. Wir haben zusammen die Methode zu Isolierung von Astrozyten aus Mäusen entwickelt und auf unsere

Anforderungen angepasst. Für die Publikation führte ich die fachgerechte Extraktion und Präparation der Gehirne durch (Pub. III, Abb. 1 und 2). Ich kultivierte und modifizierte die gewonnenen Zellkulturen zusammen mit Herr Güler (Pub III, Abb. 3,4,5). Die Aufreinigung der Kulturen gelang mir durch eine spezielle Differenzierungstechnik (Pub III, Abb.7).

8. Eidesstattliche Erklärung

Hiermit erkläre ich an Eides statt, dass ich die vorliegende Dissertation selbstständig und nur unter Verwendung der angegebenen Hilfsmittel angefertigt habe.

Ich habe keine vorherigen Promotionsversuche unternommen.

Mainz, den

Jacek Krzysko